DEVELOPMENT OF A LOW COST PRECISION POLISHING MACHINE BASED ON PARALLEL KINEMATIC SYSTEM

ZAVID MOHAMED

Supervisor: Prof. Liam A Blunt

A thesis submitted to the University of Huddersfield in partial fulfilment of the requirements for the degree of Doctor of Philosophy

The University of Huddersfield

June 2018

COPYRIGHT STATEMENT

i. The author of this thesis (including any appendices and/or schedules to this thesis) owns any copyright in it (the "Copyright") and s/he has given The University of Huddersfield the right to use such Copyright for any administrative, promotional, educational and/or teaching purposes.

ii. Copies of this thesis, either in full or in extracts, may be made only in accordance with the regulations of the University Library. Details of these regulations may be obtained from the Librarian. This page must form part of any such copies made.

iii. The ownership of any patents, designs, trademarks and any and all other intellectual property rights except for the Copyright (the "Intellectual Property Rights") and any reproductions of copyright works, for example graphs and tables ("Reproductions"), which may be described in this thesis, may not be owned by the author and may be owned by third parties. Such Intellectual Property Rights and Reproductions cannot and must not be made available for use without the prior written permission of the owner(s) of then relevant Intellectual Property Rights and/or Reproductions.

ABSTRACT

The increasing demand on mass production of high precision parts, has pushed the precision manufacturing industry to develop reliable precision finishing processes such as Bonnet polishing to address market requirements. Indeed, the nature of the surface to be polished plays an important role in the design of a possible polishing machine. A gap within the research in polishing for precision industry needs has been identified. Small parts with < 50 mm x 50 mm and possible freeform curvature containing small slopes cannot be polished with available bonnet polishing (BP) processes on market. This is caused by the tool head size and the tool holder being bigger than part curvature or the part itself. Although, the BP process has a huge potential for surface roughness improvement and form accuracy, it is generally seen in industry as an expensive solution for a non-deterministic finishing process. Therefore, this project has sought to develop a BP machine to cover the gap with an innovative and inexpensive design.

In order to develop a machine which responded to the market expectations all possible requirements were listed from a customer point of view. Based on the requirement, a machine concept was produced. Market analysis helped to identify sub-systems of the machine. FEA analysis of the design was performed to check for stress distribution and displacement due to its own mass. Additional assembly parts are designed and a prototype of the machine was produced.

The designed machine is tested for its ability as precision polishing machine. Flat surfaces of P20 tool steel were targets for polishing to nanometric surface finishes. Empirical experiments helped to identify parameters which influenced the surface roughness. Taguchi method were then used to optimise the parameters for better surface roughness. Optimum parameters conditions helped to reach less than 10 nm Ra systematically and repeatedly. The samples were also polished using re-circulating slurry techniques, and the obtained results were discussed.

Further, pre polishing, Grolishing processes capable of improving surface roughness from ground finish to mirror like finish were developed for cost effective manufacturing procedures. The material removal was analysed to identify parameters capable of improving surface roughness over a step grolishing process. Two grolishing procedures were developed. Both processes produced nanometric range surface finishes. Other variations in results were compared and discussed.

Although, machine axis has the ability to produce freeform movement, tool holders need to be improved to facilitate the identification of the distance between tool origin and workpiece origin. Therefore, a new spindle holder assembly is produced to hold the tool and an optical measurement device DRI used to evaluate accurately the distance separating the tool-workpiece origin and further align the workpiece inclination with respect to the machine axis. A CAD-CAM package is also developed to generate programme capable of performing freeform curvature.

ACKNOWLEDGEMENT

TABLE OF CONTENTS

7

LIST OF FIGURES

LIST OF TABLES

PUBLICATION LIST

1. Mohamed, Z., Blunt, L., Young, C., Tong, Z., & Li, D. (2017). Development of precision polishing machine based on a hexapod.

ABBREVIATIONS

ANOVA	Analysis of variance
BP	Bonnet polishing
C	Carbon
CAD	Computer aided design
CCI	Coherence correlation interferometry
CD1	Conceptual design 1
CDC	Centres for Disease Control and Prevention
CIPs	Carbonyl iron particles
CMA	Computer-aided manufacturing
CMM	Coordinate measuring machine
CNC	Computer numerical control
COC	Cyclo olefin copolymer
COP	Cyclo olefin polymer
Cr	Chromium
CRT	Cathode ray tubes
DLP	Digital light processing
DMD	Digital micro-mirror device
DME	Detroit Mold Engineering
DOE	Design of experiment
DRI	Dispersed reference interferometry
FCC	Field curvature correction
FEA	Finite element analysis
FJP	Fluid jet polishing
FJP	Fluid jet polishing
FTS	Fast tool servo
GCS	General Command Set
HMC	Horizontal machining centre

IR	Infrared
IRMOS	Infrared Multi-Object Spectrograph
IRP	Intelligent Robotic Polishers
LEDs	Light emitting diodes
LFTS	Long stroke fast tool servo
Mn	Manganese
Mo	Molybdenum
MR	Magnetorheological
MRF	Magnetorheological finishing
MRR	Material removal rate
MSF	Mid-Spacial frequency
NJR	National Joint Registry
NMAPs	Non-magnetic abrasive particles
OA	Osteoarthritis
OA	Orthogonal array
PALs	Progressive addition lenses
PC	Polycarbonate
PGI	Phase grating interferometer
PI	Physik Instrument
PLC	Programmable logic control
PMMA	Polymethylmethacrylate
PS	Polystyrol
PV	Peak to Valley
Ra	Roughness average
RMS	Root-mean-square
RPM	Rounds per minute
RSM	Response surface methodology
Sa	Arithmetic mean of the absolute value of the height
Si	Silicon

SiC	Silicon carbide
SPE	Society of Plastics Engineers
SPI	Society of the Plastics Industry
Spk	Reduced peak height
STS	Slow tool servo
Sz	Maximum height of the topographic surface
TKR	Total knee replacement
UHMWPE	Ultra-high molecular weight polyethylene
UPFP	Ultra-precision freeform polishing
UPM	Ultra-precision machining processes
VMC	Vertical machining centre
WC	Tungsten carbide

1. Introduction

1.1   Research Background

In the process of manufacturing precision mechanical components, the final finishing operations are always the most critical, least controllable and often the most expensive in terms of material removal. Due to tight tolerances the probability to be out of specification is high. At the same time the demand for mass production of high precision parts is constantly increasing. Industries such as medical, optical and the plastic injection moulding sector requires challenging finishing within ten nanometres surface roughness and around ten microns form accuracy [1, 2]. Indeed, the product lifespan and performance are improved with the increase of its precision. New machines and processes such as precision polishing, grinding, diamond turning and micro milling have been developed to produce precision parts and meet the market requirements.

As an exemplar, in medical industry, prosthetics devices such as knee joints are used to help patients suffering from osteoarthritis. The devices help to improve patient's quality of life by reducing the pain and restoring their mobility. The bearing surfaces requires precision freeform surfaces which are obtained through precision manufacturing. The wear of these prosthetics causes premature failure, and it is found that the surface finish and form accuracy are key to improve failure rates [3, 4]. Precision polishing using IRP200 from Zeeko for example, can be performed as final finishing process to reduce form error and improve surface roughness, hence increasing reliability [5, 6]. Developed methods have the ability to reach in surface roughness and form, well below the recommended value of ISO 7206-2:2011 for metallic bearing surface of artificial implants [1]. However, the polishing machine tool head is bulky and cannot reach middle region of the freeform femoral implant component (figure 1-1). Additionally, the cost related to the machine and the process has made the solution not feasible for many manufacturers.
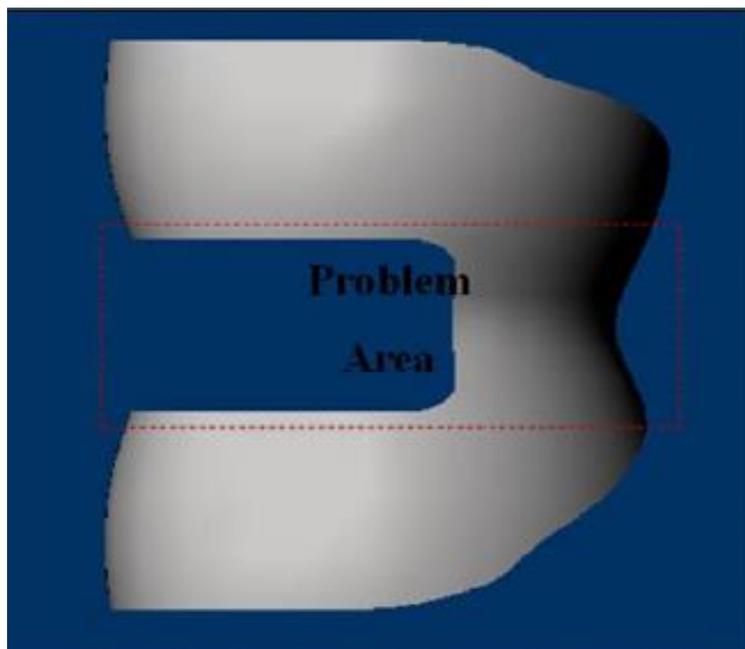
Figure 1-1:   Orthopedical knee joint: showing problem area where the polishing tool could not reach [5]

In optics industry, freeform design of optical elements has enhanced the performance of optical systems to its maximum extent. The benefits are as diverse as increased field of view, reduced number of lenses on a system, expanded field of view, simultaneous correcting aberrations, increased depth of field and so on [7, 8]. The manufacturing of these surfaces can be obtained through ultra-precision cutting, grinding and polishing processes. Materials such as, zinc selenide, zinc sulphide, germanium and polymers such as polystyrene, polycarbonates are ideal for diamond machining thanks to their material properties being compatible with ductile mode material removal. On the other hand, harder and brittle materials such as Glass used in optical application or P20 tool steel used on mould inserts, causes rapid wear of diamond tools. In this case ultra-precision grinding, grolishing and polishing are vital for the fabrication of moulds and glass optics [9, 10].

In the last two decades, ultra-precision manufacturing machines have been developed to meet industrial requirements for high precision components [11]. Precision cutting, grinding and polishing machines are available on the market for reaching the desired quality. However, cost associated with the fabrication restrain manufacturers and end users from truly benefiting from the initial design expectation. Indeed, for the process chain of manufacturing orthopedic knee prostheses, the final finish is performed on an Acme manufacturing robotic cell which offers cost effective lapping process [5]. Similarly, manufacturing of complex shapes made out of hard and brittle material is performed through deterministic fabrication methods which leaves pre-final phase machining marks, considered as mid spacial frequency errors. This weakens the designed performance of the optical element for example [12, 13].

Although, non-deterministic fabrication can remove mid spacial frequency errors, it is only benefitting a small number of applications where the removal of MSF errors is crucial such as lenses for space telescopes [14]. Indeed, non-deterministic fabrication is time consuming, expensive and requires more than one process to reach desired quality (i.e. bonnet and fluid jet polishing), depending on surface topography. Fluid jet polishing is used to overcome the accessibility issue discussed above. It has ability to improve surface roughness and reduce the scratch marks on the surface, but it tends to leave trace of tool path marks which can only be removed through a contact polishing [5, 13, 15].

The bonnet polishing process developed by Walker [16], has the ability to polish, grolish and provide form corrections. Large amounts of research have been conducted using the process which has shown its maturity and efficiency. However, the cost of the Intelligent Robotic Polishers (IRP) and processes are expensive and time consuming which refrains some industry from investing in this valuable process. Further, bulky tool heads cause accessibility issues which prevent bonnet polishing reaching its full potential. Therefore, a polishing machine using bonnet polishing process designed and manufactured to overcome issues these would be a clear advantage.

1.2   Aims and Objectives

1.2.1   Aims

The ultimate aim of this project is to design and manufacture a low cost freeform polishing machine capable of performing bonnet polishing on moulds and glass lenses to the size of around Ø60 mm. The developed machine will be evaluated on its ability to obtain the finest surface roughness on P20 tool steel. Cost effective grolishing processes capable of improving surface roughness from

machined finish to reach smooth surface will also be developed. All necessary work to perform polishing on surfaces other than flat will be implemented on the machine. Finally, machine capability as a low cost polishing machine will be discussed.

1.2.2   Objectives

The specific objectives to meet the aim are given below:

- Develop a concept design of a low cost freeform polishing machine developed to meet medical and low cost optics industry requirements.
- Integrate appropriate off the shelf sub-systems in the machine design.
- Assemble the prototype of the machine, where the form accuracy needs to be within ± 5 microns and polishing volume should cover Ø60 mm with 10 mm height.
- The machine should be capable of reaching below ten nanometres Ra/Sa surface roughness. The variation of process parameters will be studied using Taguchi approach to improve surface roughness.
- Perform re-circulating slurry polishing.
- Demonstrate cost effective surface roughness improvement process via grolishing processes developed to tackle rough surfaces such as just machined with around 0.5 µm Sa to reach surface roughness below 0.01 µm Sa using only the developed machine.
- Develop/optimise CAD/CAM software compatible to the machine motion controller, to be implemented for tool path generation.
- Developed process should be suitable on surfaces other than flat.

1.3   Structure of the Thesis

Chapter 1 introduces the research subject, thesis aims, objectives and the way the thesis is structured.

Chapter 2 offers a literature review on applications which can benefit the freeform bonnet polishing. The historical background up to recent research and development of health care and optic application is discussed in order to underline the importance of this research work.

Chapter 3 explores available machines and processes on market to produce precision freeform surfaces with pristine surface finish. It further discusses the advantages and disadvantages of those machines and processes in terms of cost, time and technical specifications.

Chapter 4 discusses the machine conceptual design, followed by market analysis to identify appropriate sub-systems for the machine. Other machine components are designed and manufactured. The prototype of the polishing machine, which comply with the machine design aim is produced.

Chapter 5 outline work carried out to understand the effect of machine parameter variability on surface roughness improvement. Polishing using paste abrasives and re-circulating slurry are performed and the obtained results are highlighted.

Chapter 6 presents the development of a grolishing process to smooth ground surfaces to mirror like surface finishes. Two grolishing processes are developed and tested. The results obtained are compared.

Chapter 7 presents the overall discussion of the thesis findings

Chapter 8 concludes the progress of the research work and contain an extended future work which briefly describes the preliminary work carried out to implement form polishing and also suggest immediate future work.

1.4 Summary of contributions

The contribution to the knowledge produced by this research work includes the following:

(1) Design and Prototype of a low cost freeform precision polishing machine based on a Hexapod.

Through literature review, a gap in research was identified. A small scale low cost precision polishing machine capable of producing freeform movement and accessing narrow surfaces is required. Bonnet polishing process were identified to have the potential to meet industrial requirements in terms of surface roughness and form accuracy. However, a cost effective machine and polishing process needed to be developed. A precision polishing machine performing bonnet polishing process is developed as a result of identifying a market gap. The designed machine having an integrated design concept, to reduce cost and time related to machine manufacturing was envisaged. The requirements of each sub-system were expressed and met to reach the global machine outcome. This concept is considered novel.

(2) Improvement of surface roughness on P20 tool steel.

Surface roughness improvement on P20 tool steel material, largely used to fabricate mould inserts was evaluated. Empirical experiments were conducted to understand the effect of machine parameters on surface roughness. Results inconsistency are noticed due to fixed parameters variation and appropriate actions were taken to produce consistent results. Taguchi method were used to improve surface roughness by optimising the variability of parameters. Re-circulating slurry polishing is also performed. The approach is a new implementation of Taguchi as applied to ultra-precision polishing.

(3) Development of grolishing process on P20 tool steel.

To reach below ten nanometres surface roughness, precision grinding before polishing is normally implemented. This requires precision grinding machines as an intermediate between CNC machining and polishing. An attempt is made using a grolishing process, to grolish rough surfaces such that as machined surfaces can be processed to give a mirror like finish. The aim of this process is to remove intermediate step, hence reduce manufacturing cost and time of precision components. Two grolishing process are developed and tested. Both reach below ten nanometres surface roughness. Grolishing at this scale on the new machine is considered novel

2 Applications which can benefit from Bonnet polishing process

This chapter will review potential applications which are using or can benefit from the bonnet polishing process. Although a number of industrial sectors use bonnet polishing technologies as a final finishing process, in the present chapter an example of an application from the medical and optics industry will be reported to emphasise the importance of the new polishing machine.

2.1 Orthopedic Implants

2.1.1 History and Statistics of Orthopedic Implants

Increases in the percentage of elderly people in the population has become a major concern in almost every country in the world. In 2017, the number of people over the age of 60 reached a record of 962 million. This represents 13% of the world population. The projection for 2050 and 2100 are respectively 2.1 and 3.2 billion people [17, 18]. The Centres for Disease Control and Prevention (CDC) estimate that 49.7% of adults over 65 or older have Arthritis in the form of Osteoarthritis (OA). OA refers to the progressive degeneration of the cartilage tissue which then for example causes damage to the femur and tibia bones which make up the knee joint. Figure 2-1 shows a schematic illustration of OA in a knee joint. The degeneration causes pain, stiffness, inflammation and also reduces the ability to move the joint. Indeed, OA is one of the major causes of disability of people over the age of 65 [19].
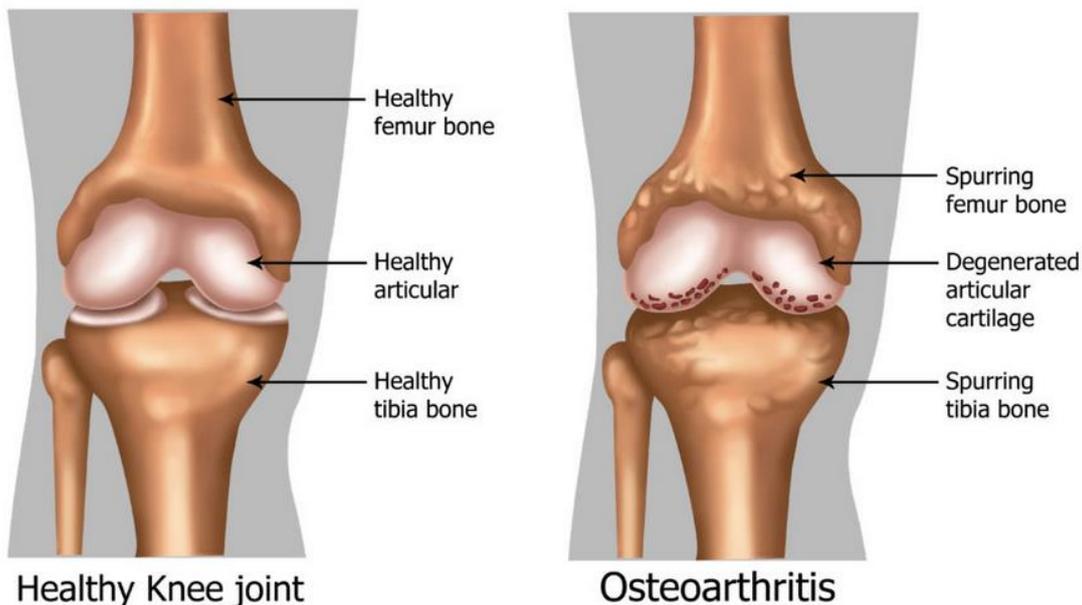
Figure 2-1:   Schematic of Knee Osteoarthritis [20]

Technological developments have allowed clinicians to replace damaged, diseased or worn cartilages and joints with artificial prostheses. This helps patients to reduce pain, improves mobility and, thus, quality of life. Artificial implants have been successfully implanted in most of the human body joints, such as shoulders [21], ankles [22, 23], wrists [24], spinal joints [25, 26], fingers [27, 28], hips and knee joints [29, 30]. The market value of orthopedic implants was $47,261 million in 2016 and is expected to rise to $74,796 million by 2023 [31]. The National Joint Registry (NJR), has

recorded surgical intervention for orthopedic implants since April 2003 in England and Wales. By December 2017, a total number of 2,284,416 procedures had been completed. Figure 2-2 shows the number of surgical procedures in different categories.
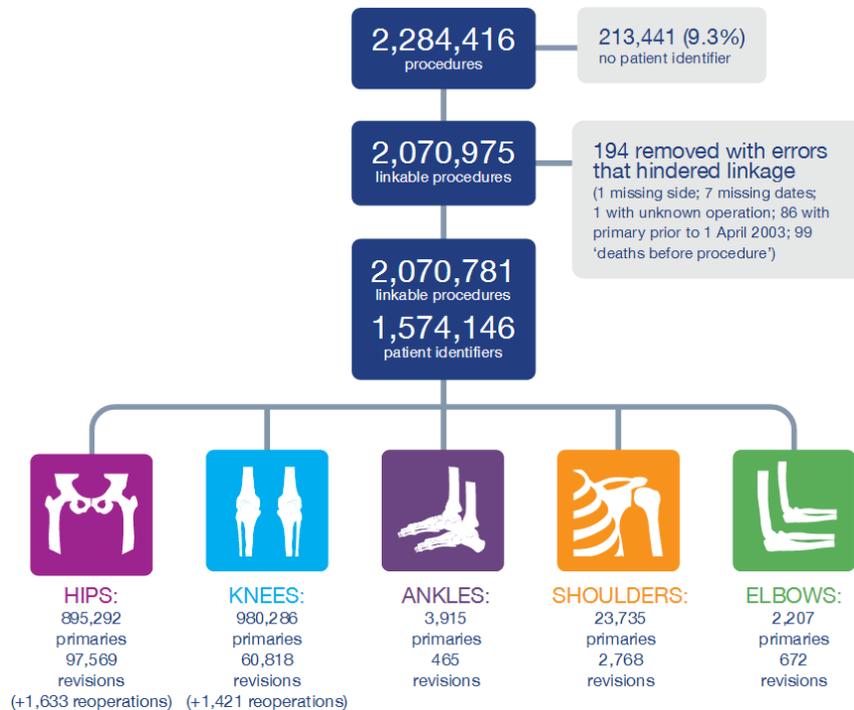
Figure 2-2:   Orthopedical implants, surgical procedures data in England and Wales by December 2017 [32]

Hip and knees joint replacements count for 98.6 % of the total number of orthopedic implants performed between 2003-2017 in England and Wales. They also have high revision and reoperation rates. In the case of hip implants, there are 97,569 revisions and 1,633 reoperations. Knee implants account for 60,818 revisions and 1,421 reoperations. Several reasons are reported for revisions and reoperations, including aseptic loosening, pain, implant wear, and infection. The main reason remains aseptic loosening, in both cases accounting for almost 50% of the reason for revision. The term 'aseptic loosening' refers to the failure of the bond between the implant and the bone, which is mainly caused by the wear debris produced from prosthetic joint articulations [33]. The particles of wear trigger an immune or inflammatory response called Osteolysis. This causes an excessive immune response the bone tissue surrounding the implants and causes osteoclast (bone resorption), which leads to loosening of the joint [34-36]. Aseptic loosening happens within 10 years of the prosthetics being implanted, resulting in premature failure and need for revision [33, 37].

2.1.2   Knee implant replacement

There are two type of knee replacement: total knee replacement (TKR) and partial knee replacement. TKR involves surgical intervention on both the femur and tibia bones, whereas partial knee replacement involves surgical intervention on one side of the two bones. Knee replacement helps patients suffering from severe pain in their knees (from rheumatoid arthritis, psoriatic arthritis, osteoporosis or trauma) to regain a better life quality. In order to replace the knee joints and mimic

the movement of the knee, the freedom of the knee joint was studied. It was found that the cartilage between the bones moves freely in six degrees of freedom [38, 39]. The TKR was initially developed by Professor Themistocles Gluck in 1891. However, the first design replicating the knee joint movement came 60 year later with the Walldius's design [40]. Even at this stage, there were several issues, such as freedom of movement, alignment, force applied on prosthetics, and other factors, which led to catastrophic failures [41, 42].

The great breakthrough in the design of knee joints was achieved by John Goodfellow (surgeon) and John O'Connor (bio-engineer) from Oxford [43]. Their design was unique in the way it mimicked all six degrees of freedom as in natural knee joints. Indeed, the femur bone was wrapped by an ingeniously designed component facilitating patella-femoral articulation. The survival rate of these TKR were much greater than any previous knee implant design. The success of the model was followed by further development of surgical jigs for accurate bone cutting, fixation devices and other improvements to increase joint lifetimes [43].

The design of the new knee implant system is referred to as a condylar prosthesis (figure 2-3). The design is composed of knee femoral component, a tibial tray and tibial insert. Additionally, it may contain a patella component, if the existing one is damaged. Tibial tray is cemented onto the tibial bone and knee femoral into the femur bone. The tibial insert is assembled on tibial tray and has inverse surface form to the knee femoral element to allow the six degrees of movement. One of the most challenging problems of artificial knee joints was the sliding movement of the knee femoral component on the tibial insert. The study of natural knee movement shows the medial side of the knee moving differently from the lateral side. The medial side has a conforming pivotal movement whereas the lateral side has a loose pivotal movement (figure 2-4). Simulating such movement with artificial knee joints is crucial to limit the sliding movement, aid stability and maintain freedom of movement [44, 45]. Freeform or blended spherical surface geometries is consequently essential on the knee femoral and tibial insert to imitate natural mechanical movements.
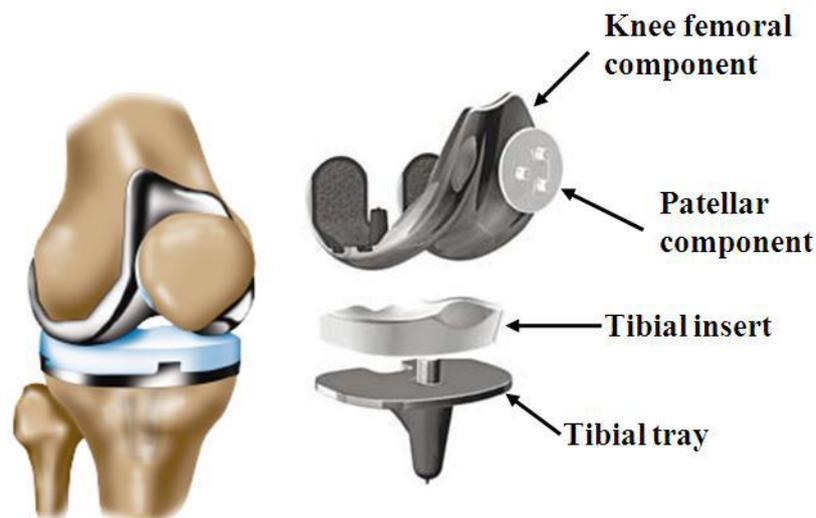
Figure 2-3:   Knee implants system [46]
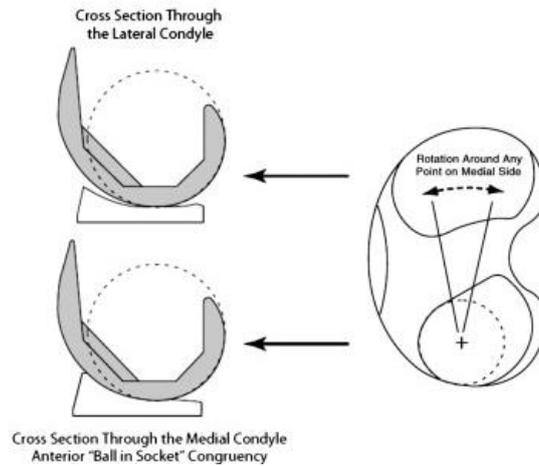
Figure 2-4:   Schematic figure showing conforming medial and looser lateral knee kinematics [44]

There are more than 150 models of condylar prosthesis available on the market. Models are adapted to the patient's age, weight, anatomy, lifestyle and physical condition of the knees. The material of the implants needs to be biocompatible to avoid body rejection of the material. In the modern TKR, the knee femoral and tibial trays are mainly made of titanium (tray) or a cobalt-chromium (femoral component) based alloys. The tibial insert is made of ultra-high molecular weight polyethylene (UHMWPE). The materials are chosen for their durability and their chemical properties having low reactivity with the body [47]. Further, the implants design may have a cruciate retainer and posterior stabilizer, depending on the condition of the patient's existing interior and posterior cruciate ligaments. The tibial insert is either fixed on the tibial tray or has some mobility freedom, depending on patient's lifestyle. Fixed bearing prostheses have a limited motion range, whereas the mobile bearing prostheses provide an additional motion range to accommodate an active lifestyle [48, 49]. However, after two years, both systems provide a similar mobility condition; therefore the mobile bearing prostheses are only reducing the time necessary to reach full motion range from two years to six months [50].

Although research has been conducted over the last three decades to improve human made artificial knee joints, there are still reports of a significant early failure rate, and this has a negative effect on patients' trust in the systems developed. Indeed, several studies report on the rate of early revision due to TKR failure [51]. The reports analyse the causes of failure based on the average number of months to revision: 24, 60 and 120 months. The causes of failure are classified based on their percentage contribution to the need for revision. The primary cause of failure in the first 24 months after implant is infection. However, the primary cause of failure, above 48 months is aseptic loosening, and it is estimated that failure due to aseptic loosening will continue to increase [52]. It is understood that aseptic loosening is caused by wear particles produced on the bearing surface between knee femoral and tibial insert [53]. Cheung, et al. studied the wear control of orthopedical implants and found that form control and improvements to surface roughness achieved on orthopedic implants using an IRP 200 polishing machine produced less material loss due to wear mechanism of bearing contact than ordinary polished surfaces [54].

2.2 Evolution of Optical lenses design

2.2.1 History of Optical lenses

The first known invention of an optic lens, the Nimrud lens, was created between 750-710 BC. The lens is made of Rock crystal, with the size of Ø38 mm and 22 mm thickness. Its function is unknown, although some authors suggest that it may have been used as a decorative stone, magnifying glass or fire stone. Archaeological research shows widespread use of lenses in antiquity, as magnifying or burning glasses [55]. However, the first referenced publication referring to the use of lenses as a burning stone is "The cloud" (424 BC) from Aristophanes, a comic playwright of ancient Athens [56]. The word lens comes from the Latin word for a lentil, because of the similarity in shape. Lentils are shaped like a double convex lens.

Lenses primarily remained as polished crystals or were used as water vessels up until the Middle Ages [57]. In the 9th century, Abbas ibn Firnas developed pure glass, which was widely used as a reading stone, through a process of converting sand into glass [58]. The foundation of scientific research on the principle of optic and visual perception was established by Ibn Al-Haytham (c. 965 – c. 1040). His "Book of Optics" [59] includes his work on vision, optics, astronomy, physics and mathematics. Ibn Al-Haytham explained the working principles of the eye as a receiver of the light rather than an emitter. He produced a clear description of the camera obscura, and explained the growing capabilities of lenses.

In the 13th century, Italian reading stone manufacturers improved their lens manufacturing techniques to produce thinner and lighter reading stones. This progress enabled the development of the first spectacles in Venice between c. 1268 – c. 1300 [60]. Figure 2-5 shows a replica of one of the earliest model of spectacles made with a wooden frame. The lenses were used both for reading and for viewing objects at close range and from afar. Indeed, by the beginning of the 17th century, Dutch Spectacle makers Hans Lippershey had developed the first refracting telescope, which, when revised by the Italian scientist Galileo Galilei, became known as the Galilean telescope. Galileo used the telescope to discover Jupiter's satellites, phases of Venus, spots on the Sun, and hills and valleys on the Moon. In 1625, Galileo modified the order of the lenses of the Galilean telescope to produce the first microscope [61]. Robert C. Hooke (c. 1635 – c. 1703) used the microscope to examine a thin cutting of cork where he noticed walls with empty space which he termed cells. He further used a microscope to study the crystal structure of objects, the anatomy of insects, and other novel discoveries, and this encouraged other scientists to explore and research the microscopic world [62]. Figure 2-6 shows, on the left, the first two telescopes developed by Galileo and, on right, the microscope, both exhibited in the Institute and Museum of the History of Science, Florence.

Figure 2-5:   Replica of Eye Spectacles model of 14th Century [63]

Figure 2-6:   Galilean Telescope 1609 (left) [64] and Galilean Microscope 1625 (right) [65]

The era of photography further put the capability of lenses to the test. At the beginning of the 19th century, simple lenses were developed to be fitted on cameras. The image produced was poor in quality and was affected by aberration and other issues. Optical aberration creates blurred or distorted images. The three main types of aberration needed to be corrected to improve the image quality are chromatic aberration, spherical aberration and coma aberration. Chromatic aberration is produced by light passing through lenses being refracted at different angles, depending on the wavelength. Spherical aberration is caused by the convergence of light rays to different focal points. Finally, coma aberration refers to the appearance of smears due to off-axis light rays.

The first commercialised photographic process called "Daguerreotype" was created using a lens developed by Charles Chevalier (figure 2-7). The lens is consisted of a biconvex lens of crown glass and a biconcave lens made of flint glass. The design of the lens and the materials used helped to reduce optical aberrations and produce a sharper image. It took 20 to 30 minutes' exposure to produce an image [66]. This lens was followed by other models designed to reduce the shooting time, increase further the sharpness of the image, requiring less light to expose the image, and totally removing aberration and stigmatism. These improvements were made possible by the development of new lens material and lens designs based on scientific formulas. Indeed, in 1890, a lens model called Zeiss Protar was developed which removed totally all aberration and stigmatism. This was the first lens model to be developed based on scientific formulas and to use a new material, barium oxide, with a high refractive index [67]. Throughout the 20th century, other lens models followed, designed to increase performance and reduce manufacturing cost. Figure 2-8 shows a schematic design of a Canon lens following the Double Gauss design. The picture shows the complexity of design, alignment, and number of optical elements to improve further the performance of the lenses [68].

Chevalier Achromat Landscape, 1839
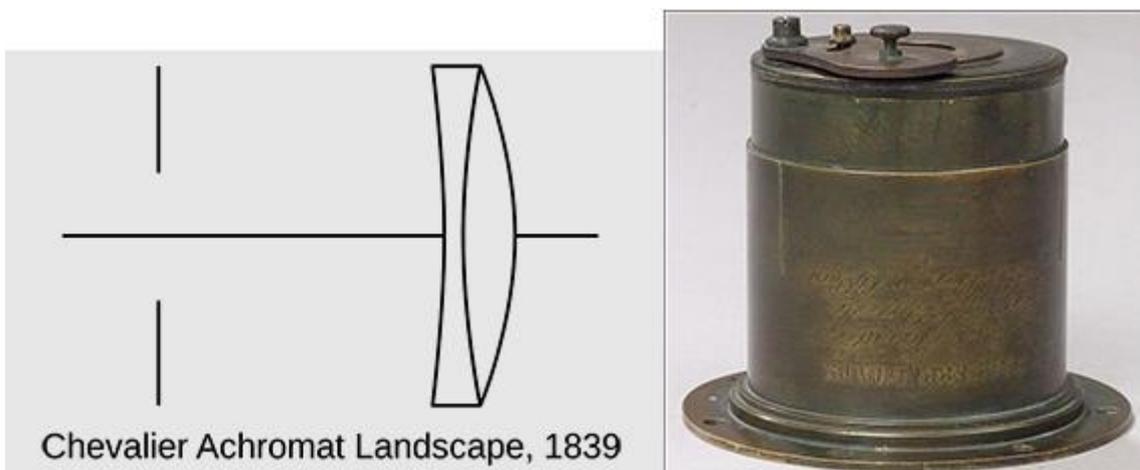
Figure 2-7:   Chevalier Achromat Landscape (1839). Schematic design of lenses (left) and first commercialised model "Daguerreotype" (right) [66]
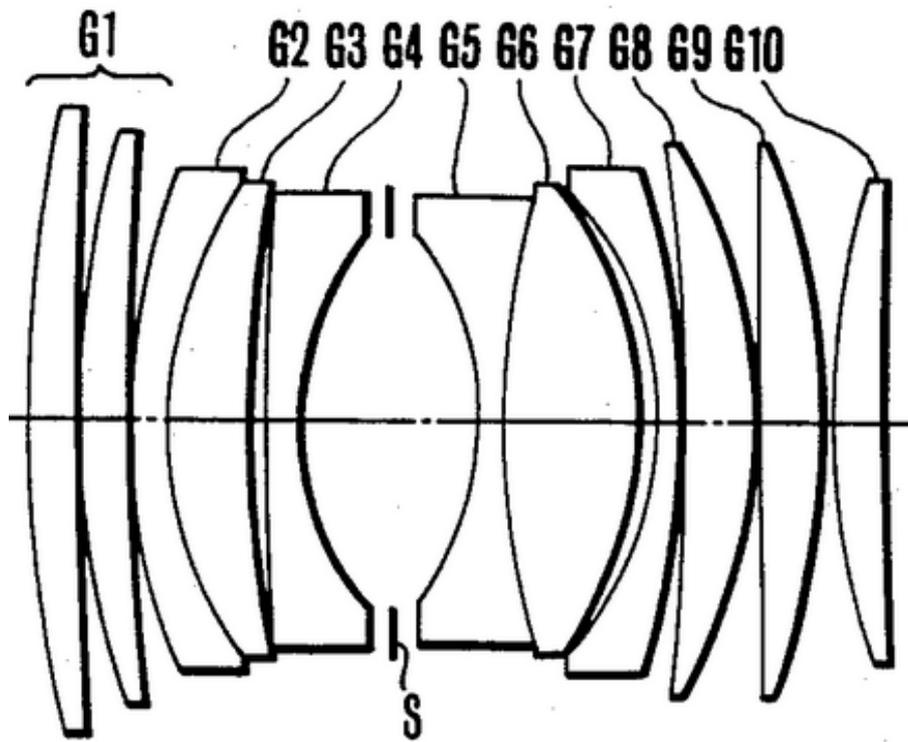
Figure 2-8:   Double Gauss schematic design, Canon lenses (1988) [68]

2.2.2   Modern lenses design and applications

Modern optical lenses are transparent in nature and made of glass or plastic. They are used to manipulate light rays by either converging or diverging them in a specifically desired way. They open the doors of the invisible world to our naked eye. Indeed, microscopes reveal micro and nano features, while telescopes enable the discovery of stars and far distant galaxies. Lenses are used in a wide range of applications, from projectors to produce large screens to domestic illumination in household lights. Lenses have at least one curve, but may have more than one, depending on the intended application. They work by refracting light beams; bending them to change their direction so that objects look smaller or larger than they actually are. There are two main types of lenses: convex and concave lenses (figure 2-9). Convex lenses produce light convergence, whereas concave lenses produce light divergence. Parallel light beams passing through a convex lens converge to reach a point called the focal point. The distance between the lens and focal point is called the focal length. On the other hand, concave lenses diverge parallel light beams outward. In both cases, the angle of refraction depends on the lens curvature.
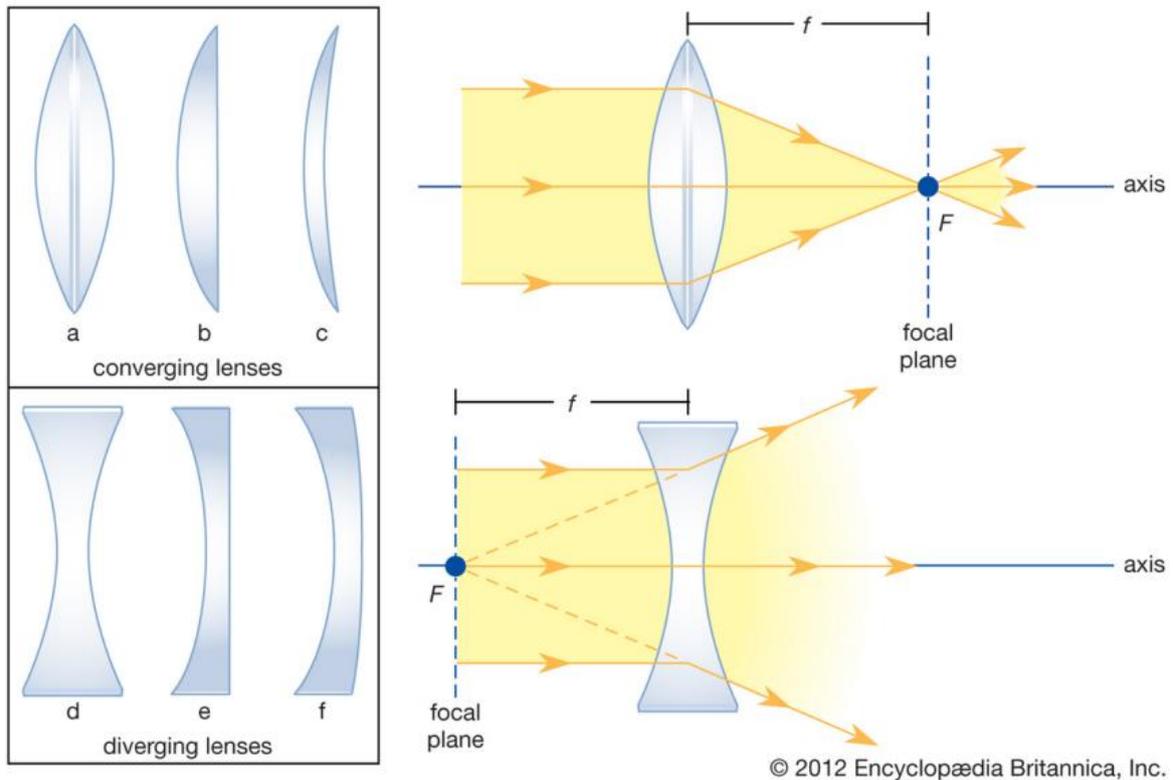
Figure 2-9: Concave and convex lenses design and their working principles [69]

Alongside improvements in the performance of lenses for better quality of image, the aspherical and freeform design approach has emerged to both reduce the size of optical systems and increase their functionality. Spherical aberration affects the quality of large diameter lenses. Aspherical lenses deviate from the spherical surface profile symmetrically to the axis of rotation, minimise spherical aberration, and reduce image distortion in wide angle lenses. Further, they help to reduce the number of optical elements used to control optical flaws, resulting in smaller, lighter, cheaper and better performing lenses (figure 2-10) [70]. A freeform surface is neither spherically symmetrical nor symmetrical of an aspherical surface. The term freeform was first used by NASA in the 1990s with the development of the Infrared Multi-Object Spectrograph (IRMOS); however, the freeform surface was used in rudimentary progressive spectacle lenses made by Owen Aves in 1907. The shape of the rudimentary progressive lenses was improved over several decades [71].
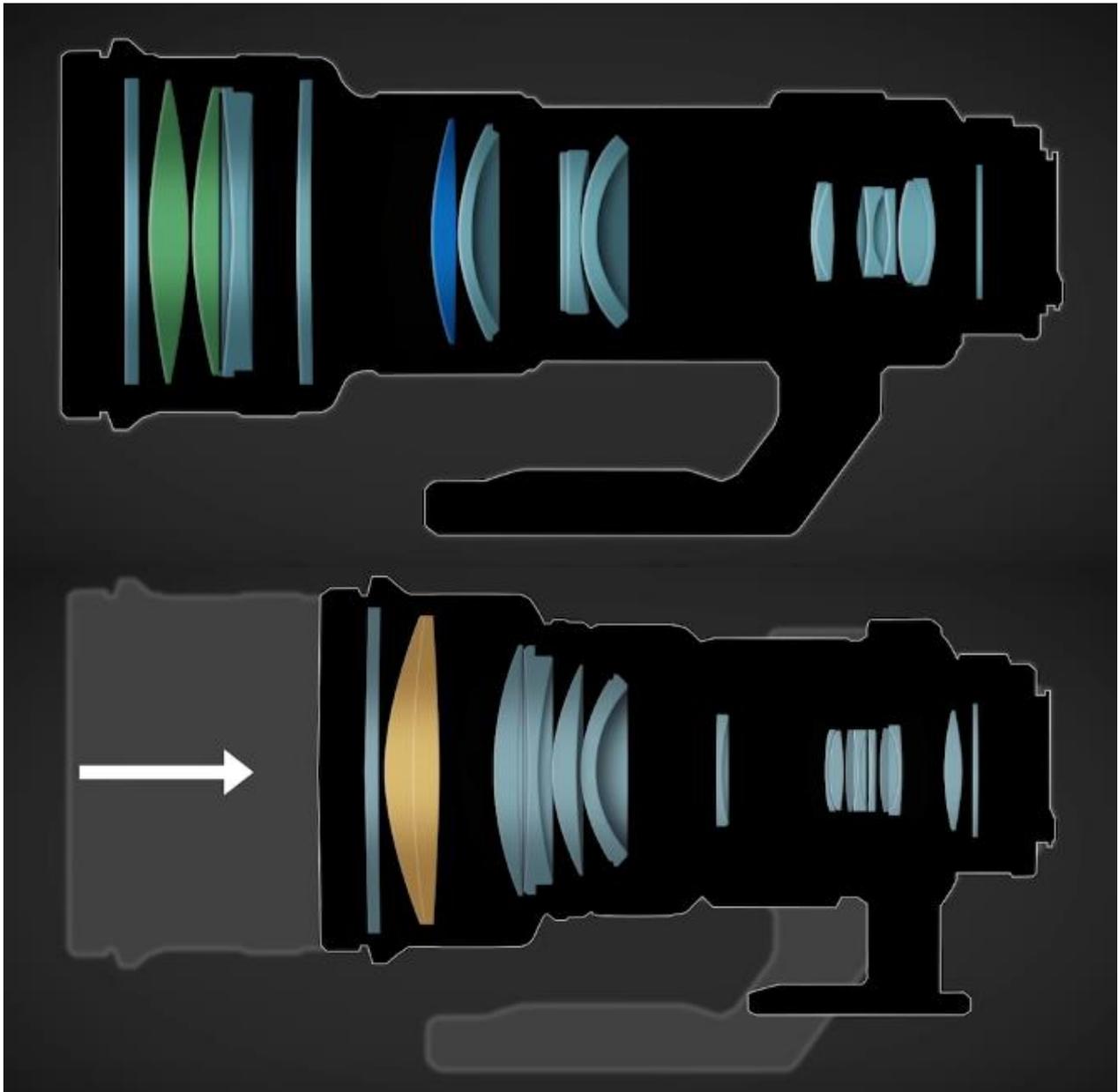
Figure 2-10:   Canon lens design: using spherical lenses (top), using aspherical lenses (bottom) [70]

By the end of 20th century and beginning of 21st century, several industries had benefitted from freeform optics within their applications. The applications could be classified into two different categories: non-imaging and imaging freeform optics [72]. In the non-imaging category, freeform optics are used to control the light direction in order to reduce energy consumption and improve light distribution uniformity. Applications include illuminations and photo scanners [73], beam shaping [74] and concentrators [75]. On the other hand, imaging freeform optics are used to improve the sharpness of the image as well as to reduce the number of optical elements within an optical system. Applications include head-mounted displays [76], projection lenses [77], off-axis reflective infrared imaging system [78], ultraviolet lithographic objectives [79] and varifocal lenses [80].

The actual design of freeform optics has been well researched over the last three decades, with the development of commercially available lens design software. In recent years, there has also been a growing research interest in the freeform machining processes as well as in material science [2].

Mass production of optical lenses is obtained through a moulding process requiring precision master mould inserts. Finally, research in the field of metrology of freeform lenses includes contact and non-contact measurement systems and the direct measurement of optical performance [81]. Optical applications which can benefit from a low cost precision polishing process are explored below.

a)   Ultrashort throw projectors

Traditional projectors using cathode ray tubes (CRT) for projecting images were initially available in the 1950's. The field was advanced by digital light processing (DLP) projectors based on digital micro-mirror device (DMD) technology using light emitting diodes (LEDs). DLP projectors offered a compact design with better brightness and higher resolution than CRT projectors. The number of applications has gradually expanded over the years, reaching education, household, business, digital cinema, and other areas. [82, 83]. Although quality and reliability have reached a satisfactory level, practicality is becoming more and more of a concern. As developed applications have matured, consumer demand has become more specific; indeed, large scale projection at an ultrashort projecting distance is demanded.

Large scale projection with high resolution is obtained either by increasing the distance between the projector and the screen or through the use of large diameter lenses to achieve a wide field of view. Both methods pose some inconvenience to the user; the first, by projecting the shadow of the presenter onto the screen. The light hits the presenter's eyes and causes discomfort. Moreover, the method requires the entire space between projector and screen to be cleared. The second solution using a large lens would make the system heavier, bulkier and more expensive. An alternative solution of using a fisheye lens capable of projecting wide images produces inevitable image distortion and affects the quality of the image [77].

To satisfy consumer demand, projector manufacturers have developed their own patented designs. Notable examples from Hitachi [84] and NEC [85] are capable of projecting a diagonal screen size of between 1.3 to 2 meters with a distance below 1 meter between projector and screen. However, the models which have been developed are large and heavy, making them unsuitable for portable use. Indeed, the surface of the reflection mirror is either concave or convex in shape, which requires several optical elements to reach the desired quality, making the system both heavy and bulky [72].

Zhenfeng Zhuang et al. have redesigned the optical system for ultra-short throw projection using refractive optical elements and an odd polynomial convex mirror (freeform) surface [77]. The design follows the field curvature correction (FCC) method to obtain large screen size with low image distortion. DMD display panels present on the structure produce the image which passes through a number of refractive optical elements, creating a curved visual image. The image is then enlarged and distortion errors corrected via a freeform convex mirror surface. The total distance the light travels within the system is 228 mm, making it one of the most compact structures. It only requires 510 mm distance between screen and freeform mirror for 1.3 meter diagonal screen projection (figure 2-11(Left)). The reflective mirror containing polynomial surface has the following dimensions; 98 mm length x 49.2 mm width x 24.6 mm height (figure 2-11(Right)).

The breakthrough in the manufacturing capabilities with the ability to accurately manufacture freeform surface have empowered optical system designers to work with more degrees of freedom in their optical design. Indeed, design optimisation could lead to the diagonal screen projection length being extended and the distance separating projectors to screen being reduced [2, 72]. Ricoh developed a portable ultra-short throw projector capable of projecting 1.3-meter diagonal screen

projection from 117 mm away from the screen using freeform mirror technology. The design requires only a 249 mm distance to project a 2-meter diagonal screen projection [86].
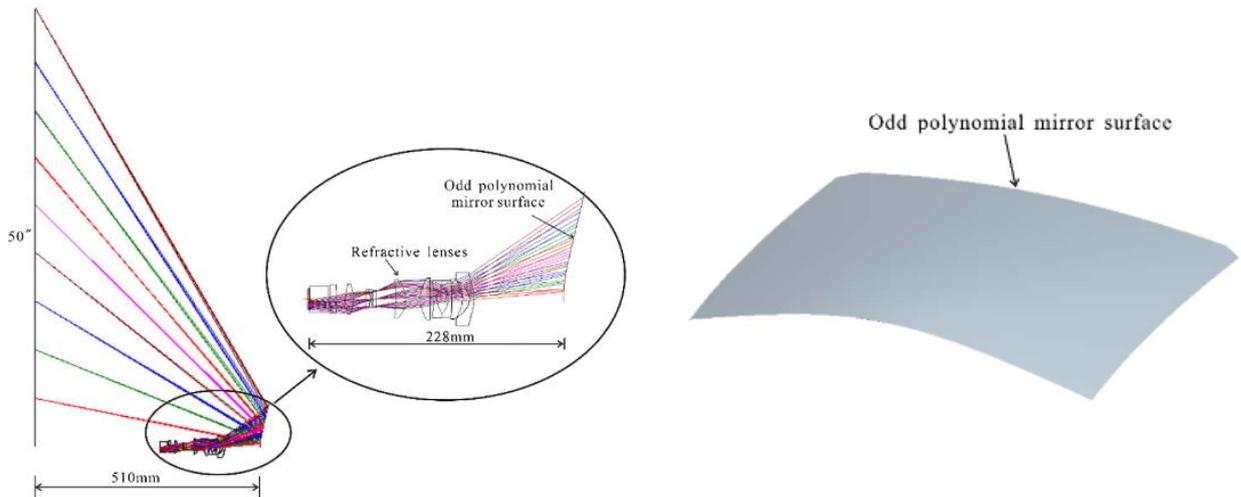
Figure 2-11: Schematic layout of projection system (left), model of odd polynomial mirror surface (right) [77]

b)   Off-axis reflective imaging system

Reflective systems are widely used in infrared imaging, ultraviolet imaging, telescopes, cameras and other applications where low mass, high transmission, uniform performance, thermal stability, and radiation resistance are required [87]. Traditional reflective systems were co-axial, causing obscuration in the middle region which negatively affected the resolution, field of view and energy concentration [88]. The obscuration problem is resolved with the use of off-axis reflective systems [89, 90]. Figure 2-12 shows an off-axis reflective system using a freeform mirror to improve image quality and reduce image distortion [91]. However, off-axis reflective systems have their own disadvantages, such as the appearance of third order coma on axis [92]. Indeed, the aberration property of the optical system is changed with off-axis positioning of optical elements. Optical systems composed of spherical and aspherical elements are incapable of correcting aberration errors caused by asymmetry and this limits the image quality. The mechanical alignments of the optical elements remain extremely difficult and expensive [93, 94].
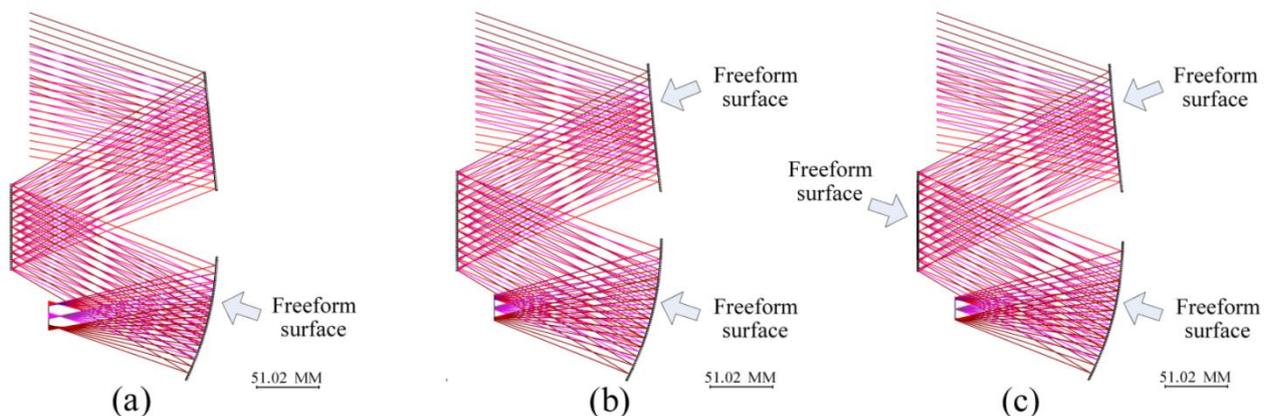
Figure 2-12: Off-axis Reflective system using freeform mirrors [91]

High performance, large field of view off-axis reflective systems can be achieved with the use of freeform optical surfaces. The design of freeform surfaces generally starts from co-axial spherical or aspherical optical elements. The obscuration in the middle is removed in the design of freeform optical elements by altering the following three aspects: (1) biased input field, (2) use of offset aperture, (3) positioning of optical elements to clear the obscurity [78, 95]. Quingyu Meng et al. have used freeform design of optical elements to integrate primary and tertiary mirrors as a monolithic mirror on an off-axis three-mirror system. The design helps to achieve large field of view and easy alignment and to reduce the weight of mirror support assembly [96]. Further, different models of off-axis optical systems have been developed based on field of view, F-number requirement [97-99].

Imaging spectrometer instruments use off-axis reflective systems to obtain a fast and reliable method for product inspection. Spectrometers are used to identify the molecular composition of a samples [100]. The spectrometer measures the light intensity as a function of its wavelength. The light source passes through a Monochromator which splits the light beam into its wavelengths. Each wavelength of the light crosses the sample and reaches the detector, which then uses the information to analyse and predict the molecular composition of the sample. Spectrometers are used in various applications; in space for more detailed satellite images, reading nutrition details of fruits and vegetables, or even help to extract information about a specific colour to reproduce the same colour [101]. Optical elements containing freeform surfaces are designed and implemented within imaging spectrometers to achieve high spectral range and resolution, combined with compactness and low weight [102].

c) *Varifocal lenses*

The muscles which control human eye lenses lose flexibility and become stiffer over age (mid-forties). Vision becomes blurred, causing difficulty in seeing small prints clearly. This phenomenon is called presbyopia [103]. Varifocal lenses, also called progressive lenses, are used to see far, near and intermediate distances using a single lens (figure 2-13). As discussed above, progressive lenses have been available since 1907 [104]. The design of the lens was complex and not easily adaptable to different wearer prescriptions. Further, the manufacturing capabilities available at the beginning of twentieth century did not allow mass production and commercialisation of this invention. The first commercially available progressive lenses were introduced in 1959 by the Société des Lunetiers (Now Essilor) [105]. This achievement was made possible by the development of a grinding / polishing machine for refractive materials capable of generating asymmetric surfaces on large scale production basis [106]. A schematic design of Bernard Maitenaz grinding machine is shown on figure 2-14. The cam on the machine is adapted to the prescription of the lenses.

Figure 2-13: Progressive lens zones [107]
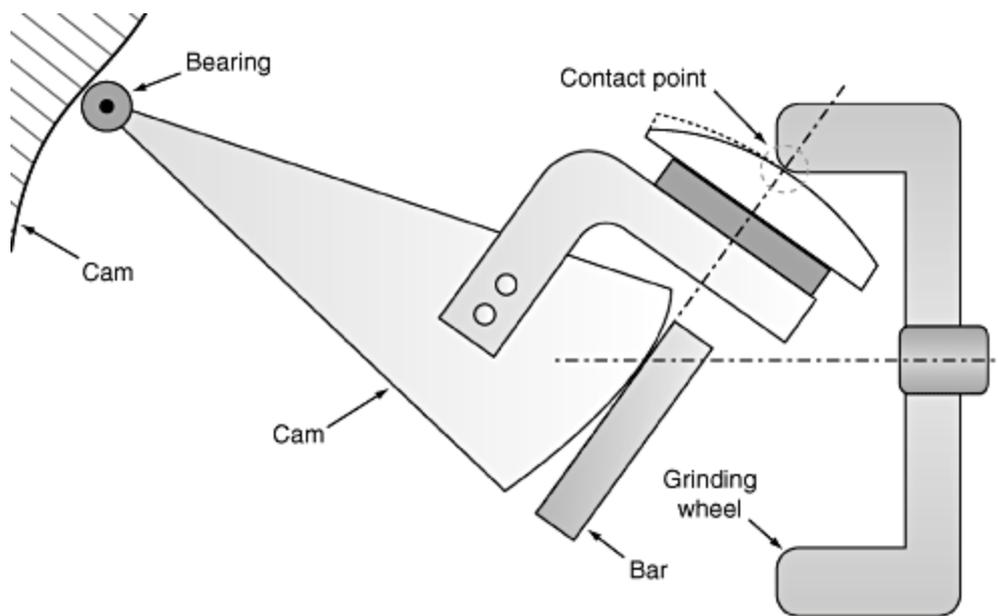
Figure 2-14: Schematic design of asymmetric grinding machine for early progressive lenses [108]

Conventional progressive lenses have an optical effect similar to that of an inverted cone, offering a gradual change in power from distance vision, with a wide zone, to near vision, with a narrow zone. Although this design was preferred to bifocal lenses, the narrow zones which limit the field of view reduce the ability to see clearly across the lens. High plus prescriptions have an even smaller vision zone [109]. As a consequence, wearers have to move their heads constantly to find a clear vision spot on the lens, causing discomfort and pain. The conventional grinding process causes astigmatism in the outer region of the triangular zone, causing blurring of vision for the wearer. Further, the lenses are not adapted to wearers' customary habits. For example, ideally, the near zone needs to be wider to accommodate someone who spends most of the time reading books, whereas, for someone spending most of their time in front of a computer, the intermediate zone needs to be wider than the other zones [110]. This cannot be achieved with conventional progressive lenses, and to counteract this, a new digital progressive design was marketed.

Digital progressive lenses use freeform surface technology to alter the shape of the lenses, based on customer daily habits. Freeform surface technology not only allows a wider zone for all vision distance in standard lenses, but aids the design of personalised lenses with varying widths of specific zones to accommodate customers' individual requirements, and thus reducing the need for the wearer to be constantly moving his/ her head [111]. Freeform surface technology allows smooth

transition between far and near zone, minimises blurring effect, and requires less adaptation time than conventional lenses. Figure 2-15 shows a picture of two freeform designs of progressive lenses. The smooth optics design provides a sharper image than a design without smooth optics. The technology is rapidly evolving to keep up with consumer demand for digital progressive lenses, and software has been developed to automatically design new lenses based on individual customer requirements, chosen frame, wearing distance, angle from the eye pupil, etc [112, 113].

with Smooth Optics   without Smooth Optics
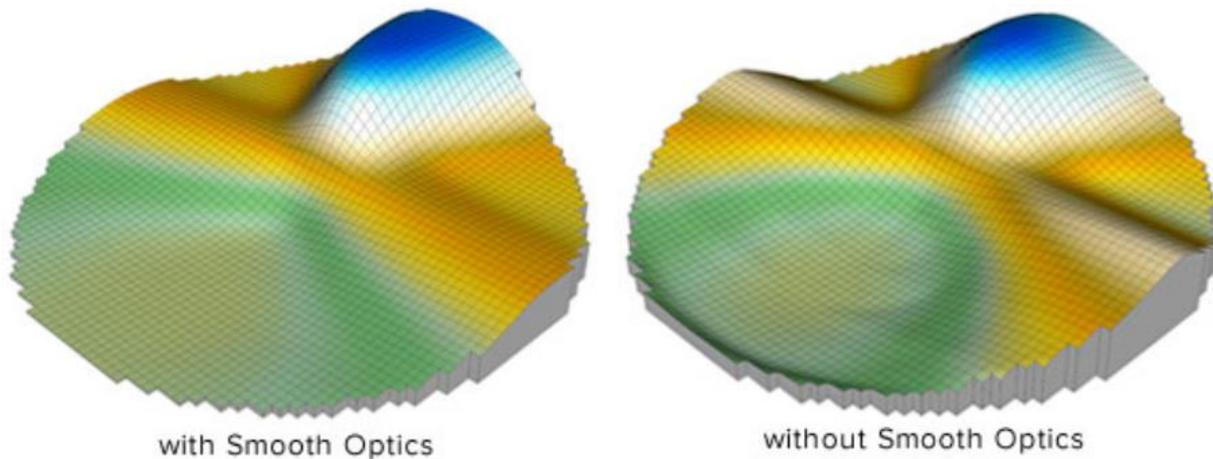
Figure 2-15:   Freeform design of Progressive lenses [114]

2.3   Precision Injection moulding

There are a variety of moulding processes available for consumer lens manufacture, such as injection moulding, insert moulding, 2 shot moulding, compression moulding and others. Precision injection moulding is a solution widely used in industries as diverse as the automotive, electronics, medical and optics industries. Injection moulding is efficient in terms of quality, cost for high volume series production, consistent repeatability of same part, high precision to cost ratio, and rapid production. It is also efficient for precision parts made from materials which involve a challenging machining process where surface cracks and internal stresses reduce the precision and feasibility of the required component [115].

Dick et al. [116] have designed and manufactured through the injection moulding process replicates of freeform optical surface with form accuracy of 2 micrometres and surface roughness of approximately 2 nm over a surface of 40 mm diameter. In order to obtain such precision on the moulded plastic part, different parameters in the process chain of injection moulding have been optimised. Generally, material used for moulded parts need to be safe from impurities and molecular confrontation. Common materials used in moulding plastic optics are PC (polycarbonate), PMMA (polymethylmethacrylate), COP (cyclo olefin polymer), PS (polystyrol) and COC (cyclo olefin copolymer) [117]. The mould tool used to produce the desired part needs to be designed by taking into consideration the shrinkage and deformation which occurs during the cooling process. The mould tool used in the manufacturing of the freeform optical surface described above is shown on figure 2-16. In this case, the mould used had a form error of 0.24 µm from P-V. Injection moulding machine parameters – melting temperature, packaging pressure, dwell pressure, dwell pressure time, tool temperature and cooling time – need to be optimized to identify the optimum level between the cycle time and peak/valley values of the moulded parts. A fast process cycle reduces the

accuracy of the produced part, whereas aiming for high accuracy slows the production rate and, thus, raises the costs of mass production.
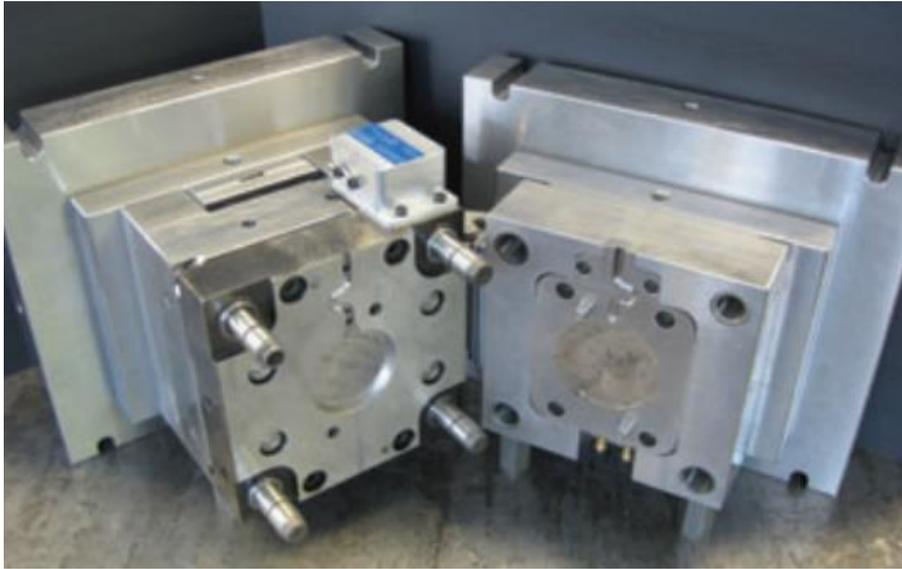
Figure 2-16:   Manufactured freeform mold tool [118]

Dick et al's research clearly shows the benefit of injection moulding for precision micro parts. High precision micro-moulded parts can be obtained for larger quantities at reduced cost. Indeed, the injection mould tool should be capable of reproducing the same part millions of, times with the same precision. Mould parts are usually sized by their weight. A part which weighs less than a gram is considered to be a micro-mould [119].

There is an increased interest from the optics, electronics and medical industries in producing high precision, micro-featured plastic parts [120]. One of the most important elements needed, to achieve precision plastic parts through the injection moulding process, is the surface finish of the injection mould tool itself. In precision moulding, the surface texture of the mould is replicated on the plastic moulded part [121, 122], making it necessary to perform an extra process, following the machining process, of grinding and polishing to remove unwanted machining marks on the surface.

2.4   Summary

This chapter has reviewed a range of different industries which can benefit from a low cost precision polishing machine: healthcare, optics/injection moulding. However, other industries may have potential applications for a low cost, precision polishing machine.

Osteoarthritis is affecting almost 50 % of people over the age of 65 years old, and, with the increase in number of ageing people reaching 3.2 billion by 2050, an expected 1.6 billion people may be affected by OA. OA causes pain, stiffness, inflammation and reduced joint mobility, resulting in high levels of disability. Fortunately, the problem has been well researched by doctors, who are now offering patients orthopedic implants to replace the worn or damaged joint. The NJR report, a total number of 2,284,416 procedures completed between 2003 and 2017, of which, 98.7% involved hip and knee joint replacement. However, these replacements lead to a high number of revisions and reoperations, the main reason for failure being aseptic loosening. Aseptic loosening affects the bond

between the bone and implant and is caused by particles of wear from the implants present on the body.

Early knee joint replacements had a high failure rate, due mainly to the complexity of movement capability of a natural joint; indeed, human knee joints have the ability of movement in six degrees of freedom. Several attempts have been made to mimic the natural movement of the knee; however, the breakthrough in the design of knee joint replacement was achieved by John Goodfellow (surgeon) and John O'Connor (bio-engineer) from Oxford [123]. Since then, different variations of their design have been developed by several suppliers to further improve freedom of movement, reduce wear and increase the life span of knee prostheses. Models have also been adapted to patients' lifestyles, sex, age, body weight and anatomy. Although TKR is now a well-researched and developed system, the early failure rate has negatively affected patients' trust. Aseptic loosening, caused by wear particles of the bearing surface, remains a major cause of failure. Cheung, et al. polished knee joint replacements using an IRP 200 polishing machine and proved that precision bonnet polishing results in better roughness and form control and, thus, delay of the wear process [124]. However, the method has not been implemented in the industrial environment due to its cost compared with the lapping process achieved using robotic arms.

The first recorded use of optical lenses by Ibn Al-Haytham was at the end of the 10th century, and improvements in manufacturing techniques to produce thinner and lighter reading stones enabled the development of the first spectacles in the 14th century. In the 17th century, lenses were used to produce the first telescope and microscope by Galileo Galilei. Together, these inventions have revolutionised the way the world around us is seen. Further advances were made in the 19th century, when lenses were used to develop cameras. However, the performance of early cameras was impaired by several issues, such as chromatic, spherical and coma aberration, which affected the quality of the image produced. In subsequent years, optical aberrations were greatly reduced by design of optical elements based on scientific formulae and improvements in the material quality of lenses. The Double Gauss design removed all aberrations and stigmatism and provided high performance at low manufacturing cost. Since then, a large number of camera models have been produced based on the Double Gauss design.

Technological evolution and consumer demand for high performance equipment have enabled the design of aspherical and freeform optical elements. These help to reduce the number of optical elements required to control optical flaws, resulting on smaller, lighter, cheaper and better performing optical systems. Applications benefiting from freeform optical elements design are classified into two categories: non-imaging and imaging freeform optics. In non-imaging optics applications, lights beam directions are controlled in order to reduce energy consumption and obtain light distribution uniformity. In imaging freeform optics, lens design achieves sharper images and a reduction in the number of optical elements in a system, making it lighter and cheaper. Several applications, such as illumination, beam shaping and concentration, head-mounted displays, projector lenses, and varifocal lenses have benefitted from freeform optical design.

Large screen projectors have been subject to inconvenience to the user for several reasons: the shadow of the presenter is projected onto the screen; projector light hits the presenter's eyes, causing discomfort; and the entire space between the projector and screen needs to be clear to avoid obstruction. Ultrashort throw projectors have been developed to overcome these problems and this has been made possible by the use of refractive lenses and freeform projecting mirrors. Reflective systems are used in applications where high transmission, uniform performance, low mass, thermal stability and other benefits are required, such as telescopes, cameras, Ultraviolet Infrared imaging. Freeform optical elements help to correct the optical aberration resulting from off-

axis reflective systems and provide a large field of view, better image quality and low image distortion. Progressive lenses are used to overcome vision problems due to presbyopia. Conventional progressive lenses have very narrow intermediate and near zones, causing discomfort to wearers as they have to move their heads constantly to find the correct focal point; moreover, they were not adapted to user habits. The freeform design of lens enables a wider intermediate and near zone, and can be custom made to accommodate users' habits, by allowing varying widths of specific zones.

Injection moulding processes are used for the mass production of high precision, complex parts at low cost and time. Dick et al. have designed and manufactured, through an injection moulding process, replicates of a freeform optical surface with a form accuracy of 2 μm and surface roughness of 2 nm Ra over 40 mm diameter. To reach such precision, the injection moulding machine parameters –melting temperature, packaging pressure, dwell pressure, tool temperature and cooling time – are suitably optimised. However, the form accuracy and surface roughness of the mould tool remains the primary and most important element in terms of precision, since the form and surface texture of the mould tool will be replicated on the plastic moulded parts. The mould tool therefore requires a finishing process, such as diamond turning or polishing. In some instances, the cost and complexity of the mould tool surface compromise with the quality and performance of the components. In such situations, which are becoming more common, low cost freeform precision polishing machines could be a valuable asset.

3 Review of precision finishing processes available on the market

The demand for mass production of high precision components is constantly increasing; however, the final finishing process in the manufacturing cycle (in terms of metal removal rates) is the most expensive and the least controllable; In addition to the precision requirement, the geometric complexity of the surface topography and form of components is an additional challenge. This chapter will review, some of the existing finishing processes currently available on the market, by outlining their capability and achievements. The surface finishing capabilities of those processes are compared with surface roughness parameters Ra and Sa.

Surface roughness measurement Ra and Sa are commonly used measurement standards (BS EN ISO 4287:2000) to quantify the surface finishing capability of any machining processes. It is a measure of the arithmetic average of the real surface with respect to the mean surface. Surface roughness of a profile measurement would provide Ra and a surface area measurement would provide Sa. The formula used to calculate the Ra is presented on 3.1 equation (L is the measuring profile length and Z(x) is the deviation from mean surface. The standard measuring length for a profile measurement is 4.8mm with cut-off length λc = 0.8mm. The equivalent for a non-contact surface measurement devise is obtained using a 20X lens.

$$Ra = \left(\frac{1}{L}\right) \int_0^L |Z(x)| dx \quad (3.1)$$

3.1 Hand finishing process

The hand polishing process is the most common finishing process practiced in industry for improving the surface quality of injection mould tools. Mould inserts are generally ground and polished after the CNC machining operation. The polishing operation is performed by highly skilled hand polishers using hand tools. In 1962, the mould manufacturing divisions of the Society of the Plastics Industry (SPI) and the Society of Plastics Engineers (SPE) cooperated to produce a classification of the surface finishes of mould tools, based on surface texture and surface roughness. The SPI-SPE standard is composed of six levels of finish, starting from SPI-SPE #1, a high polish finish, to SPI-SPE #6, a dry blasted finish [125]. Table 3-1 shows in detail the SPI-SPE finishes designation.

Table 3-1: SPI-SPE finishes designation

Name	Finish	Equipment used to obtain the Finish	Approximate Ra(µm)
SPI-SPE#1	Bright, clear, shiny, smooth	Grade #3 Diamond buff	0-0.0254
SPI-SPE#2	Semi bright, semi clear, smooth	Grade #15 Diamond buff	0.0508-0.0762
SPI-SPE#3	Lines, dull, smooth	320 Grit paper	0.2286-0.254
SPI-SPE#4	Lines, dull, semi smooth	280 Grit stone	0.9652-1.0668
SPI-SPE#5	Dull, light texture, smooth	Dry blast 240 Oxide grit	0.6604-0.8128
SPI-SPE#6	Dull, medium texture	Dry blast #24 Oxide grit	4.826-5.842

The increase in demand for plastic injection moulding at an attractive price, and the difference noticed between mould and plastic moulded components encouraged the SPI to introduce a metal plaque artefact standard indicating the expected finish texture of the moulded part. The six

standards have been split into twelve levels or "guides", which have been regrouped into four sections of three grades. In the new SPI finish designation, the capital letters indicate the type of polishing equipment used, and the number indicates the surface finish obtained. The letter A designates Diamond buff finish, B Grit paper, C Grit stone and D Dry blast finishes. Table 3-2 shows in detail the new SPI finish designation and preparation guidelines [126]. Detroit Mold Engineering (DME) have produced examples of polished surfaces with SPI standard finishes to indicate the texture finish achievable with each grade. Figure 3-1 shows the SPI standard finishes produced by DME.

Table 3-2: SPI finish designation and preparation guidelines.

NAME	Finish	Equipment used to obtain the Finish	Approximate Ra(µm)
SPI A-1	Bright, clear, shiny, smooth	Grade #3 Diamond buff	0 to 0.0254
SPI A-2	Semi bright, semi clear, smooth	Grade #6 Diamond buff	0.0254 to 0.0508
SPI A-3	Glossy, scratches	Grade #15 Diamond buff	0.0508 to 0.0762
SPI B-1	Low haze, lines scratches	600 Grit paper	0.0508 to 0.0762
SPI B-2	Hazy, lines, scratches	400 Grit paper	0.1016 to 0.127
SPI B-3	Lines, dull, smooth	320 Grit paper	0.2286 to 0.254
SPI C-1	Low haze, lines scratches	600 Grit stone	0.254 to 0.3048
SPI C-2	Hazy, lines, scratches	400 Grit stone	0.635 to 0.7112
SPI C-3	Lines, dull, semi smooth	300 Grit stone	0.9652 to 1.0668
SPI D-1	Dull, light texture	Dry blast #11 glass bead	0.254 to 0.3048
SPI D-2	Dull, light texture, smooth	Dry blast 240 Oxide grit	0.6604 to 0.8128
SPI D-3	Dull, medium texture	Dry blast #24 Oxide grit	4.826 to 5.842
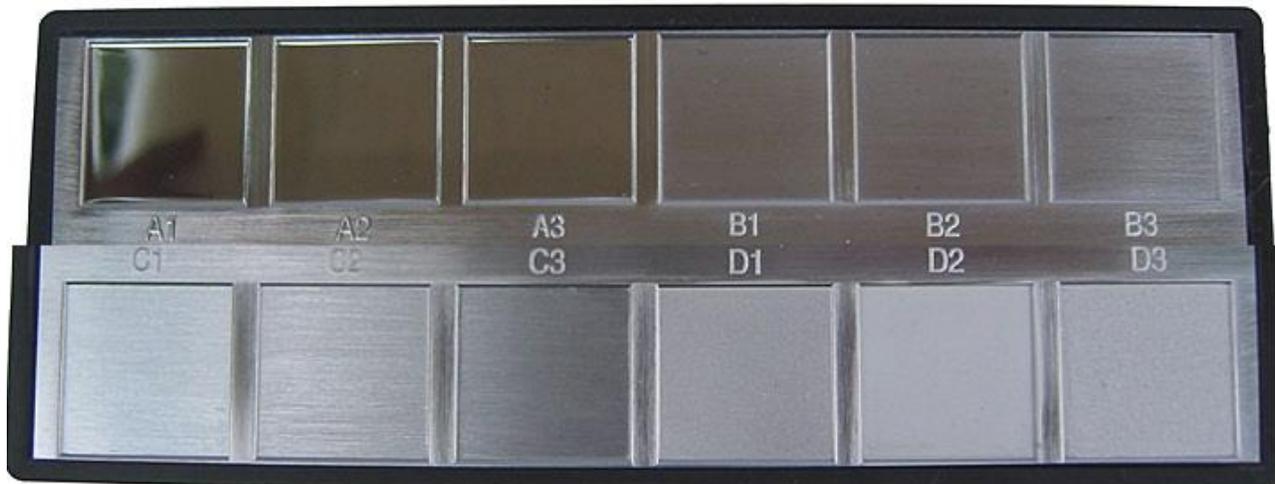
Figure 3-1:   SPI standard finishes [127]

For mould making companies, polishing the mould is a significant bottleneck process. Once the injection mould tool is designed and machined, it goes through a surface finish process where different polishing tools and methods are used to achieve the required surface finish. A better polished plastic injection mould allows manufacturers to produce more plastic parts before the mould needs a rework, and allow a quick and smooth release of the part from the mould cavities [128]. Different polishing methods are used, depending on the type of surface type to be polished and the

roughness required; however, there are some standard polishing methods which are used to pre-polish the moulds: polishing stones, sanding paper, polishing components and hand rotary polishing tools [129].

3.1.1 Sanding Paper

Figure 3-2:   Sandpaper **[130]**

Sandpaper is the name given to a paper or cloth coated with abrasive particles glued on one face (figure 3-4). Sandpapers are used to smooth a surface i.e. "polishing" or to remove a layer of unwanted surface e.g. "old paint". They are used as a tool to work metal and wood components. The abrasive particles (grit) present on the paper vary in size and material. The size of the abrasive particles ranges from P12, a very coarse sandpaper containing abrasive particles with average size of Ø1815 μm, to P2500, a sandpaper containing ultrafine abrasive with an average size of Ø8.4 μm. Grit size is determined by the number of abrasive particles per square inch [131]. Commonly used abrasive materials are: garnet, emery, aluminium oxide, silicon carbide, ceramic and diamond. Abrasive materials are adapted to the material of the polished surface, surface condition and finish requirement. Garnet is used to polish wood, and all other abrasive materials are used on metal. Aluminum oxide displays self-sharpening properties which allow the particles to crumble easily and form new edges and, therefore, to outlast other abrasives, whereas garnet abrasives produce the smoothest surfaces but wear out more rapidly. Silicon carbide is ideal for hard material and rough surface texture [132, 133].

Depending on the surface finish obtained from the pre machining process, the right size of grit paper needs to be chosen to improve the surface finish. Sandpaper can be used wet or dry; usually water is used as a lubricant if needed. Parts to be polished are rubbed against the sandpaper or vice-versa, and the rubbing process is undertaken in one direction at a time, with an equal amount of pressure throughout. Once all scratch marks have disappeared, leaving only the single direction rubbing marks, a finer grit paper is used to continue polishing at 90degrees to the previous polishing direction [132, 134].

3.1.2 Polishing stone

Polishing stones were developed to reach corners, edges and other surfaces where sandpaper are not suitable. Stones are graded and range progressively from P80 grit stone, designed for rough surfaces, to P1200 grit stone, which is the finest abrasive stone. Polishing stones can be used by hand on a profiler or mounted on an ultrasonic machine. Polishing stones are made of different materials, with each material used for a different purpose. Some are used to polish soft materiel (e.g. Aluminium), whereas others are used for harder material (e.g. steel) [125]. Figure 3-3 shows a DS-Aluminum oxide fine grit stone kit which contains five medium soft grit stones which are used for pre-heat treated steel, such as P-20, H-13, S-7, T-420 and SST.
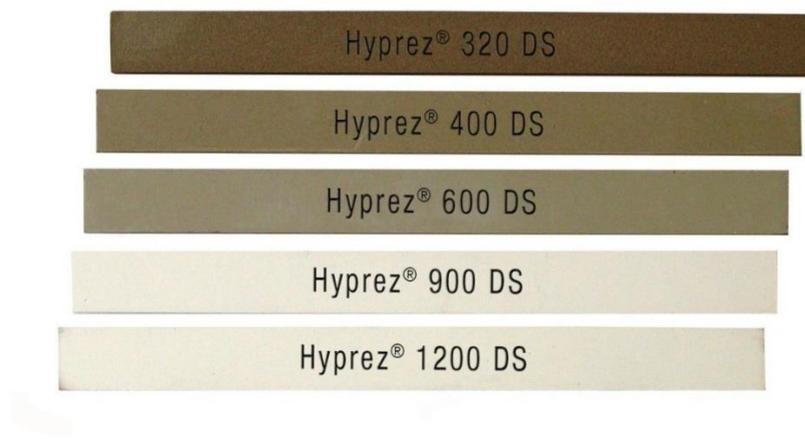
Figure 3-3:   DS-aluminum oxide fine grit stone kit used to break sharp edges and used on rough surfaces [135]

3.1.3   Hand rotary spindle and tools

Hand-held rotary spindles are often used by mould-die toolmakers for a rapid improvement of the surface finish in particular locations. Hand-held rotary spindles are used for manual grinding, smoothing, polishing and deburring a wide range of materials, from aluminium to hard steel. The spindles help to quickly remove the hard layer of EDM deposits for example, and are ideal for polishing difficult areas with complex ribs and corners. They are available in different models, based on the rotating speed of the spindle and the torque range [136]. Figure 3-4 shows a hand rotary spindle from Nakanishi designed to use for manual finishing purposes. There are a wide range of tools available for rapid polishing. The tools are generally designed to perform specific functions, based on surface geometry (internal surface, external surface, edge, etc.) and surface roughness, with tools adapted for rough or smooth surfaces [137].

Figure 3-4: Emax EVOlution hand rotary spindle [138]

3.2 Machining methods

Technological evolution has led to the development of high precision, freeform surfaces, which have the advantages of providing a cost effective solution, improved performance, and simplified system design, in addition to increased field of view and high resolution in optical systems [139]. Manufacturing of high precision complex surfaces is achieved by means of ultra-precision machining processes (UPM), such us ultra-precision milling [140], fast tool servo (FTS) [141], slow tool servo (STS) [142], ultra-precision grinding [143], and fly cutting [144]. These processes can deliver high surface accuracy, surface quality and good process stability by means of controlling machine mechanical characteristics with high frequency response, high positioning accuracy and high rigidity [145, 146]. Machine control characteristics, such as tool path planning [147], machine control algorithms [148], machine error compensation [149] and machine condition monitoring [150], form a major field of research.

A number of machining process are available for generating freeform surfaces; however, FTS is considered to be one of the most cost effective techniques for generating optical surfaces [2]. FTS assisted diamond turning machines are efficient in generating smooth freeform surfaces and microstructures. Figure 3-5 shows a picture of a diamond turning machine integrated with a FTS. The diamond tool is mounted on a tool guide mechanism. The actuator present behind the tool mechanism oscillates the tool tip at high frequencies (i.e. from several hundred hertz to several kilohertz). The tool tip oscillating movement in radial and axial directions at different depths of cut, combined with other machine axis movements, produce the freeform surface.
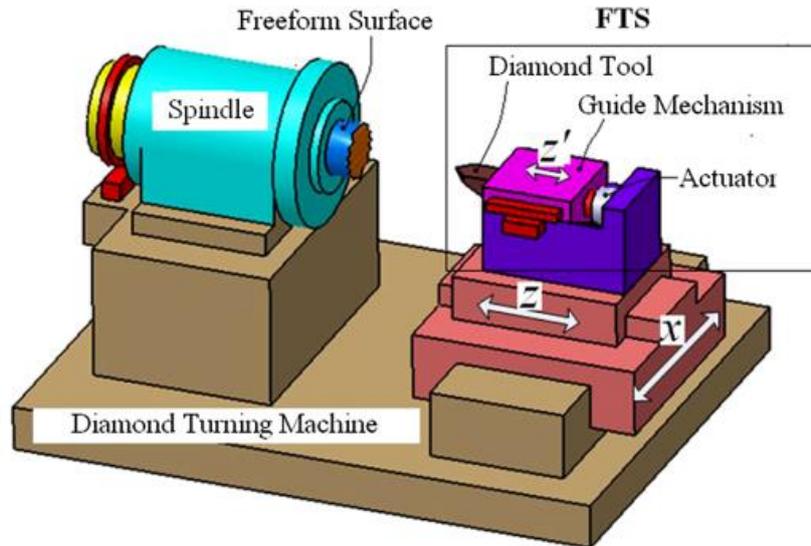
Figure 3-5:   CAD design of a FTS system integrated on a diamond turning machine [141]

Zexiao Li et al. have machined infrared (IR) material (Germanium), considered to be a brittle material, using FTS assisted diamond turning [151]. The design of the surface is a near rotational freeform surface with low rise and fall in the sagittal direction. Machining parameters (such as spindle speed, feed rate, and tool geometry) are optimised to reach the ductile mode of material removal mechanism and to achieve a nanometric range surface finish on a freeform optical surface with low defects. Cost effective mass production of freeform progressive addition lenses (PALs) is achieved using an injection moulding process, with mould tools manufactured in different materials, such as glass [152], copper [153] or aluminium [154]. The surface topography of a glass mould is generated by grinding, followed by polishing processes, whereas the surface topographies of copper and aluminium mould tools are produced by an FTS process. Although research has demonstrated the mass production capability of optical surfaces produced by injection moulding, process control remains extremely difficult, resulting in refractive index variation and geometric deformation. Indeed, the rheological properties of polymers during the moulding process cause distortion and deviation in moulded lenses, and this affects the accuracy of vision correction from prescription. Haihua Feng et al. have used a long stroke fast tool servo (LFTS) to fabricate freeform PALs on CR-39 semi-finished lenses [146]; however the LFTS process cannot be applied for direct lens machining, as it is time-consuming and ill-suited to the mass production environment.

3.3   Magnetorheological finishing

Magnetorheological (MR) is a precision finishing process developed and commercialized by QED Technologies, which is owned by the Cabot Microelectronics Corporation [155]. The magnetorheological finishing (MRF) process is widely used in optics industries, due to its capacity to polish a large variety of brittle materials [156]. The MRF process is capable of polishing a wide range of surface geometries, including flat, concave, convex and freeform. The main elements of the MRF process comprises a carrier wheel, permanent magnet, MRF fluid delivery, filtering pumps and storage system. Slurry is delivered on the carrier wheel by the slurry delivery pump, with the slurry flow forming a ribbon around the carrier wheel. An electromagnet or permanent magnet is placed around the carrier wheel to change the slurry flow regime from Newtonian viscous to visco-plastic.

The workpiece is placed under the carrier wheel, interacting with the MR slurry flow. The slurry is then sucked by the suction pump and delivered into the storage system, where it is stirred, filtered from workpiece debris and temperature controlled. Figure 3-6 shows a schematic illustration of the MRF working principles.
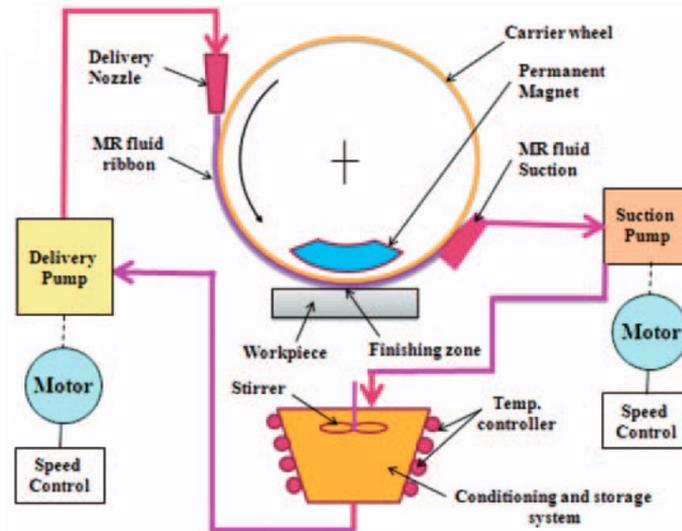
Figure 3-6: Schematic design of MRF working principles **[157]**

The slurry used in a MRF process contains magnetic carbonyl iron particles (CIPs) and non-magnetic abrasive particles (NMAPs). CIPs are used to produce the magnetorheological effect of the slurry and the NMAPs are necessary to produce material removal. The slurry behaves like a visco-plastic fluid with the presences of CIPs. The distribution of magnetic particles in MRF slurry is presented in figure 3-7. In the absence of a magnetic field, the CIPs are evenly distributed in the fluid direction (figure 3-7 (a)). The introduction of a magnetic field attracts the CIPs in the magnetic field direction (figure 3-7 (b)), and the NMAPs are introduced to the slurry as particles which are held in place by the magnetic field chain direction (figure 3-7 (c)) [157].
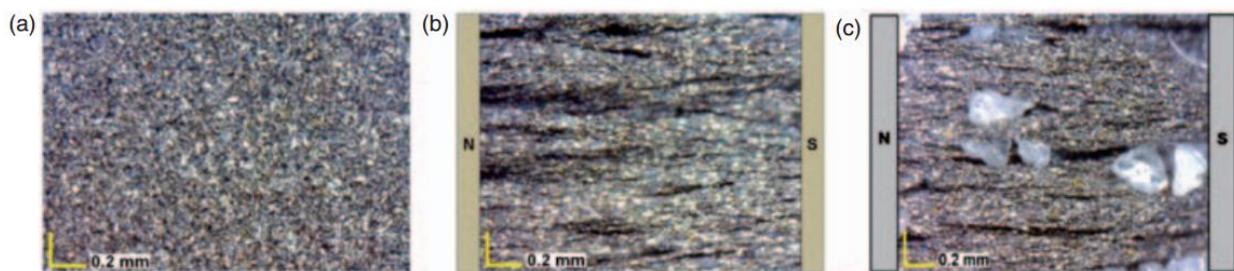
Figure 3-7: Distribution of magnetic particles: without magnetic field (a), with magnetic field (b), with CPIs and NMAPs (c) **[157]**

The yield stress and viscosity of MRF slurry has been studied by Shorey et al. [35], using a Magnetorheometer which they designed and developed. Their results show that the yield stress is proportional to the intensity of the magnetic field and CIPs concentration [158]. The effects on the concentration of CIPs, NMAPs, water and magnetic field on the yield stress and viscosity of MRF fluid has been investigated by Sidpara et al. [36]. and their results show that magnetic field is the

main factor controlling the yield stress and viscosity of the MRF slurry [159]. The effect of viscosity and yield stress on the MRF fluid is reduced after polishing for a period of time, as contamination with the material removed from the workpiece is increased. Sidpara and Jain therefore recommend that the MRF fluid should be periodically conditioned and changed for the finishing process [160].

Sidpara and Jain have used the MRF process to obtain nano finishing on the freeform surface of a prosthetic knee joint implant made of titanium (160 BHN hardness). They achieved a surface roughness varying from 28 nm to 93 nm on prosthetic knee joint implants with initial surface roughness varying from 147 nm to 524 nm [161]. Jacobs et al. have used the MRF process to polish LiF, ZnSe, CaF_2, AMTIR-I, ZnS, MgF_2 sapphire and IR materials. Optimisation of the MRF process parameters and an improved material removal rate, with the use of MRF slurry containing CeO_2, have enabled successful removal of the diamond turning marks and asymmetric grinding errors remaining from the previous machining process [162].

3.4   Bonnet polishing and grolishing process

Bonnet Polishing (BP) is a process developed by Walker et al. and has been implemented in the ultra-precision freeform polishing (UPFP) machines commercialized by Zeeko.Ltd [163]. A UPFP machine has seven axes to perform freeform movement and cover a work volume of up to 300X260X130 mm in X, Y AND Z, respectively (for standard machines). It has three linear axes, X, Y, Z, and four rotary axes, A, B, C and H. Figure 3-8 shows the IRP 200 machine axes' orientation. The first machine was an IRP 200, developed in September 2000 to meet the market requirement for a high precision finish on freeform optical lenses. Indeed, prior to the development of IRP machines, researchers used method such as large full scale tooling [164] or a series of tool setup in an array [165] for producing precision polishing on optical elements. In contrary, the Zeeko polisher has a small tool with respect to the workpiece dimension and standardised tool, which removes the need for tools designed each for a specific type of surface. The success of this concept enabled a breakthrough into other markets, such as health care, with the polishing of prosthetic implants and many other applications. Today, there are, in total, eight different Intelligent Robotic Polisher (IRP) machines on the market (figure 3-9), with the models differentiated mainly by their polishing work volume capability, ranging from IRP 50 for components below Ø50 mm to IRP 1600 designed for polishing mirrors on large telescopes.
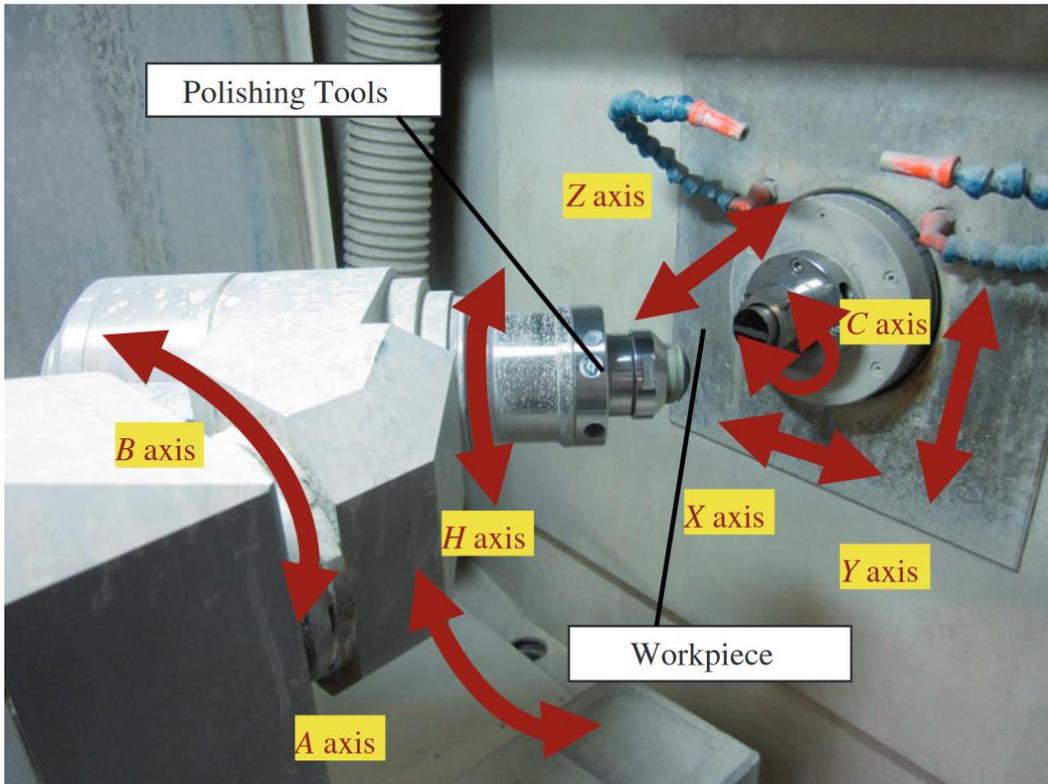
Figure 3-8: IRP 200 machine axes orientation [15]

Figure 3-9: IRP Machines available on market starting from IRP50 to IRP1600 [166]

The initial IRP machines were developed with a bonnet polishing process; however, in order to tackle more complex polishing surfaces and eager to solve other challenging problems, the company has developed other polishing processes and technologies which have been integrated into their initial machine over the course of 10 to 15 years [167]. Nowadays, IRP machines are capable of performing a range of processes: Zeeko-Classic, Zeeko-Grolish (fixed abrasives), Zeeko-Grolish (loose abrasives) and Zeeko-Jet. Technological capacities of the machine include: precession process, dwell time method, tool path generator and edge control.

3.5   Technology integrated within IRP machines

3.5.1   Precession Process

The precession process is a patented technique designed to avoid zero central speed of the rotating polishing tool during the polishing process. The tool remains in an inclined position, instead of a perpendicular position, to ensure that the surface speed never reaches zero [168]. Figure 3-10 shows the expected surface profile of a non-precession process (tool perpendicular to the surface) and precession process. The non-precession process produces a "W" shape removal profile due to the zero velocity in the middle region. On the other hand, the precession process produces repeatedly a near Gaussian shape removal. The Gaussian shape removal is very convenient for calculating and predicting the MRR. Beside its advantages of a Gaussian removal profile and ability to calculate MRR, the precession process produces surface texture with fewer defects than a non-precession process. Figure 3-11 shows the measured surface texture of a non-precession (left) and precession process (right). The non-precession leaves scuff marks on the surface, whereas the precession process produces a more uniform surface.
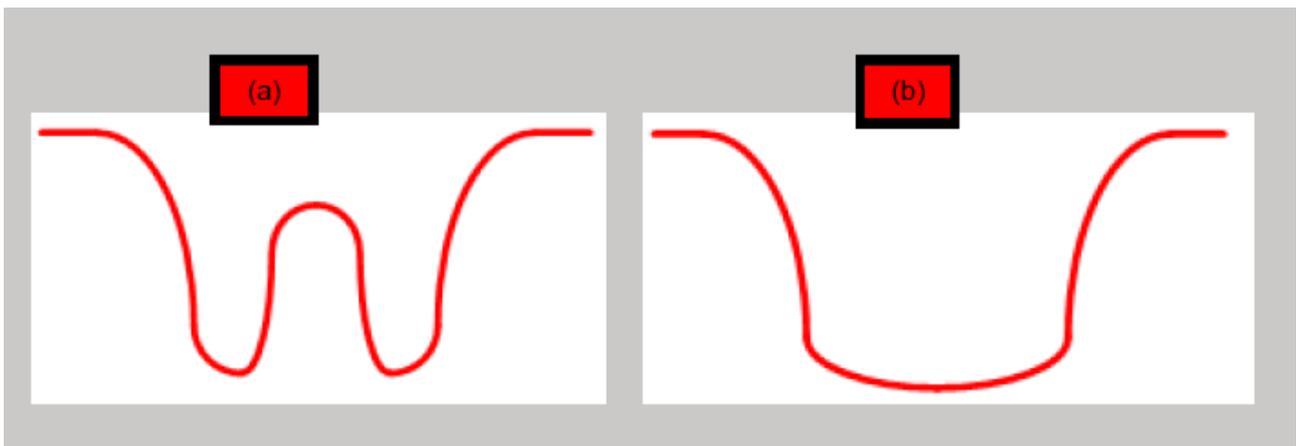
Figure 3-10:   Polishing material removal profile: Non-Precession process (left), Precession process (right) [5]
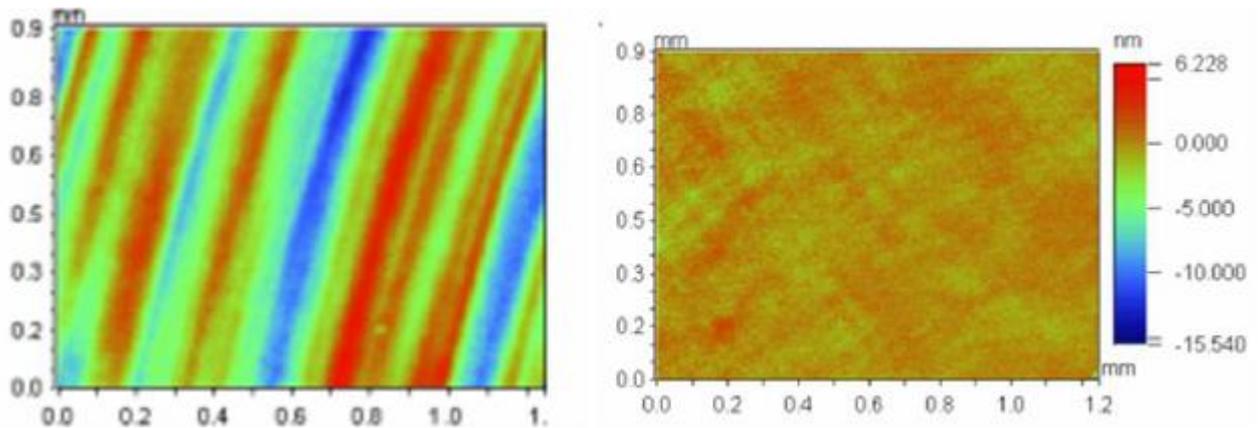
Figure 3-11: Polishing surface texture: Non-Precession process (left), Precession process (right) **[168]**

3.5.2 Dwell time

Dwell time refers to the time in seconds necessary to polish a certain area based on polishing parameters. If the parameter is kept constant and the polishing is performed on a single spot, the material removal rate is directly proportional to the time spent on that spot. Using this method, the material removal rate with a given polishing condition can be predicted. A measured form error can be corrected based on the MRR of the process. The time required to remove the excess material will be calculated by the software and performed on the specific area for obtaining the form correction [169].

3.5.3 Tool path

The polishing machine was initially developed with three types of polishing mode; Raster, Spiral and Random. The raster mode generates parallel linear tool paths, with the distance between each parallel line chosen by the programmer. The spiral mode generates a tool path with a continuous line, circular on a flat surface and spiral on a cylindrical surface. This limits the start-stop of machine movement and produces a continuous, constant feed rate [170]. The random mode generates linear tool paths, not necessarily parallel to each other, and thus ensuring that the whole surface to polish is covered by the movements. The repetitive nature of the polishing process, requiring the movement of the tool on the same path several times, prints the tool path signature on the workpiece surface, causing mid-spacial frequency errors on the surface and, thus, limiting the performance of the polished optical elements [171-173]. To overcome this problem, Dunn et al. developed a pseudo-random mode capable of covering the entire workpiece without crossing the tool path. The spacing between lines can be specified by the programmer and a complete new tool path can be generated for subsequent polishing steps, using an algorithm [174]. Figure 3-12 shows examples of available polishing tool path modes.
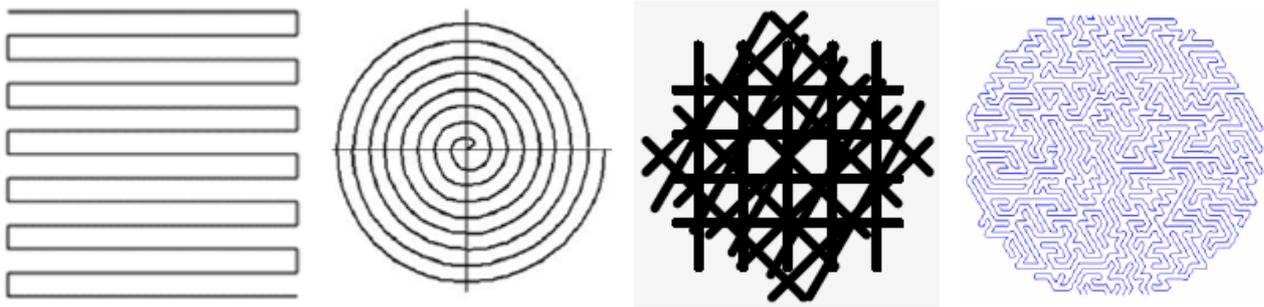
Figure 3-12:   Tool path modes (from left to right): Raster [6], Spiral [6], Random [5], Pseudo random **[174]**

3.5.4   Edge control

Non-deterministic machining processes, such as polishing, tend to roll the edges of the component during the polishing process. Lenses made for large telescopes require shaped edges in order to be able to stich images accurately between two lenses [175]. Li et al. have developed a model which will lift the tool head to ensure that the edge will not be rolled [176]. The model developed is used to produce software capable of automatically programming tool edge lifting. Based on this method, an optical mirror has been successfully polished, while preserving the edge. Further work has been conducted to predict the material removal rate on the edges [177, 178].

3.6   Polishing processes available on IRP machines

3.6.1   Zeeko-Classic

Zeeko-Classic refers to the Bonnet polishing process. The main elements of the BP process consist of a bulged bonnet, polishing cloths and slurries. The machine uses a rotating bulged bonnet as the polishing tool. The bonnet is internally pressurised with air to obtain the required tool rigidity [179] and the polishing cloth is glued to the top of the bonnet. Experiments with different cloth materials and textures, depending on the quality of the surface to polish and the material of workpiece, have been described in the literature. The role of the polishing cloth is to interact with the workpiece to maximise material removal with minimal cloth wear in order to ensure process stability [180]. A rubber inflated bonnet, holding a polishing cloth, interacts with the workpiece on a contact area called the "spot size". A flexible, rotating bonnet moves towards the workpiece, while the contact with the workpiece is detected by a load cell present behind the bonnet. It then moves further in by a predetermined distance (i.e. offset) applying pressure on to the workpiece (figure 3-13). During the polishing process, the spot size, offset and pressure applied on the workpiece remain constant. The re-circulating slurry is emitted through pipes to the contact position between polishing cloth and workpiece. The slurry is a liquid, generally water or other viscous fluid, containing particle sizes varying from several microns to 0.25 micron. The material of the particles varies depending on the surface roughness of the workpiece and its surface condition [181]. The interaction between the tool containing abrasive particles and the workpiece causes material removal by micro-chips on the workpiece. During the polishing process the abrasives present on the slurry are rubbed against the workpiece by the polishing cloth, causing micro-cutting and micro-ploughing on the workpiece surface.
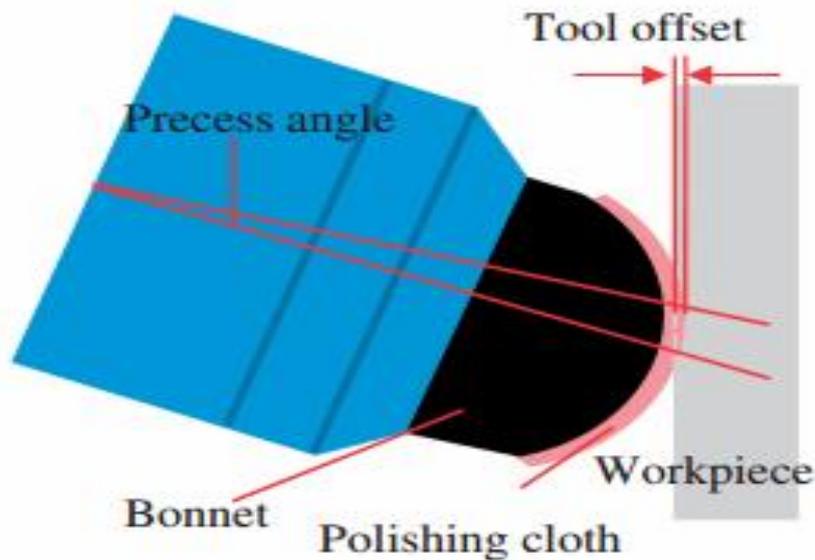
Figure 3-13 :   BP process schematic design [15]

Shengyue et al. [182] have presented results outlining the optimum polishing conditions for obtaining minimum surface roughness for CoCr alloys. The parameters with major influences on polishing surfaces were: head speed, head pressure, precess angle, tool offset, point spacing, track spacing and surface feed. However, investigation of all possible combinations of parameters was found to be time consuming, and the Taguchi method was therefore used to reduce the number of experiments. The four most important parameters selected for Taguchi analysis were found to be precess angle, head speed, tool offset and tool pressure. Precess angle describes the angular degree between the axis of the tool and the perpendicular line of the workpiece table. Head speed describes the rotating speed of the tool in terms of rounds per minute (rpm). Tool offset describes the distance by which the bonnet, once pressurised, is being squeezed when in contact with the workpiece. Tool pressure describes the amount of pressure applied internally to the bonnet. Three levels of experiments were chosen for each parameter, which gave nine possible experiments. Remaining parameters had constant values. The polishing slurry used was a 1 μm paste with a microcloth.

The experiment revealed the optimum values of each parameter: 5 degrees of precess angle; 800 rpm of head speed; 0.15mm of tool offset and 1.5 bar of tool pressure. Additional analysis, based on ANOVA, revealed the contribution to surface roughness (in percentages) of each parameter: tool pressure (48.84%), tool offset (22.68%), head speed (6.26%), and precess angle (4.44%). Using this optimum condition, the surface roughness Sa was improved from 24nm to 7nm. Shengyue et al. also investigated material removal models of the BP process using CoCr alloy. CoCr alloy is a bio-compatible material used in the medical industry to manufacture artificial prostheses. The relative contributions to the MRR of precess angle, head speed, tool offset and tool pressure was investigated. Precess angle was found to have the greatest effect on MRR, with 0.06mm^3/min at 30-degree angle, followed by tool offset, with 0.035mm^3/min at 0.4mm – above 0.4mm, the MRR was reduced due to the distortion of the bonnet; tool pressure, with 0.022mm^3/min at 2 bar; and, finally, head speed, which had the least impact on MRR, with 0.012mm^3/min at 1800rpm [183].

Anthony et al. carried out some work on ceramic material, tungsten carbide (WC), and achieved a surface roughness of 1nm Ra using bonnet polishing. In the optics industry, the development of glass press moulding offers the possibility of producing replicates of high precision lenses at low cost. Tungsten carbide is a material used to make precision injection moulds. Samples of WC are ground before polishing and a surface roughness of 8-9nm Ra is obtained from the grinding process. The samples are then polished for 10 minutes, using a 3µm diamond abrasive suspension, and this produces a surface roughness of 4.07nm Ra. Further polishing for 40 minutes, using 1µm abrasives produces a surface roughness of 2.56nm Ra. The same method is followed, using 0.25µm abrasives, to achieve a surface roughness of 1.6nm Ra. Finally, an optical polishing pitch is used to improve the surface texture to below 1nm Ra [184].

a.   Material removal mechanism

In the BP process, material removal is effected by abrasives in contact with the tool and workpiece. The abrasives used are micro particles of different sizes and with different materials, depending on the characteristics of the surface to polish. Particle size ranges from several microns to less than a micron. Reducing the size of abrasive particles improves the surface roughness and reduces the material removal rate. The material composition of abrasives varies according to the hardness of the surface to polish and the chemical reaction of the surface with the workpiece [185]. Examples of abrasive materials include: cerium oxide, aluminium oxide, silicon carbide, boron carbide, and diamond powder. The abrasives can be mixed with a polishing paste and become paste slurry or with polishing fluid and become fluid slurry.

The abrasive particles suspended in the paste or fluid interact in two different modes when in contact with the workpiece – two-body or three-body abrasion. Two-body abrasion consists of abrasive particles sticking to or penetrating the polishing pad and becoming fixed during the polishing process; material removal is achieved by micro-ploughing or micro-cutting of the surface. Three-body abrasion consists of abrasive particles rolling and sliding freely between the pad and workpiece, and material removal is caused by micro-fatigue and micro-fracture of the polished surface (figure 3-14).
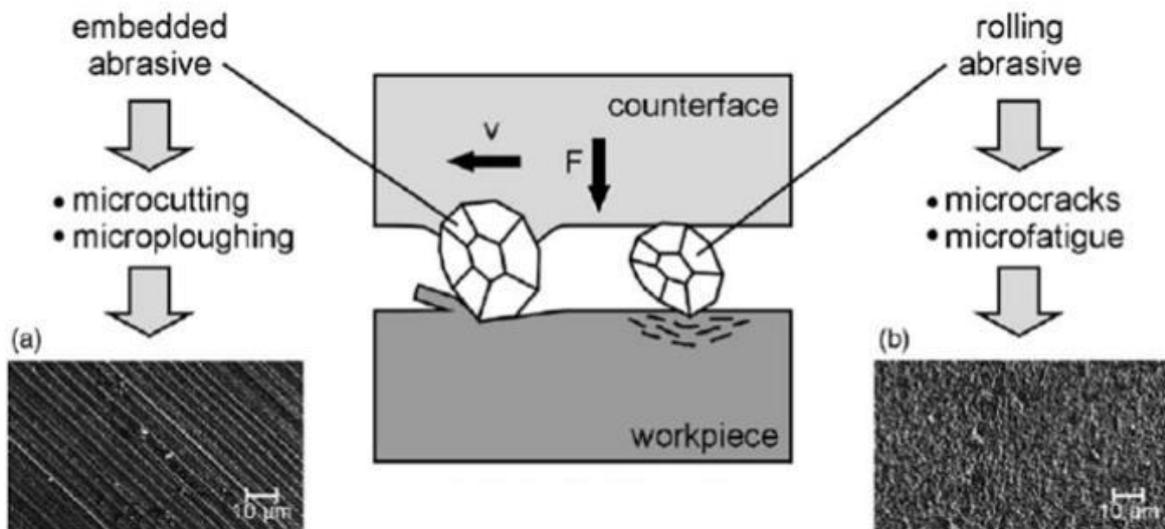
Figure 3-14:   Two-body and Three-body material removal mechanism [186]

b.   *Preston equation*

The Preston equation is one of the basic equations used to determine the MRR in a Bonnet polishing process. As discussed above, the mechanical polishing can be classified as two-body or three-body abrasion with possible additional chemical reactions [186]; however, two-body abrasion with abrasives bonded to the pad is considered to be the most efficient material removal mode. The factors influencing the MRR are: normal load, particle size, abrasive material, material of polishing sample, concentration of abrasives, and bonnet pad properties. The Preston equation is expressed as followed [187]:

$$\frac{dz}{dt} = K_p \times P \times V_r$$

dz refers to the film thickness and *dt* to the polishing time or dwell time. K_p is the Preston coefficient which covers all other factors not directly expressed on the equation. This coefficient needs to be obtained through experiments for each polishing process. *P* is the down force from polishing tool contact with the workpiece. V_r is the relative velocity between the polishing tool and the workpiece. The MRR is a volumetric measure expressed in $\frac{mm^3}{min}$, and is defined as the ratio of film thickness removal over time [188]. Bonnet polishing is a well-researched process which is precise, stable and predictable. It has the ability to reach nanometric range surface roughness, with microns form accuracy through a controlled MRR using the Preston equation as compared with other polishing methods.

3.6.2   Zeeko Grolish (fixed and loose abrasives)

Zeeko grolish is a process developed to reduce the pre-polishing time necessary to bring a machined only finish to a relatively smooth finish with a surface roughness within the hundreds of nanometre range [189]. Pre-polishing removes sub-surface damage, although it is time-consuming and it generates mid-spacial frequency errors on the surface [173]. The grolishing process is designed to reduce the pre-polishing time, by improving the surface roughness and reducing sub-surface damage on the surface. In the fixed abrasives grolishing process, the abrasive particles are bonded to the polishing cloth, whereas, in the loose abrasive grolishing process, a rigid cloth is glued onto the bonnet. Re-circulating slurry or paste containing abrasive particles designed for rough surfaces are used as the polishing medium.

The grolishing process relies largely on the tool performance. Walker et al [190], have developed different types of tool for fixed and loose abrasives and conducted experiments on Zerodur and silicon carbide (figure 3-15). There are three types of tool: hard tool (1 & 2), inflated tool with bonded abrasives (3 to 6 & 8), and inflated tool with loose abrasives (7). Picture nine shows a new bonnet for comparison. The hard tool produces a poor finish, mainly due to the machine structure not being designed for hard contact. Bonded and loose abrasive bonnets produced acceptable results in terms of material removal rate, surface uniformity, and sub-surface damage level. The researchers therefore concluded that these processes can be developed and implemented successfully as an intermediate step between form generation and polishing.

Figure 1 metal-bonded diamond pellets on hard tool

Figure 2 resin-bonded diamond hard ring tool

Figure 3 nickel-bonded diamond pellets on 40mm bonnet

Figure 4 Single metal-bonded diamond pellet on 40mm bonnet

Figure 5 stainless steel washers on 40mm bonnet

Figure 6 brass washers on 40mm bonnet

Figure 7 Polyurethane on 40mm bonnet

Figure 8 3M Trizact ™ on 40mm bonnet

Figure 9 New bonnet with no active surface attached

Figure 3-15: Pictures showing the pad/cloth used for grolishing process experiments performed by Walker et al. [190]

3.6.3 Fluid Jet polishing

Fluid jet polishing (FJP) is a process in which a pressurised slurry containing polishing abrasives is projected through a nozzle towards the area to be polished on the workpiece. The variable parameters of the FJP process are: fluid pressure, abrasive type, abrasive concentration, nozzle diameter, angle of jet projection, and nozzle-workpiece stand-off distance. The fluid jet hits the workpiece directly without the need for physical tool contact. The material removal rate is linearly proportional to the slurry concentration; however, the impact velocity and MRR have non-linear dependency. There are three main reasons for the non-linear relation between impact velocity and MRR. Indeed, at low impact velocity, the minimum velocity required to remove material did not occur. Increases in the delivery velocity increased the particle delivery rate. Finally, there is square relation between velocity and particle delivery energy. The choice of abrasive material, particle size and flow rate are important to obtain a stable MRR and reach a ductile mode of material removal [191].

L. Yang et al. investigated the FJP process and reported that the material removal mechanism operates through a combination of shear and collision force [192]. In order to perform the FJP process on Zeeko IRP machines, the bonnet tool head is replaced with a nozzle. The process is integrated into the machine for polishing surfaces with limited access for the BP process. Figure 3-16 shows a picture of the FJP process performed on a Zeeko IRP 200 to polish a cylinder.

Figure 3-16:   FJP process performed on a IRP 200 [184]

3.7   Polishing consumables

BP is a form of machining process which uses abrasive particles trapped in the porosity of the polishing cloth to remove the unwanted layer of surface material in order to reach the desired smoothness and geometrical accuracy [193]. Although the accuracy of the polishing machine and polishing parameters are important for improving the performance of a process, the key to success is the selection of the appropriate polishing cloth and abrasives [194].

3.7.1   Polishing cloth / pad

Polishing cloths or pads are a wearable product used to drive-in the abrasives and drive-out the swarf from the contact area. They ensure a uniform contact for a controlled material removal process. The surface texture is designed to improve the performance of the pad (i.e. increase MRR and reduce the wear process). Indeed, the texture of the cloth is adapted to the condition of the workpiece surface to facilitate the penetration of abrasives and smooth ejection of swarf, with minimal heat generation in the interaction region between tool and workpiece [195]. In precision polishing, polyurethane pads and polishing cloths made of woven, non-woven and flocked material are used as an abrasive carrier.

Polyurethane pads are generally used to polish optical surfaces. The pads are formed from the solidification of polyurethane plastic, producing a microcellular foam structure on its surface, called

porosity. There are three types of pad available on the market, distinguished mainly by their material composition and hardness of pad. Table 3-3 shows the characteristics of these polishing pads. Research studies show that the pad density is inversely proportional to the porosity of the pad and MRR [196]. McGrath has shown that the polishing process wears out the pad within several hours of use, depending on the polishing condition (of the surface/pad), which dramatically affects the MRR [197]. The wear is mainly caused by the plastic deformation of the pad [198].

Table 3-3:   Characteristics of polyurethane polishing pads

Polyurethane pad type	Shore hardness "D"	Density [g/cm^3]	Thickness [mm]	Filler	Picture
LP57	35	0.48-0.64	0.51	Not filled	
LP66	25	0.35-0.51	0.51	Cerium oxide	
GR35	37	0.56-0.67	0.51	Zirconium oxide	
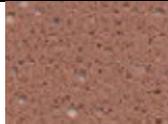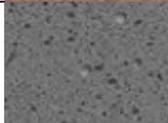
As mentioned earlier, polishing cloths are generally categorised into three groups: woven, non-woven and flocked. Woven cloths are made with fibres of different sizes and materials. The back of the cloth is laminated to ensure that polishing abrasives do not exit through the fibre weaves during the polishing process. Woven cloths are developed for polishing rough surfaces [199]. Non-woven, napless cloths are stiff cloths created with a mixture of short and long fibres obtained from plastic, latex, elastomer, and similar substances. The fibres are bonded together with mechano-chemical treatments. Non-woven cloths are used to polish hard materials and in the finishing phase of light alloys. Flocked cloths are used to obtain a mirror-like finish on metallic materials, and are made of flock of different lengths, density and grade. Polishing cloths manufacturers, such as Buehler or Kemet, advise shortening the polishing time when using flocked cloths in order to avoid possible inclusion pullout [200]. Buehler provide guidance on choice of polishing cloths, based on the surface roughness condition of the sample (figure 3-17).

Coarse

UltraPad™
Hard woven, no nap
6μm & up, Diamond

UltraPol™
Hard woven,
nonaggressive silk cloth
6μm & up, Diamond

Nylon
Oil resistant, medium hard woven,
no nap
6μm & up, Diamond

TexMet™ P
Hard perforated,
non-woven cloth
6μm & up, Diamond

Intermediate

TriDent™
Soft, durable, synthetic woven
cloth, no nap
15 to 0.02μm, Diamond

TexMet C
Non-woven pressed cloth
15 to 0.02μm, Diamond, Al_2O_3,
SiO_2

VelTex
Short napped synthetic velvet cloth
9 to 1μm, Diamond

VerduTex
Durable, medium hard synthetic
silk cloth
9 to 1μm, Diamond

WhiteFelt™
Soft, durable matted wool cloth
6 to 0.02μm, Diamond, Al_2O_3,
SiO_2

PoliCloth
Medium hard, woven wool cloth
6 to 1μm, Diamond

Fine

MicroFloc
Soft, long napped cloth
3 to 0.02μm, Diamond, Al_2O_3, SiO_2

MicroCloth™
Soft, versatile, long napped
synthetic rayon cloth
5 to 0.02μm, Diamond, Al_2O_3,
SiO_2

MasterTex™
Soft synthetic velvet with low nap
1 to 0.05μm, Al_2O_3, SiO_2

ChemoMet™
Soft, porous, chemically resistant,
synthetic cloth
1 to 0.02μm, Al_2O_3, SiO_2

Figure 3-17: Buehler polishing cloth guide, design based on workpiece material, chemical reactions and categorised into surface roughness condition of samples [201]

Polishing pads are also available with embedded abrasive on the surface of the pad. Abrasives, such as silicon carbide or diamond, are bonded on flexible or semi-flexible materials, like paper, cloth, resin or metal, to form the fixed abrasive polishing cloth. Fixed abrasive cloths have the advantage of continuously exposing fresh cutting edges for polishing when the previous one becomes worn away, a process known as self-sharpening (figure 3-18). Fixed abrasives also have the ability to produce uniform polished surfaces with low defects with the use of a new polishing pad; whereas, a worn pad has a concave profile which affects the polishing performance and control of form accuracy [202].

(1) Partially bonded abrasive particle with cutting edge protruding
(2) Fully bond abrasive particle
(3) Bonding material
(4) Rounding of cutting edges (abrasive action on contact with workpiece) of partially bonded particle with some wear of bonding material around the particle
(5) Further wear of bonding material particle rounded particle begins to work loose
(6) Further wear of bonding material creates void
(7) Rounded particle breaks loose
(8) New abrasive particle revealed which was once a fully bonded particle

Figure 3-18:   Fixed abrasive cloth wear process and self-sharpening [5]

3.7.2   Polishing abrasives

Polishing abrasives are the cutting tool of the BP process and are made of both natural and synthetic products. They are generally used as a slurry or a paste (figure 3-19). In the slurry version, water (deionised) is the polishing medium which carries the abrasives, with added agents which modify the density, viscosity, thermal conductivity and other physical properties of the polishing fluid in order to improve the effectiveness of the process [185]. In the paste version, diamond and silicon carbide abrasives are the two most popular polishing pastes. The abrasives are uniformly suspended in a variety of substances, including: fatty acid, stearic acid, lanolin, Vaseline, paraffin wax, glycerine monostearate, iron oxide, and rosin; although the detailed paste composition is usually kept secret by the manufacturer. Only for common slurry, such as alumina slurry, is the detailed composition known [194].

Figure 3-19:   Polishing paste (left) and polishing slurry (right) **[203]**

There are three key factors related to the performance of slurry and paste: grain concentration, grain size and grain material. Grain concentration refers to the volumetric concentration of abrasives present in the paste or slurry; grain size refers to the average size of abrasive particles; grain materials are either soft or hard, depending on the desired MRR [185]. Diamond, silicon carbide, cerium oxide, aluminium oxide and colloidal silica are the most popular polishing abrasives. Diamond abrasives have the additional characteristic of shape of abrasives – monocrystalline or polycrystalline. Monocrystalline diamonds have clean and sharper edges, with fewer cutting facets, whereas polycrystalline diamonds are blocky-shaped, with numerous cutting facets. Polycrystalline diamonds produce higher MRR than monocrystalline, due to their increased number of cutting facets (figure 3-20); however, the latter produce a clean and defect-free finish, making them ideal for final finishing.

Monocrystalline diamonds   Polycrystalline diamonds
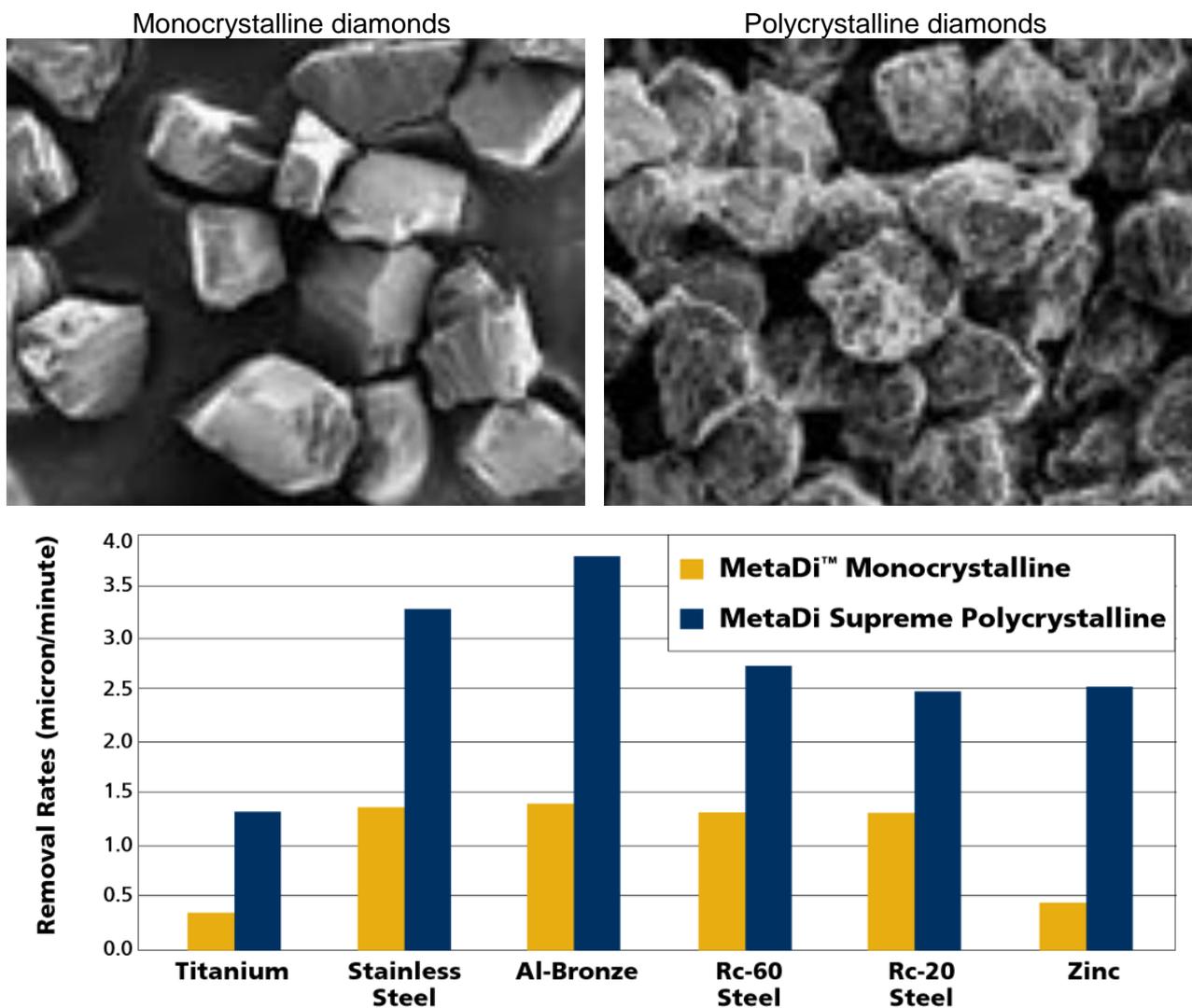
Figure 3-20:   Diamond abrasives shape (top), Diamond abrasives MRR (bottom) **[201]**

3.8   Summary

This chapter reviews the available finishing process capable of achieving a nanometric scale surface finish and microns scale form accuracy. The least expensive and most commonly used is the hand polishing method performed by a highly skilled tool maker. However, the process is unstable, prone

to failure due to human error and the numbers of skilled engineering in this area is rapidly diminishing. The SPI standard delimits twelve levels of surface finish for an injection moulded component, and, in order to reach the required level and obtain the desired surface texture, a range of hand polishing tools are necessary. Hand tools, such as sand paper, polishing stones and hand-held electric spindles are among a range of tools available on the market. Hand tools are available with a range of grit sizes and abrasive materials. Grit size refers to the average size of the abrasives present on the tool, with lower numbers indicating coarse abrasives and higher numbers fine abrasives. Sand papers are ideal for improving surface roughness on large areas; polishing stones are better suited to reaching corners and edges of the workpiece, whereas tools with an electric spindle are used for polishing difficult areas with complex ribs and corners.

Machining methods, such as ultra-precision milling, ultra-precision grinding, fast tool servo, slow tool servo and fly cutting, provide high finish capability with good process stability by means of controlling the mechanical characteristics of the machine. FTS is considered to be the most cost effective solution for optical applications owing to its ability to convert a pre-formed component into a final finished component in a comparatively short time. However, the machining preparation for production and programming remain a time consuming and challenging job, making the process unsuitable for one-off manufacturing projects. MRF processes are largely used to polish brittle material. The presence of CIPs in the slurry transform the slurry flow from Newtonian viscous to visco-plastic regime, helping to grip the NMAPs in the contact region and providing more efficient MRR. The process is relatively expensive, with the disadvantage of being time consuming.

The Bonnet polishing process has been developed to overcome the problems faced in the optics industry with the development of full scale tooling for any new design of optical mirror. The BP process implemented in Zeeko IRP machines has successfully achieved surface finishes in the nanometric range and correction to form error. The machine can also perform the grolishing process and FJP. The grolishing process improves the surface roughness of machined only or ground finishes to a pre-polished stage with less than 100 nm Ra without modifying the form accuracy or printing tool path marks. Moreover, the grolishing process helps to remove machining marks and any other periodic marks which would create mid-spacial frequency errors on the surface. The FJP process can achieve a smooth finish on a surface without the need of a physical tool contact. Optimum parameter conditions for a given material enable the process to reach the ductile mode of the material removal. The process has been successfully used to polish surface curvatures which cannot be polished using contact polishing methods due to tool access restriction.

Zeeko IRP machines have some integrated technology for ensuring a controlled and repeatable polishing process. This includes precession, dwell time, tool path and edge control. The precession process requires the tool to reach the workpiece in an inclined position to avoid zero surface speed and to produce a Gaussian shape material removal function. This helps to predict the MRR, and hence perform form correction accurately. Dwell time refers to the time required to spend on an unwanted layer of material to successfully remove that material layer, and is calculated based on the MRR. Different tool paths are categorised as raster, spiral, random or pseudo-random, and appropriate tool path methods can be applied to maximise the polishing performance. Finally, edge control was developed to meet the requirement of optical mirrors for sharp edges, where ordinary polishing processes would roll the edges due to polishing force. Edge control technology helps to lift the tool vertically upwards while the tool approaches the edge in order to avoid chipping or rolling the edge. Models have been developed to predict the process and, thus, control edge shape.

Polishing pads and cloths are necessary to carry-in the abrasives and carry-out the swarf from the contact area. They are made of wearable material and ensure a predictable material removal

process. Polyurethane pads are made from the solidification of polyurethane plastic which produces porosity during the formation process. The porosity traps the abrasive particles and uses them as a cutting tool to remove material. Tool preparation time using the pad is extremely long and the pad can wear within several hours of use, depending on the polishing condition. Further, the wear affects the removal rate and process stability. On the other hand, polishing cloths, generally made of plastic, latex or elastomer fibres, are available in a woven, non-woven or flocked form. There are a large number of polishing cloths available on the market, and choice of cloth is based on the surface condition and material of the polishing sample. Polishing cloths are available as self-adhesive cloths, making the tool preparation process both easier and quicker.

4 Prototyped Machine design methodology

4.1 Introduction

Design of a new precision machine requires knowledge of the principal of precision machine design. This implies understanding and obtaining accuracy, repeatability and resolution by controlling various factors such as design, errors, budget, timescale, etc. Along with the literature review to identify a gap in research pertaining to inexpensive polishing machine design, further general background study has been completed to identify the best strategy for design of a general precision machine. The design process has largely followed the principles outlined in the seminal publication "Precision Machine Design" by Alexander Slocum [204]. According to Slocum (1992), A good design methodology requires some sequent steps to be followed (figure 4-1). He also said "*There is no room for prejudice in design. One must take what exists, use it to fullest potential and then improve upon it.*" The diagram below shows the basic steps to follow to produce a machine which responds to specific needs. At the same time ensuring nothing is being omitted in the development of this process.

```
Task          Conceptual      Layout        Detail        Design
definition     design         design        design       follow-up
```

Figure 4-1:   Design methodology followed for the development of the polishing machine

This chapter describes the development of a low cost precision polishing machine based on chemical/mechanical polishing process. The functionality and performance of the designed machine is outlined. The chapter then states the requirements of sub-systems of the machine to satisfy the desired performance of the machine. Several conceptual design are discussed to identify the advantages and disadvantages. This is then followed by layout design section where research is conducted to determine the type of product which can fulfil the needs. A detail design section provides in depth information on sub-systems to validate their match with task definitions. Finally, the overall machine assembly is discussed along with its challenges.

4.2 Principle sub-systems task definition

Initially a need was identified for designing and building a new machine to perform a specific function. From the viewpoint of a customer who will be using the new equipment all the necessary functions that the new machine should perform are gathered. From this "task definition", conceptual designs need to be produced. Conceptual designs give an overall view of the machine design and basic sketches which describes the physical structure of the machine and the relationship of components within the machine. It also includes diagrams which explain how the machine functions. Once several conceptual designs are produced one need to be selected to expand in detail through layout design. During this stage the actual size of components is defined. Calculations are undertaken to evaluate the designed machine accuracy and capacity. Rough assembly drawings of the conceptual designs are produced. Based on the rough assembly drawings cost estimation and feasibility studies can be undertaken. From the one rough assembly drawing the detailed drawings can be developed. At this stage some modification to the design can be made to suit cost or accuracy of the new machine.

During the detailed design stage every necessary task is completed to make the design into a product. Finally, in the design follow-up stage the maintenance plans and associated documentations are created.

4.2.1   The Polishing machine

The task definition of the polishing machine can be identified by analysing the literature review in Chapter 2 & 3 and actual products available on market. As identified a precision polishing machine based on bonnet polishing process is needed for small parts such as complex prosthetic knee joints or polymer injection moulds with specific defined surfaces forms where available bonnet polishing heads would not suit due to its large dimensions. The proposed machine should polish hard materials such as glasses as well as softer metallic materials. The cost of such machine be less than £40k. The polishing cycle time should be no greater or more expensive than commercial systems. To achieve these requirements, the newly designed prototype polishing machine should have the following assets:

- Polish parts of up to 50 mm diameter and up to 30 mm thick.
- Polish spherical, aspherical and freeform surfaces with about 5 to 10 degrees max slope.
- Capable of achieving ± 10 μm precision in form accuracy.
- Achieve surface roughness of less than 10nm Sa.
- Polish corners and edges.
- Be able to polish small grooves down to 10mm width (note; not vertical sides)
- Reduce the polishing process time compare to other machines.

In addition to all these tasks expected from this machine the main effort should be put towards keeping the machine cost as low as possible, £40K without compromising on requirements depending on their importance. The design should remove contamination effects between different polishing particle sizes and materials by simplifying the circulation flow and allowing accessibility for cleaning. Moreover, polishing methods needs developing to achieve sub nanometre surface roughness from as rough as ground finish. Thus helping industry to reduce manufacturing cost and time. Finally, the overall machine dimension should be kept as small as possible ($< 2m^3$).

In order to obtain the stated requirements on the designed machine, the equipment sub elements which composed the machine needed to be well chosen. Analysing the above requirements helps to identify four main sub-systems. These are the i) polishing tool ii), multi-axis movements system which allows freeform movement iii) spindle, and iv) overall machine frame. Task definitions for each of these four sub-systems were made. These task definitions then helped to identify the right sub-system elements.

4.2.2   Polishing tools

The polishing tool is the key element that is in contact with the workpiece. It has the role to transmit the rotational movement of the spindle combined with the movement provided by the machine axis system allowing the tool to interact across the whole workpiece surface. Zeeko polishing machines use a spherical pressurised inflated bonnet as a polishing tool. The tool diameter ranges from Ø40

mm to Ø320 mm. In BP processes, pressurised areal contact is used to facilitate the polishing action. To obtain such contact there are two methods; an inflated bonnet pressed on to the surfaces or solid rubber bonnet pressed onto the specimen surface.

In the designed machine the tool will be a combination of three main elements which are solid shaft, a rubber bonnet and the polishing pad adhered to the bonnet surface. The solid shaft will be mounted in the chuck of the spindle and the rubber bonnet will be bonded on to the solid shaft. The bonnet provides the pressurized contact with the workpiece. The bonnet should be stiff enough to not deflect to much due to the force transmitted during polishing. Finally, the polishing pad is bonded to the rubber bonnet. The pad is used to contain the abrasive pastes/fluids and provides the polishing action to the surface. The pad is subject to wear during extended polishing. Therefore, this can be removed and replaced before damage occurs to the rubber bonnet. The design of the bonnet which in contact with the workpiece should be designed according the geometry of the specimen surface geometry. Indeed, the geometry of the bonnet can be adapted to the type of surface to polish to obtained better results. A flat disc bonnet can be used to polish flat surfaces. Spherical geometry bonnet can be used for flat, spherical, aspherical and freeform surfaces. Cylindrical geometry can be used for grooves or side wall polishing. Conical geometry can be used to polish V-grooves.

4.2.3 Multi-axis movement system

A Multi-axis movement system is the element of the machine which will provide displacement within the polishing machine working volume. The precision, accuracy and stability of the multi-axis movement system plays an important role on the polishing process. Indeed, the precision on the axis movement will set the ability of the designed polishing machine to achieve dimensional targets (e.g. 10±0.001 mm). The accuracy of the machine will be obtained through the ability of the multi-axis system to reproduce the same length of movement repeatedly within a given range. Finally, the stability also referred to as stiffness allows a controlled movement without any structural deformation due to the mass of components or the forces polishing encountered.

Furthermore, the machine design has to have at least three linear and two rotary axes to provide possible freeform movements [205]. The travel ranges in each axes should be enough to polish a workpiece within the volumetric range of 50mm^3. The feed rate of axis movement should be similar to currently available precision bonnet polishing machines on market. For example, when polishing cobalt chrome alloy a medical grade alloy, 7nm Sa surface roughness is obtained after conventional BP processes with the optimum parameters, the feed rate chosen is 1500mm/min [206]. Therefore, the developed machine should have similar feed rate capability.

4.2.4 Polishing spindle

To produce a spindle task definition, it is important to understand the role of the spindle within a precision polishing machine and numerate elements which are beneficial and non-beneficial to the machine. The spindle provides axial rotation to the tool in contact with the workpiece. Zeng S, Blunt L, et al. have investigated material removal by bonnet polishing and showed that spindle rotation speed has a linear effect on material removal rate [183]. Existing bonnet polishing processes have maximum spindle rotation speeds of up to 2,000 rpm. This is mainly because polishing is used only

as a final processing step. However, in the presently designed machined it is aimed to pre polish rough surfaces. The material removal rate should be higher when removing material on rough surfaces to gain in productivity. Therefore, the spindle should have starting speed of 500 rpm up to 10,000 rpm. The spindle runout should be as low as possible to obtain high form accuracy. In order to ensure that the friction force does not reduce the rotating speed, the torque produced by the spindle should be higher than the friction force produced by polishing process. Experiments only can provide the friction force, therefore it is important to check the application for which the spindle is designed and ensure the torque produced is enough for the polishing process. Further the spindle should be thermally stable to allow long cycle time polishing and also not affecting the precision by deformation. The spindle weight needs to be low to avoid any deflection. Finally, the spindle dimension should be small to achieve a compact machine design. The spindle needs to have the following features to satisfy all the requirements identified above:

- The rotational speed of the spindle needs to be variable.
- Rotation speed ranging from 500 rpm to 10,000 rpm.
- The torque provided by the spindle should be 50 N or above at any speed.
- The spindle rotation runout needs to be ≤ 1µm precision.
- The spindle should have a low amount of thermal expansion.
- Spindle weight should be as low as possible.
- The overall dimension of the spindle should be small.

4.2.5 Machine structure frame

The machine body will be the element which provides fixtures for each sub-system in the optimum position. It should have a stiff design to avoid vibration and deflection due to the masses of objects fixed on them. The stiffness of the frame should be higher than the force generated by the polishing process to avoid any deformation larger than the precision of the machine. The design should ensure easy access for the following equipment:

- In BP process the polishing pad are changed regularly, therefore easy access to the tool is required.
- The machine aims to polish parts such injection mould tools, which are relatively big and can be heavier than 10 kg.
- The particles of liquid based slurries can contaminate the whole machine if not well protected. The design should ensure that all surfaces inside machine are accessible for cleaning.
- Slurry flow design needs to be done to ensure that abrasives do not stick the machine structure.
- Easy access is needed for maintenance of machine elements.

4.2.6 Slurry system

There are two main type of abrasives used during BP processes, these comprise re-circulating slurry circulation and abrasive paste. In mass production and long cycle polishing the slurry circulating system is used for its quality and consistency. Abrasive particles are mixed with water (deionised) and re-circulated via a pump to the polishing part. The circulation provides consistent polishing and

thermal stability over polishing area. The disadvantages of this process are the time consumption, cost and risk of contamination within particular slurry abrasives regimes. On the other hand, the paste component is used for short cycles and for experimental development stages. The process is very simple and cost effective. There is less chance of abrasive contamination and it is very quick to switch between abrasive sizes. However, there is a high risk of uneven paste distribution on the polishing surface which leads into uneven polishing. Use of paste could also have potential thermal issue if the process is long (dwell time).

Designed machine should run these both type of abrasives polishing. Therefore, to provide slurry circulation system the machine should have a slurry tank. The surrounding parts which may contact the slurry liquid should be designed to allow the flow directed towards outlet direction.

4.2.7   Additional parts

The task definition of the core sub-systems is expressed in the above sections. There will be subsequent parts which are required to assemble the designed machine. These parts will depend on the layout design of the identified sub-systems and the conceptual design of the machine. There are several parts identifiable at an early stage of the design, such as machine base, slurry drainage tray, workpiece holding unit and spindle holding element, multi-axis movement system mounts to machine frame, etc. However, the task definition of these parts can only be expressed once full knowledge is acquired of the conceptual design and core sub-systems. During the design and implementing process of these parts efforts were put in to make parts fit for purpose and cost effective to keep the overall machine cost lower.

4.3   Conceptual and layout design process

4.3.1   Conceptual Design process

The task definition outlined in the previous sections, helped to clarify the view of the requirements expected from each element of the designed machine. However, the assembly of sub-systems and parts have not yet been discussed. There are many possible concept designs to explore and discuss. The BP process can be assimilated to CNC milling process, the interaction will be between the tool and the workpiece. The tool is fixed on the spindle and the workpiece attached to its holding fixture. There are three options at this point. The spindle with the tool could be attached to the machine axis movement system and the workpiece fixed on the machine base or vice versa. Both solutions will have similar results on polishing process unless the mass of these equipment can potentially reduce the precision of the machine. There is an additional solution where the spindle is attached to the linear axis and the workpiece on one of the two rotary axis needed to perform freeform polishing for example. The designed machine aims to polish injection moulds and other metal parts where the mass will be heavy or not easily predictable. Therefore, aiming to attach the workpiece on the axis system might deflect the axis linearity and reduce precision. Consequently, the spindle with the tool needs to be attached to the machine axis system and the workpiece attached to the machine base or in one of the rotary axis depending on the multi axis system chosen for this machine.

The other important element of the conceptual design is the machine axis orientation. Indeed, the axis of the spindle needs to be aligned with the workpiece vertically and/or horizontally. In other words, a vertical machining centre (VMC) or horizontal machining centre (HMC). Each one of these has their own advantages and disadvantages. A horizontally aligned machine allows the chips from a cutting process to fly away from the surface due to gravity. This reduces the surface defects due to chips being dragged on the surface. However, the precision of the axis could be affected due to the mass of the tool, spindle and workpiece hanging on the axis horizontally. On the other hand, the vertically aligned machines will deflect only on the vertical axis due to its mass which can be predicted and compensated. Moreover, the visibility of the manufacturing process and the accessibility of the workpiece are high compared to a horizontal machine centre. Conversely the chips from the cutting process can cause damage to the machined surfaced if the chip are not effectively removed from the surface [207].

In terms of the bonnet polishing process there are vertically and horizontally aligned machines available on market. If the designed machined aims to polish only using a slurry circulation system, then HMC and VMC are suitable. Whereas the designed machine aims to use the slurry circulating system in addition to "dry" polishing using paste and polishing suspensions. In the case of "dry" polishing the machine orientation needs to be vertically aligned to ensure the polishing paste remains in contact with the workpiece during the polishing process.

There are three design possibilities, based on machine task definition and the elements to consider on the conceptual design discussed above. All three are vertically aligned machines. They all contain sub-systems identified by the task definition sections. Sketches of these different possible combinations are presented below. In addition to the known information the allowable machine dimensions are introduced in these sketches. This helps to picture the overall machine dimension and the sub-system dimension.
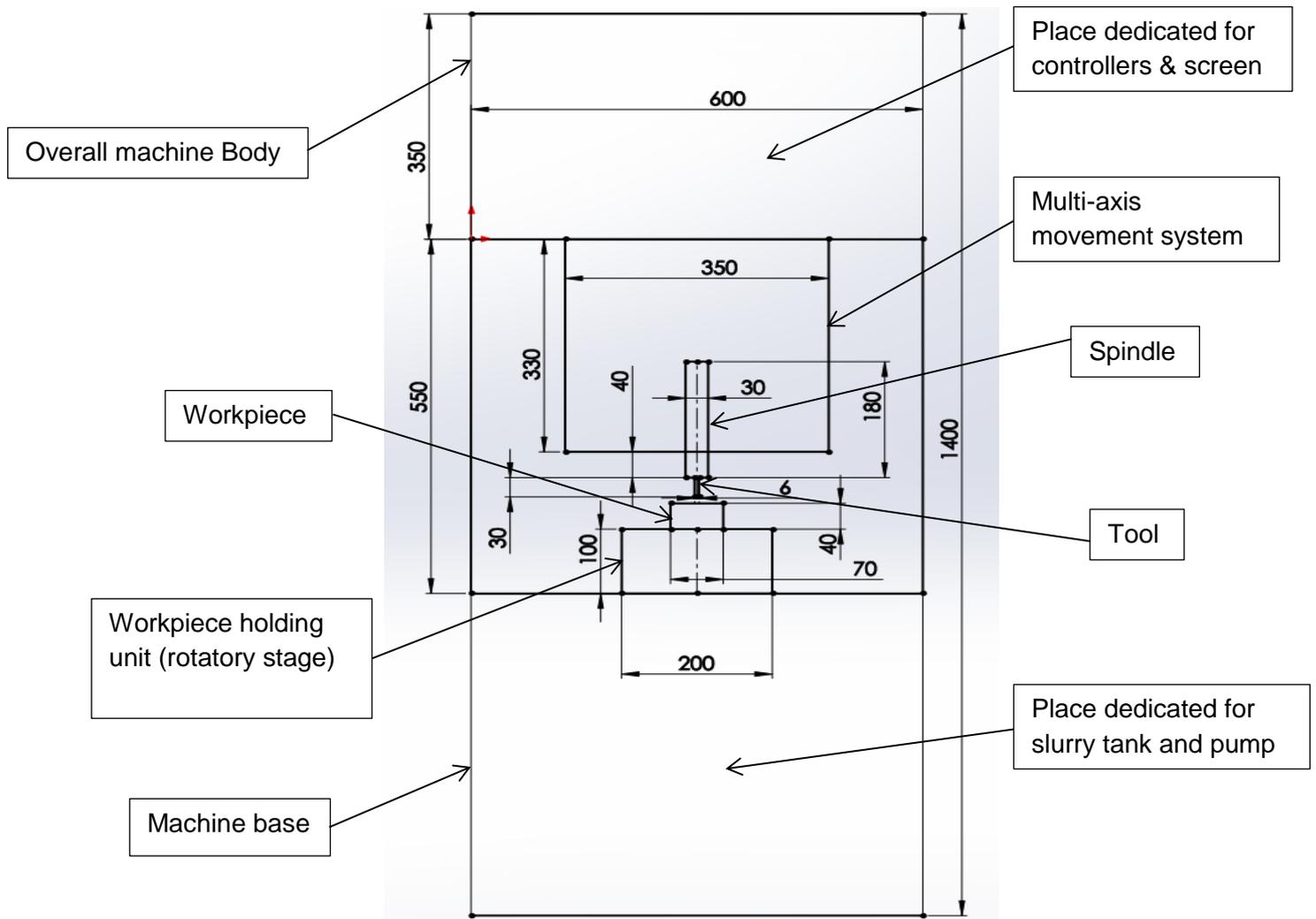
Figure 4-2: Conceptual design 1, with vertical machine alignment containing all sub-systems with their approximate dimensions

Conceptual design 1 (CD1) shows the profile view of one example of polishing machine (figure 4-2). This sketch shows a design setup with the multi-axis movement system holding the spindle. The spindle holds the tool and the end of the tool will be the controlled to perform any pre-programmed movement. The workpiece is held by a rotary stage. The use of a rotary stage would be more appropriate for polishing spherical and cylindrical parts. This would facilitate the program of rotationally symmetric parts. The machine should sit on solid machine base. The space inside the base can be used for implementing slurry tank and the pump. The space above the machine can be used to place the controllers from all sub-systems and screen to monitor them. The overall machine dimensions will be around L1900mm, W600mm and D600mm.
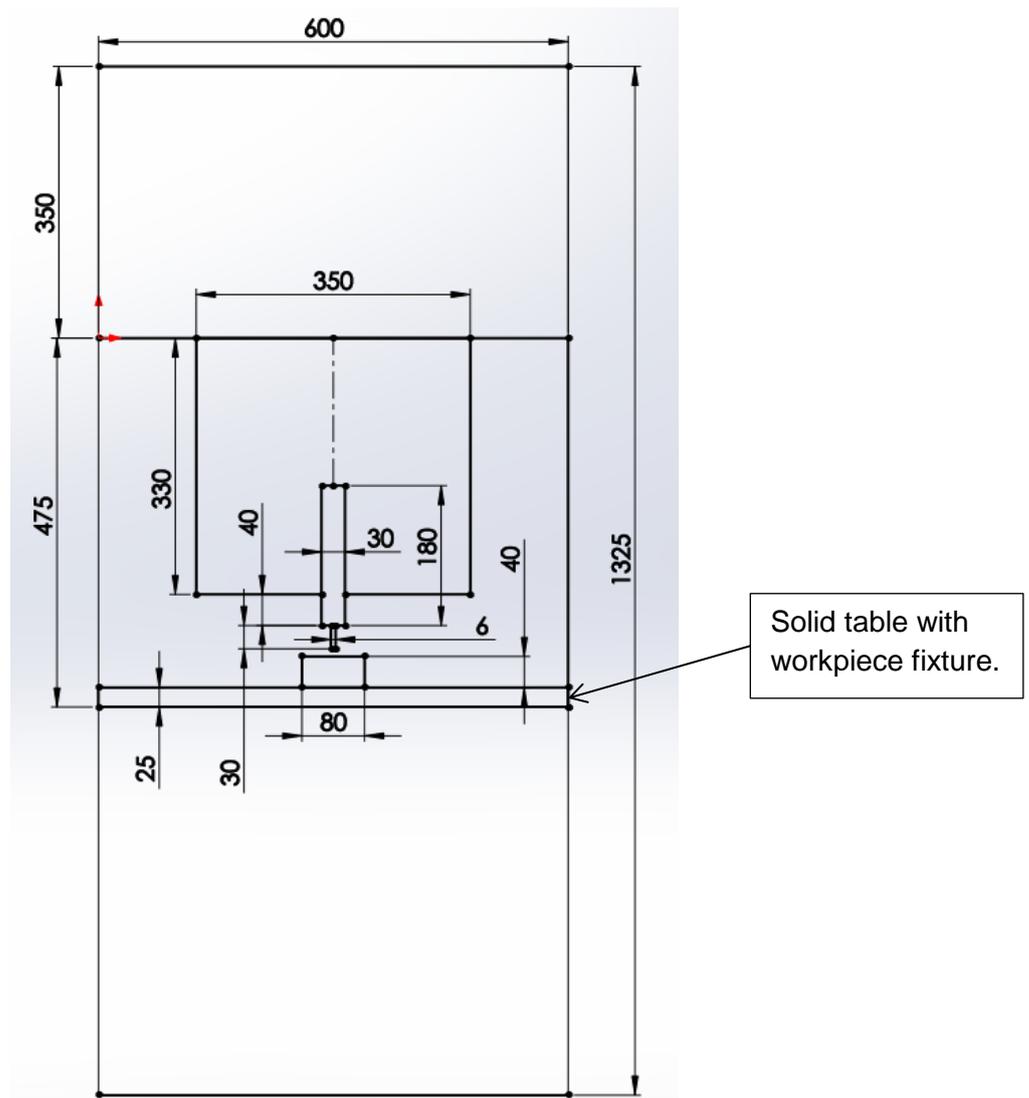
Figure 4-3:   Conceptual design 2, with vertical machine alignment.

The difference between CD1 and CD2 is the workpiece holding table (figure 4-3). Indeed, in this case a fixed table replaces the rotatory stage. The solid table is a cost-effective solution. However, the workspace area is limited to the movement of the multi-axis system. The length of overall machine body dimension change and becomes L1825mm, W600mm and D600.
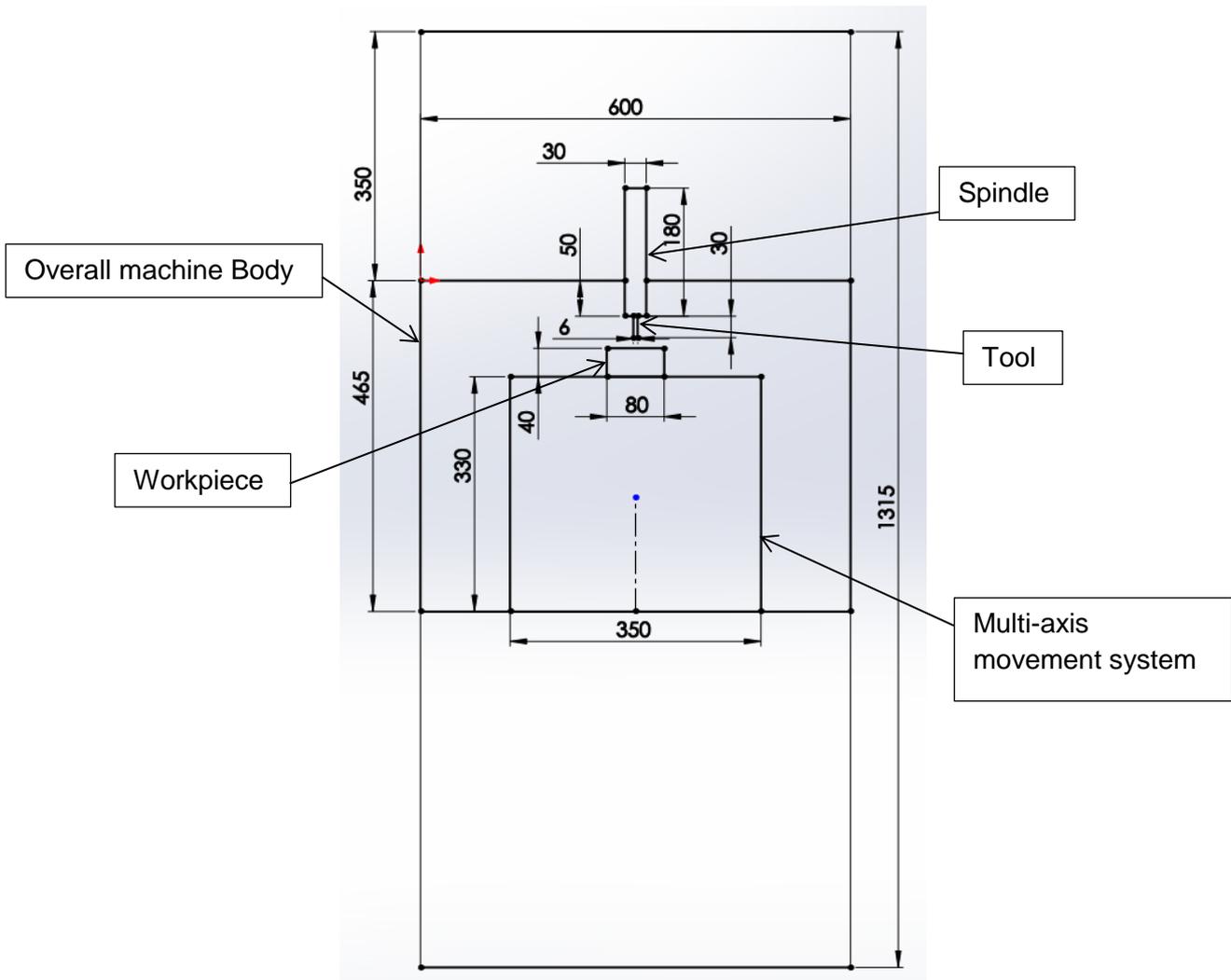
Figure 4-4: Conceptual design 3, with vertical machine alignment. The multi-axis movement system holds the workpiece.

The third conceptual design scenario CD3 is to fix the spindle solidly on the top surface vertically down (figure 4-4). The multi axis movement system is used to hold the workpiece. In contrast to the two-previous scenario the workpiece will move to be polished by the stationary spindle. Most of the mass of the machine is attached to the machine base. The spindle is the only part which is hanging, therefore the is less possibility of deflection in this conceptual design. The overall dimension change slightly and become L1815mm, W600mm and D600.

Conceptual designs were compared to identify the most appropriate design for the polishing machine. CD1 and CD2 are very similar except the rotary stage. The CD3 has a different concept. Although the CD3 would be more precise due to its structure design, as a polishing machine designed to polish heavy parts such as injection mould tool, it might lose precision by carrying heavy

masses. The other problem could be the contamination of multi-axis movement system by the slurry circulation. Therefore, CD3 was considered not suitable for the purpose of the proposed machine.

CD1 and CD2 were both suitable for the design of a polishing machine. For this project simplicity is preferred to validate machine design concept. Therefore, CD2 was selected to expand in detail through layout design and CD1 was kept for further development once CD2 was satisfied. During the layout design process each identified sub-system was fully developed.

Market analysis was conducted for each sub-system to identify existing products which match the sub-system required criteria. If the required product is not available on market it will be designed and manufactured.

4.3.2   Multi-axis movement system Layout design

The layout design was carried out initially on a multi-axis movement device as it is the main sub-system element of the machine. To polish defined geometry surfaces a minimum of five axes is required. Three translational and two rotational axes would enable freeform movement for example. Serial kinematic systems and parallel kinematic systems are the two ways to obtain freeform movement available on market. Serial kinematics are used on manufacturing and measurement systems. The parallel kinematics are used on flight simulation, telescope mirrors alignment and other applications where heavy loads need to be handled with high precision.

Serial kinematic stages systems have errors which affect the precision of the machine. There are two main categories of error affecting the positioning accuracy of machine, which are systematic and random error [208]. Systematic errors can be predicted and compensated whereas random errors are dependent on an external error source. In serial kinematic set ups the axes are stacked together. This creates an unbalanced mass distribution. Some axes carry more weight than others. The runout and tilt errors are accumulated over the number of axes which reduces the machine precision. The cable connection of each axis causes friction with the surrounding parts which affects the reliability and the repeatability of the system [209].

The parallel kinematic stage is designed to be stiffer than serial kinematic stages. Parallel kinematic systems (such as a hexapod) are different from serial kinematic in their structure with six struts moving simultaneously to move from one position to another. The actuators on struts are actuated simultaneously. The way the actuators are arranged optimizes the structural stiffness of for example a hexapod design [210]. A hexapod design allows movement in three translational and three rotational axes. This structure enables high stiffness and compact design to be embedded in the system. It provides relatively small incremental motion which is repeatable. It has the capacity to move a load from one position to another with micron precision. The positioning error is not accumulated. The cables are not moving which increases the reliability and repeatability of the system. The downside of the hexapod design is that the workspace volume is limited to the size of the struts and their relative distance between each other.

Market analysis shows that five axis stacked serial kinematic stages are (not embedded into a machine system) are commercially available as an OEM product which can be utilised by the designed machine. To obtain a serial kinematic stage, the axes needs to be purchased individually and assembled manually within the design. Once assembled a controller is required allow programming of axes movements. On the other hand, parallel kinematic systems such as the

hexapod design are commercialised as a single unit with the associated controllers. Although they have restricted workspace access, a hexapod with the work range required for the present machine can be identified. Therefore, further market analysis was conducted to identify the right model of the hexapod for the designed machine.

Three models appear to be close to the requirements in terms of travel range, velocity, overall hexapod dimensions, minimum incremental motion, load capacity and rigidity. The final decision was made based on overall quality and cost of the hexapod. All three hexapods were sold with their controllers. The Table 4-1 below shows their level of compatibility with the task definition of multi axis movement system. High compatibility are presented with a (+) sign, acceptable compatibility will be presented with (o) sign and non-acceptable\ compatibility will have (-) sign. The technical data of these three models can be found on Appendix 4-1.

Table 4-1:   Hexapod model compatibility comparison

	HXP100-MECA(Newport)	BREVA (Symetrie)	H-840.D2 (Physik Instrumente)
Travel range	-	+	+
Velocity	-	o	+
Overall hexapod dimensions	+	o	+
Minimum incremental motion	+	+	o
Load capacity	o	+	+
Controller	o	o	+
Cost	+	-	+

a   HXE100-MECA hexapod from Newport

Newport has a hexapod model which matches the requirements [211]. The model HXP100-MECA had interesting price and overall dimensions (figure 4-5). The quoted price was £23,769. Although this model had the price corresponding to the budget, other criteria had medium or poor compatibility. Indeed, the travel range and velocity were a lot lower than the requirements.

Figure 4-5:   HXE100-MECA hexapod from Newport [211]

One the other hand, the Symetrie's hexapod models called BREVA is either highly or medium compatible except the cost [212]. BREVA have a very good travel range, high load capacity and good rigidity (figure 4-6). The overall dimensions were twice those desired and the price was too expensive. The cost of a BREVA with its controller was £41,500, which was a lot higher than the budget.

SYMETRIE_BREVA Hexapod with C axis top

Figure 4-6:   Hexapod BREVA from Symetrie [212]

c   *Hexapod H-840.D12 from PhysikInstrument*

A hexapod model H-840.D2 from PI (Physik Instrument) [213] has high compatibility with the requirements identified on the Table 4-1. All the requirements are highly compatible with this model except the minimum incremental motion which has a medium compatibility. This model is the only model which has higher compatibility with the controller. The cost of the hexapod with its controller is just below £25,000 which is within the budget. Therefore, H-840.D12 present on figure 4-7 is chosen for detailed review before the purchase.

H-840 6-Axis Hexapod
High Velocity, Medium Load, Affordable

- Load capacity to 30 kg
- Travel ranges to 100 mm / 60°
- Actuator resolution to 16 nm
- Repeatability to ±0.4 µm
- MTBF 20,000 h
- Velocity to 50 mm/s
- Works in any orientation
- Rapid response
- Sophisticated controller using vector algorithms, virtual pivot point
- Extensive software support

Figure 4-7: Hexapod H-840.D12 from PhysikInstrument [213]

4.3.3 Spindle Layout design

There is no specifically designed spindle for CNC polishing operations available on the market. However, there are spindles which match the requirements for a polishing process (see table 4-2). The conceptual design identifies the location, allowed dimensions and weight of the spindle. Based on this available information, market analysis was conducted to find the appropriate spindle for the machine. Electric spindles, pneumatic spindles and air bearing electric driven spindles are the three types of spindles available on market which fit the requirements mentioned above, however they need to be further studied for matches with other requirements. An image of the spindle models chosen for the following analysis are shown in table 4-2. Electric spindles are designed for manual and hand operations. Pneumatic spindles are designed for high speed machining. Air bearing electric driven spindles are designed for CNC turning, milling and drilling operations. The table 4-3 below offers a more detailed review of these three types of spindles based on our requirements.

Table 4-2: Spindle Models

Electric Spindle	Pneumatic Spindle	Air bearing electric spindle

Table 4-3: Comparison of spindle specification

	Electric Spindle	Pneumatic Spindle	Air bearing electric spindle
Speed range	From 1,000rpm to 40,000rpm	From 5,000rpm to 160,000rpm	From 500rpm to 80,000rpm
Rotating speed control	The desired speed is controlled via a manual controller.	These spindles are designed to run at one single speed. However, in some models the air flow can be controlled which can vary the rotating speed. This method does not allow an accurate control of the rotating speed.	The electric signal to run these spindles is sent through a controller which can be programmed. Desired rotating speed is obtained within the spindle working range.
Runout	Not provided	Less than 1 μm runout error can be obtained.	Less than 1μm runout error can be obtained.
Torque	Maximum torque of 4.8 Cn.m is delivered.	Maximum torque of 5 Cn.m is delivered.	Maximum torque of 35 Cn.m is delivered.
Thermal expansion	These spindles are not designed for long cycles or precision operations. Therefore, on long cycles thermal expansion could be an issue which affects the precision.	Thermal expansion is negligible in these spindles.	Even though the motor is electric, air is used as the bearing medium and spindle cooling solution. Therefore, the spindle is thermally stable.

The table above clearly shows that the air bearing electric driven spindle is the most suitable for the requirements identified via the task definition. Indeed, it covers the speed range required for polishing. The controller allows the control of the rotating speed. The air bearing provides runout error to be less than 1 μm and allows the air to flow around the motor which controls thermal expansion of the spindle. The torque produced by the spindle are far more than needed for the polishing processes. Therefore, further research was carried out on this category of spindle.

4.3.4 Polishing tool Layout design

Polishing tool is the part which will be in contact with the workpiece. Depending on the type of surface to polish the tool design can be adapted. The polishing tool is composed of three parts: shaft/shank, flexible bonnet and polishing pad.

The Shank was designed to be a solid rod attached to the chuck of the spindle. The diameter of the shank can range from 1 to 6 mm in diameter. Smaller diameter of the shank was aimed for use in narrow workpiece zones. The end of the shank was designed to accommodate the flexible bonnet.

The flexible bonnet was glued to the end of the shank. The flexibility of the bonnet created a pressurized areal contact. The stiffness of the bonnet will define the pressure applied to the surface. The tool offset is related to the contact area. (See section on offset measure for more details on the effect of the offset.)

In use, a polishing pad is glued on top of the bonnet. The material of the pad used for polishing varies from the material of the workpiece surface and the surface quality priory to the polishing process. The polishing pad also called polishing cloth holds the paste or slurry abrasives against the workpiece surface. The pad is expected to wear due to the force generated in the interaction with the workpiece. For BP processes the pads are either dressed or replaced with new one if it shows sign of wear. To simplify the pad changing process the skank was made of two pieces which were screwed together. This method helped to save time in pad changing process.

Industrial BP machines such as the Zeeko IRP 200 uses an inflated spherical rubber bonnet with the pad glued on top for polishing. However, inflated bonnets can only be used from 20 mm diameter tools. If a smaller tool is needed, then a solid spherical rubber is used to replace the inflated bonnet. Based on this principle the same spherical bonnet will be used to polish flat, spherical and freeform surfaces. Nevertheless, spherical design of the bonnet is not suitable for polishing internal grooves or side walls. Therefore, different type of bonnets need development in future depending on the type of surface to polish.

4.3.5 Machine frame layout design

The machine frame has the purpose of holding in position all sub-systems according to the conceptual design. At the same time, it must ensure that all criteria expressed on the task definition section are fulfilled. To hold the hexapod, spindle and tool in place aluminium extrusion frame was chosen as a proof of concept design. Aluminium extrusions are easy to cut and assemble to the shape required for the prototype design. They are inexpensive and allow easy access for workpiece, cleaning, tool changing and maintenance as required in the task definition.

The aluminium extrusion frames are available with different profile shapes and dimensions. Each are designed for certain types of application. In the present case the frame was aimed to position the hexapod and the spindle vertically downwards. To obtain a stiffer structure a model designed for factory equipment is chosen. It is a 40 x 40 mm square cross section with the following profile (figure 4-8 left), which has a weight of 2.47 kg/m. The dimensioning detail of the cross section is not provided by the manufacturer. This profile of the cross section is modelled on Solidworks based on the profile sketch and measured dimensions to extruded over 1-meter length (figure 4-8 right). The inner radiuses of cross section are altered to match the weight information provided but he manufacturer. The aim was to verify the validity of the profile using available weight information for further Finite element analysis (FEA) analysis in the detailed design section. The obtained results showed a good correlation between the model and the real weight with the weight of the model being 2.473 kg/m.
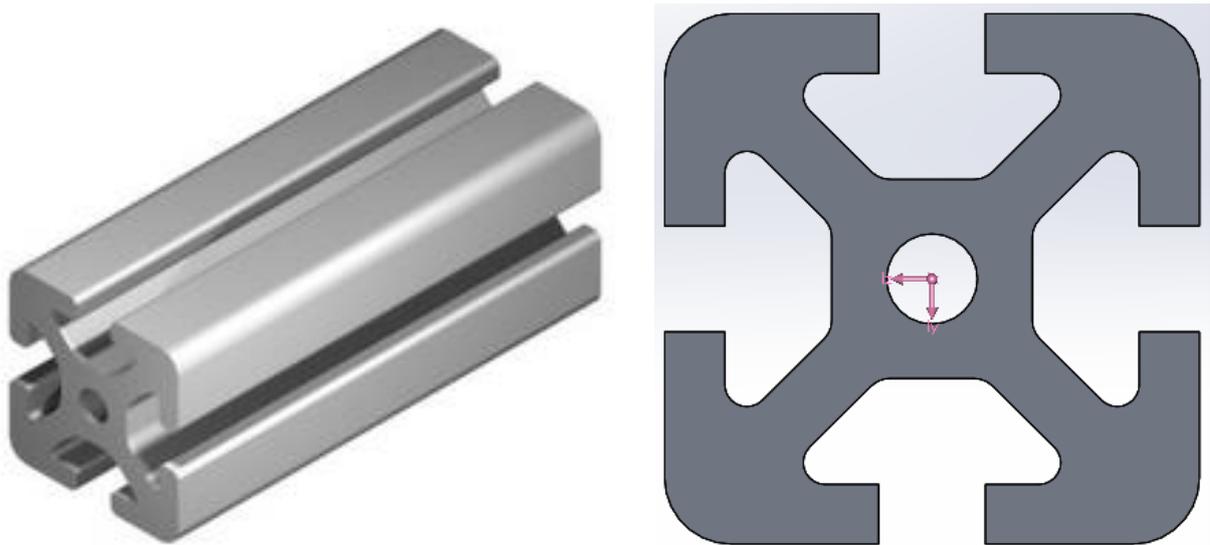
Figure 4-8: Aluminium extrusion profile picture (left) [214], and CAD designed aluminium extrusion (right)

4.3.6 Slurry pump layout design

The slurry tank was not a commercialised product which could be purchased, hence it needed to be designed and manufactured. The purpose of the slurry pump system was to continually mix the abrasives with the polishing fluid and deliver it towards the contact area through a pump.

There are three main parts required to develop the slurry pump system. These are the container tank, pump and an abrasive mixer. To begin, the necessary capacity of the tank was decided. There should be enough fluid in the tank to obtain the slurry circulation cycle between the polishing surface and the tank. At the same time a larger capacity tank than necessary will increase the process cost dramatically. In polishing using slurry the abrasives such as cerium oxide used for polishing glass is expensive. The concentration of these abrasives in the polishing fluid has an impact on the polishing time and the surface finish [215]. A bigger tank would use more abrasive than a smaller tank. Based on the distance separating the slurry tank and the workpiece, a tank with 5 litres capacity is chosen for development. The container needs to be cylindrical to ensure that abrasives are circulating without stagnating at any corners. For a cost effective prototype, a stainless steel 6 litres capacity container was purchased. In terms of the pump, an industrial pump used for coolant circulation in CNC operation was identified and purchased.

4.4 Detailed design and analysis

4.4.1 Hexapod H-840.D12 detail design

The Hexapod, the most expensive sub-system of the polishing machine, provides precision movement to the polishing head. The precision finish achievable by the polishing machine depends mainly on the precision of the Hexapod. All the criteria used to select the most appropriate model of

hexapod have a direct impact on the precision of the final polishing machine. It was therefore important to review all requirements to ensure that the chosen hexapod matched the criteria.

a   Travel range

The travel range of the hexapod is its movement capability in each axis, and this defines the work volume. The chosen model has a travel range of ±50 mm in the X and Y axes and ±25 mm in Z axis. It can rotate ±15 degrees around the X and Y axes and rotates ±30 degrees around Z axis. For this hexapod, the maximum travel range specified per axis can only be achieved if other axes are at zero position. It is important to check the availability of workspace on polishing conditions. PI offers hexapod simulation software which allows the prediction of workspace availability under a given condition. Initially, all axes are at zero position, and the available workspace can be seen in figure 4-9. The left and right images show the same work volume in different axis orientations. In Z axis, the travel range is 50 mm in the middle, but, moving away from the middle, in the X and Y axes, the Z range reduces gradually to reach a value close to zero towards the extreme limits of the X and Y axes.
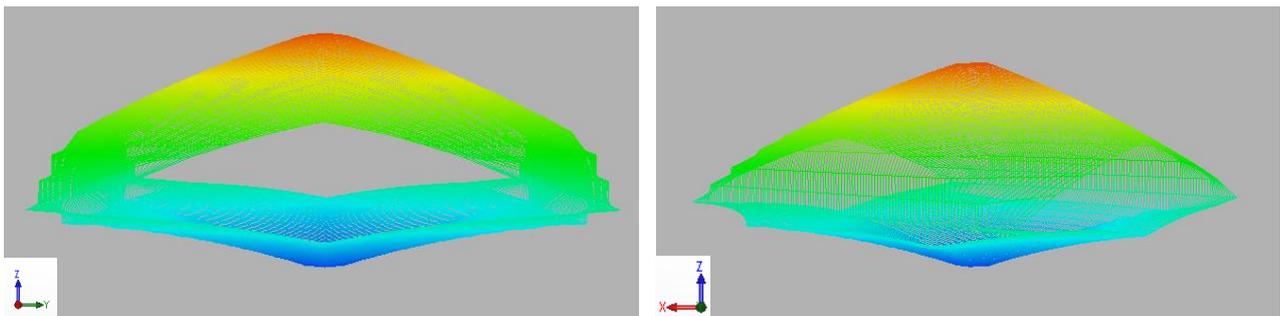
Figure 4-9:   Grid lines showing available hexapod workspace volume; in YZ axis (left) and XZ axis (right). Overall: X, Y 100mm and Z 50mm (Colours used only for visual aspect of work volume purposes).
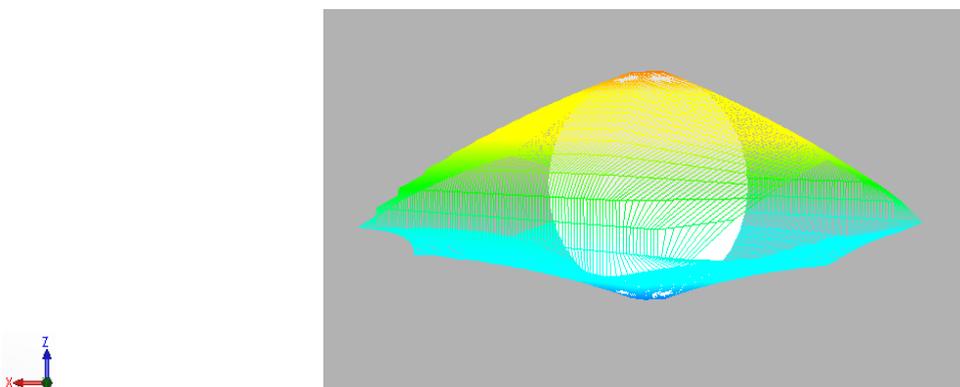
Figure 4-10:   50mm diameter sphere size sample can be reached with available workspace volume.

Figure 4-10 shows a sphere of 50mm diameter inside the available workspace area. Any position within micron precision within the workspace area can be reached. However, the literature review

on bonnet polishing shows that an angle to the bonnet provides a Gaussian shape material removal function. This allows the prediction of the material removal rate using Gaussian function for form error correction [169]. Shengyue et al. have polished CoCr material and achieved a surface roughness of 7 nm Sa from 24 nm Sa, with an angle given to the tool of 5° [206]. A rotation of 5° is given around the X axis for the present design and the results show that only a sphere of 18 mm radius can be reached, as movement range on the Z axis is reduced (figure 4-11). However, if the workpiece has a lower depth in Z, such as a thin plate with a low slope, then the machine can polish a workpiece of size X65 mm, Y65 mm and Z5 mm (figure 4-12). Further increasing the angle reduces the workspace volume.
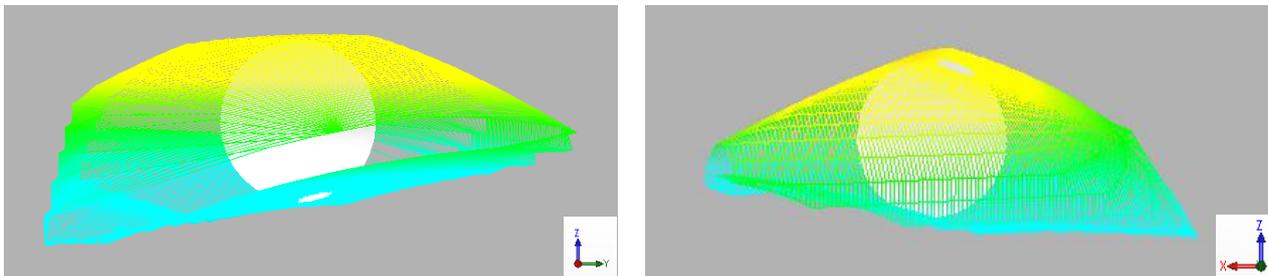
Figure 4-11:   Workspace available with 5° angle on hexapod. Workspace volume of X, Y 84 mm and Z 20 mm, 18 mm diameter sphere sample can be reached inside.
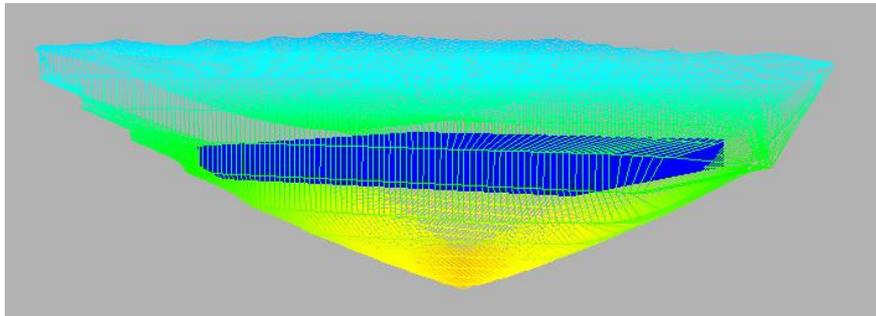
Figure 4-12:   Square plate of 65 mm^2 with 5 mm thickness can be reached inside the workspace volume of X, Y 84 mm and Z 20 mm.

b   Velocity

Velocity indicates the feed rate of the polishing machine. In the polishing process, the dwell time and feed rate have a direct relation – calculation of the material removal mechanism is based on dwell time, which is then converted into feed rate for form correction. The feed rate determines the amount of time the tool spends at each positioning coordinate. Slow feed rates generate heat in the polishing environment and, thus, affect the polished surface quality. The feed rate also has an influence on the depth of the removal profile [216]. Shengyue et al. used a feed rate between 600 mm/min to 1,000 mm/min with the Zeeko IRP200 polishing machine to investigate material removal and optimise parameters for surface roughness improvement [217]. Feed rate has therefore an important influence on the surface finish that can be achieved. Therefore, similar feed rates to those used by Shengyue et al. will need to be performed by the designed polishing machine. There are two models of Hexapod in the H-840 range from PI: The G models have a maximum velocity of 150 mm/min,

with minimum incremental motion of 1 µm and maximum load capacity of 30 kg; D models have maximum velocity of 3,000 mm/min, with minimum incremental motion of 3 µm and a maximum load capacity of 10 kg. H-840. D models cover the feed rate which is required for polishing, with acceptable load capacity and minimum incremental motion; hence it was the D model that was chosen.

c   Overall hexapod dimensions

In the conceptual design, the dimension allowed for the multi-axis movement device is around 300 mm^3. This specification is intended to design a rigid/compact polishing machine. The H-840.D2 has a diameter of 348 mm and 328 mm height, which is relatively close to the requirements. The figure 4-13 below shows the technical drawing of the hexapod.
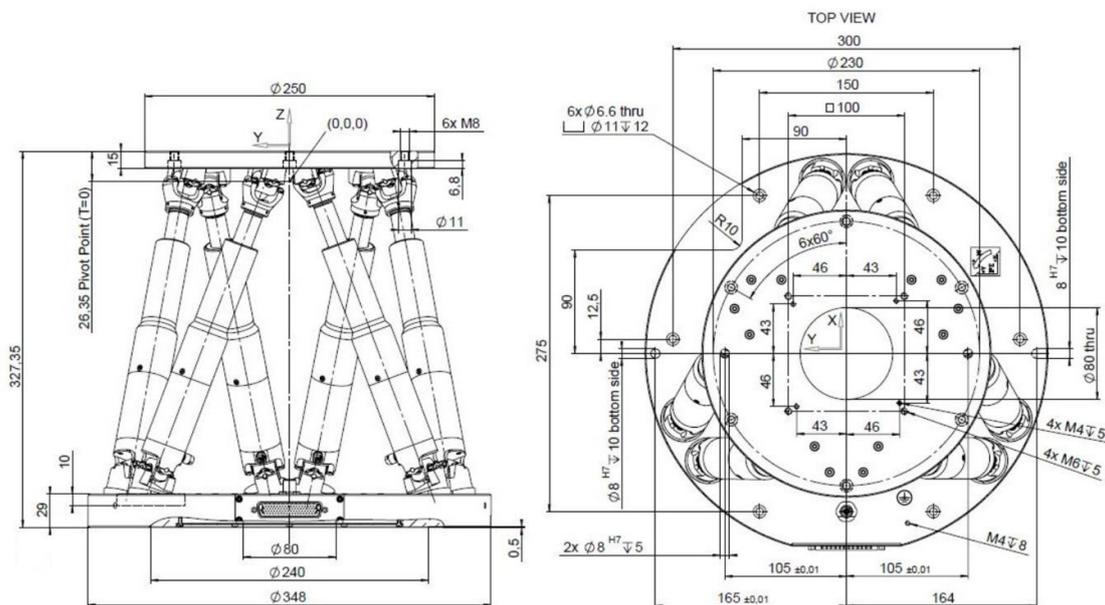
Figure 4-13:   Hexapod H840.D2 technical Drawing [213]

d   Minimum incremental motion

Minimum incremental motion indicates the smallest step movement that can be achieved with the hexapod. The H-840.D2 has a minimum incremental motion in translation of 3 µm in X and Y axes and 1 µm in Z axis, and a minimum incremental motion in rotation of 5 µrad in X, Y and Z axes. Minimum incremental motion has a direct relation to the machine's ability to obtain form accuracy. Indeed, the hexapod controller executes a step movement: if a circle is specified only with three points, a triangle is produced. Defining a curve via programming using points will therefore be limited to the minimum incremental motion capability of the hexapod. The minimum incremental motion specified above is sufficient for achieving 50 µm form accuracy defined on task definition.

The load capacity indicates the amount of load that the hexapod can hold and move from one defined position to another without losing precision. It also indicates the stiffness of the hexapod, with heavy load capacity hexapods having a stiffer design [218]. In this project, the spindle EMR-3008K is planned to be fixed to the hexapod. The spindle has a weight of 0.65 kg. H-840.D2. has a maximum load capacity of 10 kg on vertical positioning and a capacity of 3 kg in any orientation. The chosen spindle with wires and assembly features will be less than 3 kg. The precision of the hexapod will not, therefore, be lost due to the mass carried by the hexapod.

f   *Controller*

The controller is the device which takes commands and sends an electrical signal to the hexapod to execute movements. As the Hexapod is designed mainly for positioning purposes, it uses robot commands called General Command Set (GCS). It is easier to program simple flat movements using GCS commands. However, the aim of this project is to polish precision spherical and defined surfaces where the programming would need a computer-aided manufacturing (CAM) software to generate the polishing path. The positioning command of the program can be read by GCS commands as long as the letter preceding the values are X, Y and Z for translation movement and U, V and W for rotational movement.

If other commands (such as machining velocity, homing or approach velocity, tool radius compensation or any other commands) need to be used in the machining environment, a programmable logic control (PLC) can be used to translate the g-codes into GCS command and send them to the controller via an EtherCAT.

4.4.2   Machine Spindle Detail design

NSK Nakanishi is a Japanese firm producing precision spindles for CNC machining operations. They have a series of spindle called E3000, which are mainly electric driven spindles with air bearings. The motors of these spindles are designed to run between 2,000 – 80,000 rpm. Only few models are available at low speed. These models possess a gearbox to reduce spindle speed and increase torque. Depending on the ratio of the gearbox, the spindle speed can be altered. A brushless motor spindle EMR – 3008K from Nakanishi was assessed to be the most suitable for the present machine (figure 4-14). This spindle had a maximum rotating speed of 32,000 rpm, and a gearbox with 1 to 4 ratios, which brought the maximum speed down to 8,000 rpm. The dimension of the spindle is 30 mm in diameter and 183.5 mm in overall length, and its weight is 0.65 kg. It has a spindle runout of less than 1 µm. The output torque is constant at 35 Cn.m. The spindle was designed to be used for drilling and grinding purposes. It was therefore assumed that it will overcome required force for a soft contact to perform the polishing process. The collect chuck diameter to hold the polishing tool can vary from 0.5 mm to 6 mm in diameter. This allows the possibility to design a micro tool for polishing micro parts.

The spindle was sold with a controller E3000 (figure 4-15) and connecting cables. The controller E3000 allowed manual selection of the rotating speed and rotating direction. It has a digital screen to read the speed and also an errors code in the case of problems. There are DB-type connectors for command input and information output. The on/off motor switch, rotating speed and directions can be programmed and send as a command to be executed. The motor current, warning, errors and some other data can be monitored.

ELECTRIC SYSTEM	Brushless Motor Spindle EMR-3008K	O.D.	Max. Rotating Speed at The Cutting Tool	Reduction Ratio	Max. Allowable Motor Speed for The Spindle	Spindle Runout	Max. Power	Weight
		ø30mm	8,000min^{-1*}	$\frac{1}{4}$	32,000min^{-1} (Allowable Rotating Speed)	Within 1 µm	350w	650g

Code No. 1757   Model EMR-3008K

< Standard Equipment · Accessories >
• Collet Chuck ø3.0mm (CHK-3.0) • Chuck Nut (K-265) • Spanner (12 x 14) : 2pcs. • Grease for Reducer (10mL)

< Optional >

Collet Chuck (CHK Group)	: ø0.5~ø6.0mm See Page 34 for details
Motor Cord	: Length 3m (1778), 4m (1768), 6m (1767), 8m (1766)
Metal Saw Axis (KCH-03)	: For ø6.0 (I.D.) x within ø30mm (O.D.)
Grindstone Axis (AGM-03)	: For grinding wheel with I.D. of ø5.0mm

⚠ To extend the life expectancy of the Speed Reducer, inject grease every 70 to 100 hours. Grease injection prevents friction of the internal gears as well as heat generation. Adding grease also prevents the degradation of the existing grease in the reducer. Please maintain a reducer grease maintenance program.

Figure 4-14:   Picture of brushless motor spindle EMR-3008K and its technical characteristics [138].

Figure 4-15: E3000 Series spindle controller [138].

4.4.3   Tool detail design

To manufacture the polishing tool, a 6 mm diameter stainless steel rod was cut to a length of 100 mm. One end of the shank was threaded to screw in the second part of the shank. The other part of the shank was designed according to the bonnet design discussed above. A spherical rubber bonnet was used; a 20 mm diameter sphere, cut at 4 mm height, which gives a flat end diameter of 12 mm, with a positioning hole in the centre. In order to glue this on to the shank correctly, the end of the shank was designed with a flat end of diameter 12 mm with the same type of cylinder to match with the bonnet.

The pad was cut at 10 mm diameter using a punch. Normal polyurethane pads were soaked in hot water to make them more flexible. Contact adhesive (EVO-STIK IMPACT) was applied to the pad and the bonnet. The complete adhesive cure took 4 hours. By contrast, self-adhesive pads could be stuck on to the bonnet loaded with abrasive paste and used immediately. This method saved time in tool preparation. Both pads with their adhesive bonding method showed some irregularity. The pad, once glued, did not follow the spherical shape of the rubber. To solve this problem, the tool was pressed against the 20 mm diameter spherical shape using a drill stand. Using this method, a spherical shape following the rubber profile was obtained. Table 4-4 illustrates the tool manufacturing process with pictures.

Table 4-4:   Polishing tool manufacturing process

Polishing shank with one end tapped. The rod can vary between 1 to 6 mm in diameter.

Treaded cylinder designed to accommodate rubber on one side and screwed to the rod on the other

Table 4.4 continued

Spherical rubber bonnets are used to create pressurised and areal contact to maximize polishing efficiency. Different size and shapes of rubbers can be used, depending on the geometry and size of the polishing surface.

Rubber is then glued to the cylinder.
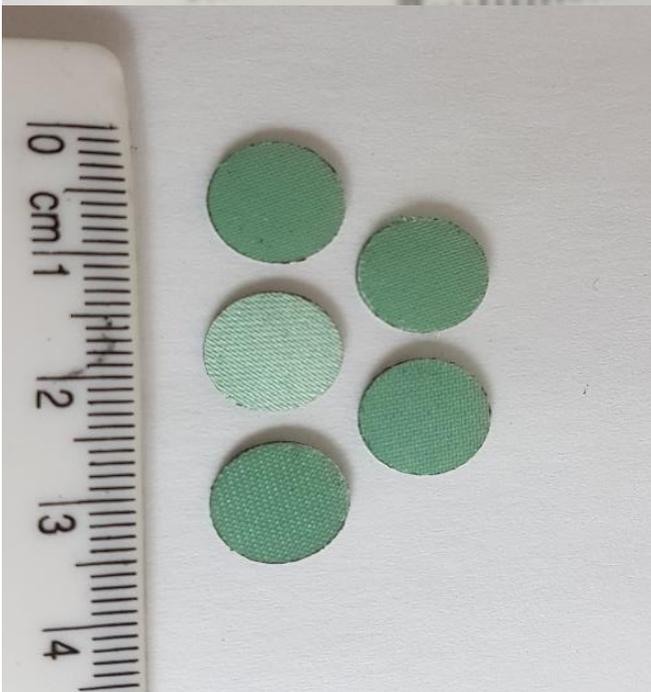
Polishing pads/cloths are then cut to fit the rubber bonnet, using a punch.

Table 4.4 continued

The pad is then stuck to the rubber. However, as can be seen in this picture, the pad does not stick correctly to the rubber, due to its small size.

To obtain uniformity in the bonding process, a shaping tool containing the same size spherical surface was manufactured.

Table 4.4 continued

The polishing tool is then attached to the drill stand and pressed against the shaping tool.

After 10 minutes, the tool was ready, with the pad being stuck correctly on to the tool. The detachable design between the shank and the cylinder of the polishing tool enables the preparation of a new pad while another one is being used for polishing.

4.4.4 Machine frame detail design

The stiffness of the aluminium extrusion frame needed simulation to evaluate the deformation and stress distribution due to the hexapod and the spindle being suspended in the middle of the frame. The type of frame chosen for purchase was, therefore, designed and assembled as required in the CAD package Solidworks, and subjected to an FEA analysis to identify any unwanted stresses or displacement in the model. To simplify and reduce the simulation running time, only the frame with hexapod, spindle and tool was simulated. In order to simulate the working condition, initial conditions were applied. The hexapod with the spindle had a total mass of 15 kg within the model, which took into account 12 kg of hexapod and 3 kg for the spindle and assembly features. The bottom of the frame was selected to be fixed geometry. An external force of 50 N/m^2 was applied on the tool bonnet with the gravity of 9.81 N/kg downwards for all parts (figure 4-16). This applied load was generally higher than expected during the polishing process

The stress analysis shows a maximum stress of 34.1 MN/m^2 in the middle region where the hexapod is fixed, which is almost nine times smaller than the yield stress for this material (275 MN/m^2). The overall structure did not have a high amount of stresses (figure 4-17). The displacement results showed maximum displacement in the middle of the cross frame. The amount of the displacement is less than 13 μm (figure 4-18). The 50 N external force applied on the tool produced no significant effect on the model. Based on these analyses, it was concluded that the structural frame which had been designed was sufficiently stiff for the purposes for which it was designed.

Gravity acting downwards

50 N/m^2 Polishing force acting on the bonnet upwards.

Fixed geometry fixture on the bottom the frame
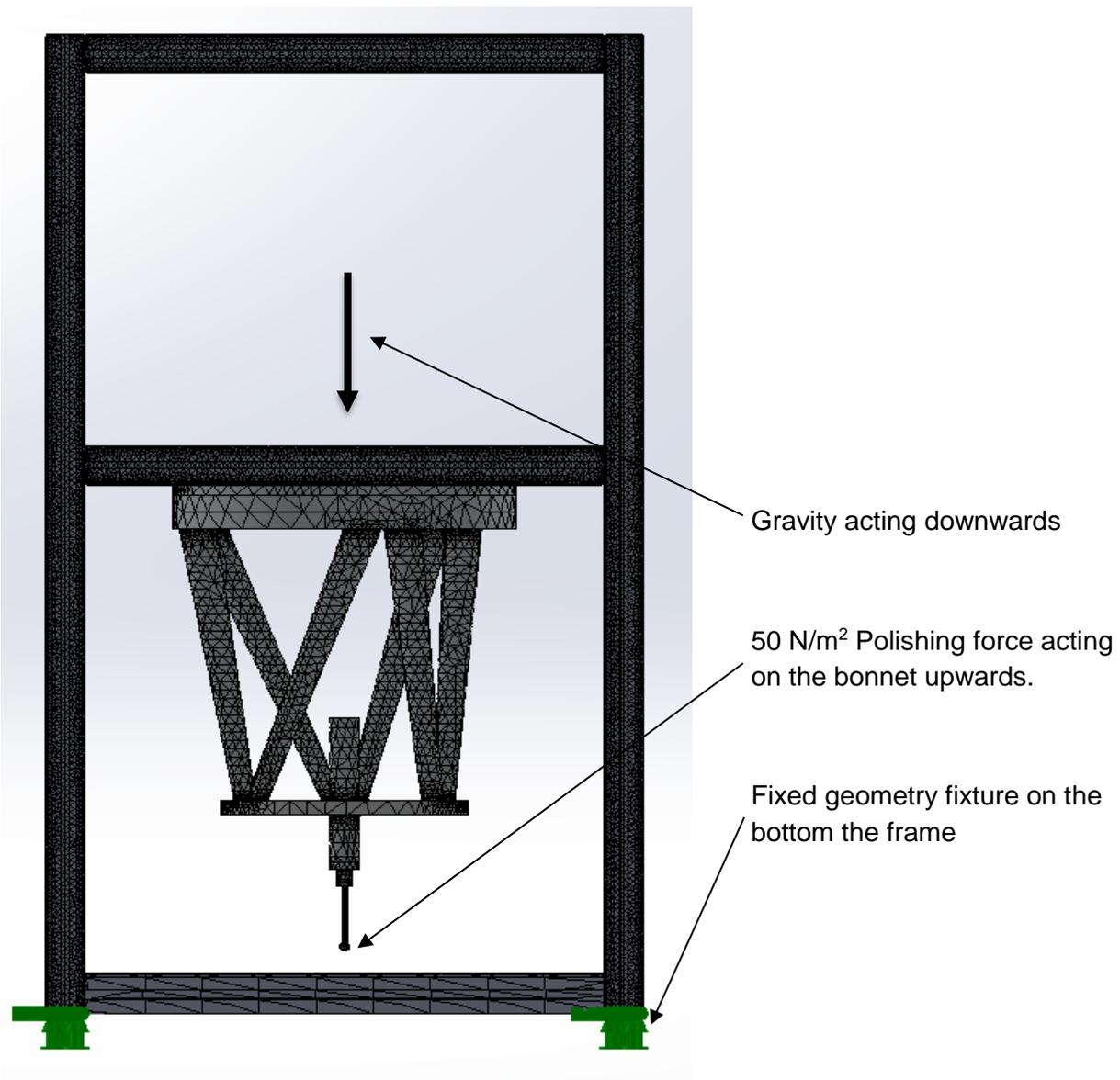
Figure 4-16:   Machine frame FEA initial conditions
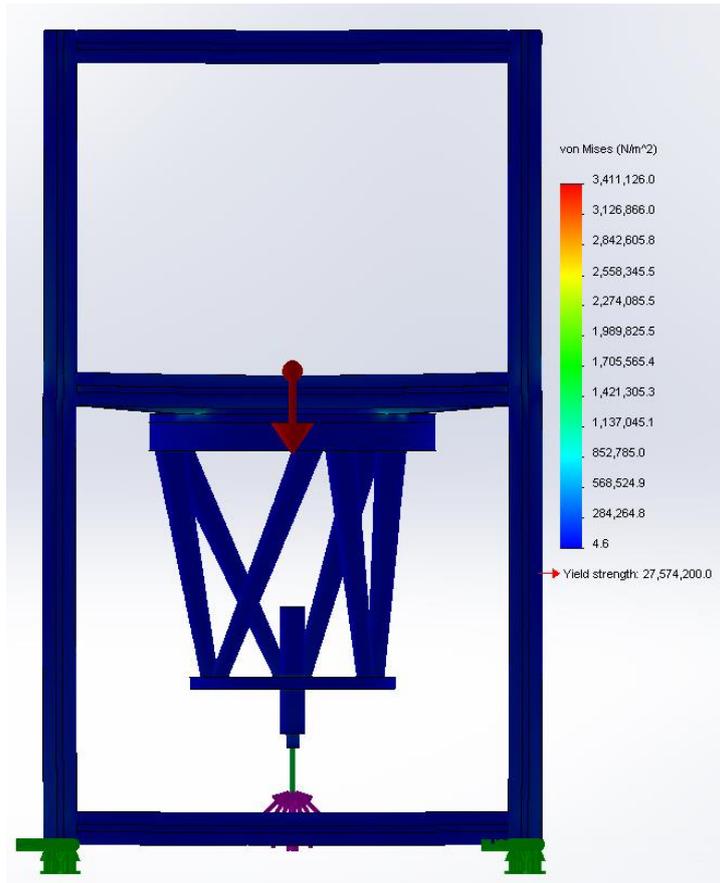
Figure 4-17:   Machine frame Von Mises stress
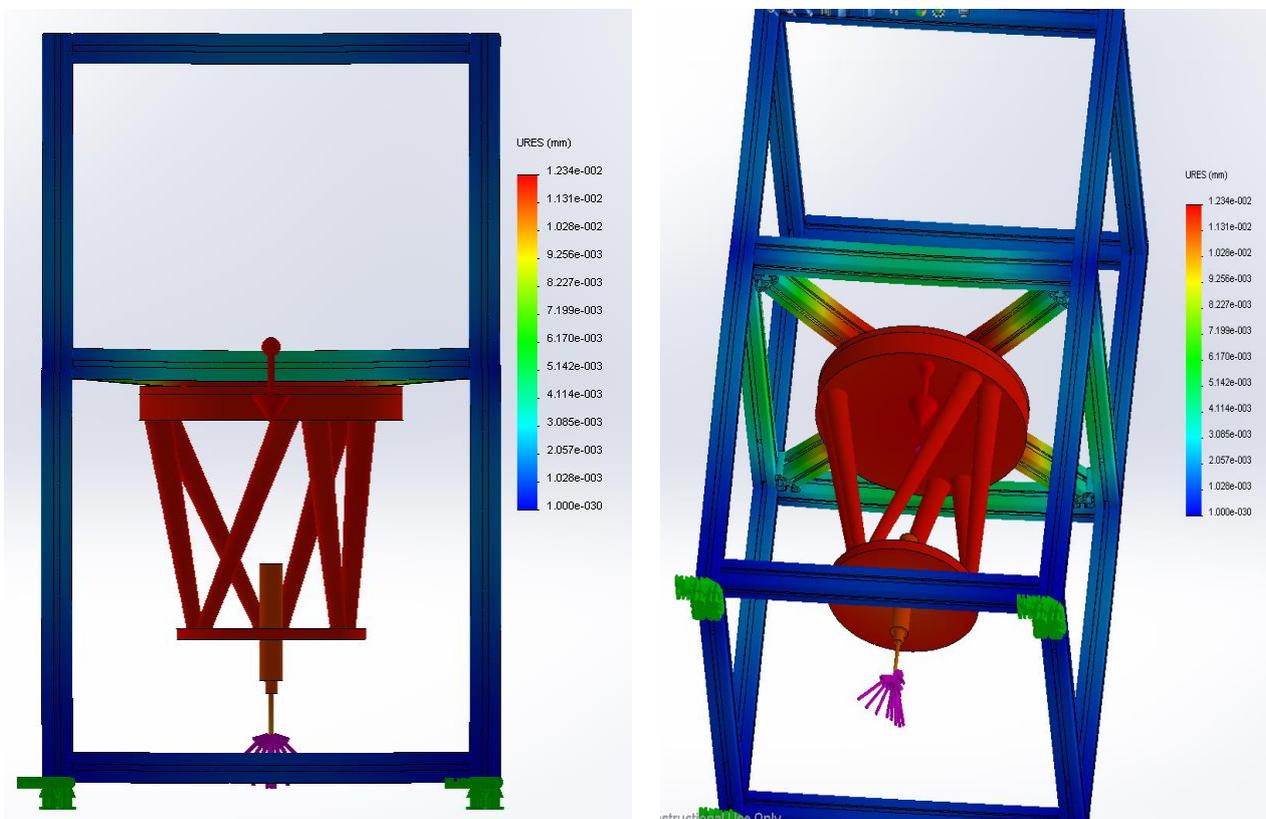
Figure 4-18:   Machine frame displacement analysis

4.4.5   Slurry pump detail design

Finally, a system was needed to mix the abrasives while pumping. In order to obtain the abrasive mixture without an additional system the cover which seals around the pump impeller was redesigned. The spinning force of the impeller creates a flow inside the cover which surrounds it. Redesigning this cover with incorporated impellers (inside and outside) which are connected through a bearing would transmit the inside flow to the outside without compromising the pumping force. The parts were designed and assembled in SolidWorks. The figure 4-19 shows the CAD design process with all individual parts and the assembly. The designed parts were 3D printed, expect the bearing. This was chosen from the standard waterproof bearings available on the market.
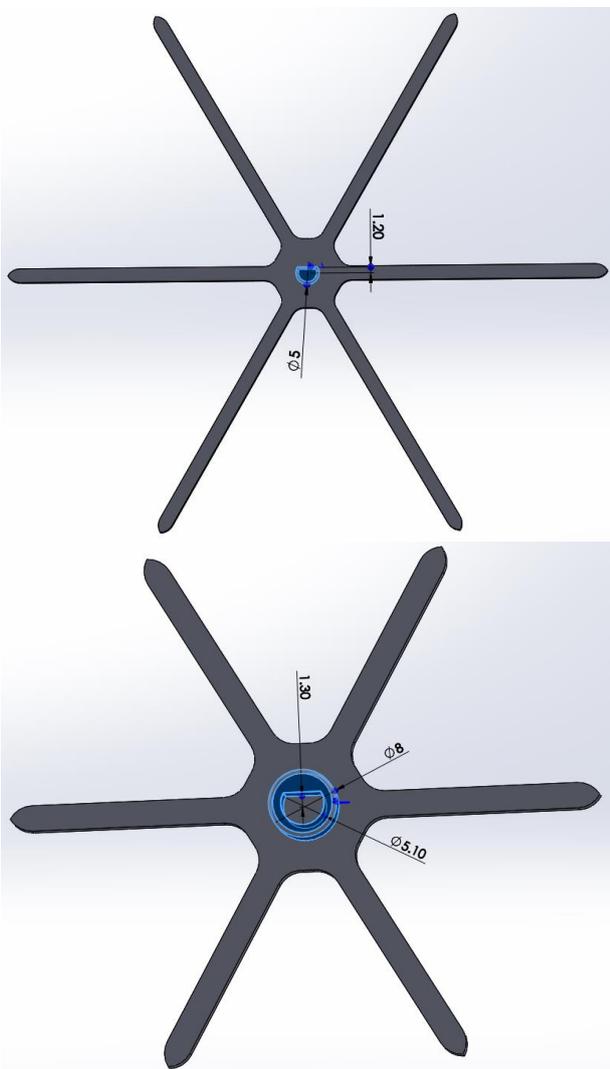
Outer impeller of the pump cover.

Inner impeller which has the fixture to connect the outer impeller. The diameter of the outside cylinder was designed to have a tight fit connection with the bearing.
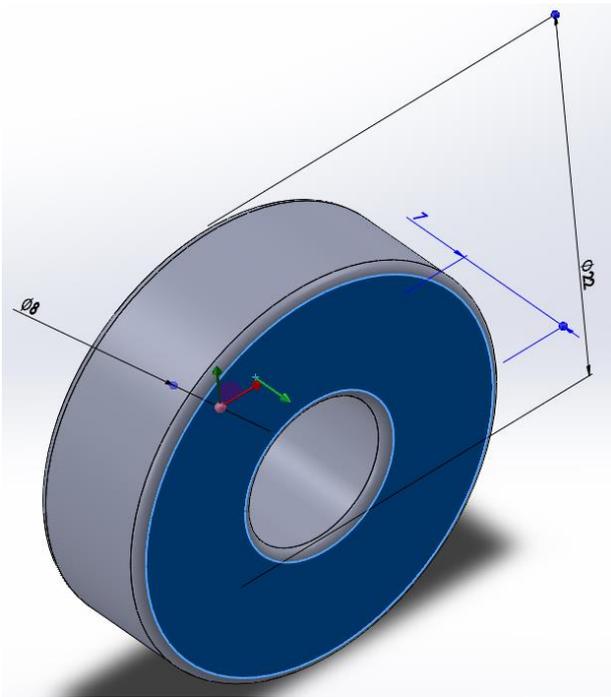
Standard bearing with waterproof housing.
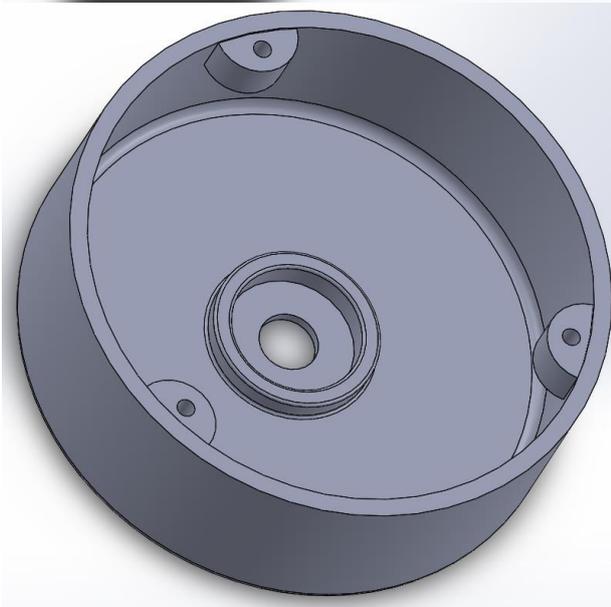
The redesigned cover has the same dimensions as the original. The cylinder in the middle was added to hold the bearing. The hole was to allow the cylinder of the inner impeller to reach the outer impeller.
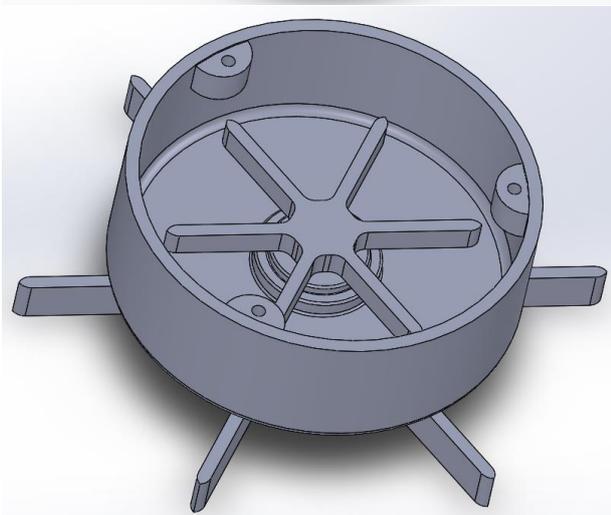
The picture shows the design of the pump housing cover to create a slurry mixer capability, using the flow force inside the housing cover.

Figure 4-19:   Impeller cover CAD Design assembly process

The 3D printed cover was fastened to the pump base to cover the area around the impellor which rotates to direct the flow towards the intake pipe. The pump was fastened to the container lid. The container depth and the 3D printed cover were designed to obtain a maximum distance of 2 mm between the outer impellor of the 3D printed cover and the base of the container. The aim was to reduce the possibility of abrasive stagnating at the bottom of the container. Figure 4-20 shows the 3D printed cover and the full assembly of the slurry tank.

Figure 4-20:   3D printed pump cover on left and slurry tank on the right

4.4.6   Additional parts task definition to detail design

The core sub-systems were obtained through design and manufacturing, or purchased as an integral sub-system. Having chosen the conceptual design and the core sub-systems in the layout design section, it was much easier to identify the requirements of all surrounding parts which were necessary to combine the sub-systems as a functional polishing machine based on the machine requirements.

a   Machine base

The machine base needed to have a stiff design which could hold all the other parts of the machine without causing deflection or vibrations. In terms of dimension the base height needed to be based around a standard table size to ensure easy handling with workpiece and tool. The area of the base should be bigger than the diameter of the hexapod and be able to hold components such as an

injection mould tool. The base plate needed to have three-point contact to correct flatness error propagated from floor and difference in size with base legs. Fortunately, the research centre had a machine base corresponding the requirement. The available base was made from cast iron. The dimensions were measured to be L839 mm, W608 mm and D608 mm. It was then designed in SolidWorks to assemble with the other components of the machine and to identify fixing hole positions (figure 4-21). The holes on the edges are made to fix the aluminium extrusion frame and the holes in the middle are to assemble the workpiece holding unit. The holes are then drilled and tapped as necessary. To absorb vibrations from the floor, damping pads are placed under the legs.
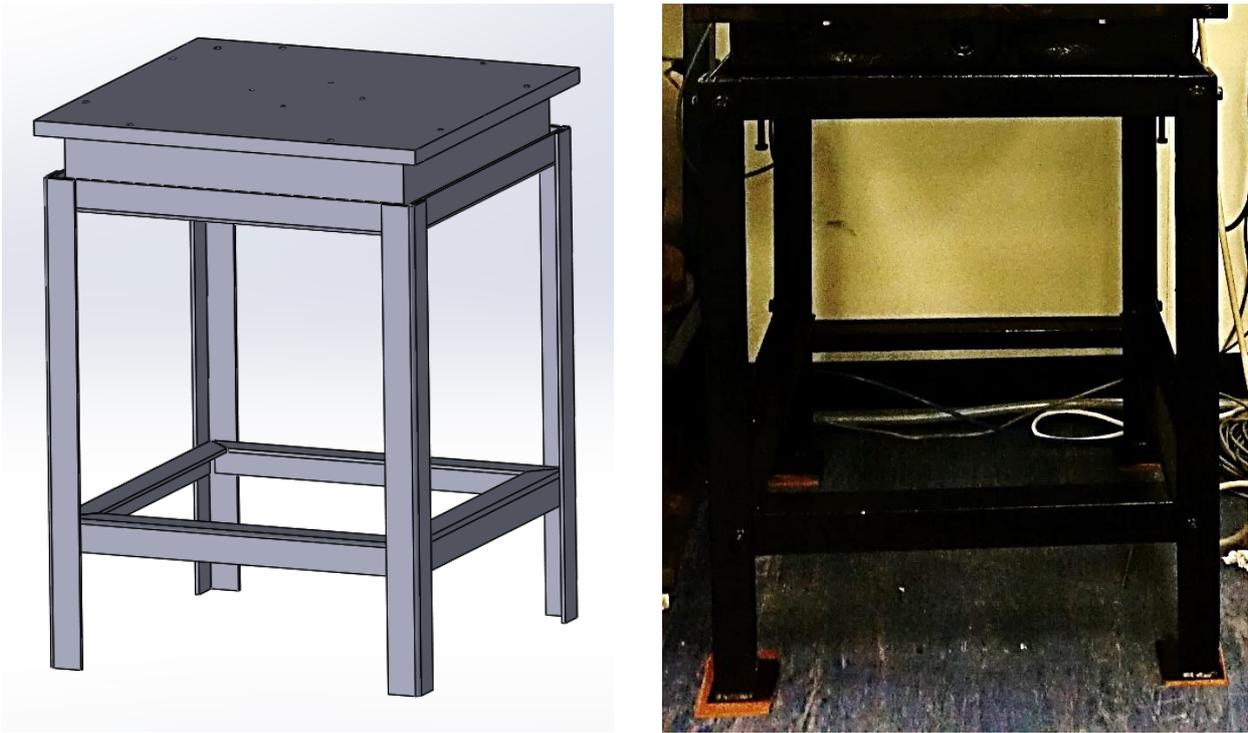
Figure 4-21:   Polishing machine base table (left: CAD model and right: Actual table)

b   Workpiece holding unit

The workpiece holding unit acts as a fixture base for the workpiece assembly. The facilitate this, a series of M5 tapped holes were integrated. The M6 through holes were to be used to fasten the workpiece holding unit to the machine base (figure 4-22).
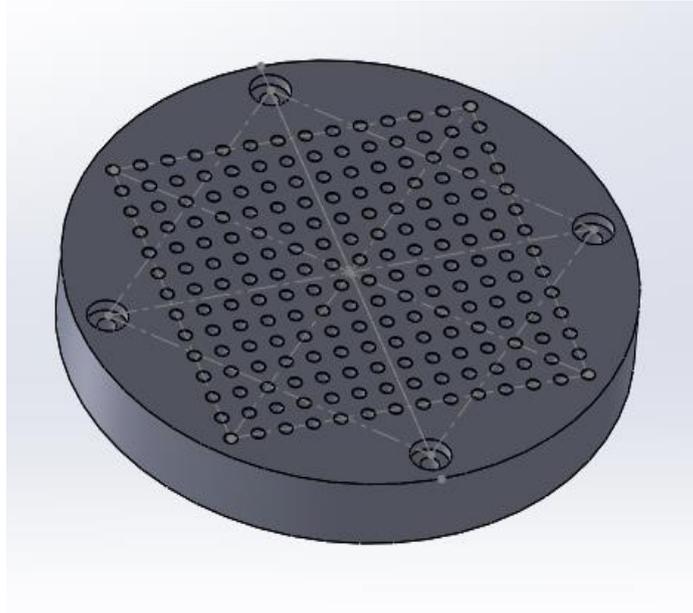
Figure 4-22:   Workpiece holding unit

c   *Base cover tray*

The base cover tray was designed to cover the machine base (figure 4-23). The edges of the tray were fastened on the aluminium extrusion to fully cover the base and, thus, avoid fluid/slurry contamination. The tray was designed for easy cleaning, with bends to direct the slurry flow in one corner towards the front of the machine, and was made of stainless steel to avoid corrosion. The hole in the middle was to allow access to the workpiece holder unit. Silicone sealant was applied to the gaps between these two components to protect from leakage.
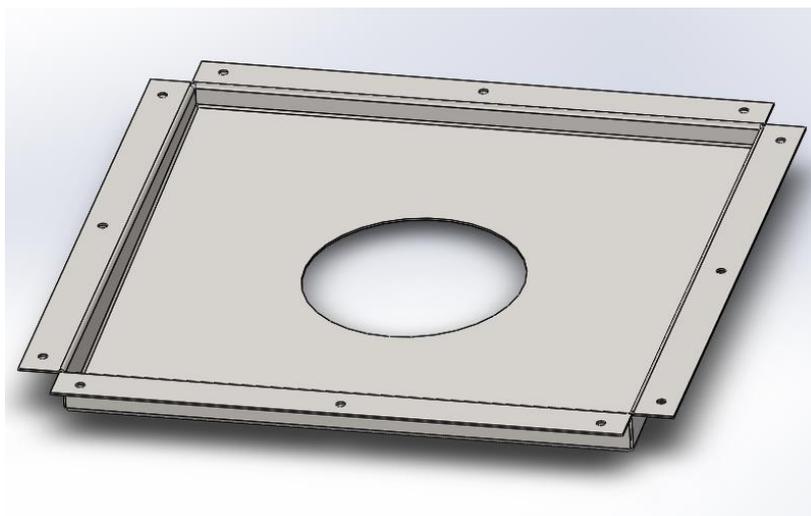
Figure 4-23:   Base cover tray

To ensure a good slurry flow to the machine, the part which surrounds the workpiece holder needed to be designed to avoid slurry flow stagnation. Stagnation of large size abrasives, for example, would cause contamination to the process when a smaller size abrasive was used for smoother polishing.

96

The slurry drainage tray was designed to surround the polishing area. The circular hole in the middle contoured the workpiece holder.

d   Hexapod Holding plate

This plate was designed to fix the hexapod into the frame (figure 4-24), and has six M5 tapped holes for the purpose. It also has five Ø7.5 mm through holes aligned and fastened with the aluminium extrusion frame. The intermediate assembly disc was made of aluminium, Ø348 mm 10 mm thick to provide sufficient room for the hexapod to be assembled.
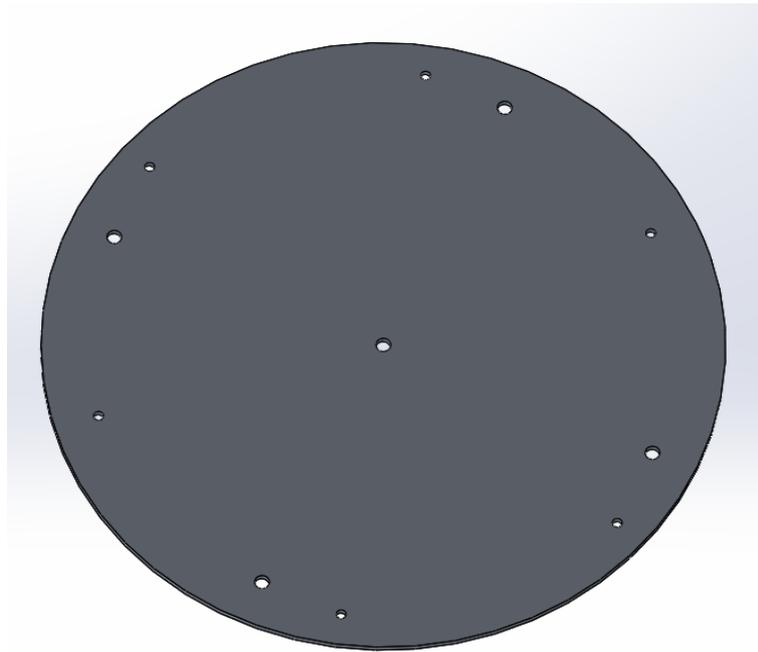
Figure 4-24:   Hexapod holding disc

e   Spindle holding assembly

The aim was to hold the spindle in the middle of the hexapod. The hexapod has a Ø80 mm hole in the middle of the bottom horizontal plate and four M6 tapped hole arranged equally spaced in a square. These features were used to create an assembly of three parts to assemble the spindle in the middle of the hexapod assembly. These three parts are described, with their design consideration, below.

Based on these hole positions, a plate was designed with a Ø40 mm hole in the middle (figure 4-25). There was also a Ø80 mm step used to create concentricity between the centre axis of this plate and the centre of the hexapod hole. The three equally spaced Ø5 mm through holes were for further assembly.
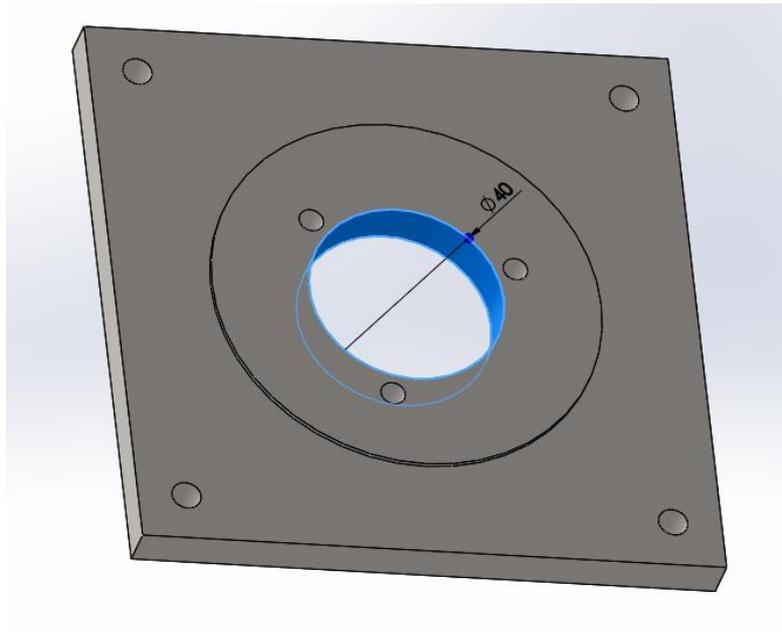
Figure 4-25:   Spindle assembly plate

The Nakanishi spindle EMR – 3008K came with fitting instructions to avoid damage to the internal components. The spindle installation instruction recommended avoiding the use of a fastening screw directly to the spindle; rather, the use a bush with a slit as an intermediate between spindle and holder was recommended. Following these instructions, a slit bush with internal Ø30 mm and external Ø35 mm was designed (figure 4-26). The spindle holder had an internal Ø35 mm diameter which corresponded with the slit bush, and three equally spaced Ø5 mm fixing holes which corresponded with the spindle assembly plate (figure 4-27). Figure 4-28 shows the assembly of the spindle holder on to the spindle assembly plate.
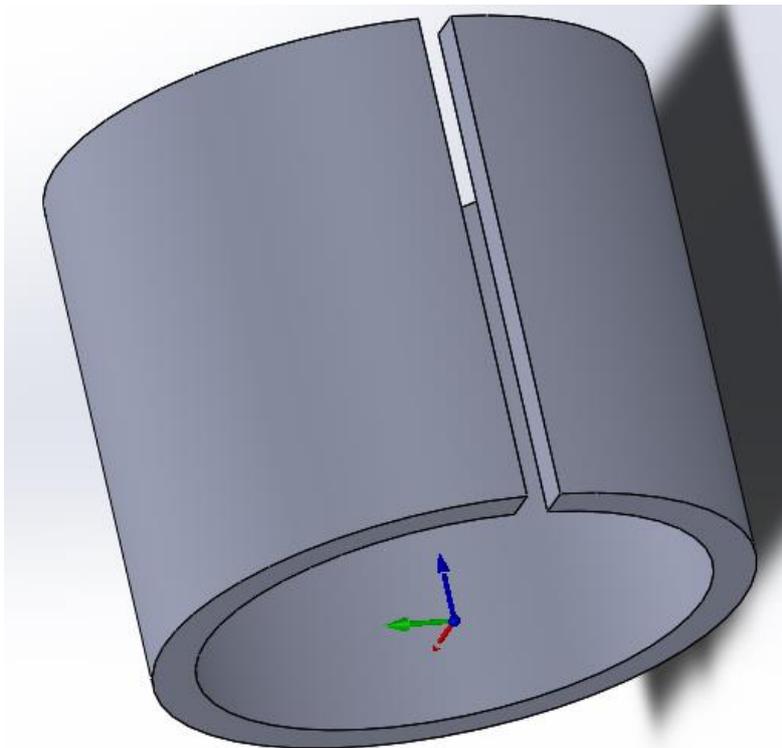
Figure 4-26:   Slit bush
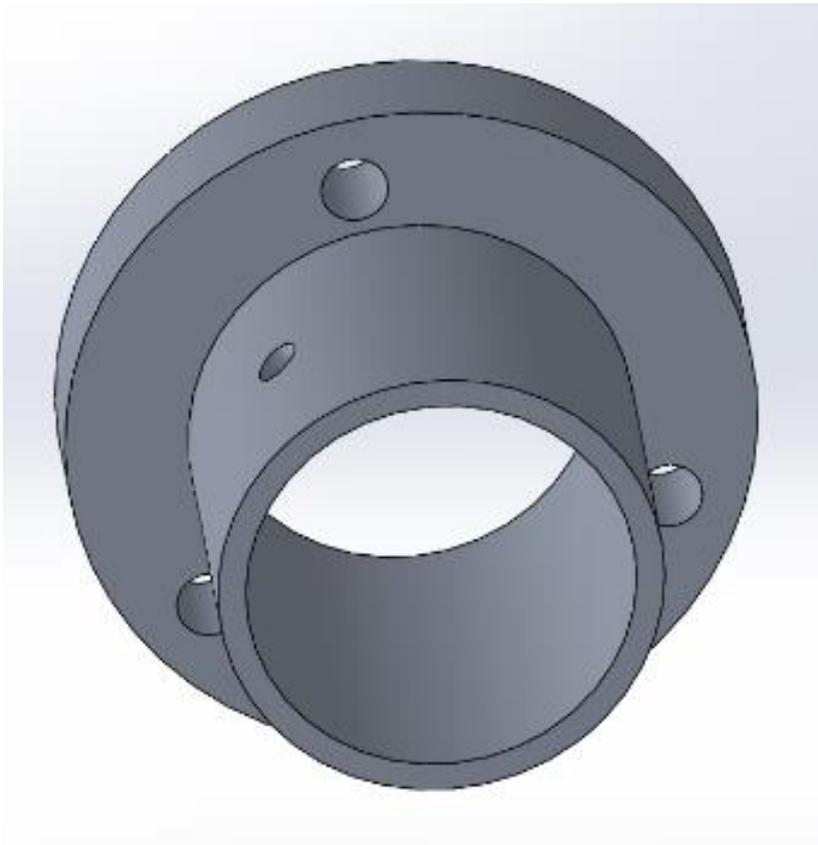
Figure 4-27: Spindle holder
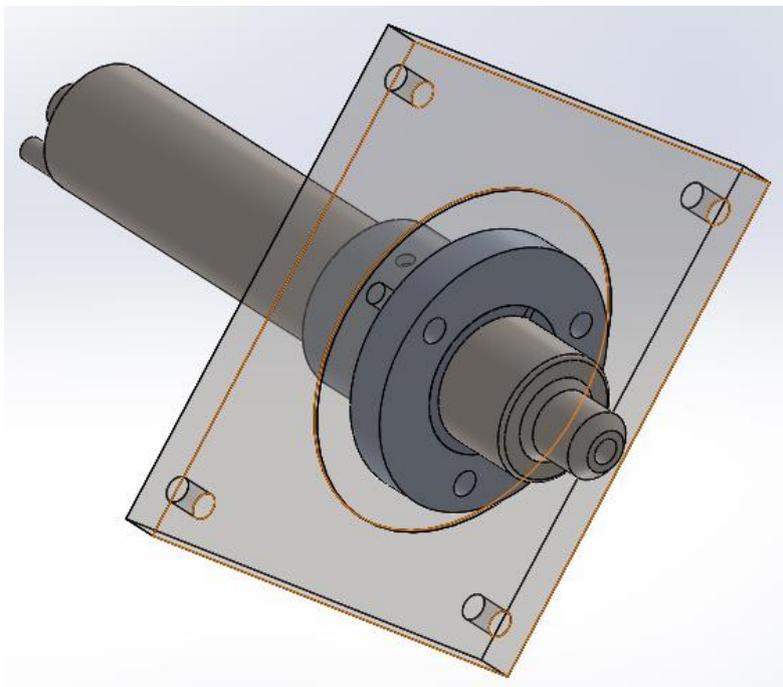
Figure 4-28: Assembly of the spindle holder

4.4.7 Overall machine assembly

The machine was initially assembled in SolidWorks. This provided detail on the overall dimensions of the machine. The machine foot print was L1839 mm, W608 mm and D608 mm. The space available below the machine base was to be used to accommodate the slurry tank. Space above the hexapod was available for possible placement of both the hexapod and spindle controllers. Figure 4-29 shows the CAD model of the assembly on the left and fully constructed prototype machine on the right.

The biggest challenge during the assembly process was to align accurately the different elements of the machine so as not to lose machine precision. Tilt error within the sub-system could result in geometrical error in the polished component. There were two different methods to resolve this issue. In the first, all designed components would have high tolerances and geometrical specification to ensure accuracy of the alignment during assembly; however, this method would be expensive as a means to provide the least added error in the relation between workpiece and tool. The second method, which would be more cost effective, would accept a standard finish for the machined component, with errors built into the relation between workpiece and tool. Some major errors required manual alignment, but minor errors could be measured and accounted for, using hexapod virtual referencing.

A primary concern was the parallelism between the workpiece and hexapod X and Y axes. The errors could build from the floor up to the workpiece. On the other hand, errors could accumulate from the cross aluminium frame down to the tool end. Major errors could originate from floor level and differences in leg size of the machine base, as well as from machine frame alignment with respect to the machine base. Minor errors were generated mainly in parallelism between the bottom and top faces of the workpiece holding unit and the hexapod holding plate. Additional errors emanate from the workpiece holder and the workpiece itself.

The base was initially placed on the vibration absorption pad and the workpiece holding unit was fastened to the machine base, which had tripod levelling points. The top of the workpiece holding unit was levelled in X and Y plane of the machine using a precision level. The frame which held the hexapod was also levelled using the precision level. Before levelling, an appropriate height position of the frame with respect to the machine base was determined. The hexapod had only a 50 mm travel range in Z direction; the position of the cross frame, therefore, needed to be in accordance with the workpiece position. An initial experiment was conducted on Ø30 mm P20 hard steel. The samples were cut to 20 mm height, ground, and held using a 3-point chuck. The chuck was assembled on a plate which was used to align the top surface of the workpiece with respect to the axis of the hexapod, once the height had been determined based on the above information.
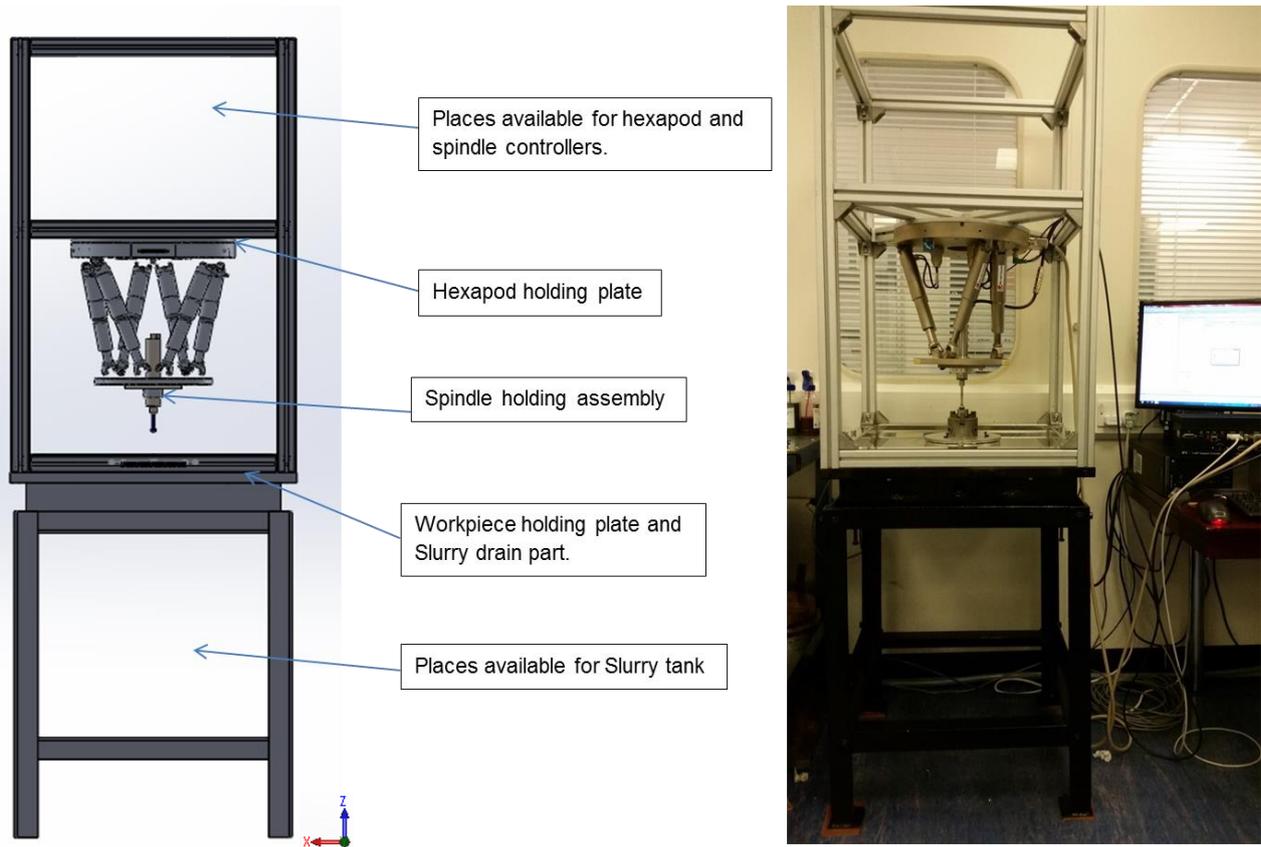
Figure 4-29: Assembly design and prototype of the polishing machine

4.5 Summary

This chapter has discussed the development of a novel design to fulfil the design of a precision polishing machine based on mechanical chemical polishing processes. The aim was to design a machine that could be developed at low cost in order to attract a wide range of market uses, from optics, healthcare to injection moulding. The design process follows a methodology which enables a clear statement of the capability and performance objectives of the proposed machine [1]. Based on these objectives, sub-systems were meticulously developed. All sub-systems were used to their full potential to ensure that they were cost effective and fit for purpose. The costs of manufacturing the machine were also kept low by designing an integrated system. The full machine can be assembled in half day by two engineers, which saves costs related to machine assembly. The overall machine foot print is slightly over 600 mm^2, which is ideal for mass production industrial environments. The total power consumption of the machine does not exceed 1 kW.

The machine spindle axis design was vertically downward. This design was chosen over other configurations for several reasons. Although a horizontal spindle alignment machine is generally considered to be more accurate, it was not suitable for this machine which was designed to use paste based abrasives as well as slurry, where the paste can slip from the polishing surface due to gravity. Additionally, the deflection caused by the mass of spindle and hexapod acting on the frame as a single point caused a simple downward displacement. FEA results showed a displacement of 13 μm, which would not affect the form accuracy (±50 μm) expected from the machine. Moreover, in

the vertical orientation, the hexapod has a higher load capacity (10 Kg) compared with any other orientation (3 Kg). A vertical machine alignment was therefore considered more appropriate.

The hexapod H-840.D2 was used as a precision, multi-axis movement system, allowing possible freeform movements. The work volume cannot be formulated as an absolute value. Indeed, the design of hexapod, with six parallel legs moving together to reach a specific target, does not allow the evaluation of a fixed universal workspace volume, and this is a problem of the design. However, the workspace simulation software provided can define the workspace range with given pre-conditions. Based on this information, it is understood that that gentle freeform surfaces could be finished using the hexapod based machine designed. Further, the minimum incremental motion and the feed rate range corresponded with the requirements of the machine.

The Nakanishi EMR 3008K spindle was chosen over other available spindles on the market. Indeed, this air bearing electric driven spindle had a runout precision within 1 μm. It allowed rotational speed to be controlled either manually or through command. The speed range and torque available on the spindle should enable polishing of rough surfaces at high speed to bring down the surface roughness very quickly. It also had the speed range required for final polishing.

The polishing tool is composed of a stainless steel shaft, rubber bonnet and polishing pad/cloth. The shaft is attached to the spindle, the bonnet glued on the rod, and pad glued on top of the bonnet. The design allowed for the tool head to be screwed and unscrewed in order to facilitate, and reduce the time needed for, tool preparation. A convex shape mould was developed and used to press against the spherical tool to ensure that the pad adhered to the bonnet surface correctly. A slurry pump was developed for polishing, using re-circulating slurry with a 6 litre capacity tank. An ordinary pump was used, but the housing was redesigned to ensure that abrasives did not stagnate at the bottom of the tank.

Additional parts were developed to obtain the desired machine functionality. During the assembly process, the table and the hexapod frame were levelled in the X and Y axes to remove major parallelism errors between the workpiece and hexapod axis. It was assumed that there would be some minor errors within the range of hundreds of microns. These minor errors could be adjusted for specific samples, using a tripod levelling base for each workpiece individually.

5 Precision polishing process development on the Hexapod polisher

5.1 Introduction

The literature review in Chapters 2 & 3 indicated the benefit of precision surface roughness and form accuracy in different industries. As an example the mass production of precision polymer or even glass components requires a precision mould tool. Mould tools for polymer production are often made out of hard tool steels for process reliability. Tool steel such as P20 are hard to machine when sub-nanometre surface roughness is needed. A.M. Zanatta et al. polished two different tool steel materials called WNr. 1.2738 (also called P20) and WNr. 1.4305, using automated and manual polishing. It was noted that WNr 1.4305 presented surface deterioration, such as pitting, on the surface due to the polishing process and a poor material characteristic. On the other hand, P20 achieved Rz = 0.08 µm without any visible defects on the surface [219]. This research showed the excellent surface obtained by polishing on P20 hard steel using an automatic flat polishing machine. However, no research is available on surface roughness improvement by polishing of P20 for surfaces other than flat such as injection mould tools. The developed machine in this study was used to polish primarily flat samples of P20 to enable comparison with previous work in order to evaluate the machine capability as a precision polishing machine. In future the developed process will be applied for form polishing.

A novel freeform polisher was designed and a prototype of the machine was produced. One of the main expected outcomes of the machine is to achieve less than 10 nm Sa, surface roughness. Before undertaking an experimental study to try to achieve the aim expressed above, it was important to understand the machine behaviour under different working conditions to better plan future experiments. Indeed, the hexapod polisher has certain differences to the well-established and previously reported Zeeko polisher [168]. The Zeeko polishing machine uses an inflated bonnet as the polishing tool whereas the hexapod polisher uses a solid rubber bonnet as the polishing tool. Zeeko machines polish with the tool being oblique to the workpiece normal face between 5 to 20 degrees to obtain an even surface speed and also a Gaussian shape material removal function for predicting material removal and hence form correction. In contrast, with the hexapod polisher, the use of a tool angle would reduce the workspace capacity considerably (see Chapter 4 – Hexapod workspace volume). Therefore, in terms of practical use, it was decided that the hexapod polisher would always polish normal to the polished surface. Moreover, the difference in machine kinematics, tool size, and other differences suggested an empirical study should be completed to understand the influential machine parameters in terms of improving specimen surface roughness.

The Taguchi method was used to optimize the range in the influential parameters. The Taguchi method is a tool developed by Dr Genichi Taguchi for improving the quality of products [220]. The philosophy behind the method is to emphasize the design of experiment (DOE) to obtain the optimum combination of variables. The Taguchi method also allows researchers to reduce the number of experiments using the Taguchi's orthogonal array (OA) approach. Indeed, a process with four variables with each having three levels would require (3^4) a total of 81 experiments using conventional or fractional factorial design of experiments. Fortunately, using Taguchi OA L9 (3^4), only nine experiments are necessary.

In the precision machining industry, the variables influencing surface finish and precision have been extensively studied using the Taguchi method. Shengyue, for example Blunt et al. have previously

polished artificial knee joints made of CoCr using Bonnet polishing processes. The samples were pre-polished to 24 nm Sa. Surface roughness of Sa >7 nm was then obtained by optimising polishing parameters using a Taguchi approach. They used a standard 3-level orthogonal array L9 (3^4) for the design of experiment. This allowed four variable parameters at three chosen levels. All other parameters were fixed with a given value [206]. As further example of the approach, in the grinding process, the form control is very critical. There are several parameters, such as wheel speed, table speed, depth of cut and grain size, that influence the geometrical error. The Taguchi method is used by Kwak et al. to understand the cause of these errors and find the optimum condition to reduce them, They found that the depth of cut followed by grain size are the two major causes of geometrical error [221]. Tsai et al. have applied the Taguchi and experimental investigation to improve the surface roughness of mould steel SKD61 by abrasive jet polishing. The Taguchi design of experiment enabled them to polish a EDM machine surface which was at 1.03 µm to 0.13 µm Ra. They have further identified that the gas pressure and impact angle of the flow have the greatest effect on surface roughness. A 1:1 mixture of water and oil as the additive reduces the cutting force and helps to obtain mirror-like polishing [222].

The following chapter will describe the initial work carried out for preparing the polishing process. It is then followed by the empirical experiments which helped to identify inconsistency in the obtained results for the same parameters. Once the problems related to result inconsistency are solved, the Taguchi DOE is tested and the obtained results are analysed. Finally, the identified optimum parameters from Taguchi experiment are applied on the re-circulating slurry polishing process.

5.2   Polishing preparation

5.2.1   Polishing program on GSC command

A polishing program was created using GSC command on Excel. The program created moves only in X and Y directions following a raster profile (figure 5-1 a). The program was made to cover 28 mm^2 with a 0.5 mm step size. The program was manually written to execute the profile available on figure 5-1 b. Once this profile was expressed as a step movement, it was then converted into a program using MOV function with X and Y values. Between each line of command "WAC ONT? X =1" was inserted to ensure that the previous line of command was executed before reading the next line of command (figure 5-1 c). These 4 line commands were repeated with a step change of 0.5 mm to cover the whole sample. The left column with yellow coloured lines on figure 5.1 is used to create the raster program, parallel to X axis and the blue coloured lines used to create the raster program, parallel to Y axis.

Figure 5-1: Polishing program GSC commands a) Raster tool path (Top left) b) Programmed path on excel (Top right) c) Generated program (Bottom)

#	Left (X=28)	Middle GSC commands	Right (X=28) generated program
1	X 28 X Y -		X 28 X Y
2	y 0.5 14 14	MOV X 14 Y 14	Y 0.5 14 14 — MOV X 14 Y 14
3		WAC ONT? X = 1	WAC ONT? X = 1
4	-14 14	MOV X -14 Y 14	14 -14 — MOV X 14 Y -14
5		WAC ONT? X = 1	WAC ONT? X = 1
6	-14 13.5	MOV X -14 Y 13.5	13.5 -14 — MOV X 13.5 Y -14
7		WAC ONT? X = 1	WAC ONT? X = 1
8	14 13.5	MOV X 14 Y 13.5	13.5 14 — MOV X 13.5 Y 14
9		WAC ONT? X = 1	WAC ONT? X = 1
10	14 13	MOV X 14 Y 13	13 14 — MOV X 13 Y 14
11		WAC ONT? X = 1	WAC ONT? X = 1
12	-14 13	MOV X -14 Y 13	13 -14 — MOV X 13 Y -14
13		WAC ONT? X = 1	WAC ONT? X = 1
14	-14 12.5	MOV X -14 Y 12.5	12.5 -14 — MOV X 12.5 Y -14
15		WAC ONT? X = 1	WAC ONT? X = 1
16	14 12.5	MOV X 14 Y 12.5	12.5 14 — MOV X 12.5 Y 14
17		WAC ONT? X = 1	WAC ONT? X = 1
18	14 12	MOV X 14 Y 12	12 14 — MOV X 12 Y 14
19		WAC ONT? X = 1	WAC ONT? X = 1
20	-14 12	MOV X -14 Y 12	12 -14 — MOV X 12 Y -14
21		WAC ONT? X = 1	WAC ONT? X = 1
22	-14 11.5	MOV X -14 Y 11.5	11.5 -14 — MOV X 11.5 Y -14
23		WAC ONT? X = 1	WAC ONT? X = 1
24	14 11.5	MOV X 14 Y 11.5	11.5 14 — MOV X 11.5 Y 14
25		WAC ONT? X = 1	WAC ONT? X = 1
26	14 11	MOV X 14 Y 11	11 14 — MOV X 11 Y 14
27		WAC ONT? X = 1	WAC ONT? X = 1
28	-14 11	MOV X -14 Y 11	11 -14 — MOV X 11 Y -14
29		WAC ONT? X = 1	WAC ONT? X = 1
30	-14 10.5	MOV X -14 Y 10.5	10.5 -14 — MOV X 10.5 Y -14
31		WAC ONT? X = 1	WAC ONT? X = 1
32	14 10.5	MOV X 14 Y 10.5	10.5 14 — MOV X 10.5 Y 14
33		WAC ONT? X = 1	WAC ONT? X = 1
34	14 10	MOV X 14 Y 10	10 14 — MOV X 10 Y 14
35		WAC ONT? X = 1	WAC ONT? X = 1
36	-14 10	MOV X -14 Y 10	10 -14 — MOV X 10 Y -14
37		WAC ONT? X = 1	WAC ONT? X = 1
38	-14 9.5	MOV X -14 Y 9.5	9.5 -14 — MOV X 9.5 Y -14
39		WAC ONT? X = 1	WAC ONT? X = 1

5.2.2 Workpiece holder

The workpiece was held on a three-point chuck available in the laboratory for primary polishing. However, it required an intermediate plate to hold the chuck in the middle and to allow it to be fastened in the machine workpiece holding unit. The intermediate plate designed has three holes in the middle to attach the chuck. It also has three holes in line with the threaded holes of the workpiece holder for fixing. Further, there were threaded holes nearby these through holes to be used to

position the workpiece top surface parallel to the hexapod X and Y axis. The chuck and its assembly plate fastened to the machine workpiece holding unit are shown in figure 5-2.
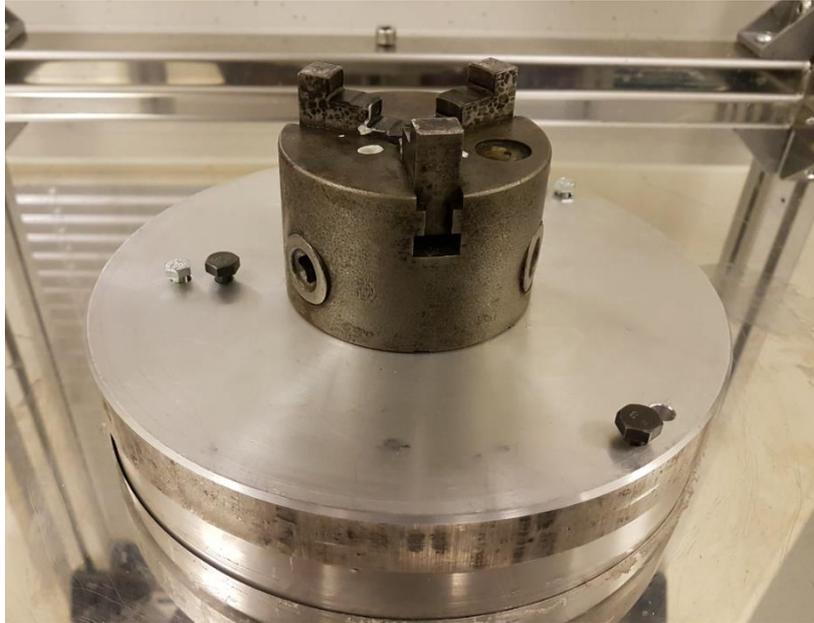
Figure 5-2:   Three point chuck for holding workpiece

5.3   Hexapod – workpiece alignment

5.3.1   Center alignment

The centre of the chuck needed to be aligned with the centre of the Hexapod. Two sharp cones designed for machine alignment were used to join the intersection point between X and Y axes. One cone was attached to the spindle collet and the other was attached to the chuck (figure 5-3 (a) and (b)). The hexapod was moved to be in line with the cone attached on the chuck. A digital microscope was used to identify any deviation from the alignment. The deviation from the hexapod origin can be read on the PI software used to control the hexapod movements. In this case, the hexapod had to move -0.36 mm in X axes and 0.46 mm in Y axes to align itself with the centre of the chuck. There is a tab on the bottom named "Define Home Coordinate System (KSF)" which was used to define the new home position for the hexapod (figure 5-3 (c)). Once the KSF was active, all movements would be executed with respect to that position.
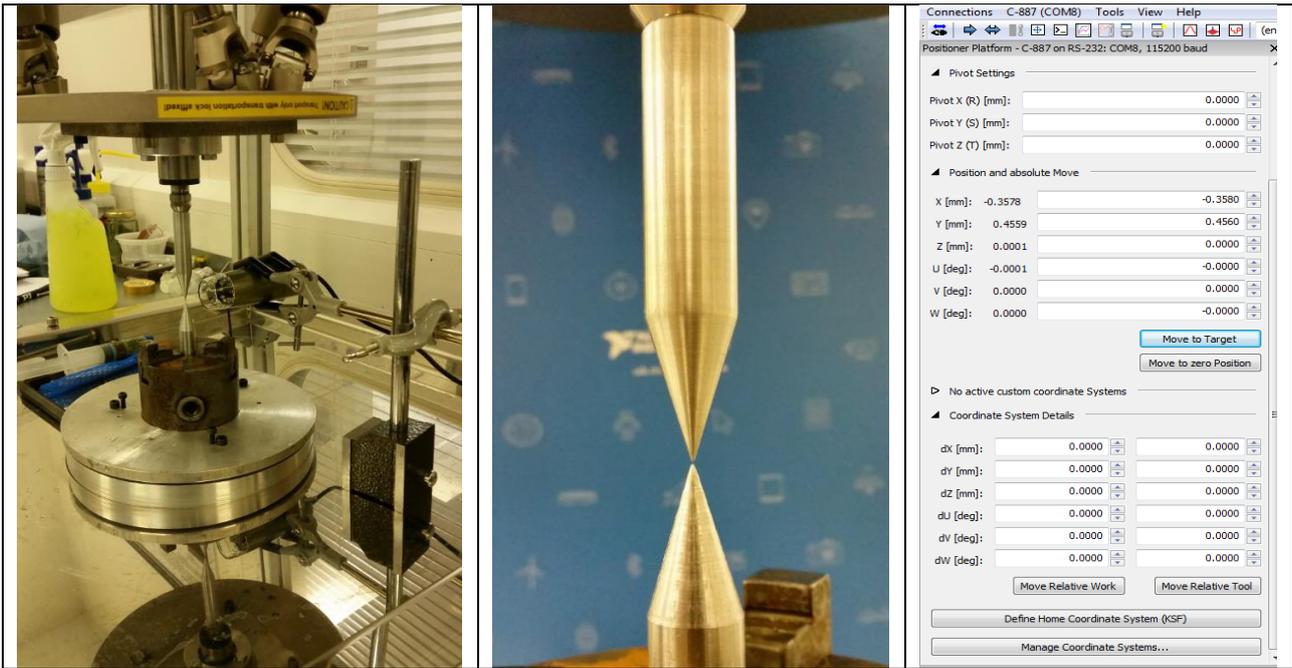
Figure 5-3: Hexapod - Workpiece center alignment(Left – Alignment assembly (a) ; Middle – Aligned position (b) ; Right – PI Software input (c))

5.3.2   Contact and parallelism

Identifying the contact between the tool and the workpiece is a challenging task. Indeed, the tool was a soft bonnet and the workpiece made of a hard material. The contact force was not measured at this stage, but assumed to be relatively small within 1 N. To measure this would require a load cell or force sensor with load range between 5 g to 5 kg. It also needs to be sensitive to detect even a 5 g change. These type of load sensors cost in the range of £3,000 and upwards. It was considered too expensive for this project where its purpose would only be to detect contact and measure the force in the experimental stage. At this stage for polishing a flat surface, a thin shim of known thickness was placed between the tool and workpiece to evaluate the gap and move to the contact position accordingly.

To obtain parallelism between workpiece and hexapod X and Y axis, the hexapod was moved towards the extremity of workpiece in X and Y axis with Z axis being at contact position. Fine threaded screws are used to align the workpiece parallel to the hexapod XY plane. Once in position, the bolt nearby the fine threaded screws is used to clamp the workpiece in place. The alignment is verified again once the intermediate plate is clamped to ensure that the clamping process did not change the alignment. Perfect parallel alignment in the region of 20 μm is not considered necessary due to the compliant nature of the polishing bonnet.

5.4   Empirical experiment

Literature reviews on bonnet polishing process using the Zeeko polishing machine were very useful to understand the influential parameters on polishing process. However, the same behaviour could not be expected from the presently designed machine, as the working principles of the machine differs from Zeeko polisher in certain aspects. As explained in the introduction, it is important to

understand the influences of polishing parameters, as the working principles of the machine differs from the Zeeko polisher. Indeed, it allowed the DOE for Taguchi to be more efficient. The experiments were conducted to understand the effect of parameters and their influences on surface roughness. Parameters, such as feed, speed, offset, number of passes, polishing paste grain size, were considered in this analysis. Initial results showed the hexapod polisher's ability to reach less than 10 nm Sa roughness; however, suddenly, after several experiments, the obtained results were always above 15 nm Sa. All experimental trial parameters were recorded and logged. Trials with the same parameter conditions were repeated and the obtained results were different (Table 5-1).

Table 5-1: Empirical experiment results

	Feed Rate (mm/sec)	Speed (rpm)	Offset (mm)	No Pass	Diamond Paste Grain size (µm)	Average Initial Sa (nm)	Average Final Sa (nm)	Variation
Sample 012	15	1000	0.2	10	6 µm	15.6	9.3	-6.3
Sample 024	15	1000	0.2	10	6 µm	14.8	15.4	0.6
Sample 007	20	700	0.3	15	6 µm	22	24.5	2.5
Sample 027	20	700	0.3	15	6 µm	23.1	20.6	-2.5

Table 5-1 shows samples 012 and 024 had the same parameters and initial surface roughness condition. However, the obtained results show inconsistency. In Sample 012, the Sa of the surface improved, whereas, in Sample 024, the Sa of the surface deteriorated. On the other hand, Sample 007 initially showed deterioration of Sa of the surface, which when tested again in Sample 027, showed improvement of the Sa of the surface. This clearly indicates that other factors than those thought to be influential affected the results. Therefore, these experiments were further investigated. It was found that there were several factors which were initially not considered to affect the outcome.

The Hy57 polyurethane pad was used as a polishing pad for the samples discussed on Table 5-1. The pad was used for more than one experiment. The wear of the pad changes the initial condition of the polishing process; therefore, it was decided to use a new pad for each experiment. The second problem was with the amount of polishing paste applied on the workpiece. Indeed, it changes the concentration of the abrasives on the polishing surfaces, which affects the removal rate, hence Sa value. To ensure consistency, the amount of paste applied was measured on a precise balance, and the same amount was used for each experiment. The final factor which influenced the result was the amount of polishing fluid applied on the workpiece. During the initial experiment, some periodic scratch marks were noticed on the workpiece (figure 5-4). The application of polishing fluid helped to remove or reduce the intensity of those marks and helped to obtain a mirror-like finish. It was later understood that the scratch marks were caused by a high concentration of paste for an initial relatively smooth surface (20 nm Ra); the application of polishing fluid helped to remove agglomeration of abrasives which reduced the intensity of scratch marks on the surface. To solve this problem, two actions were taken. First, the amount of paste applied was related to the initial surface roughness of the workpiece. Secondly, the polishing fluid was placed on a spray gun and applied once on the polishing surface at the beginning of the experiment for all samples to ensure consistency.
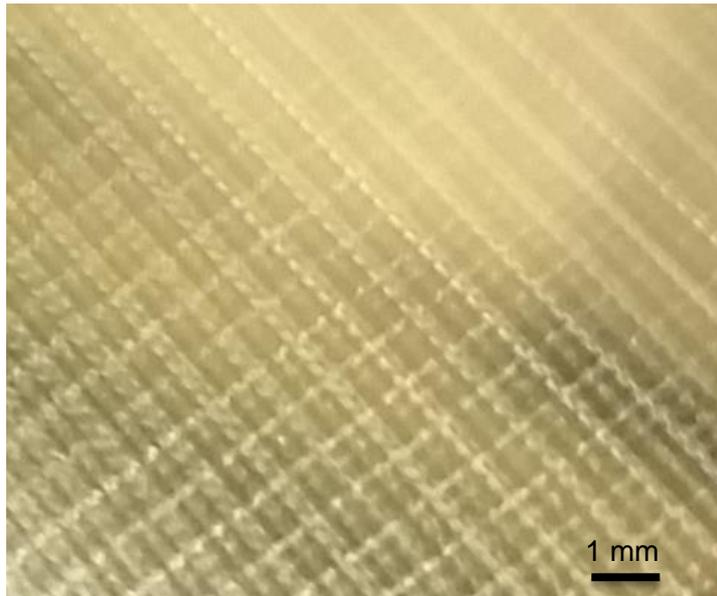
Figure 5-4: Optical image of the periodic scratch marks on polished surface

5.5 Taguchi experimental procedure

5.5.1 Experimental design

In this experiment, the aim was to evaluate the machine capability as a final finishing process to improve surface roughness of P20 tool steel. P20 is a commonly used material in plastic injection moulds and dies for its good material composition, hardness and durability. The material is delivered in the pre-hardened condition and is chosen generally for its good machinability, hardness (Brinell 300/33), homogeneous microstructure, temperature stability and polishability. The chemical composition of the material was measured on XRF (X-ray fluorescence) and shown in Table 5-2. The P20 steel of Ø30 mm was cut and ground to equal lengths. Further, they were hand abraded using SiC abrasive papers from 80 grit up to 400 grit to obtain a baseline surface topography. The surface roughness Ra is around <30 nm at this stage.

Although all factors influence surface roughness, four varying parameters of the machine need to be optimized in order to achieve the smoothest surface roughness within given initial conditions. The varying parameters were: i) feed rate (mm/sec) of the hexapod, ii) rotating speed (rpm) of the spindle, iii) tool offset (mm), which refers to the distance, the bonnet being pressed against the workpiece and iv) number of passes, which refers to the number of times the raster program is repeated. All fixed polishing parameters are shown in Table 5-3. A standard OA L9 (3^4) was chosen for the DOE. The range of these parameters is based on empirical experiments (Table 5-4).

Table 5-2: P20 material chemical composition

Material	Carbon (C)	Manganese (Mn)	Molybdenum (Mo)	Silicon (Si)	Chromium (Cr)
P20	0.4	1	0.35	0.4	1.2

Table 5-3:   Taguchi experiment fixed parameters

Tool angle	0 degrees
Step change	0.5 mm
Bonnet type	Hy57 polyurethane polishing pad
Bonnet radius	10 mm
Abrasives	0.006g of 1 µm diamond paste spread over the polishing surface
Polishing Fluid	Sprayed once before polishing

Table 5-4:   Design matrix for L9 (3^4)

	Feed Rate (mm/min)	Speed (rpm)	Offset (mm)	No of Passes
Sample 1	15	500	0.2	8
Sample 2	15	700	0.25	12
Sample 3	15	1000	0.3	16
Sample 4	20	500	0.25	16
Sample 5	20	700	0.3	8
Sample 6	20	1000	0.2	12
Sample 7	25	500	0.3	12
Sample 8	25	700	0.2	16
Sample 9	25	1000	0.25	8

5.5.2   Experimental Results and Analysis

a)   Experimental Results

The samples were measured before and after polishing, using a Dektak XT stylus profiler. Five measures are taken over the surface, with one in the middle and four others around the edges. Approximately the same location is used during measurement to increase the validity of the experiment. The measurement length is 4.8 mm long using a Gaussian regression filter with standard cut-off Lc (0.8 mm) and Ls (0.025 mm). Table 5-5 shows the average of the initial condition, average of the final condition, variance, S.R. ratio and S/N ratio (Signal to Noise Ratio). The variance is the difference between the average initial and final results. The S.R. ratio is calculated using the equation (5.1) and it represents the proportion of the variance with respect to initial value. The S/N ratio is a measure of signal power relative to noise power. It helps to identify the robustness of signal over noise to reduce variability in parameters in order to obtain the combination with highest signal [220]. There are different formulae of S/N ratio based on the experimental goal. In this chapter, the aim was to achieve the smoothest surface possible with the biggest S.R. ratio. Therefore, the S.N ratio was based on "larger the better" case. The formula used to calculate the S/N ratio is shown on equation (5.2).

$$S.R.ratio = \frac{Ra\ before\ polishing\ (nm) - Ra\ after\ polishing\ (nm)}{Ra\ before\ polishing\ (nm)} \quad (5.1)$$

S/N ratio $= -10Log(\sum(\frac{1}{Y^2})/n)$ (5.2)

Where Y is S.R. ratio

Table 5-5:   Taguchi experimental results

Samples	Ra before polishing (nm)	Ra after polishing (nm)	Variation (nm) ΔRa= Ra before - Ra after	S.R. ratio	S/N ratio
1	34.476	21.168	13.308	0.39	-8.27
2	28.05	14.93	13.12	0.47	-6.60
3	25.546	5.604	19.942	0.78	-2.15
4	26.726	16.934	9.792	0.37	-8.72
5	37.742	12.78	24.962	0.66	-3.59
6	25.482	11.904	13.578	0.53	-5.47
7	26.386	10.764	15.622	0.59	-4.55
8	29.136	16.446	12.69	0.44	-7.22
9	33.06	10.984	22.076	0.67	-3.51

Parameter based S/N ratios (Table 5-6) were calculated using S/N ratio values of individual experiments. The figure 5-5 shows the effect of S/N ratio for each parameter with their levels. The variations within parameters are named level 1, 2, 3 in sequential order (i.e. feed rate: 15=1; 20=2; 25=3) This helps to identify the optimum level of each parameter based on the condition considered on DOE experiments. In this case the optimum levels of each parameter are:

-   Feed rate 25 mm/sec
-   Speed 1,000 rpm
-   Offset 0.3 mm
-   Number of passes is 8

Table 5-6:   S/N ratio response table

Level	Feed Rate (mm/sec)	Speed (rpm)	Offset (mm)	No of Passes
1	-5.673	-7.181	-6.985	-5.122
2	-5.927	-5.803	-6.276	-5.54
3	-5.093	-3.709	-3.432	-6.031
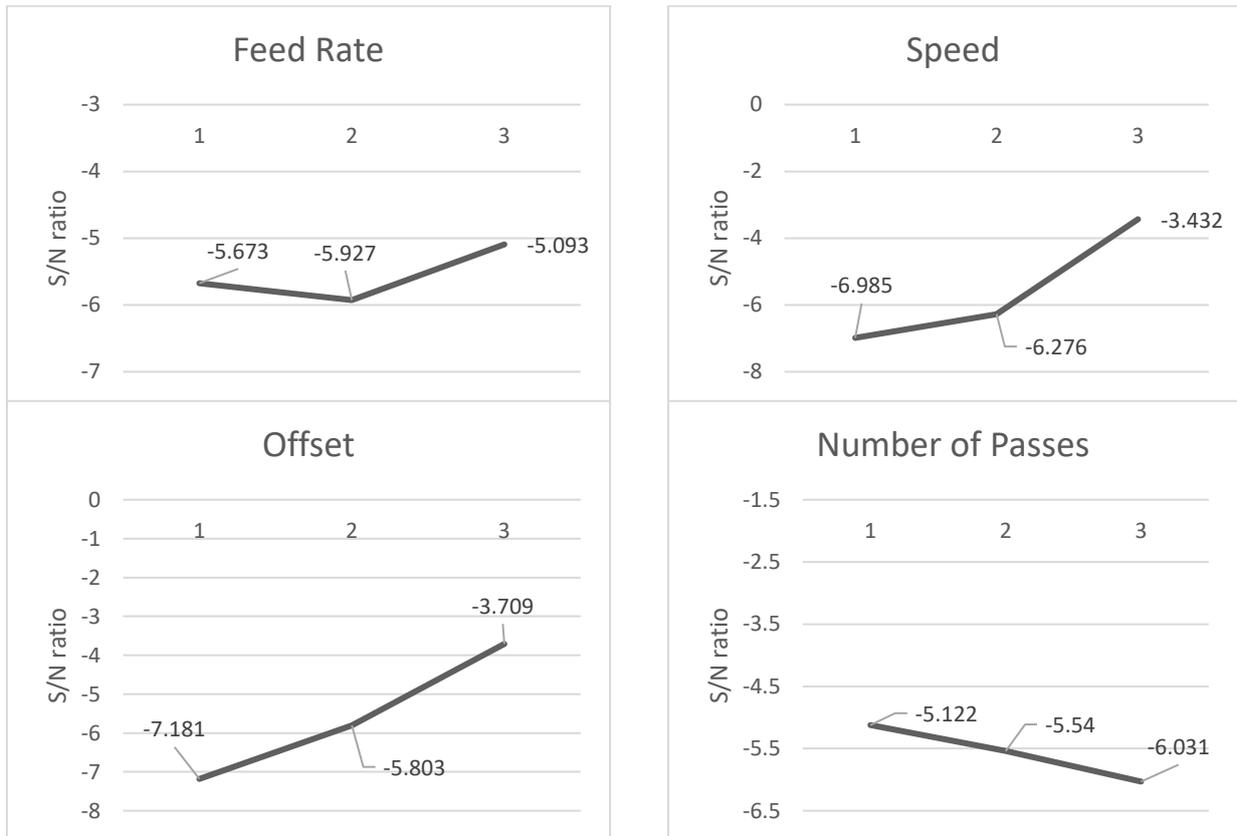
Figure 5-5: The effect of S/N ratio on level of parameters

b) ANOVA

The variance in experimental results is analysed using a statistical method called Analysis of Variance (ANOVA). ANOVA helps to identify the percentage contribution of each analysed parameter with respect to overall output. The following formulae were used to calculate values presented in Table 5-7 which helped to identify the percentage contribution.

(1) Degrees of Freedom (DOF)

DOF depends on the variability of the experiment and helps in obtaining the independent amount of data which can be used for calculation.

$$f = Number\ of\ level - 1$$

$$f_{Total} = Number\ of\ experiment - 1$$

(2) Sum of Squares

The deviation from the mean value of the experimental data is calculated using sum of squares. The total deviation is obtained through the sum of all squared deviation.

$$S_T = \sum_{i=1}^{n}(Y_I - \bar{Y})^2 \quad (5.3)$$

S_T is the total deviation, Y_i is the ith experimental data and $\bar{Y}$ is the average value of Y_i.

112

(3) Variance

Variance spreads the average of data.

$$V = \frac{S}{f} \quad (5.4)$$

S is the sum of square of each parameter and f is the DOF of each parameter

(4) F-value

F-value, also called F statistic, is used to calculate the ratio of variance with respect to the variance error.

$$F = \frac{V}{V_e} \quad (5.5)$$

V_e is the variance due to error factor. $V_e = S_e/f_e$

(5) Pure sum of squares

Pure sum of squares removes the variability error due to noise factor. This can be obtained using the following equation:

$$S'_i = S_i - f_i \times V_e \quad (5.6)$$

(6) Percentage of contribution

It calculates the percentage of contribution of each parameter using information from pure sum of squares and the total sum of squares.

$$P_i = S'_i \times 100/ S_T \quad (5.7)$$

Table 5-7: ANOVA

	DOF	Sum of squares	Variance	F-Value	Pure sum of squares	Percentage of Contribution	Rank
Feed rate	2	2.085	1.0425	2.11	1.095	2.34%	4
Speed	2	19.327	9.6635	19.52	18.337	39.14%	2
Offset	2	22.213	11.1065	22.44	21.223	45.30%	1
No of Passes	2	2.23	1.115	2.25	1.24	2.65%	3
Error	2	0.99	0.495	1.00	4.96	10.59%	
Total	8	46.845	5.855625			100.00%	

Table 5-7 presents the results from the calculation carried out using equation from (5.3) to (5.7). The results show that the greatest contribution to improving surface roughness is provided by the offset, counting for 45.3%, followed by speed (39.1%), number of passes (2.65%) and finally the feed rate (2.34%), which has the least contribution. It is interesting to note that the work carried out by Zeng et al. on improving the surface roughness on CoCr using Zeeko IRP200 showed that tool pressure (48.84%) has the greatest contribution, followed by tool offset (22.68%), head speed (6.26%) and precess angle (4.44%) [206]. The tool pressure and offset are both related to the pressure applied by the tool onto the workpiece. In the present case, the offset itself applies the pressure onto the workpiece and has the highest contribution. In Zeng's work, the head speed was the next contributor to roughness improvement, which corresponds with the present experiment in that it also shows the speed after offset. This indicates that on bonnet polishing surface roughness, improvement relies mainly on the pressure applied by the tool onto the workpiece, followed by the surface speed on the interaction between tool-workpiece. This is reminiscent of the well-known Preston equation (5.8) in which the material removal rate (MRR) is obtained from the multiplication of K (Preston coefficient), P (contact pressure) and V (tool velocity relative to workpiece).

$$MRR = K \times P \times V \quad (5.8)$$

c) *Confirmation Test*

The results obtained from the DOE were analysed and the optimum combination of parameters identified. Table 5-8 summarises the optimum conditions. The expected improvement in surface roughness is $Y_{expected} = 0.84$. Two samples were polished with the optimum conditions and the results obtained are presented in Table 5-9. Test1 and Test 2 have respectively 22.81 nm and 27.41 nm Ra as the average initial surface roughness. After the polishing, the average Ra reduced to 5.66 nm and 6.98 nm, respectively. Both tests provided an improvement of almost identical S.R ratio of around 75%, with the expected S.R ratio to be 84%. A areal map of the test specimens was obtained using a white light interferometer CCI (Taylor Hobson) and is presented in figures 5-6. The surface topography shows that most of the intensity of scratch marks has been greatly reduced by this polishing process. However, some deeper marks are still present on the surface.

Table 5-8: Taguchi optimum polishing conditions

Feed Rate	Speed	Offset	No of Passes
25	1000	0.3	8

Table 5-9: Confirmation test results

	Ra before polishing (nm)	Ra After polishing (nm)	S.R ratio	Expected S.R ratio
Test 1	22.81	5.66	75.19%	84%
Test 2	27.41	6.98	74.53%	

	Before Polishing	After polishing
Test 1		
Test 2		
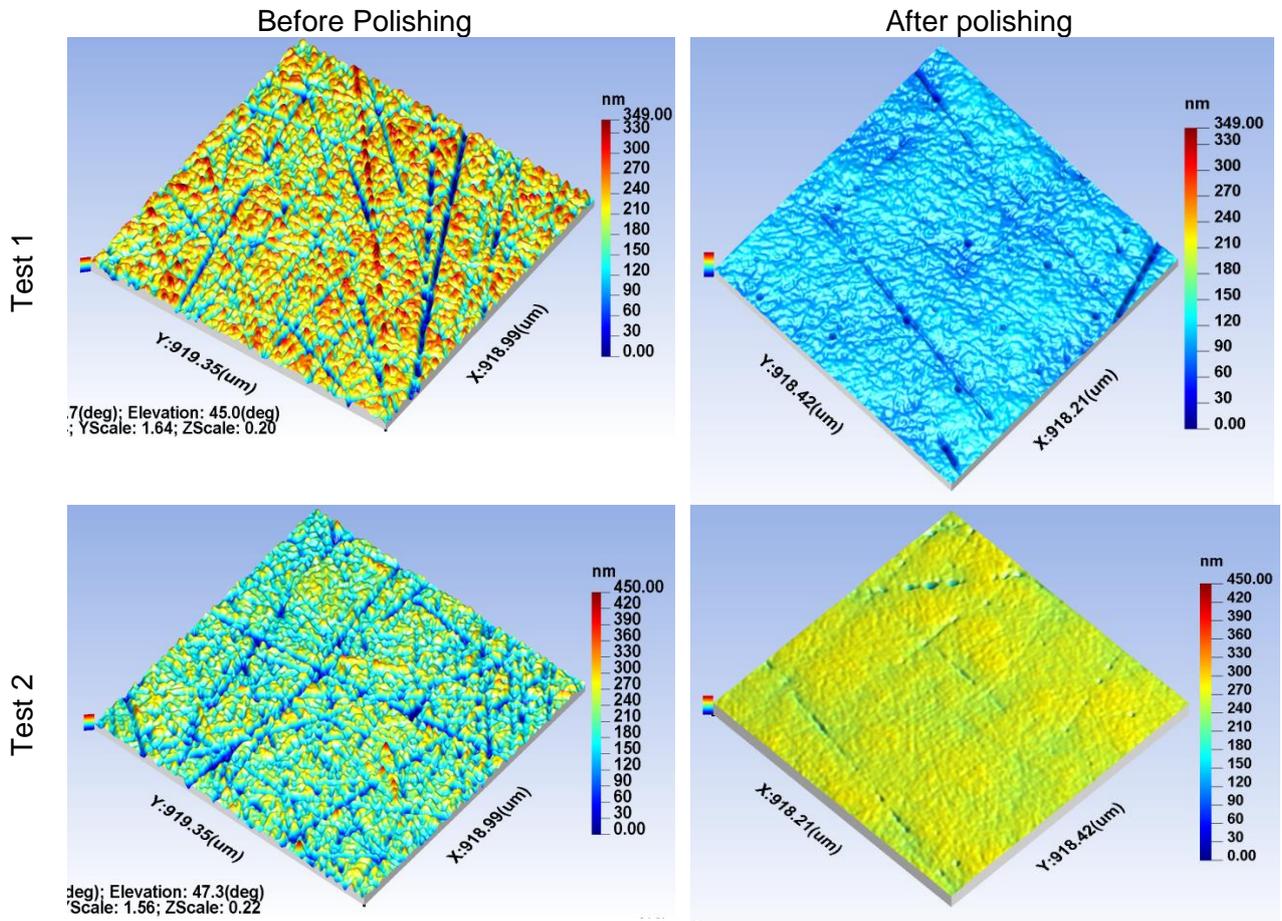
Figure 5-6:   3D surface topography of before and after Taguchi test polishing

5.6   Polishing with re-circulating slurry

It is commonly considered that recirculating slurry polishing has the ability to provide a more reliable surface finishing than other polishing components, such as paste, suspension, etc. Recirculating slurry polishing improves the stability of the polishing process by various factors. The amount and the concentration of abrasive present on the contact area between the polishing cloth and the workpiece is controlled over the entire polishing surface. The temperature around the contact area is also better controlled. It can further reduce the surface roughness beyond the roughness achieved using paste. Therefore, industrial polishing processes use re-circulating polishing as their final finishing process.

5.6.1   Workpiece holder for re-circulating slurry process

The designed machine has a re-circulating slurry system as presented in chapter 4. Pipes are available to circulate the slurry flow. However, the workpiece holder using the chuck is not designed

for this purpose. It would let the slurry flow freely allowing it to be collected at the corner of the base tray cover. A new workpiece holder was designed to avoid the slurry contaminated the surrounding components and to enable the flow to return to the tank. The bill of materials is presented in Table 5-10.

Table 5-10:   Design of workpiece holder for re-circulating slurry.

	Container: The new workpiece holder is designed to hold only a Ø30 mm cylinder. It has the form of a container with the workpiece held in the middle. The side wall is raised to contain the slurry and a hole in the container directs the slurry towards the inlet pipe of the re-circulating slurry system. This container is designed to be 3D printed, as the machining of such a component would be relatively expensive.
	Fastening plate: The container is fastened to a plate with matching holes. The plate also has a M8 thread in the middle to be fastened with the three point aligning disc.
	Cylinder: To avoid the bending of inlet pipe, a cylinder of Ø60 mm and length of 100 mm is used to raise the workpiece position from the three-point levelling disc. It has a Ø8.5 mm through hole to allow the M8 long screw to go through.
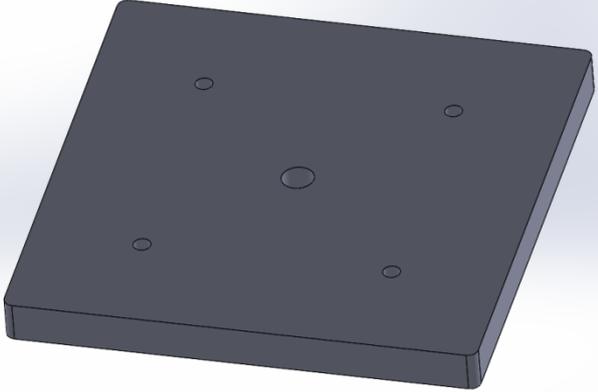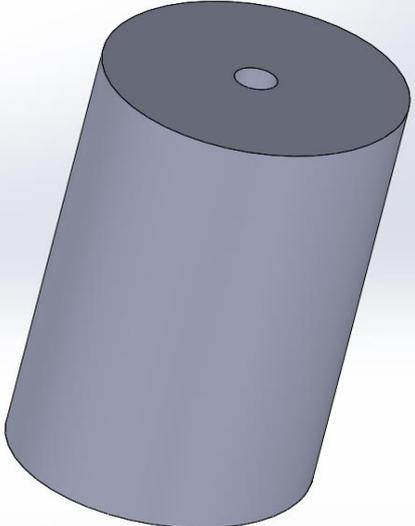
Table 5.10 continued:	
	Three points aligning plate: This plate has a hole in the middle to fit the M8 counterbore screw. There are also three equally spaced, fine treaded M6 holes designed to align the workpiece with respect to hexapod axis. The through holes near the M6 threaded holes are in line with threaded holes of the workpiece holding unit. Once the workpiece is aligned, it will be fastened to the workpiece holding unit via these through holes.
	Design Assembly: The figure on the left shows the section view of the assembly. The container is 3D printed. All other components of the assembly are machined in aluminium and painted in black. Container Fastening plate Cylinder Three points aligning plate Workpiece holding unit
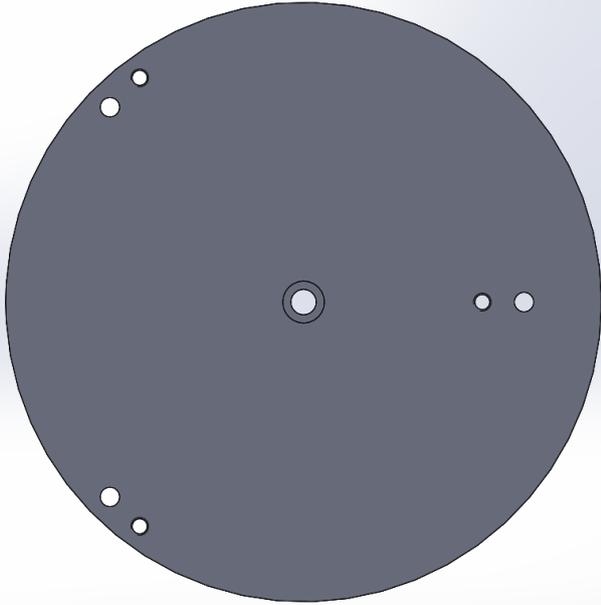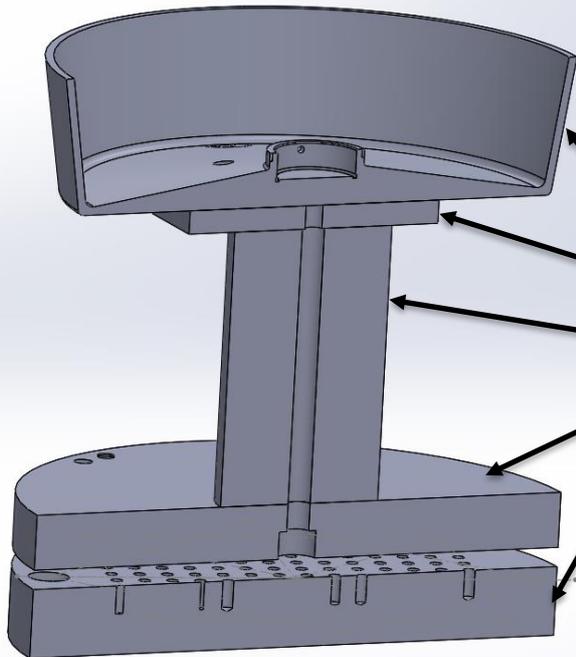
The new workpiece holding assembly was mounted on the polishing machine and connected to the slurry tank. Figure 5-7 shows the outlet pipe from the tank being directed on to the workpiece surface. The inlet pipe collects the slurry from the container and sends it back to the tank.
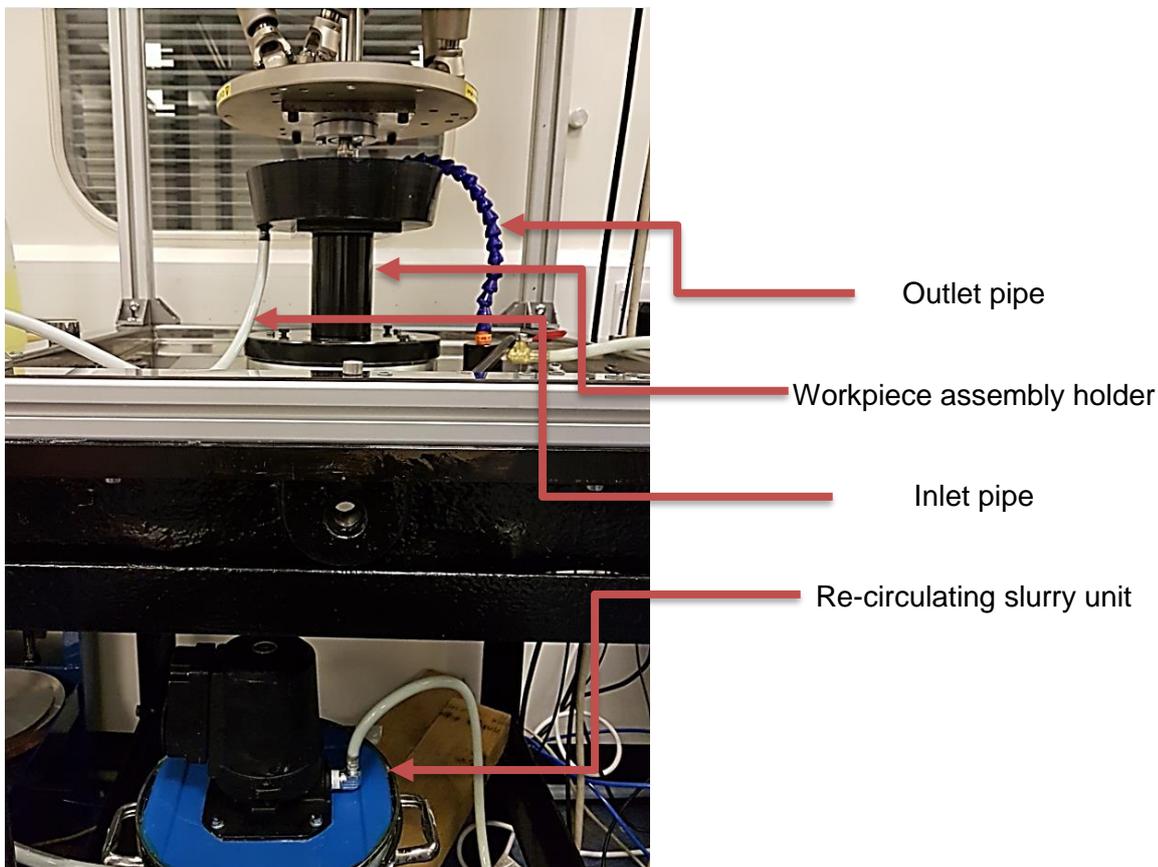
Figure 5-7:   Slurry flow working principles

5.6.2   Kistler load cell contact detection

a)   Force sensor calibration

As explained above, the contact between the workpiece and the tool was initially identified visually and with the help of shims. However, visual contact detection is not possible for the new workpiece holder with the container's side wall higher than the workpiece surface. A force sensor (type 9031A) from Kistler was therefore used to detect the contact between workpiece and tool. The same instrument was used to align the workpiece parallel to the hexapod X and Y axis. Objects with known masses were placed on it in order to obtain accurate results from the sensor and understand it's sensitivity. The results obtained were verified against the object's own forces. The masses of small objects used for sensor calibration process were comparable to the force applied while polishing. These masses were measured on a balance and converted into forces and placed on the force sensor; the measured force from the sensor was then compared with force obtained from the balance. Table 5-11 below presents the results obtained. A very good correlation between the scale and the force sensor from 0.1 N of force was observed. The table 5-10 below also indicates the smallest force that the sensor can detect accurately, which is around 0.1 N.

Table 5-11: Force sensor calibration

Object mass on scale (Kg)	Force (N)	Force measured using the sensor (N)
$1.5*10^{-3}$	0.015	Cannot read any change
$4.4*10^{-3}$	0.043	0.015
$9.1*10^{-3}$	0.09	0.1
$27.7*10^{-3}$	0.27	0.28
$87.1*10^{-3}$	0.85	0.85
$197.6*10^{-3}$	1.94	1.95

b) First contact and offset force measurement

The tool was mounted into the spindle and brought down with small increments until a contact was detected. There was no contact until it reached 20.54 mm away from the origin. At 20.55 mm, the sensor detected a contact and showed a force of 0.1 N on the screen (figure 5-8). This shows a clear contact between tool and the workpiece with 10 µm accuracy. The hexapod was then moved towards the edges of the workpiece sample in X and Y axes and the same method of contact was followed produced to obtain a parallelism between workpiece and hexapod.
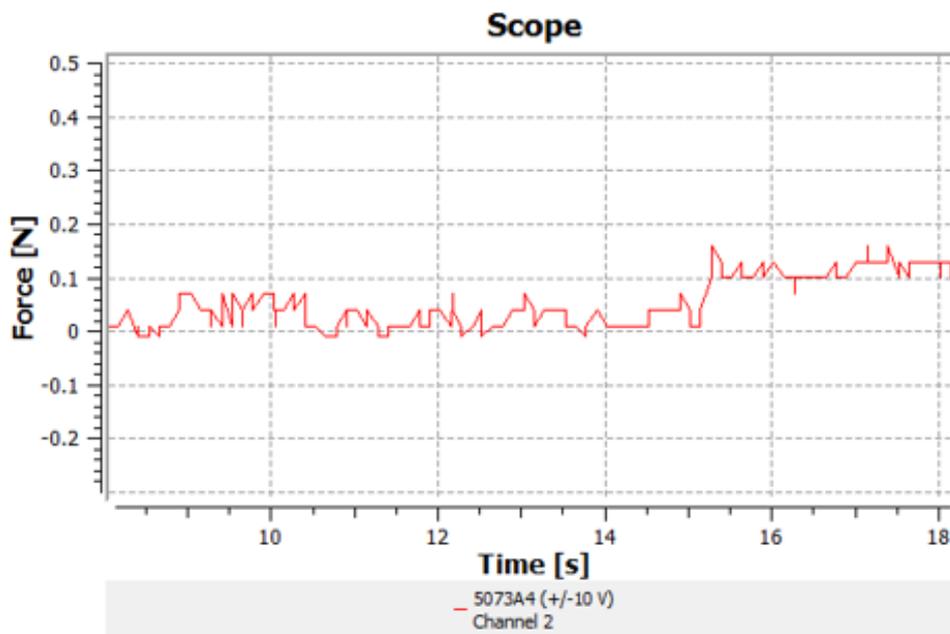
Figure 5-8: Tool-workpiece contact detection with 0.1 N force detected at time 15 seconds

5.6.3 Re-circulating polishing experiment

a) Polishing sample preparation

The polishing sample was initially ground on a conventional grinding machine. It was then turned on a Nanoform diamond turning machine using a CBM tool. The sample was again ground using an ultra-precision grinding spindle which rotates at 80,000 rpm. Figure 5-9 shows the surface roughness of the sample at this stage. The results show an average of 39.4 nm Sa on CCI (Taylor Hobson) with

five measured spots. The sample was then polished using the optimum Taguchi parameters. At this stage, the sample was measured to be 6.4 nm Sa (figure 5-10). This provided an improvement of 84%, as predicted by Taguchi results analysis. The slurry was prepared with alumina suspension abrasives. The particles size was 0.25 µm with specific gravity of 1.040.
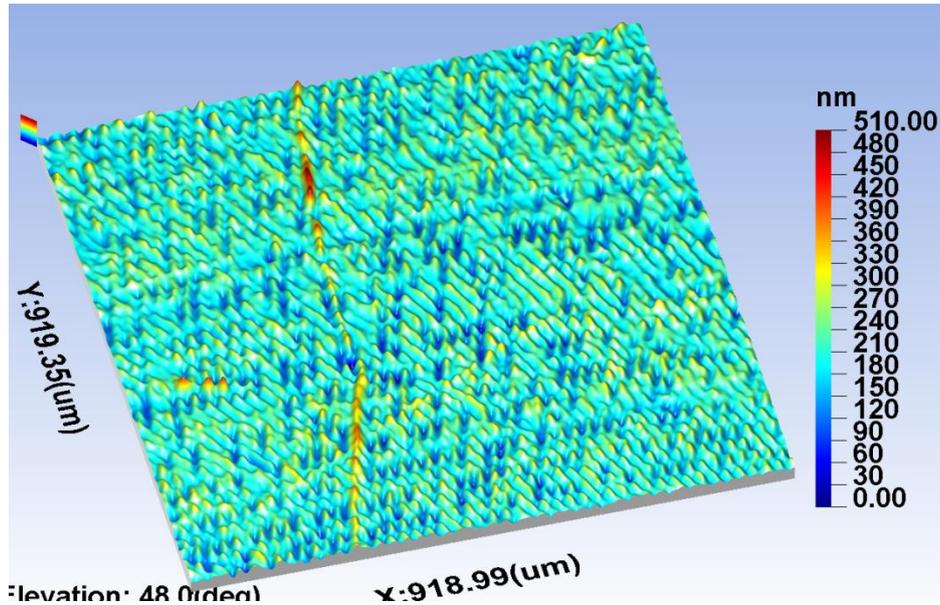
Figure 5-9:   Ultra - precision ground surface
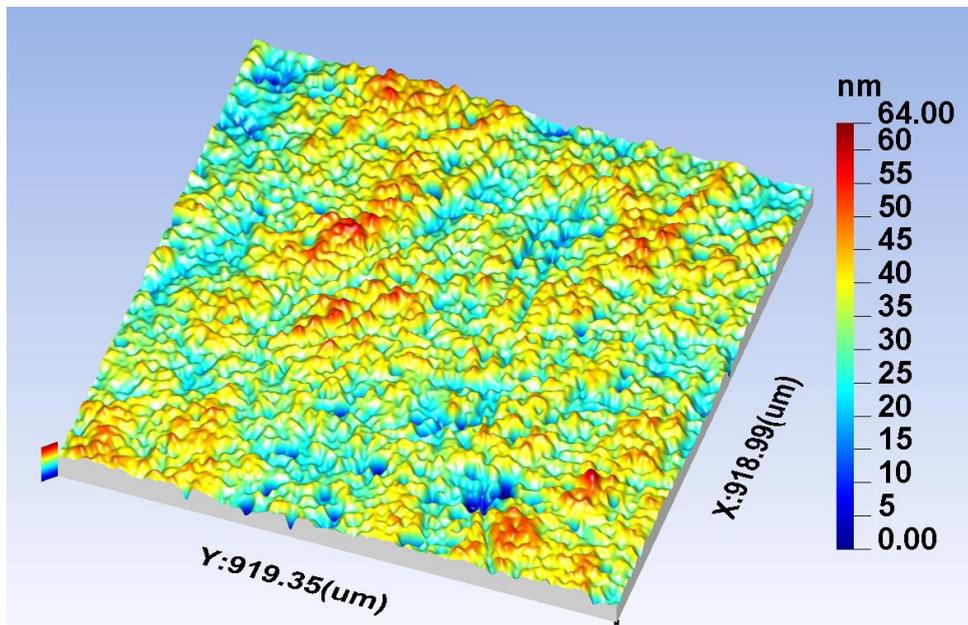
Figure 5-10: 1 µm diamond paste polished surface

b) Re-circulating slurry polishing result

The parameters for polishing were those used in the optimum polishing conditions (Table 5-7), except for the number of passes. As the particles size is small and the slurry concentration is different from paste condition, 25 passes were performed. An average surface roughness of 7.44 nm Sa was obtained after this polishing process. Considering that these parameters were not optimised for this type of initial condition, the results obtained are just a proof of concept for re-circulating polishing. Figure 5-11 shows the image of surface topography after the polishing process.
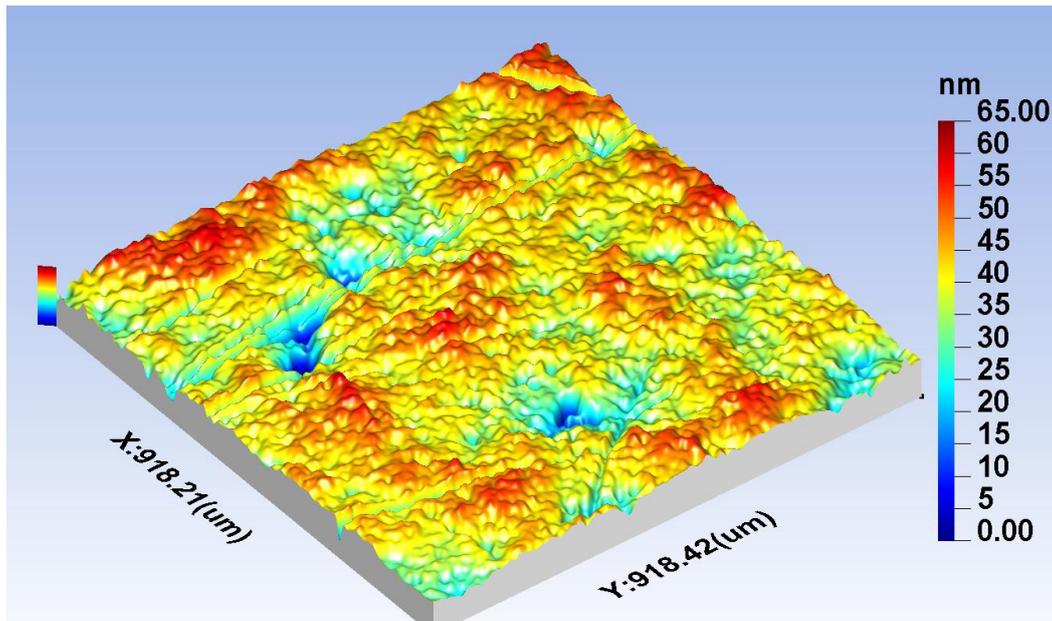
Figure 5-11:   0.25 μm re-circulating slurry polished surface

5.7   Summary

This chapter describes the experiments designed to improve the capability of the designed machine as a final finishing process to reduce surface roughness. P20 hard steel was chosen to polish in these experiments. This material is widely used in the injection moulding industry for its quality, reliability and performance. The hexapod was programmed using robotic commands called general command set (GSC). A program for polishing flat surfaces which cover 28 mm^2 was created using excel. The workpiece is a Ø30 mm cylinder, cut to equal length and ground on a conventional grinding machine. The samples were further hand polished to reach approximately 40 nm Ra surface roughness. The workpiece was held on a three-point chuck which is centred and aligned to hexapod origins.

Empirical experiments were initially performed to understand the influence of parameters on surface roughness variation. Inconsistency in the results obtained were identified. For same parameters and initial surface conditions, polishing results showed large variation in roughness. The investigation reveals the importance of other factors such as polishing pad, abrasive and polishing liquid. It was found that the wear of the pad affects the force applied on the workpiece for the same amount of offset. The amount of paste applied over the polishing surface affects the removal rate, hence

surface roughness. Polishing fluid helps to reduce the visibility of scratch marks; however, the amount of liquid applied needs to be controlled to obtain a consistent result. Once these parameter conditions were fixed, consistency in results was obtained.

The Taguchi method was used to optimise the parameters for surface roughness reduction. Four parameters with three levels were considered for the experimental analysis. A standard OA L9 (3^4) was chosen for the DOE. Optimising parameters were feed rate, speed, offset and number of passes. The variation between initial and final surface roughness Ra values were used to calculate the S/N ratio. The optimum polishing conditions were identified using S/N ratio effects on parameters level. Feed rate (25 mm/sec), speed (1,000 rpm), offset (0.3 mm) and 8 number of passes were the optimum conditions based on experimental design for surface roughness improvement. A reduction of 84 % in surface roughness was predicted. Two test samples were polished with the optimum parameters. Both samples achieved around 75 % improvement with a slight difference from the prediction. The Taguchi method was therefore considered to be fairly robust.

A statistical method called ANOVA was used to evaluate the impact of each parameter on surface roughness reduction. Several statistics, including Degrees of Freedom, Sum of Squares, Variance, F-value, Pure sum of squares and Percentage of contribution were calculated. Results from this analysis of variance indicate that the greatest impact on surface roughness reduction is obtained from the offset (45.3 % of contribution), followed by speed (39.14 % of contribution), number of passes (2.65 % contribution) and, finally, feed rate (2.34 % of contribution). There are also 10.59 % contributed to error which refers to the noise ratio of the experimental process. It was also observed that the two main contributors follow the Preston equation on material removal rate. Other studies conducted on the bonnet polishing process have similar results.

Finally, polishing using a re-circulating slurry system was also tested. A new workpiece holding system was designed and produced to ensure the flow of slurry around the workpiece and the tank without contamination from the external environment. A force sensor from Kistler was used to identify the contact between tool and workpiece. The same instrument was used to align the workpiece surface parallel to the X and Y axes of the hexapod. This polishing experiment was conducted with parameters identified as optimum in the Taguchi experiment, except for the number of passes chosen to be 25. The slurry contained alumina oxide abrasives with particle size of 0.25 μm and gravity 1.040. Experimental results showed a slight deterioration of surface roughness after 25 passes, going from 6.4 nm Sa to 7.4 nm Sa average. The parameters need to be optimised using Taguchi for further improvement.

6 Development of grolishing process for P20 tool steel

6.1 Introduction

Grolishing is a process first developed by Walker et al. [190]. It is aimed to be used as an intermediate process between grinding and polishing. Grolishing process helps to reduce considerably the pre-polishing time thus rendering it suitable in industrial environments. It also removes the undesirable effect of manual rough polishing which is prone to cause form errors and uneven surface finish to the final component. This also helps to remove the need for expensive machines for an intermediate step between machined finish and polished finish. Moreover, the Grolishing process helps to remove mid-spacial frequency errors resulting from the machining and precision grinding process. Polishing a component which has previously been ground is difficult. Machined and ground marks are not totally removed, which are undesirable for optical applications. The grolishing process remove previously machined marks and enables a faster removal rate for smoothing the surface and also facilitates form correction [14, 189].

There are a number of grolishing techniques described in the literature. These can be categorised into three different groups. The first uses a hard tool with bonded abrasives, the second soft bonnet with bonded abrasives, and the third soft bonnet with loose abrasives. Walker el al. have studied the effects of these three grolishing techniques on Zerodur and silicon carbide [190]. The hard tool shows non-uniform removal using IRP600. The authors explain that this could be due to machine bearing errors, since the bearings are designed for soft contact rather than hard contact. The soft tool acts as a damping system which absorbs vibration, whereas the hard tool tends to replicate the dynamic effects of the machine onto the workpiece surface. The author discusses the uniformity of the results obtained, the material removal rate, surface roughness and sub-surface damage. He concludes that several processes have acceptable results which need to be adapted to individual situations.

Charlton and Blunt have studied the performances of grolishing pads on cobalt chrome medical grade material [5]. Two types of pads were evaluated: diamond and non-woven alumina oxide pads. Diamond abrasive cloths are nickel plated. Figure 6-1 shows magnified pictures of a nickel plated diamond cloth made by KSG Diamond (Switzerland). It shows the best and worst case after a single run. Grolishing results show an aggressive material removal; however, after one run, the pad shows signs of wear. Examination of the pad suggested evidence of a chemical reaction due to shell electrons reaction. The reaction caused graphitisation and diamonds were pulled from the electroplated nickel, with remaining diamonds worn smooth in the worst case example. It was concluded that this pad has conclusive results on small areas only due to excessive wear. On the other hand, the non-wooven alumina oxide pads were offered a more consistent cut through their

lifetime by exposing fresh abrasives as the pads wear. This indicates that the wear rate of pads using bonded abrasives could have a significant effect on the consistency of the delivery [5].
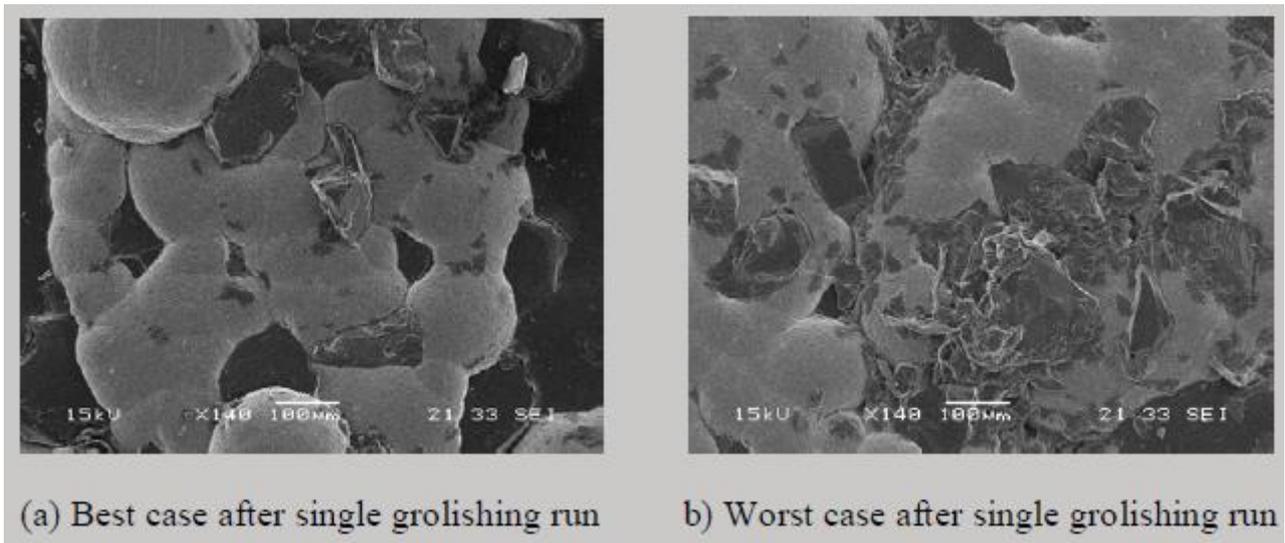
Figure 6-1:   Magnified image of Nickel plated Diamond cloth; (a) Best case with clean and sharp diamond abrasives after first run, (b) Worst case with damaged abrasives due to chemical reactions [4]

Grolishing techniques have proven their importance in reducing mid-spatial frequency errors. Mid spatial frequency errors are periodic wavelengths of different amplitude produced by the precursor manufacturing process. They are considered to be a process error, as they are neither in the surface roughness range nor in the form range. In optical applications, mid spatial frequency errors have a huge impact on the performance of optical components, and can cause light scattering, undesired refraction and other problems affecting the performance of the equipment [12]. Identifying and removing or reducing mid spatial frequency errors is therefore crucial to achieving the desired performance. Literature review shows that grolishing process can reduce the mid spatial frequencies errors quicker than the polishing process on its own. Three main types of grolishing technique have been developed by Walker et al. [190] and their capabilities have been proven to be conclusive. One of the three techniques can be chosen to develop further, based on the specific requirements of the application, such as surface roughness after grolishing, process time, P-V values, sub-surface damage and other requirements. Charlton and Blunt's work using abrasives bonded pads showed that consistent removal can be achieved which is free from chemical reaction between pad and workpiece surfaces [5].

The research on grolishing techniques using loose abrasives mainly focuses on methods using re-circulating slurry. The use of paste has received comparatively little experimental attention, although this method has been proven to be ideal in improving surface roughness and reducing P-V values [190]. Indeed, the combination of polyurethane cloth and 8 μm diamond paste achieved 28.7 nm Sa and 0.729 μm P-V for an initial condition of 136 nm Sa and 3.28 μm P-V, respectively, on silicon carbide. This chapter describes the experimental use of a hexapod polisher to evaluate its capability for grolishing. A hard tool cannot be used with the actual prototype structure, as this would transfer the hexapod motion error and vibration due to hard contact with the workpiece; however, the two other techniques using soft bonnet tools can be performed on the designed machine. The methods using a soft tool and paste abrasives will be investigated, as they are more appropriate for non-flat surfaces and would provide consistent removal over the full test piece surface.

In order to plan the grolishing process accurately, it is important to have information on CNC finish capability of P20 tool steel. In the milling process, the surface quality left by the tool on the component is widely characterised in industry using surface roughness as a measure. The main factors affecting the surface roughness in milling are workpiece material, machining conditions and tool geometry. In order to optimize and obtain low surface roughness, all parameters from those factors are studied using the Taguchi method and response surface methodology (RSM). It was found that both the Taguchi and RSM gave similar results. Using the optimum conditions, Vandhan et al. have obtained surface roughness Ra = 0.615 μm on P20 hard steel [223].

The developing grolishing process will therefore aim to remove machining marks by reducing both the surface roughness and P-V values. The aim is to reach a surface roughness of less than 30 nm Sa and less than 0.7 μm P-V on a flat surface. This chapter describes experiments using two grolishing processes. Results from both approaches will be examined and compared.

6.2   Grolishing experiments preparation

P20 tool steel was obtained as a rod of Ø30 mm. The rod was then cut to equal lengths and the end faces ground flat on a conventional grinding machine. An image obtained from the white light interferometer (CCI from Taylor Hobson) using 20X lens can be seen in figure 6-2. The ground surface finish obtained was equivalent to the type of surface roughness achieved in industry using CNC machining. The grinding marks are clearly visible. At this stage, the surface roughness of the samples was measured to be 0.56 μm Sa. The Sz value was 4.77 μm. The aim of the grolishing process is to reduce both the Sz and Sa value at the same time.
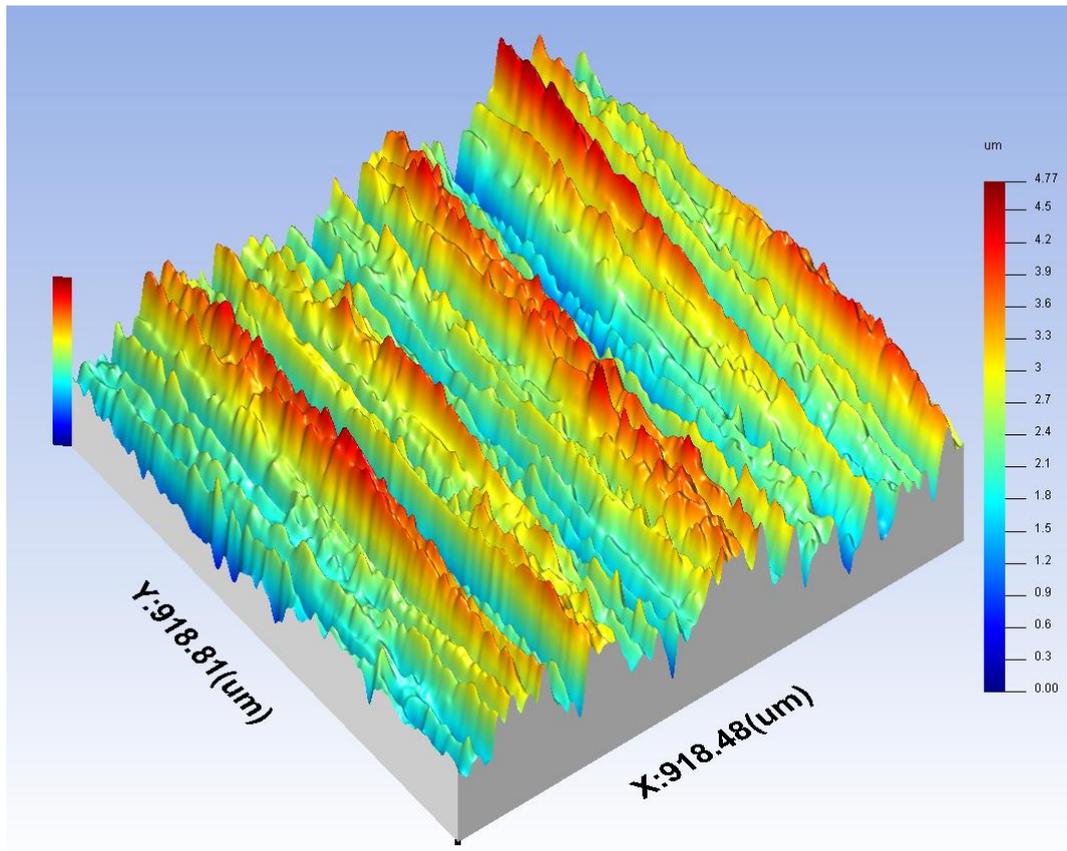
Figure 6-2: P20 tool steel ground finish showing rough surface finish left from manual grinding machine.

6.2.1 Grolishing cloth and abrasive selections

a. Cloth selection

The identification of the grolishing cloth and abrasive paste was essential to the success of the experiment. A polyurethane pad was used at the beginning and it was noticed that, in terms of surface roughness obtained (0.6 μm Sa), the wear of the pad was an issue. The tool preparation time using these pads was also a major concern. Indeed, the pad needed to be soaked in hot water and to be placed on a mould containing the bonnet shape. The mould was then placed in an oven for an hour to allow the pad to take the form of the mould. It was then cut around the circumference and glued onto the bonnet using multi-purpose adhesives. It needed to be left to dry for at least 4h to 24h to reach full strength. The process was therefore time consuming, expensive and not suitable for an industrial environment.

Market analysis helped to identify a range of polishing cloths developed by Buehler. The cloths are designed based on the surface condition of the polishing specimen and material (figure 6-3). P20 tool steel can be considered as soft steel or stainless steel based on material hardness and composition for cloth selection from the table present on figure 6-3. The guidelines provided for P20

indicate the use of UltraPad™ for a coarse surface. UltraPad™ is a hard woven cloth designed for high material removal. For intermediate surfaces, there are several options. VerduTex containing medium hard synthetic silk cloth was chosen because this pad is recommended for almost all types of material (figure 6-4). The pads, which are self-adhesive and 8-inch diameter in size, can be cut to Ø10 mm circles and prepared for polishing within 10 minutes (Table 4-4).

Material Type	COARSE				INTERMEDIATE							FINE		
	UltraPad™	UltraPol™	TexMet™ P	Nylon	TexMet C	TriDent™	VerduTex	VelTex	WhiteFelt™	PoliCloth	MicroCloth™	MicroFloc	MasterTex™	ChemoMet™
Aluminum	●			●	●	●	●	●	●	●	●	●		●
Cast Iron	●		●		●	●	●		●		●	●	●	
Ceramic		●	●			●	●				●			
Ceramic Thermal Spray	●				●	●	●							●
Copper			●	●				●	●	●	●	●		●
Generic Bulk Mount		●	●		●	●	●				●			
Generic Thin Section		●	●		●	●	●				●			
Hard Steels		●	●	●	●	●			●		●	●		●
Heat Treated Steels		●	●						●		●	●		●
High Temperature Solder in Ceramic	●		●				●	●			●			●
Metallic Thermal Spray							●	●						●
Micro-Electronic Material	●		●				●	●			●		●	●
Nickel Base Alloys		●	●	●	●	●	●		●	●	●	●		●
Non Populated PCB	●				●	●	●				●		●	●
Polymers					●						●	●		
Silicon in Micro-Electronics					●	●					●		●	●
Sintered Carbides		●	●				●							●
Soft Steels	●			●	●	●	●	●	●	●	●	●	●	●
Stainless Steel	●			●	●	●	●	●	●		●	●		●
Titanium	●	●		●	●				●		●	●		●

Figure 6-3: Buehler polishing cloths guidelines based on workpiece material and initial surface roughness condition [224]

UltraPad™
Hard woven, no nap
6µm & up, Diamond

VerduTex
Durable, medium hard synthetic silk cloth
9 to 1µm, Diamond
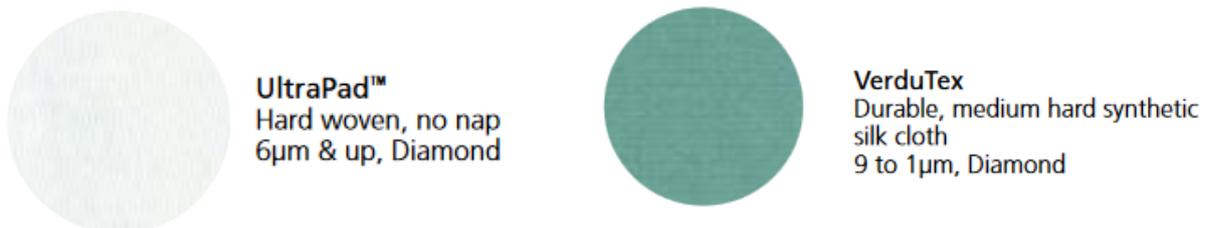
Figure 6-4: Grolishing pads chosen for experiment : Coarse Surface roughness (left) Intermediate surface roughness (right) [224]

b. Abrasive selection

At this stage of the experiment, paste based abrasives are preferred to re-circulating slurry, since they are quicker, cheaper and provide meaningful results without the need for major "polishing machine clean downs". During the empirical experiment, different abrasive grain sizes were tested. It was observed that fine abrasive did not improve the surface roughness of the coarse surface and that large abrasives increased surface roughness when applied to the smooth surface. Abrasive

grain sizes should therefore be adapted to the initial surface condition of samples. Paste containing 45 µm diamond abrasives is used on rough surfaces, followed by 9 µm paste to remove scratch marks left from the previous process and further improve the surface roughness in preparation for final polishing stage.

6.2.2 Tool – Workpiece contact area (Spot size)

a. Theoretical spot size
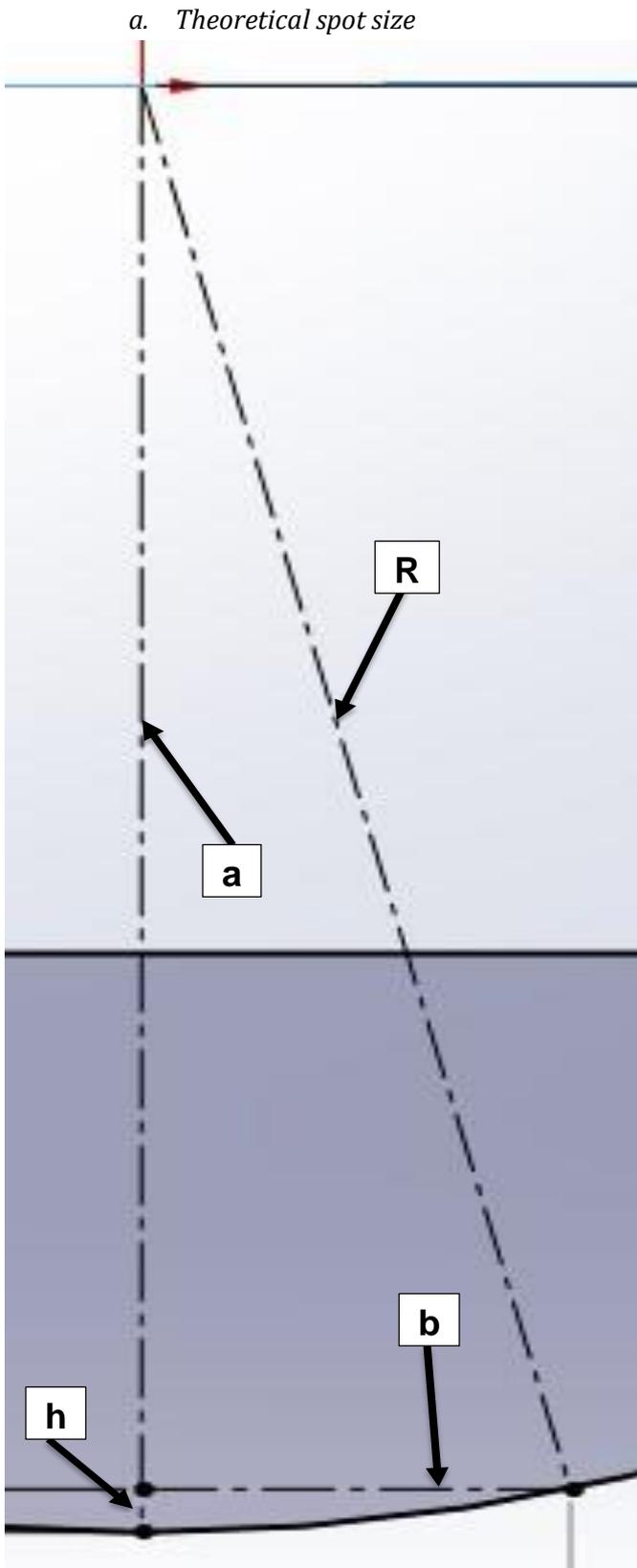
Figure 6-5: Spot size calculation diagram

The term spot size refers to the contact area between tool and workpiece, depending on the tool offset. Calculation of the theoretical spot size is based on the diameter of the tool rubber bonnet with the polishing pad on the bonnet. The mould used has Ø20 mm. The bonnet and the pad are pressed against the Ø20 mm mould. Therefore, it is assumed that the polishing tool will have Ø20 mm at the bonnet surface. The diagram used for calculation is shown on figure 6-5.

Pythagorean theorem:

$$R^2 = a^2 + b^2$$

$$a^2 = R^2 - h^2$$

- ❖ R is the tool rubber bonnet radius. In this case, this should be 10mm radius.

- ❖ h is the tool offset. Three different offsets are used: 0.1mm, 0.2mm and 0.3mm

- ❖ b is the offset radius.

- ❖ a is the distance between the origin of bonnet radius and the origin of offset radius.

So for 0.3mm offset:

$$b^2 = R^2 - (R^2 - h^2)$$

$$= 10^2 - (10 - 0.3)^2$$
$$b^2 = 5.91$$
$$b = \sqrt{5.91} = 2.43mm$$

The diameter of the theoretical spot size for 0.3 mm offset is Ø4.86 mm. The same equation is used to calculate the theoretical spot size when using a 0.2 and 0.1 mm offset. These values are calculated to compare with the actual spot size for different offsets.

b. Experimental spot size

The tool was prepared with the UltraPad™ cloth. The spindle speed was 5,000 rpm. Diamond paste containing 45 μm abrasives was applied on the workpiece surface. The tool was brought into contact with the workpiece at different offsets and left in that position for 2 minutes. The contact area was measured using a Dino capture microscope. The microscope was used to take pictures of the surface. The software has measuring facilities with microns precision. A ruler was used to calibrate the microscope.

All offsets were measured on Dino capture 2.0. For each offset, there were two circles (blue and red) covering the contacted area. The blue circle covered the whole contact area whereas the red circle only covered the impact area (where material removal is noticeable). Figure 6-6 contains all three offset pictures. The pictures of these three offset show no removal in the middle, the main reason being that that the surface speed approaching the center of the tool was effectively zero. The grolishing produced in the red circle region is caused by two body abrasion. The abrasives embed in the polishing cloth and cause removal by micro cutting and micro ploughing. This produces circular micro grooves on the grolishing surface reflecting the rotating movement of the spindle. The spot size reflecting two body abrasion (red circle) will be called impact spot size. The region covered between red and blue circles has only scratch marks without actual penetration of abrasives into the workpiece. This is called "three body abrasion", where the abrasives roll between the grolishing cloth and the workpiece causing micro cracks and micro fatigue. This produces micro indentation on the workpiece surface[186, 225]. Blue circle covers the overall area of contact between tool and workpiece and will be called contact spot size. All three offsets have two body abrasion in the middle and three body abrasion in the outer region. This can be explained using Hertz contact theory[171] for a spherical surface in contact with a flat surface. The middle of the contact area has high pressure which causes removal by micro cutting, but, moving towards the circumference the pressure reduces to zero where the abrasives roll between polishing cloth and workpiece.

0.1 mm Offset   0.2 mm Offset   0.3 mm Offset
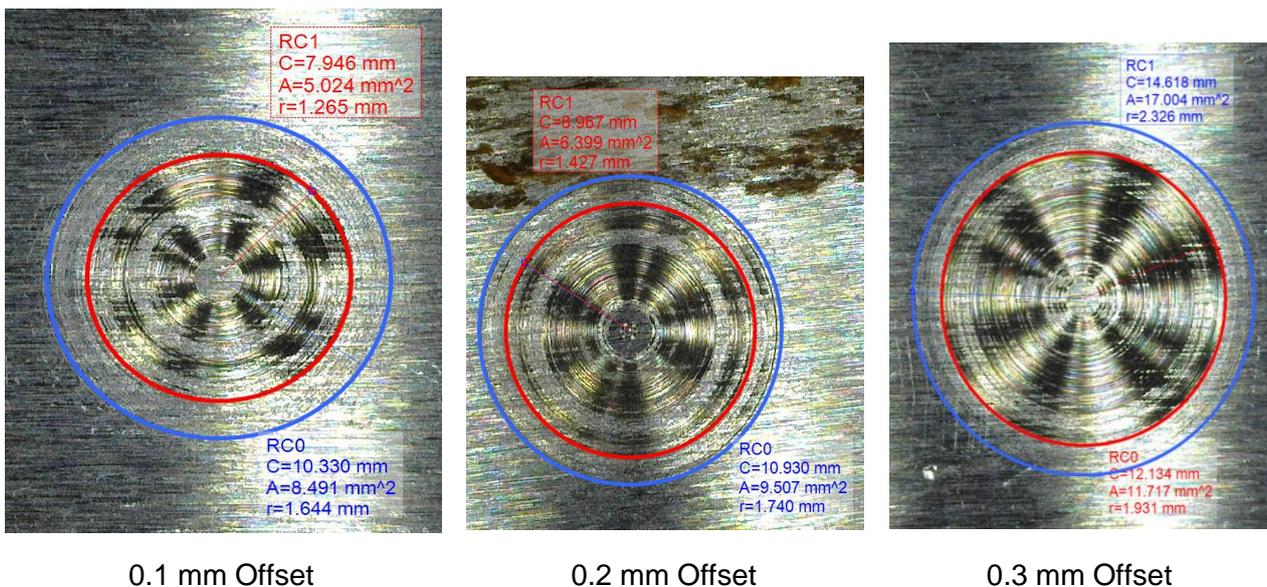
Figure 6-6:   Offset measurements on Dino microscope

The theoretical and measured results are combined in figure 6-7. The line with round marker shows the diameter of theoretical spot size, square marker shows the diameter of contact spot size and triangle marker shows the diameter of impact spot size. The theoretical and contact spots are very close in size. However, for 0.1 mm offset, the contact spot size is slightly bigger than the theoretical spot size and, for the other offsets, the contact diameters are slightly smaller than the theoretical spot size. The thick layer of 45 µm diamond abrasives is affecting the contact diameter for 0.1 mm offset. Otherwise, the discrepancy in results between theoretical and contact spot size comes mainly from the contact position error between tool and workpiece. Indeed, a 20 µm error on the contact position would increase the theoretical spot size of 0.1 mm offset to Ø3.09 mm instead of Ø2.82 mm. On the other hand, the impact spot size is dependent on the pressure applied from the tool offset. It follows the contact spot trend with smaller diameter. In the grolishing process, a large amount of material needs to be removed in a short period of time to ensure that the process is efficient. Two body abrasion obtained through impact spot size will therefore be considered for the development of the grolishing process. The force sensor from Kistler used to measure the contact detection (Chapter 5) was also used to measure the offset force. The data collected was used to produce the graph presented in figure 6-8, which gives information on the amount of force applied for each offset and can be used in future to predict the material removal rate for form corrections. The force applied on the workpiece increases linearly with the increase of offset. A force of 8 N was measured for an offset of 0.3 mm.
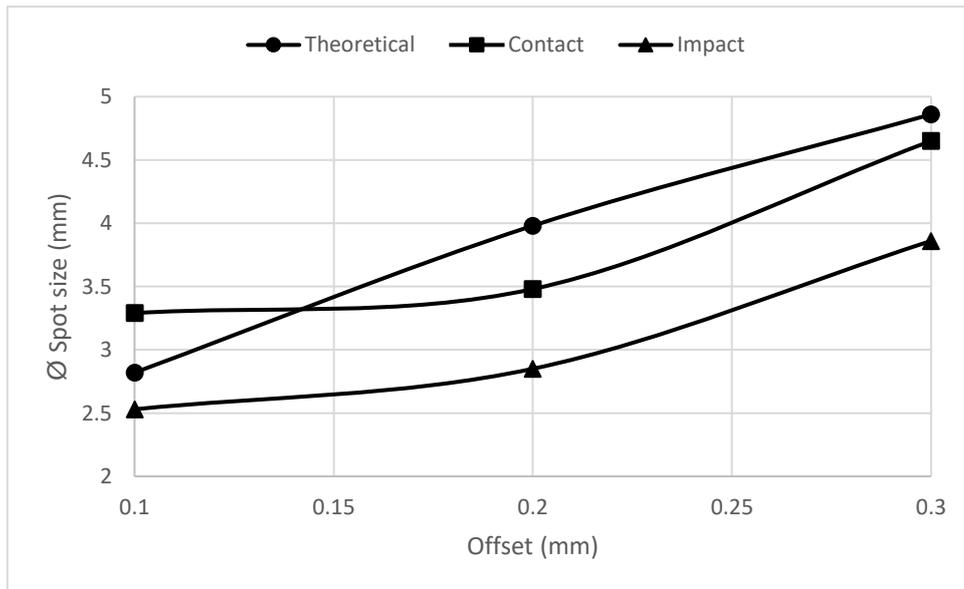
Figure 6-7:   The change in theoretical and experimental spot size with respect to tool offset.
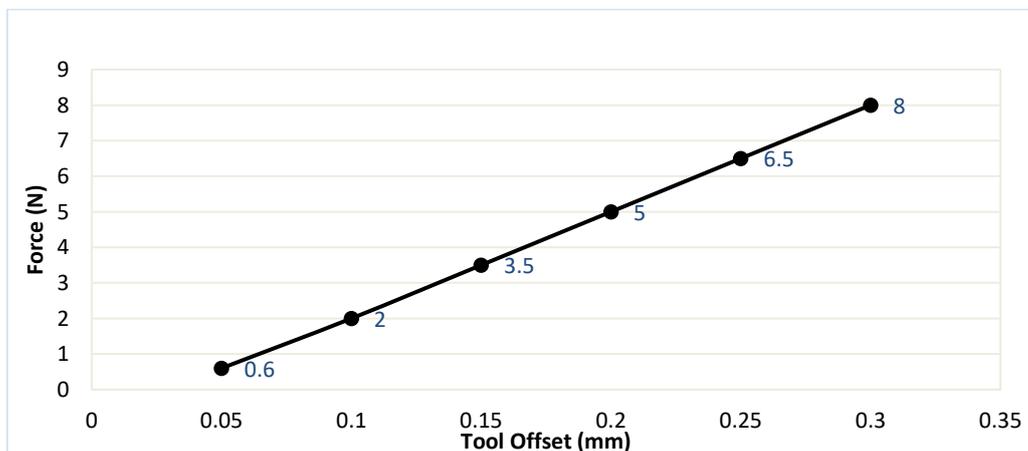
Figure 6-8:   Force (N) obtained from tool offset (mm

131

6.2.3 Grolishing trials

a. Line grolishing

During the polishing or grolishing process, the tool will always be in movement at the selected feed rate. It is important to understand the additive effect of the feed rate on the material removal process. In practice, grolishing processes with a linear line movement is produced on a workpiece. All three offsets were tested. The produced program moves 10 mm in the X axis and returns on the path to the initial position. The selected feed rate was 1 mm/sec. Figure 6-9 shows the grolished surface waviness profile of these three offsets which are measured using a contacting stylus instrument (PGI Taylor Hobson).
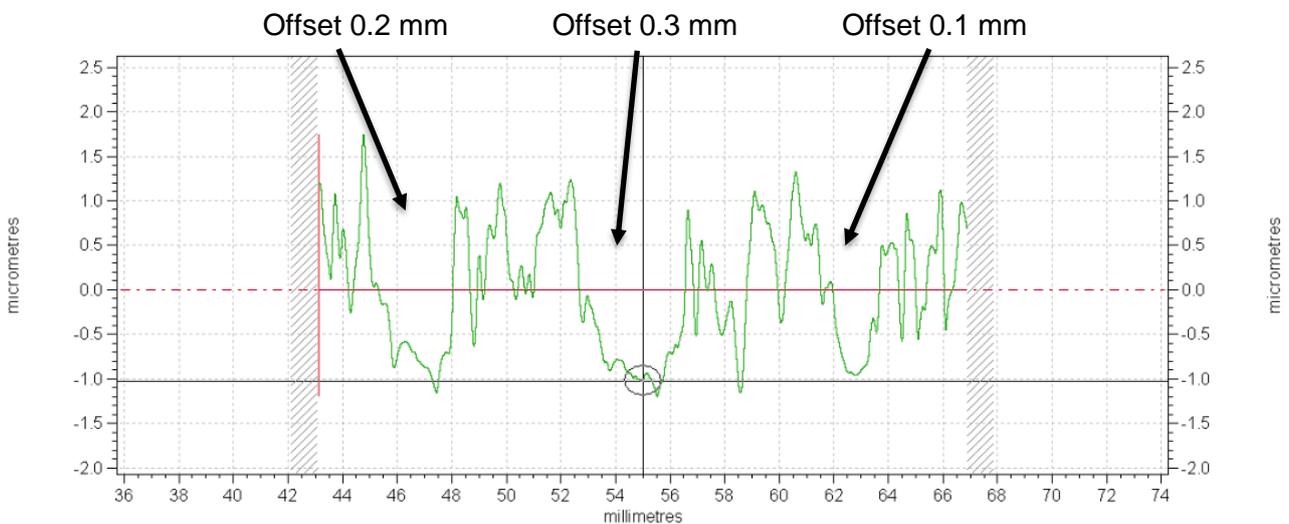
Figure 6-9:   Line grolishing results on PGI, showing the depth and width of removal for different offsets

The result indicates that all three offsets achieved a depth of two micrometres from the initial rough surface. The width of the profile was observed to be approximately three millimetres for 0.2 mm offset, four millimetres for 0.3 mm offset and 2.3 mm for 0.1 mm offset. These widths were consistent with the impact spot size measured previously. It is interesting to note that the effect of the feed allows material removal in the middle, although the surface speed is null in the middle. Indeed, while the tool is in movement on the workpiece, each segment of the workpiece is crossed by the tool full contact area. This produces material removal in the middle.

b. Grolishing small area

A grolishing program was created to cover 5 mm². This was a raster program with 0.5 mm step size. The program initially runs parallel to the X axis and then parallel to the Y axis of the machine. The feed rate was set at 1 mm/sec, with 0.3 mm offset and 45 µm diamond paste applied on the surface. Once the grolishing process was completed, the surface was measured using a contacting stylus in areal mode (PGI Taylor Hobson) to identify the depth of material removal. A picture of the surface after the grolishing process is shown in figure 6-10. The circular spot on the side of the square patch

shows tool entry-exit. In the figure the square patch covers 9 mm². The program drives the tool center position. The tool offset would produce a Ø4 mm impact spot which, added to the 5 mm program, gives the 9 mm² contact area. The black line in the middle indicates the place where the profile measurement is taken. The measured result is filtered to show the waviness profile as this is more appropriate measure to identify the depth and form of material removal process.
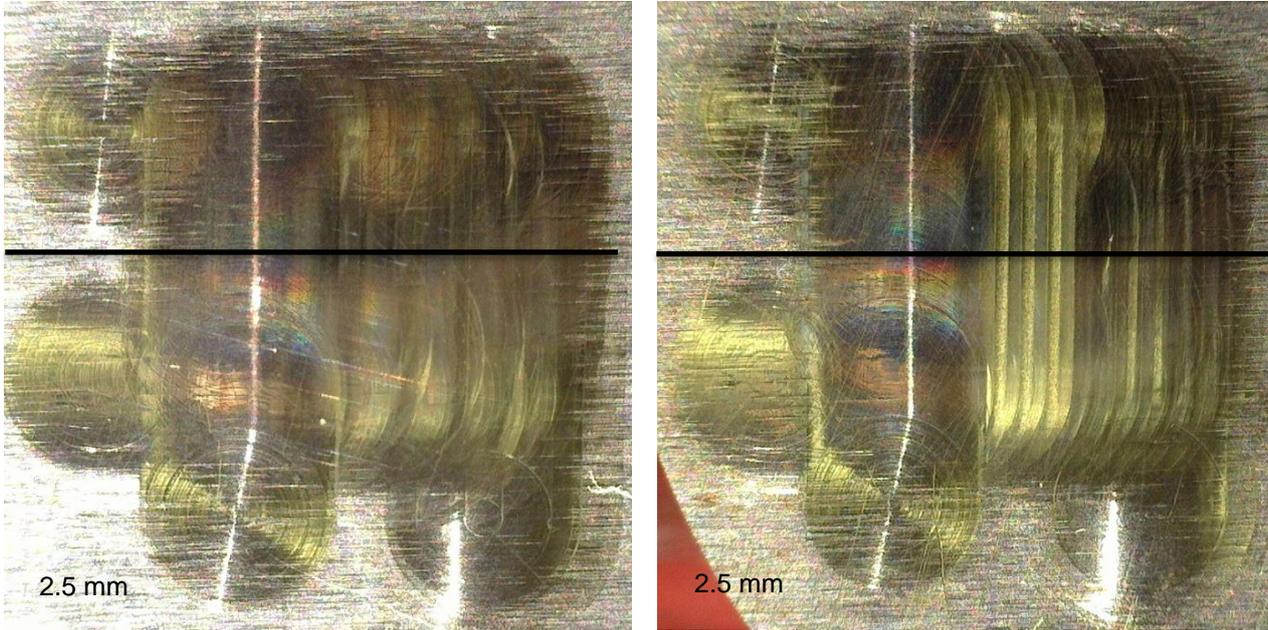
Figure 6-10:   Grolishing test with 0.5 mm step movement (left) and 0.25 mm step movement (right)

The measured waviness profile shows a depth of 2.5 μm material removal in the middle after the grolishing test (figure 6-11). The black vertical lines delimit the distance where the material removal is obtained through grolishing. The distance between these two black lines is 9 mm, which covers the programmed distance (5 mm) and 2 mm either side due to the impact spot. The red lines show the program start and end position with respect to the overall distance. The green lines show the area where the depth of removal is high. Indeed, the tool is in contact with the workpiece in this area more that the outer area due to the raster program. It is positioned symmetrically to the center and covers a distance of 3 mm. The removal is constant in that area, allowing a flat surface.
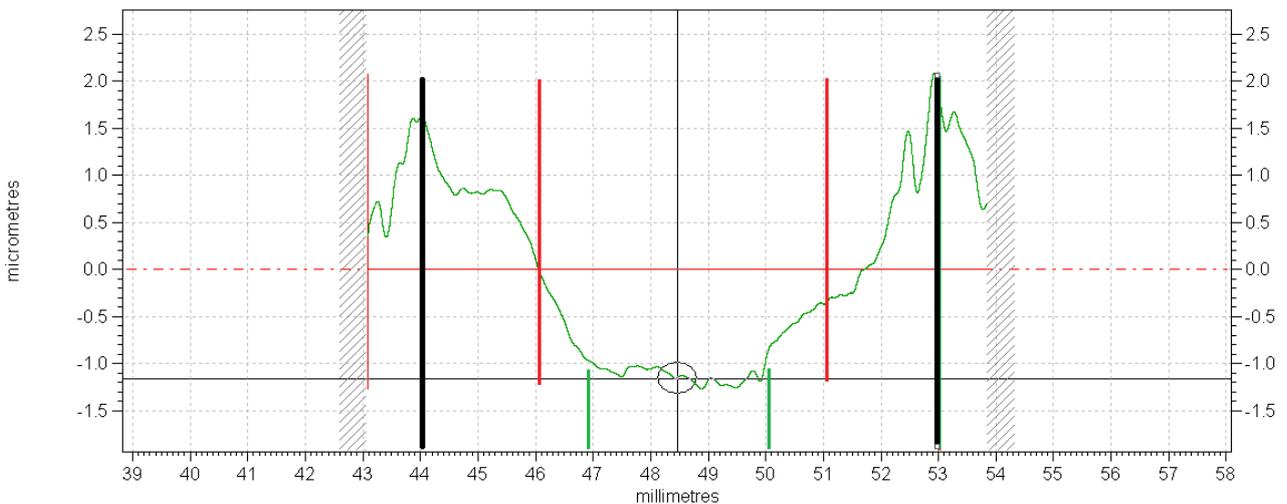
Figure 6-11:   Material removal profile of 0.5 mm step grolishing test

The conventional ground surface is measured to have Sz = 4.77 µm (figure 6-2). The aim of the grolishing process is to reach a depth greater than 4.7 µm in order to remove all grinding marks from the surface and to improve the surface roughness. The 0.5 mm step grolishing process provides a stable removal of around 2.5 µm depth, which does not reach the 4.7 µm depth removal required. The grolishing test program was therefore modified with a 0.25 mm step size to evaluate whether a smaller step size which would increase the amount of grolishing time performed on each segment of the workpiece, would affect the depth of material removal. All other parameters were the same as in the previous grolishing test. Figure 6-10 (right) shows the picture of a 0.25 mm step grolishing test. The measured profile of the grolishing test with a 0.25 mm step is presented in figure 6-12.
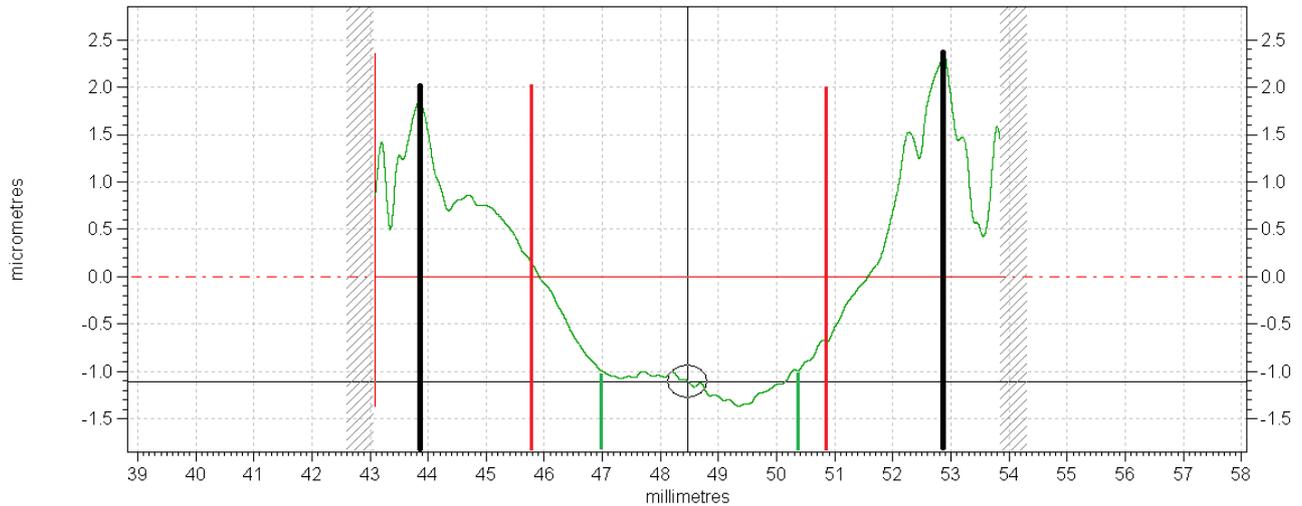
Figure 6-12:   Material removal profile of 0.25 mm step grolishing test

The depth of removal in the modified grolishing test remained very similar to the previous test, with around 2.5 µm depth. The material removal was achieved over 9 mm distance, as would be expected for a 0.3 mm offset and 5 mm^2 program. The distance between the green lines was approximately 3.3 mm compared to 3 mm in the previous experiment. This difference in distance between green lines could be the effect of the 0.25 mm step size. The depth of removal did not change significantly, although the grolishing time was doubled since the step size was divided by two. The 0.5 mm step will therefore be used in the developing grolishing process.

c.   Pad wear

The pad used for the grolishing process was an Ultrapad™ from Buehler. Although the pad is designed for materials with a hardness of P20 and in a coarse condition, it is important to verify the performance of the pad to ensure that pad wear will not affect the consistency of the grolishing process. Pictures of the pad were taken before and after the grolishing process using a Keyence digital microscope (figure 6-13). The picture taken after the grolishing process does not show signs of wear. The hard woven pad was not affected by the aggressiveness of the grolishing process using 45 µm diamond abrasives and 5,000 rpm spindle speed. Diamond abrasives and grolishing process debris were lodged between the hard woven stitches.
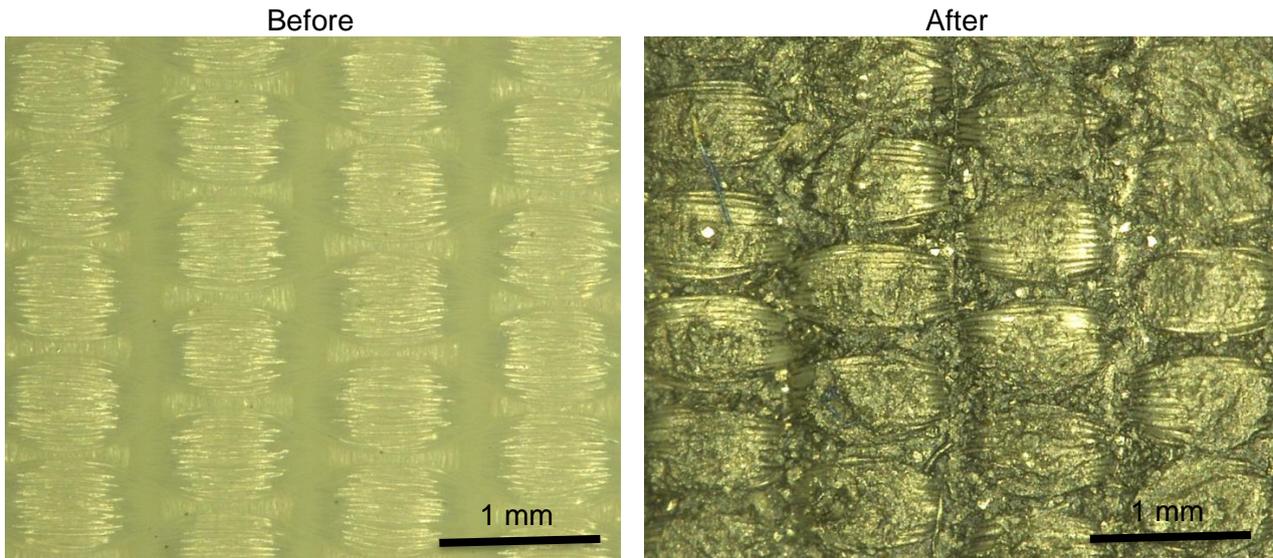
Before   After

Figure 6-13: Ultrapad™ before and after grolishing process

6.3 Grolishing Experiment

The Grolishing process was mainly developed to remove mid-spacial frequency errors from a previous manufacturing process; however, it has other useful advantages, such us improving surface roughness and correcting form errors [189]. In the experiments described below, the main aim was to improve surface roughness by the grolishing process. In automated and manual lapping machines, surface roughness improvement is obtained via a series of polishing steps determined by the nature of the workpiece material and its initial surface roughness. Polishing consumables manufacturers, such as Buehler, have studied improvement to surface roughness using their products and provide basic guidelines on how to achieve improvement [224]. The guidelines for improving surface roughness suggest a series of polishing steps to convert a rough surface into a smooth surface. For each step, the material of the polishing cloth and size of abrasives are adapted to the initial surface roughness condition of the workpiece (figure 6-14).

Material		Grinding Steps	Polishing Step 1	Polishing Step 2	Polishing Step 3
Stainless & Maraging Steel		CarbiMet 120grit [P120] - 320grit [P400]	UltraPad 9μm MetaDi Supreme Diamond Suspension	TriDent 3μm MetaDi Supreme Diamond	ChemoMet MasterPrep Alumina

Figure 6-14: Buehler polishing guidelines on selecting polishing cloth and abrasives [224]

A step grolishing process was developed to improve the surface roughness of components with a surface form not adapted to conventional lapping/polishing machines. The process developed should grolish components which have only been CNC machined to achieve a mirror like finish. This chapter describes the development of two grolishing processes. Grolishing parameters and results obtained using those parameters are presented below. Before each step in the grolishing process, the samples were measured using a white light interferometer with a 20X lens.

Mid-spacial frequency errors are usually identified at a certain frequency, so the grolishing process is developed to attenuate the amplitude of that frequency. At this stage of grolishing process development, although there were no specific errors that needed to be targeted, it was important to

understand the progress of surface roughness improvement in terms of frequency distribution. The results from CCI were therefore saved as a spacial data file (SDF) file. MATLAB software was used to extract a linear roughness profile which was then used to analyse the results in the spatial frequency domain. The measurement length was 918.48 μm with a resolution of 0.898 nm / pixel. A Matlab code was used to extract information from the surface roughness profile and transpose it into the frequency amplitude domain. The written code was initially tested using an equation with known frequency. The tested equation has a frequency of 4 and 20 Hz. The result obtained on a single-sided amplitude spectrum shows clearly these two frequencies with their corresponding amplitude (figure 6-15).

```
x =linspace(0,1000,1000);
z=sin(2*pi/250*x)+2*sin(2*pi/50*x)
```
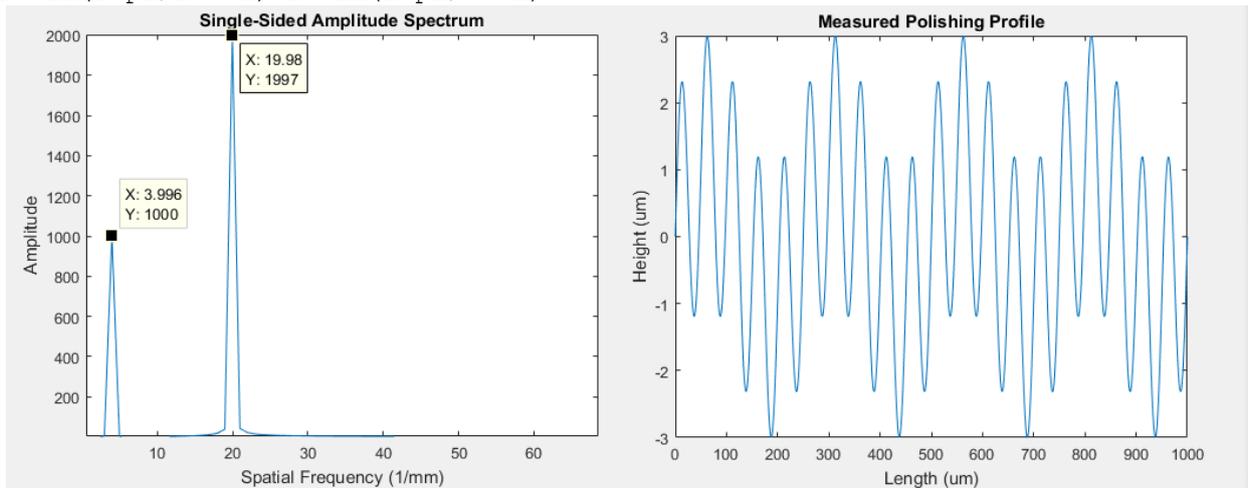

Figure 6-15:   Test equation (top); amplitude in frequency domain (bottom left) and equation profile (bottom right)

Both literature review and knowledge gained through empirical experiments were used to select the grolishing parameters. The Preston equation shows that the surface speed is linearly proportional to the MRR. Indeed, SY Zeng et al. have studied the material removal rate of CoCr with respect to several parameters, including tool speed. The material removal rate (MRR) has a steep linear response with tool speed [179]. This indicates that higher speed would increase the MRR. The increase in offset would also increase the MRR until bonnet distortion occurs. In the same way the increase in offset would increase the spot size. Therefore, grolishing spot size obtained from the tool offset needs to consider the surface topography to preserve the form accuracy. The feed rate and number of passes are both related to the time the tool spends on each spot. However, high feed with high speed ejects the grolishing abrasives away from the surface, whereas low feed keeps the abrasives on the workpiece surface. On the other hand, low feed and high speed results in deterioration of a smooth surface, whereas high feed and low speed improves further the surface roughness. The parameter selection of each polishing step is dependent on the initial surface roughness condition. High speed and low feed were selected for rough surfaces; low speed and high feed for smooth surfaces.

6.3.1 Four step grolishing process

a. Parameter condition and results

Table 6-1: Four step grolishing parameters & results (step 0)

Step 0	Surface condition from grinding process obtained from Semi- Automatic grinding machine
Average Sa after grinding process	461 nm
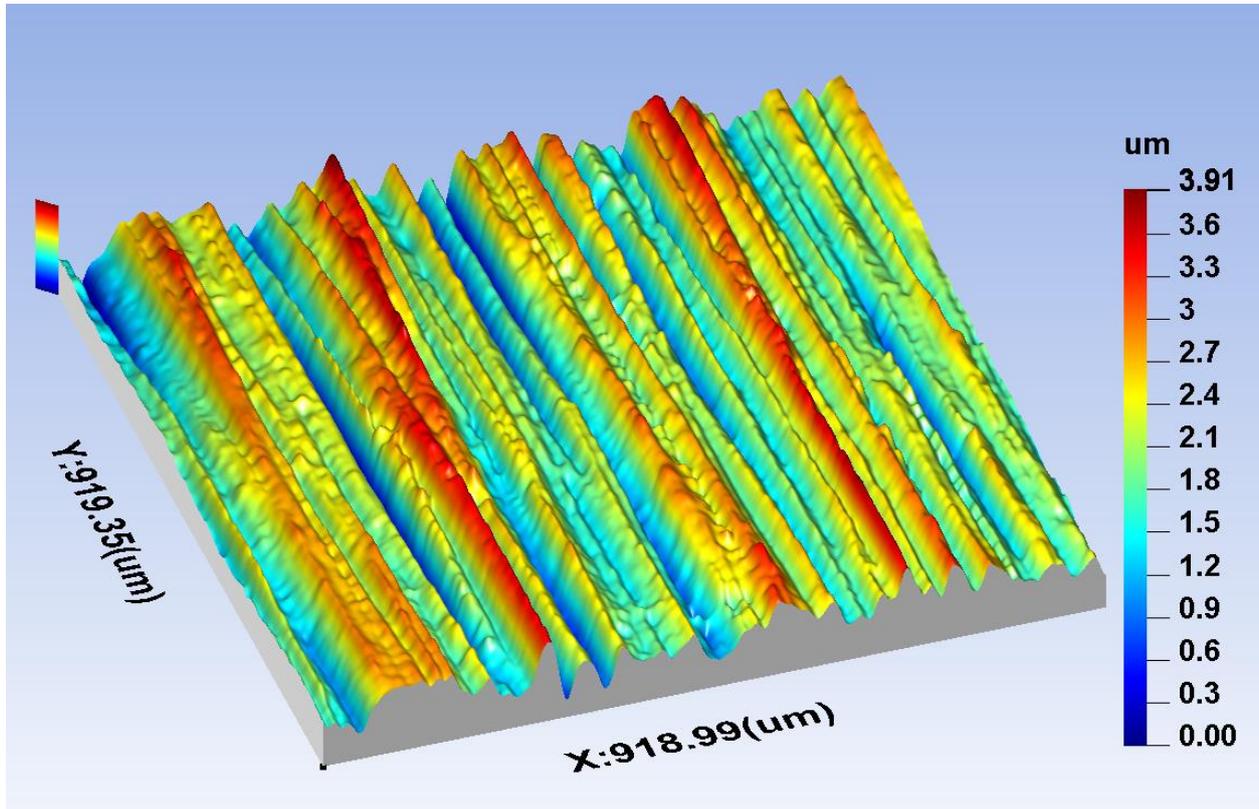
Figure 6-16:   Four step grolishing step 0 surface topography
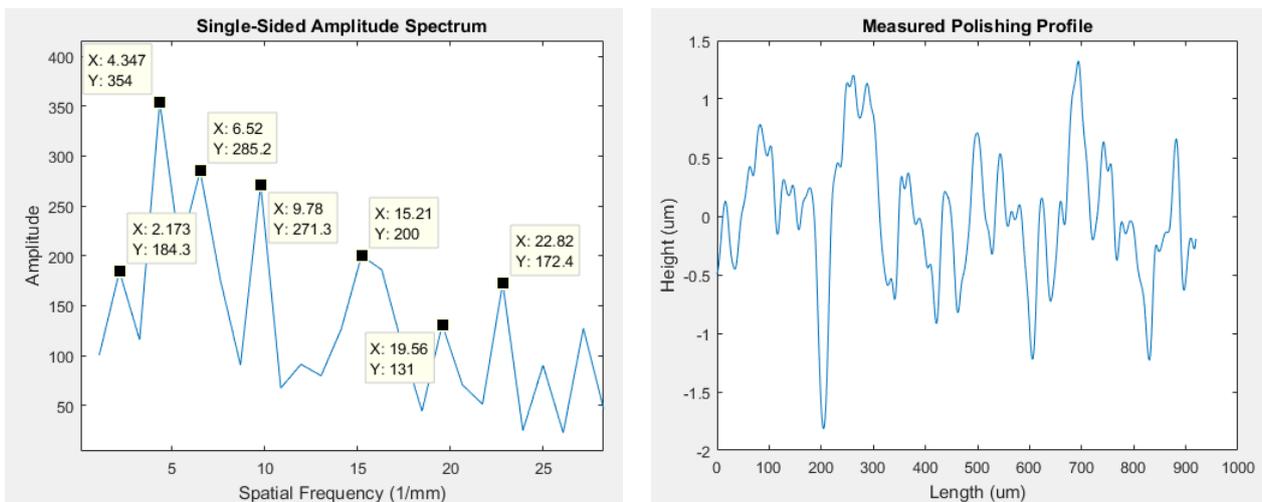
Figure 6-17:   Four step grolishing step 0, amplitude in frequency domain (left) and surface profile (right)

Table 6-2:   Four step grolishing parameters & results (step 1)

Step 1	Speed (rpm)	Offset (mm)	Feed (mm/sec)	Number of Passes	Programme path direction	Abrasive size	Polishing Pad
	6500	0.3	0.75	1	Parallel to X & Y Machine axis	45µm	Ultrapad
Average Sa before grolishing process			461 nm				
Average Sa after grolishing process			100 nm				
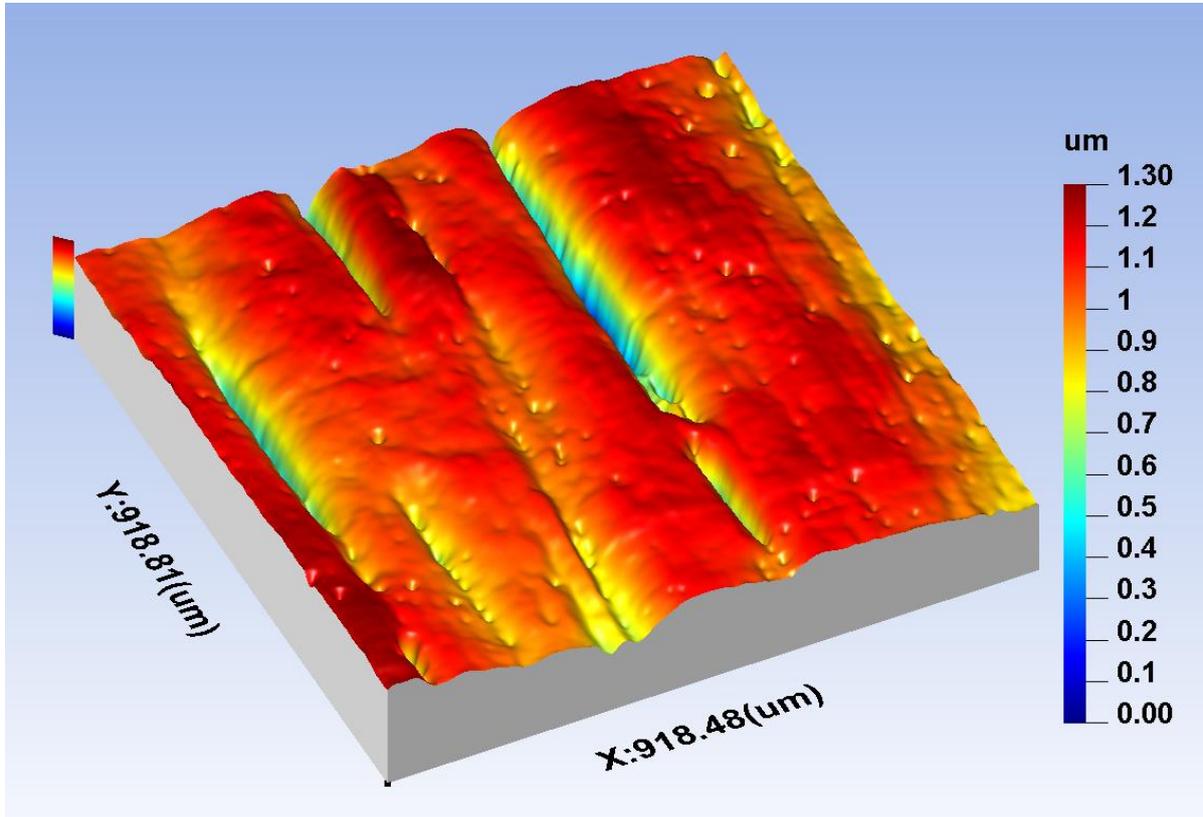
Figure 6-18:   Four step grolishing step 1 surface topography.
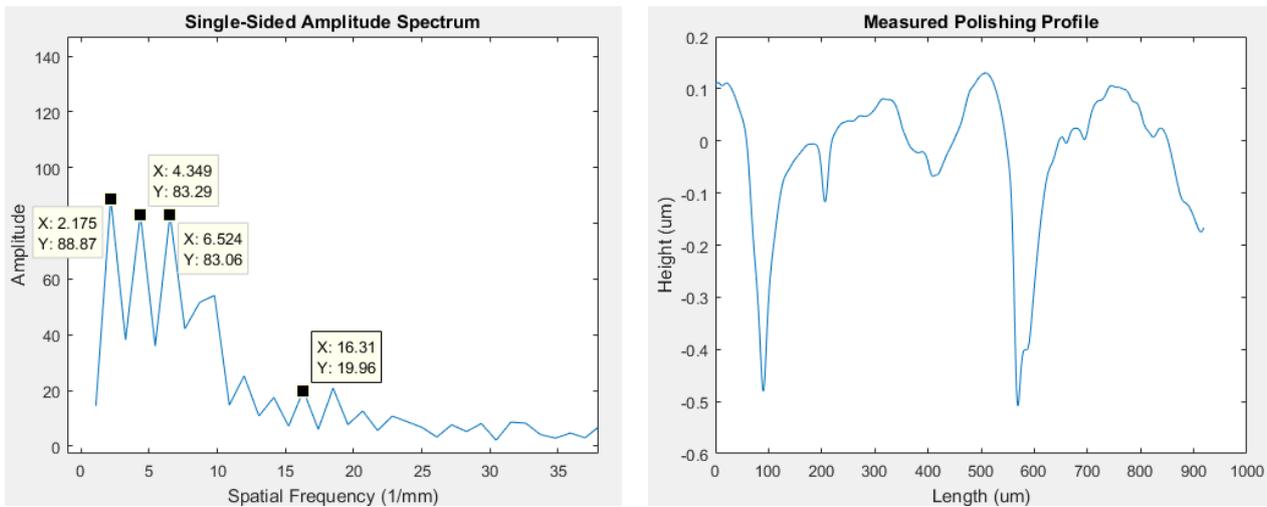
Figure 6-19:   Four step grolishing step 1, Amplitude in frequency domain (left) and surface profile (right)

Table 6-3:   Four step grolishing parameters & results (step 2)

Step 2	Speed (rpm)	Offset (mm)	Feed (mm/sec)	Number of Passes	Programme path direction	Abrasive size	Polishing Pad
	6500	0.3	0.75	1	Parallel to X & Y Machine axis	45µm	Ultrapad
Average Sa before grolishing process				100 nm			
Average Sa after grolishing process				53 nm			
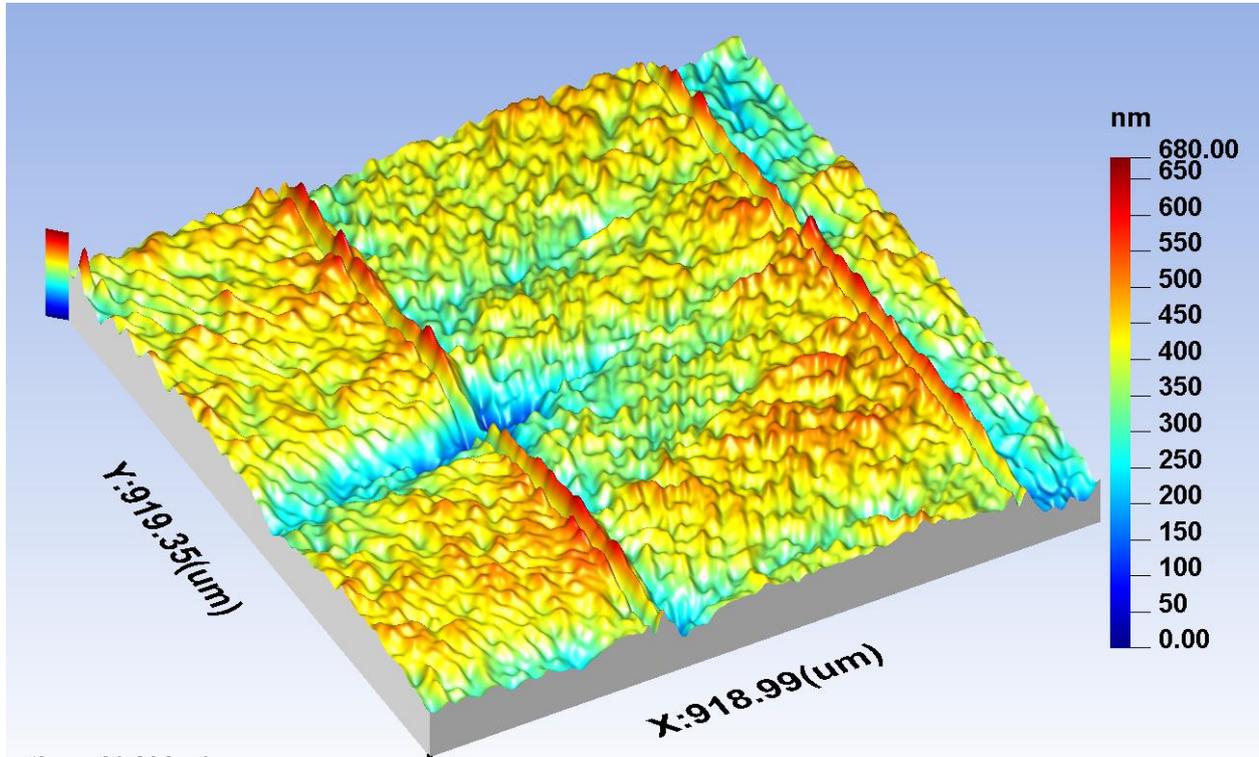
Figure 6-20:   Four step grolishing step 2 surface topography
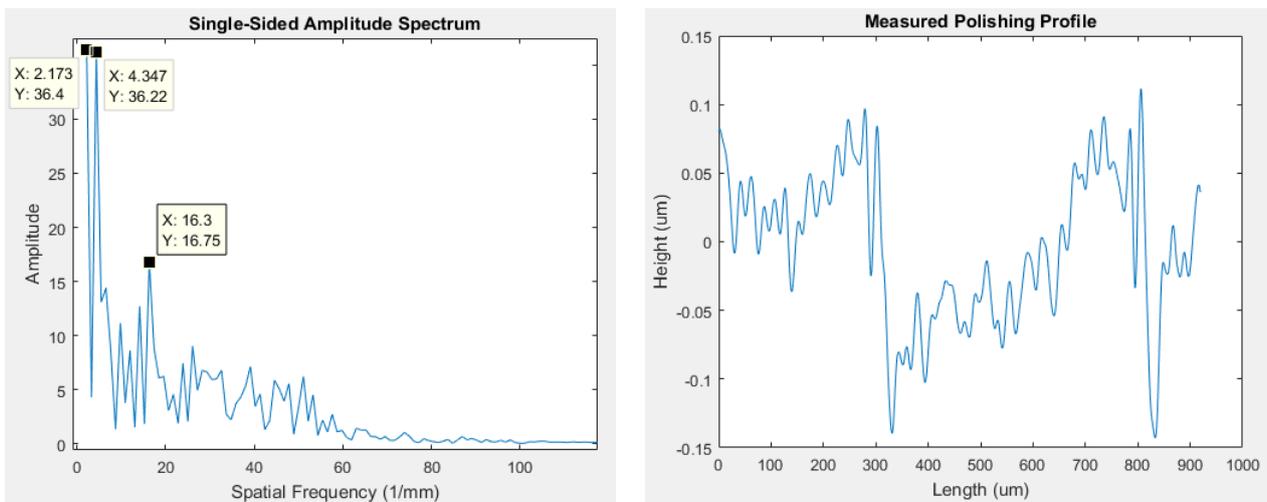
Figure 6-21:   Four step grolishing step 2, Amplitude in frequency domain (left) and surface profile (right)

Table 6-4:   Four step grolishing parameters & results (step 3)

Step 3	Speed (rpm)	Offset (mm)	Feed (mm/sec)	Number of Passes	Programme path direction	Abrasive size	Polishing Pad
	5000	0.3	5	5	Parallel to X & Y Machine axis	9μm	Verdutex™
Average Sa before grolishing process			53 nm				
Average Sa after grolishing process			21 nm				
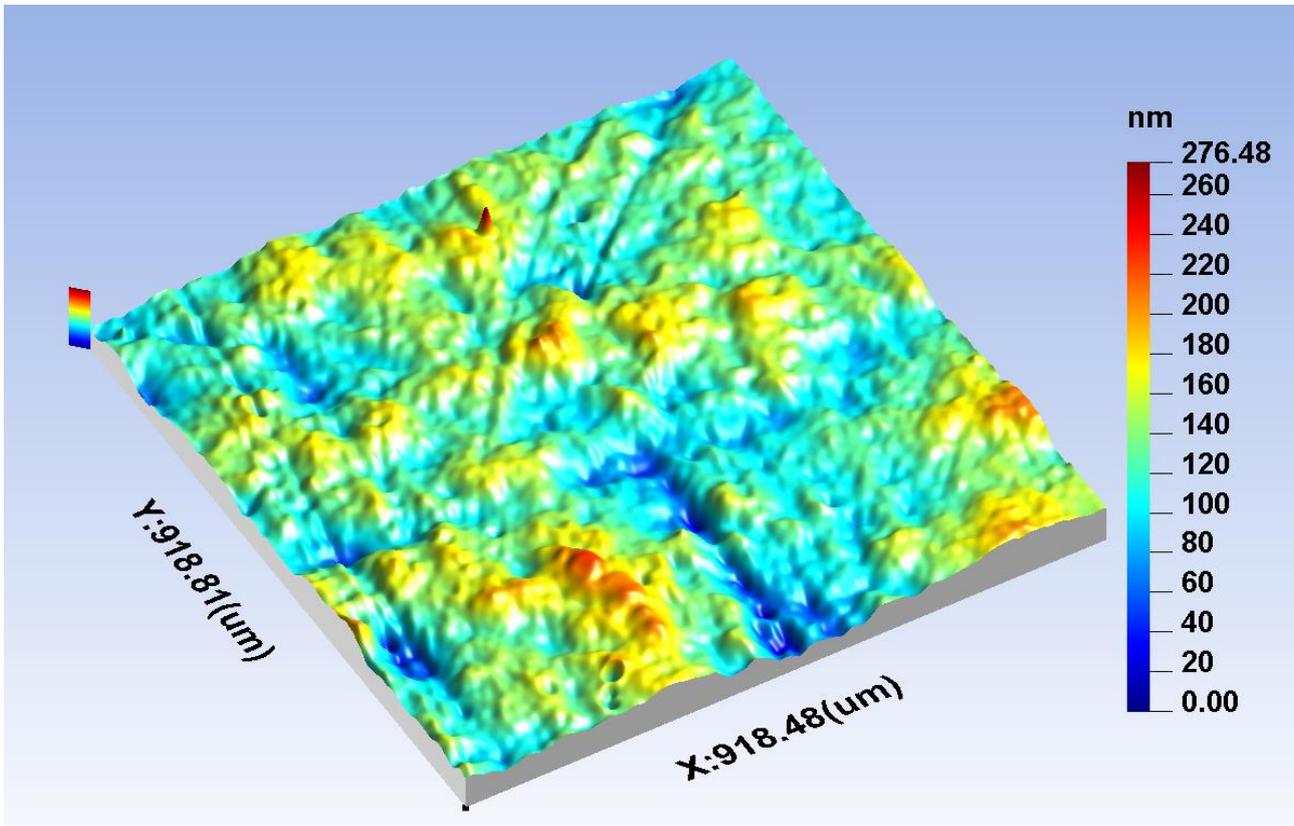
Figure 6-22:   Four step grolishing step 3 surface topography
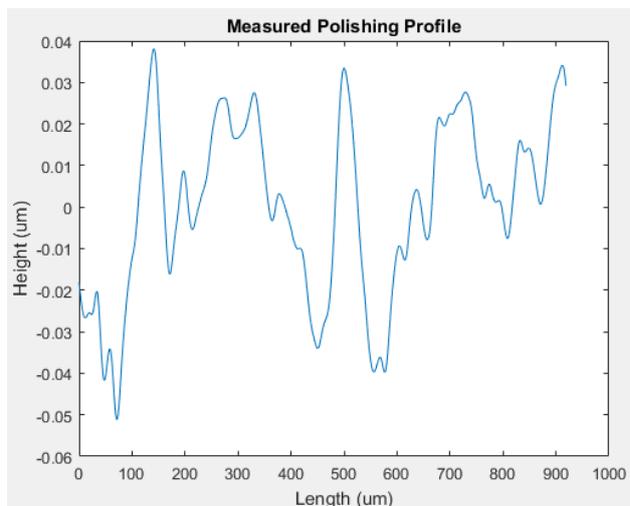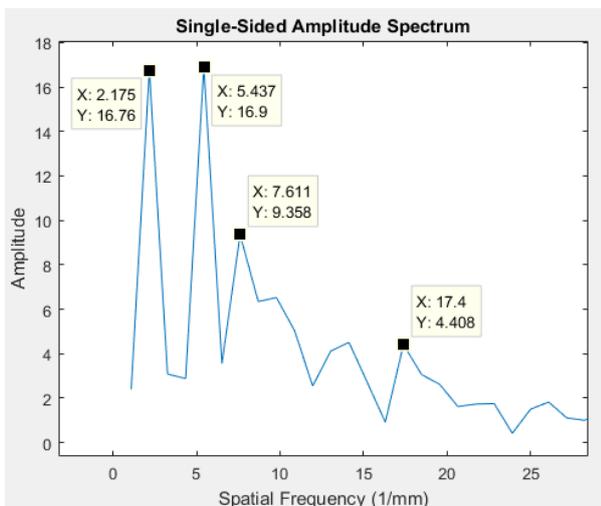
Figure 6-23:   Four step grolishing step 3, Amplitude in frequency domain (left) and surface profile (right)

140

Table 6-5: Four step grolishing parameters & results (step 4)

Step 4	Speed (rpm)	Offset (mm)	Feed (mm/sec)	Number of Passes	Programme path direction	Abrasive size	Polishing Pad
	1000	0.3	15	4	Parallel to X & Y Machine axis	1µm	Verdutex
Average Sa before grolishing process				21 nm			
Average Sa after grolishing process				4 nm			
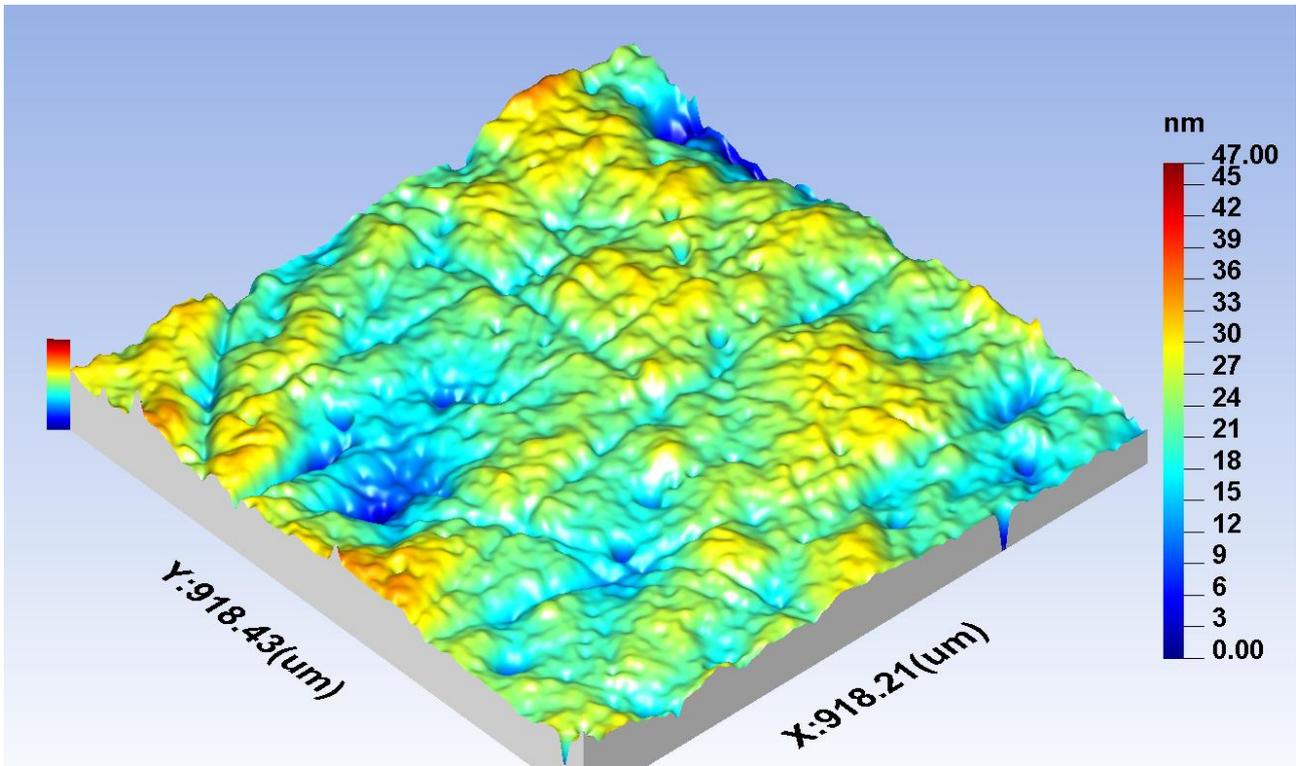
Figure 6-24:   Four step grolishing step 4 surface topography
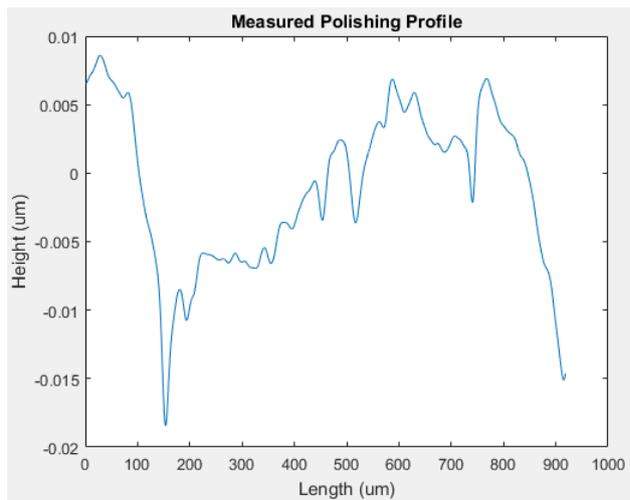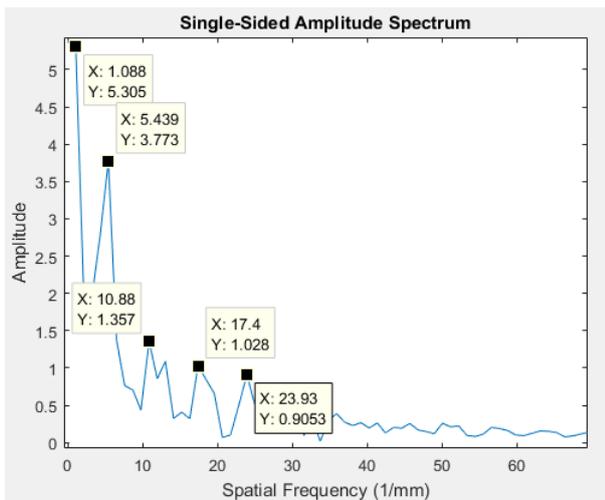
Figure 6-25:   Four step grolishing step 4, Amplitude in frequency domain (left) and surface profile (right)

b. Result analysis

In the step 1 grolishing, the surface was improved from 461 nm Sa to 100 nm Sa (Table 6-2); however, the grinding marks were still clearly visible (figure 6-18). A second grolishing process (step 2) was therefore performed with same parameter conditions and this brought the Sa down to 53 nm (Table 6-3). The grinding marks were considerably softened but remained visible optically and in the frequency domain (figure 6-20). The aggressiveness of the grolishing process started to print the tool path on the surface, aided by the low feed rate (0.75 mm/sec). In step 3, the speed was reduced slightly to 5,000 rpm to cope with the 5 mm/sec feed rate (Table 6-4). The number of passes was increased to ensure the removal of the tool path printed on the surface, while the surface roughness was improved. The grolishing cloth and abrasive size were changed to correspond with the initial surface roughness condition (53 nm Sa). The result shows a Sa of 21 nm at step 3 (figure 6-22). Finally, the speed was reduced to 1000 rpm and the feed increased to 15 mm/sec, with the number of passes set to four (Table 6-5). One micron diamonds abrasive was applied to further smooth the surface, and this brought down the Sa to 5 nm (figure 6-24).

The workpiece measured result was computed using Fast Fourier Transform (FFT) to highlight the amplitude of surface roughness peaks in the frequency domain. The ground surface shows high amplitude at 4.347 Hz which corresponds to repeated pikes, spaced at an interval of 230 μm (figure 6-16). There are also further noticeable peaks at 2.175, 6.52, 9.78 and 15.21 Hz. The step 1 grolishing process attenuated the amplitude from 354 to 83, for 4.34 Hz frequency (figure 6-19). Step 2 grolishing process has further attenuated the amplitude of all peaks. Those with noticeable amplitude are still dominating the frequency response with lower amplitude (figure 6-20). In step 3, the grolishing parameters were changed, causing frequency shift from 4.347 to 5.437 Hz, 6.52 to 7.6 Hz and 16.3 to 17.4 Hz (figure 6-23). The final step in the grolishing process, with parameters similar to a polishing process have further attenuated the amplitude of all peaks. The dominant peak present at 2.175 Hz from the ground finishing process have shifted to 1.088 Hz.

Figure 6-27 shows a four step grolished sample. The grolished part with mirror like finish can be distinguished from the outer ring with only a ground finish. Although the roughness is improved by the grolishing process, some form error can still be seen on a surface supposed to be flat. When the waviness of the ground and 4 step grolished surfaces were compared (Table 6-6), it was observed that, although the grolishing process had removed the waviness error from the grinding process, it had also printed its own waviness from the tool path movements. The ground surface had a W_t of 1.33 μm and the grolishing process had reduced the W_t to 0.61 μm. The spacing between peaks had also changed from WS = 828 μm to WS = 3048 μm.

The four step grolishing process reduced the PV of the waviness and also increased the spacing between peaks, which greatly improved the surface topography. However, deep grinding marks become visible once the surface becomes reflective (figure 6-28). To remove these marks, further grolishing steps, which would amplify the waviness present on the surface, are required. Therefore, an attempt was made with a new step in the grolishing process designed to remove totally the grinding marks and to reduce the waviness effect from the tool path.

Figure 6-26:   Four step grolished sample

Table 6-6:   Surface waviness ground surface (top) & 4 step grolished (bottom)
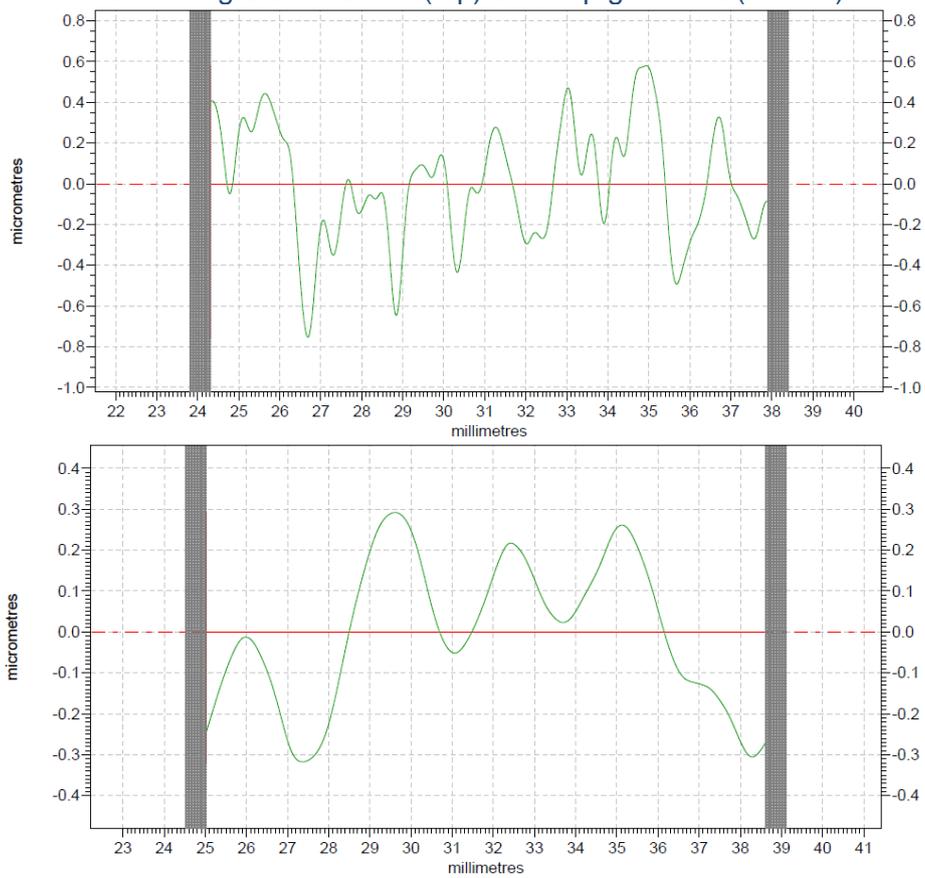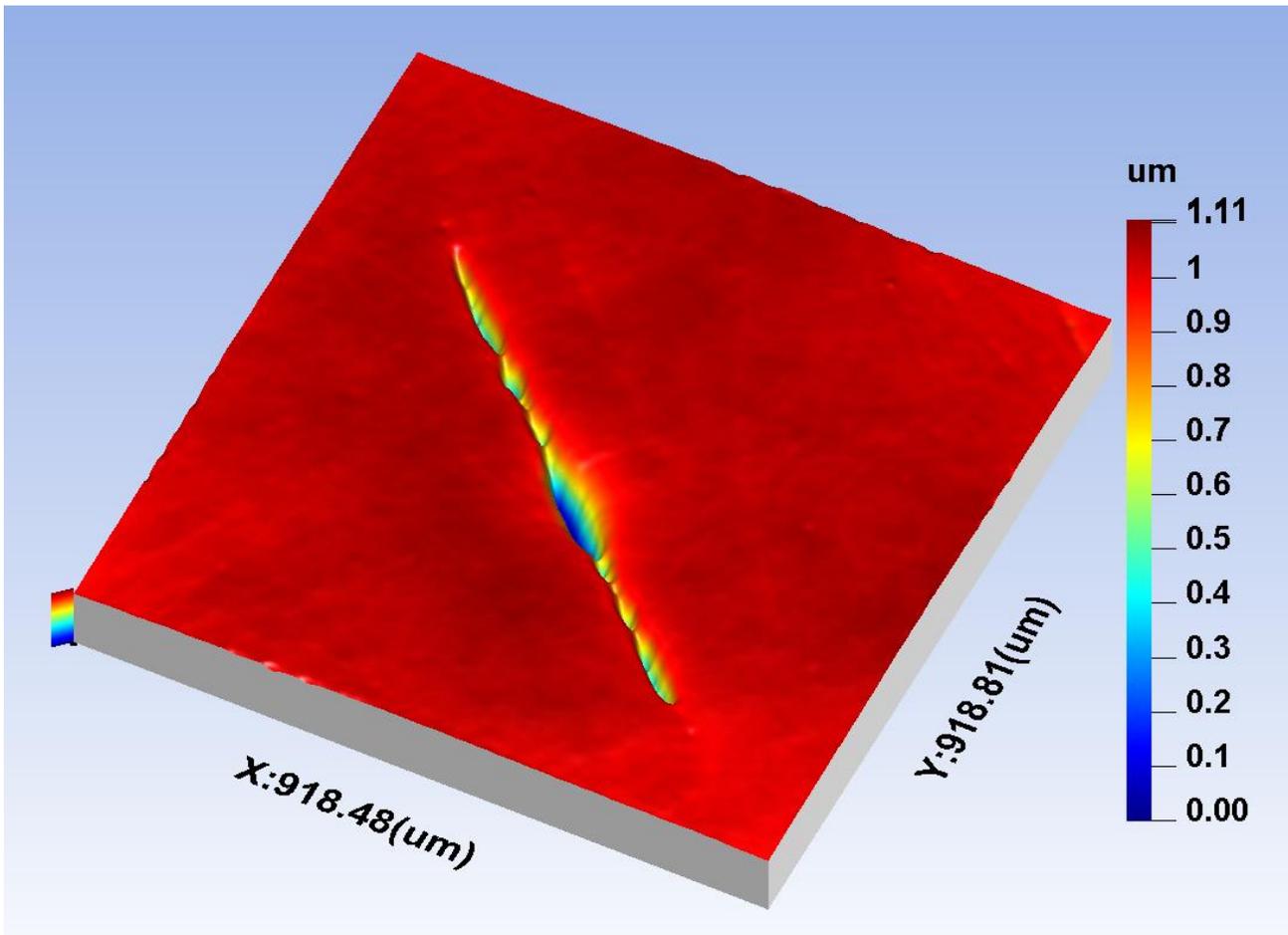
Figure 6-27:   Visible grinding marks after four step grolishing

6.3.2   Seven step grolishing experiment and results analysis

To remove the grinding marks totally, the aggressive steps with high speed and low feed using larger abrasives need to be repeated. However, repeating the same programme would increase the form error on the surface. Therefore, an attempt was made by using the raster program with the tool path set at 45 degrees to the hexapod X and Y axes. This was used in addition to the raster program with the tool path parallel to the X and Y axes of the hexapod. Each step of the grolishing process was designed so that each set of parameters was performed on all four sides (Table 6-7). Step 3 was designed to remove the excess grinding marks noticed in the previous grolishing process. Steps four to seven replace steps three and four of the four step grolishing process. In practice steps one and two can be merged, as can steps four and five, and steps six and seven. However, these are split to better understand surface roughness improvement process.

Table 6-7: Seven step grolishing parameters

	Speed (rpm)	Offset (mm)	Feed (mm/sec)	Number of Passes	Program path direction	Abrasive size	Polishing Pad
Step 1	5000	0.3	0.75	1	Parallel to X & Y Machine axis	45µm	Ultrapad
Step 2	5000	0.3	0.75	1	45 Degree to X & Y Machine axis	45µm	Ultrapad
Step 3	3000	0.3	3	1	Parallel & 45 Degrees to X & Y axis	45µm	Ultrapad
Step 4	2500	0.3	5	1	Parallel to X & Y Machine axis	9µm	Verdutex
Step 5	2500	0.3	5	1	45 Degree to X & Y Machine axis	9µm	Verdutex
Step 6	1000	0.3	15	1	Parallel to X & Y Machine axis	1µm	Verdutex
Step 7	1000	0.3	15	1	45 Degree to X & Y Machine axis	1µm	Verdutex

The ground sample has a surface roughness of 575 nm Sa. The Seven Step grolishing process provided an average of 7 nm Sa. The roughness results, surface topography and amplitude spectrum in frequency domain of each grolishing step are available in Appendix 6.1. The amplitude spectrum shows a trend very similar to the previous grolishing process, with each step attenuating the amplitude of peaks. The dominant peak at 2.175 Hz remains dominant until step 6. The final polishing step shifts the frequency from 2.175 Hz to 1.087 Hz, as it did in the final step of the previous (Four Step) grolishing process. The CCI image taken after step 2 shows an attempt to remove the tool path marks from step 1 (figure 6-28). This is obtained by setting the tool path at 45 degrees to the machine X and Y axes, whereas, in four step grolishing, step 2 involves printing the tool path on the workpiece. (figure 6-20). The CCI image shows that the tool path has influence on the surface topography. Indeed, until step 5, the CCI image shows a correlation between tool path direction and workpiece topography. However, steps six and seven do not affect the topography, but rather improve the roughness by attenuating the amplitude of peaks.
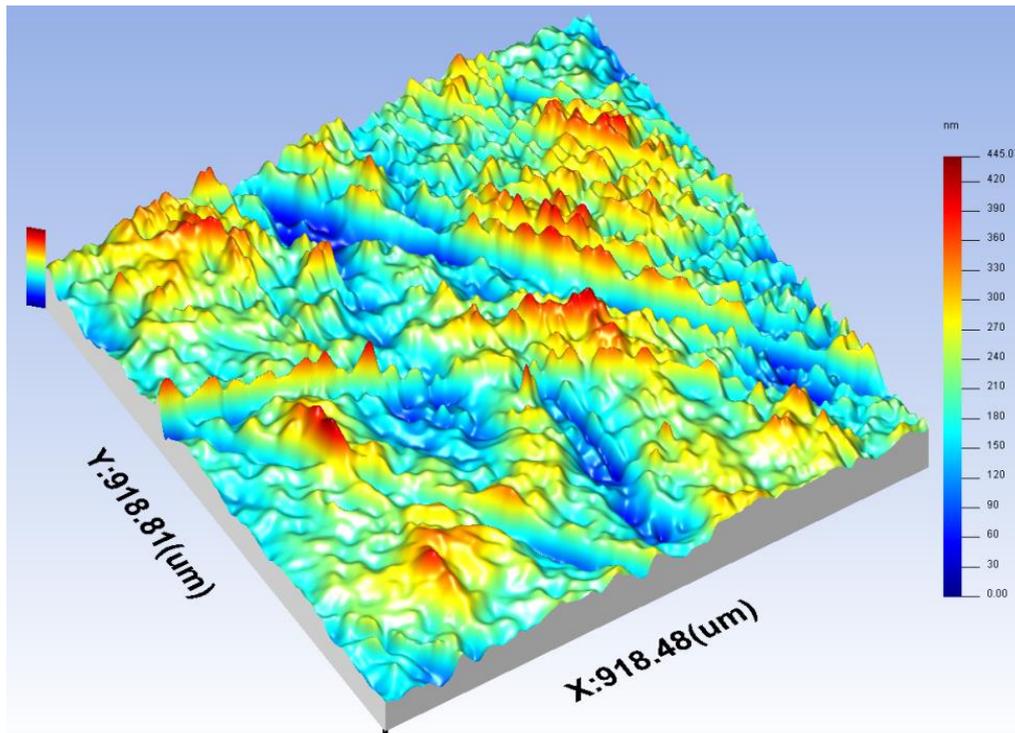
Figure 6-28:   Seven step grolishing, step 2 surface topography

The waviness is measured on a 15 mm long profile on PGI (Table 6-8). The ground surface has a Wt of 1.44 µm and the grolished surface has a Wt of 0.5 µm. The peak spacing moved from WS = 1138 µm to WS = 2084 µm. This indicates that the Seven Step grolishing process has the ability to attenuate PV of waviness better than the Four Step process. However, the new tool path programming has less effect on the spacing distance between peaks. Both Four and Seven Step grolished samples were measured on CCI with 5X magnification (figure 6-29). In this way, it was possible to both obtain and to measure the surface topography of 3.68 mm^2. The results were filtered to expose wavelengths between 0.025 mm and 0.8 mm corresponding to the wavelength used for roughness measurement. The yellow contour height patch shown on the Four Step grolished sample highlights the waviness error from the tool path movement, whereas the yellow contour height patch on the Seven Step grolished sample shows less effect. The grinding marks are less visible on the surface after the Seven Step grolishing process. In applications where these waviness errors are undesirable, form correction needs to be performed before the final polishing.

146

Table 6-8:   Surface waviness ground surface (top) & Seven step grolished (bottom)
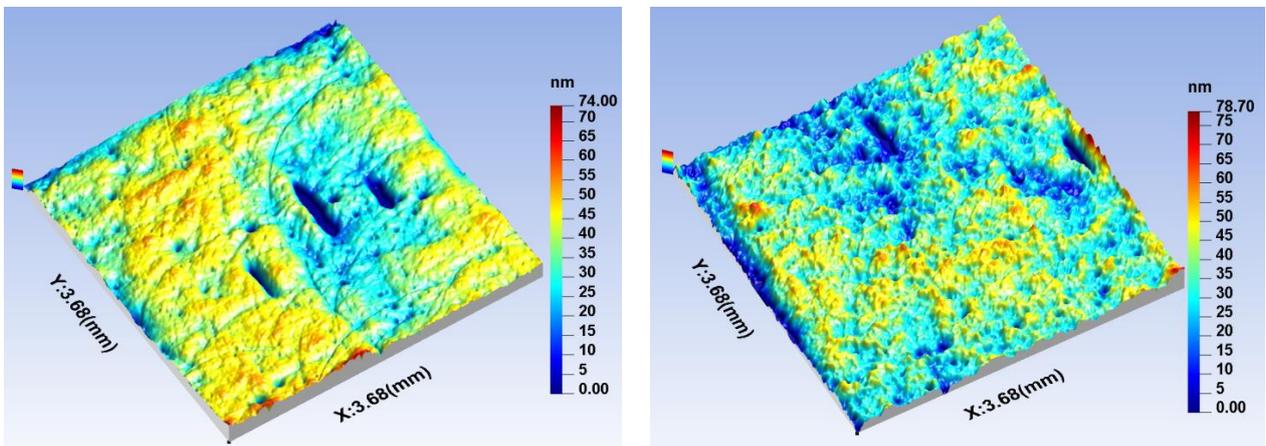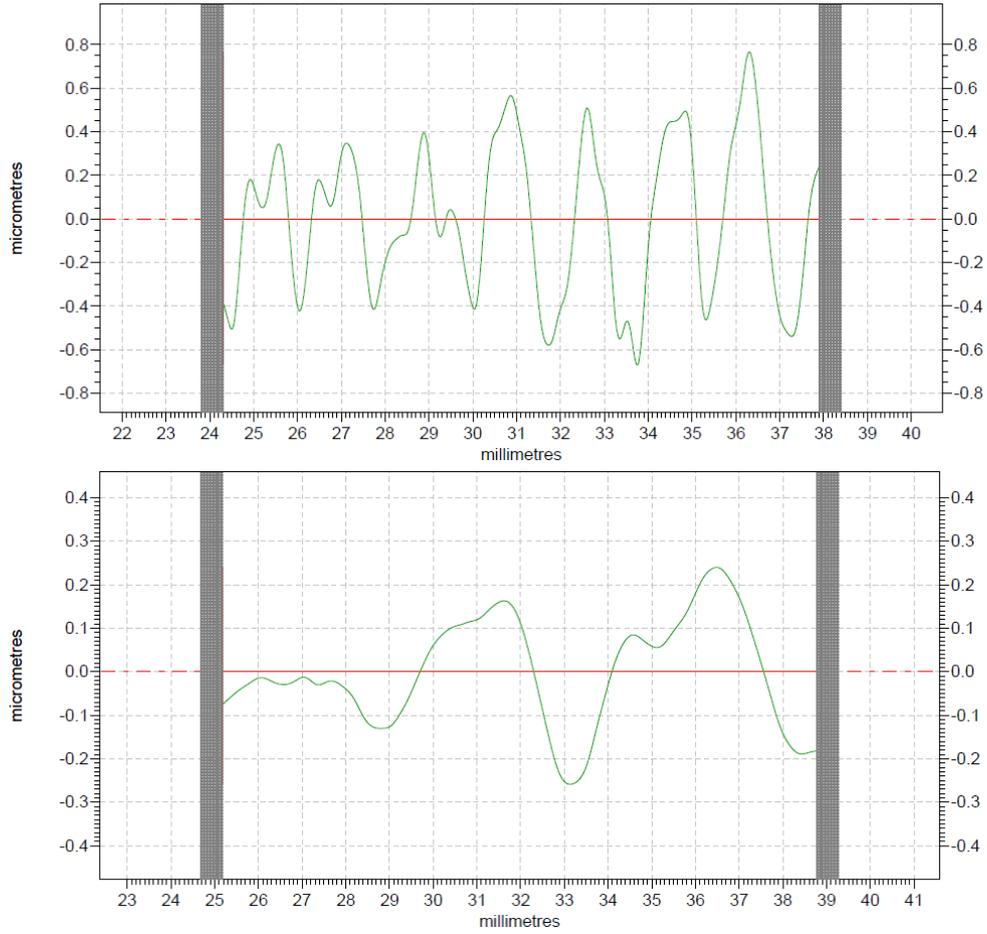
Figure 6-29:   Grolished surface topography: Four step (left) & Seven step (right)

6.3.3   Multi-scale Wavelet analysis

a. Four step Grolishing

In section 6.3.1, the four step grolishing process results are analysed with data pre-filtered to expose the surface roughness. In this section it is aimed to analyse the surface waviness using multi - scale wavelet analysis to identify the removal process of grinding marks and expose the tool path imprint of grolishing process (MSF error) on the workpiece. There are four wavelet ranges used for results analysis which are; (1) 14.4 µm -28.8 µm, (2) 28.8 µm – 57.6 µm, (3) 57.6 µm – 115.2 µm. (4) 115.2 µm – 230.4 µm. Measurement data analysis software Surfstand produce images exposing only the chosen range for wavelet analysis. The figure 6-30 shows images of step 0, step 2 and step 4 of four step grolishing process in all four wavelet ranges. The full data with all steps of grolishing process are available in Appendix 6-2.1.

(µm)	STEP0	STEP2	STEP4
14.4-28.8			
28.8-57.6			
57.6-115.2			
115.2-230.4			
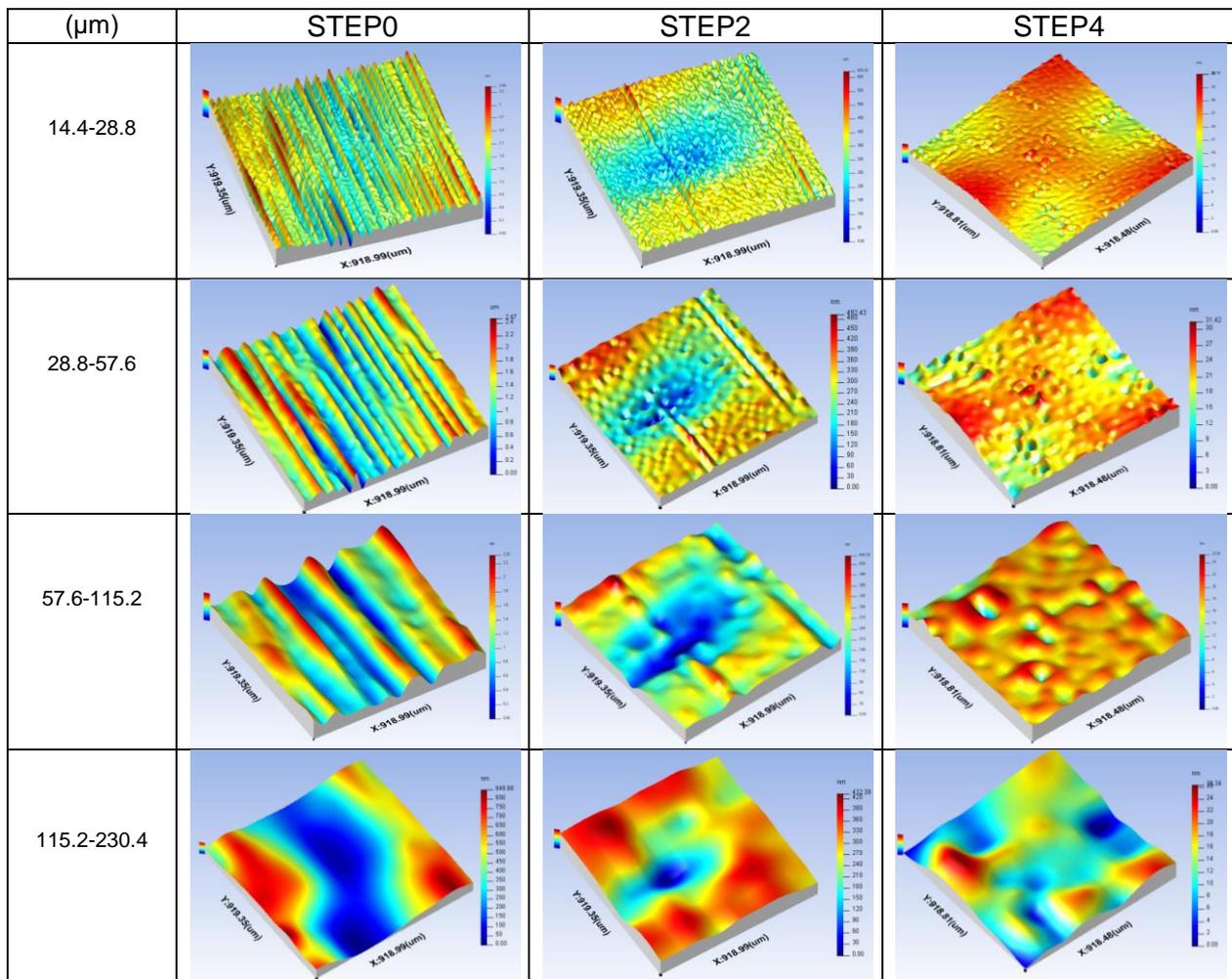
Figure 6-30:   Multi-scale wavelet analysis: Partial results from four step grolishing process exposing tool path imprint on the workpiece studied at four levels of wavelet ranges

The results indicate that the grinding marks are gradually suppressed from the surface through a series of grolishing steps. However, some square patches can be clearly identified from step 2 onwards indicating the imprint of the grolishing tool path on the surface. These square patches attenuate in intensity by step 4 of the grolishing process. Surface roughness parameter Sa helped to evaluate the grinding marks removal process, however Sa parameter do not quantify the surface waviness. Therefore, Sal (fastest decay auto correlation length) parameter is used to analyse the tool path imprint on the surface over the series of step grolishing. The figure 6-31 shows a graph produced using Sal surface parameter results.

The grinding process have printer unidirectional tool marks on the surface at all wavelet ranges. The grolishing process removes the marks from all wavelet ranges and places its own marks at around 0.18 mm spacing distance on Sal parameter. Towards the step 4 of the grolishing process, the imprinted tool marks attenuate in intensity which reflects on the diminution of Sal spacing to around 0.13 mm for all wavelet ranges.

Four step grolishing Sal parameter analysis

	STEP0	STEP1	STEP2	STEP3	STEP4
14.4-28.8	0.012	0.185	0.18	0.187	0.143
28.8-57.6	0.023	0.177	0.176	0.185	0.132
57.6-115.2	0.054	0.125	0.175	0.19	0.096
115.2-230.4	0.111	0.108	0.178	0.171	0.127
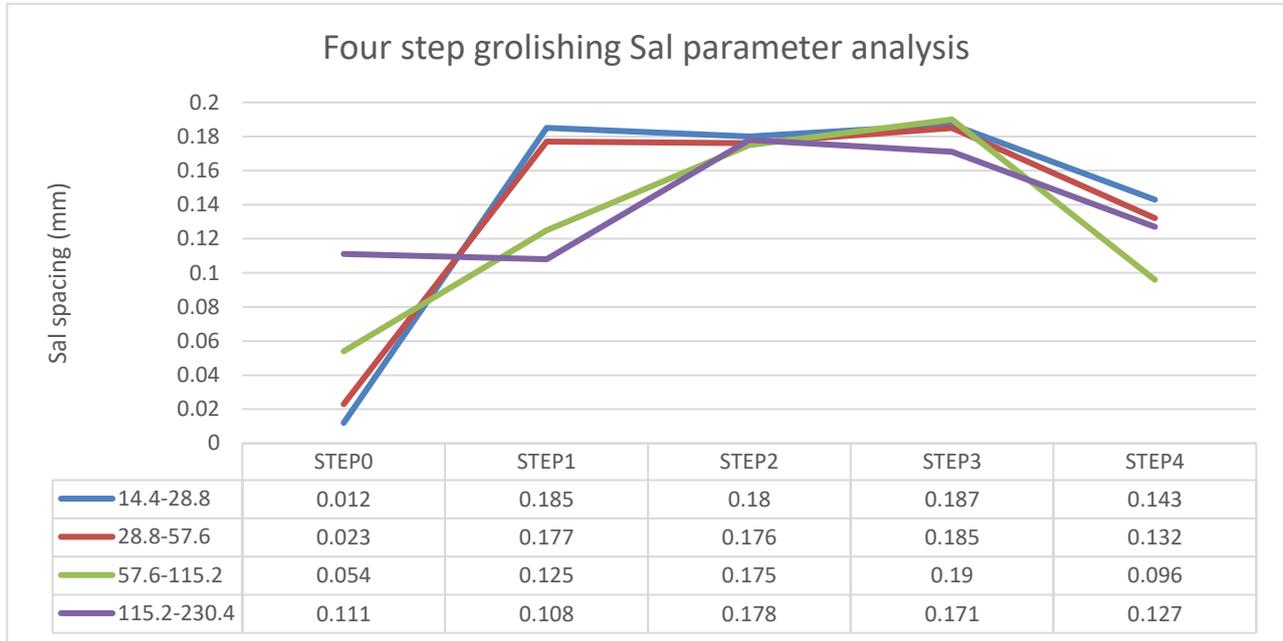
Figure 6-31:   Sal parameter analysis from four step grolishing results showing the trend of tool path imprint on workpiece

b.   *Seven step Grolishing*

Multi-scale wavelet analysis is also carried out on seven step grolishing process. The seven step grolishing process is designed to tackle two issues faced with four step grolishing process. The first one is to reinforce the grolishing process to remove the presence of deep grinding marks and the second one is to reduce the effect of the tool path imprint on the workpiece. The full version of the wavelet analysis results is available on Appendix 6-2.2. Figure 6-32 shows the step 2, step 3 and step 7 results in all four chosen wavelet ranges.

In step 2 for the grolishing process the tool path direction is deviated from the original by 45 degrees. This is clearly visible on the results of step two where the grolishing process tend to remove the marks from previous process and imprint its own mark at 45 degrees from X and Y axis. In step 3, parallel and 45 degrees to X and Y axis are performed respectively. Although, the step 3 grolishing finished with 45 degrees tool path direction, tool marks from parallel to X and Y axis are clearly visible at wavelet range (57.6 – 115.2) μm and (115.2-230.4) μm. However, in wavelet range (14.4 – 28.8) μm the direction of tool marks follows 45 degrees to machine axis direction. The step 3 grolishing results filtered foe roughness analysis also shows tool path from 45 degrees to machine axis printed on the surface (Appendix 6.1 Figure 7). This indicates that long grolishing process does not have influences on the surface waviness of ranges (57.6 – 115.2) μm and above. The final step (step 7 results) grolishing results shows less tool marks than the final step grolishing results obtained from four step grolishing process.

(µm)	STEP2	STEP3	STEP7
14.4-28.8			
28.8-57.6			
57.6-115.2			
115.2-230.4			
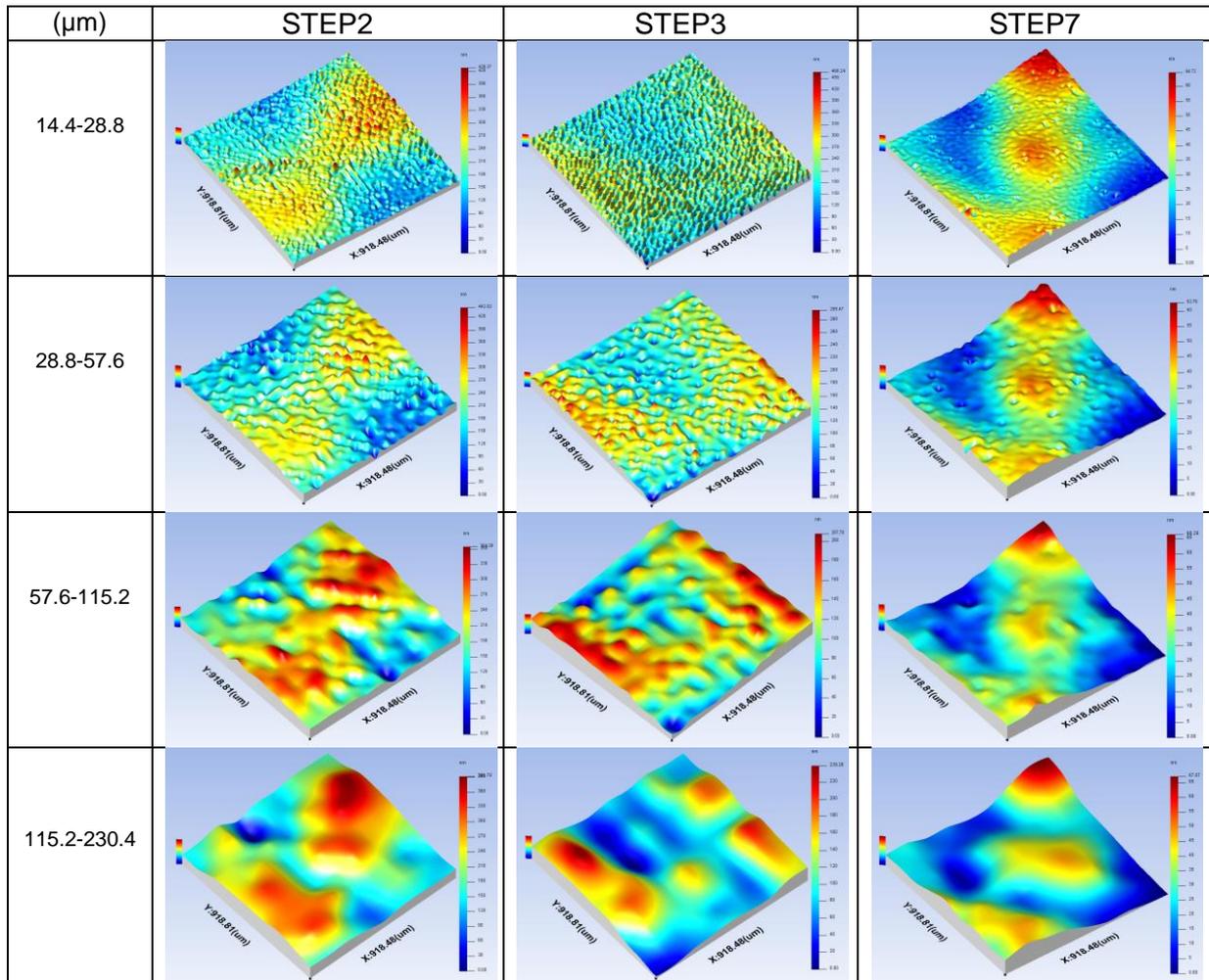
Figure 6-32:   Multi-scale wavelet analysis: Partial results from seven step grolishing process exposing tool path imprint on the workpiece studied at four levels of wavelet ranges

The Sal parameter is also used to analyse the seven step grolishing results (figure 6-33). The result shows similar trend to four step grolishing results with initial spacing from grinding process at each wavelet range, regrouped around 0.2 mm spacing for grolishing processes from step 1 to 6. The step 3 grolishing result at wavelet range (14.4 – 28.8) µm is the only result which does not follow the trend. Indeed, the results on that specific wavelet range shows tool path marks being directed all in one direction. In step 7 of the results all spacing from Sal parameter drops at the lowest spacing distance of around 0.13 mm in all four wavelet ranges.

Four step grolishing Sal parameter analysis

	STEP0	STEP1	STEP2	STEP3	STEP4	STEP5	STEP6	STEP7
14.4-28.8	0.01	0.212	0.201	0.014	0.19	0.158	0.201	0.135
28.8-57.6	0.019	0.212	0.199	0.181	0.191	0.158	0.205	0.136
57.6-115.2	0.046	0.206	0.195	0.19	0.191	0.152	0.203	0.124
115.2-230.4	0.087	0.161	0.193	0.152	0.142	0.154	0.159	0.139
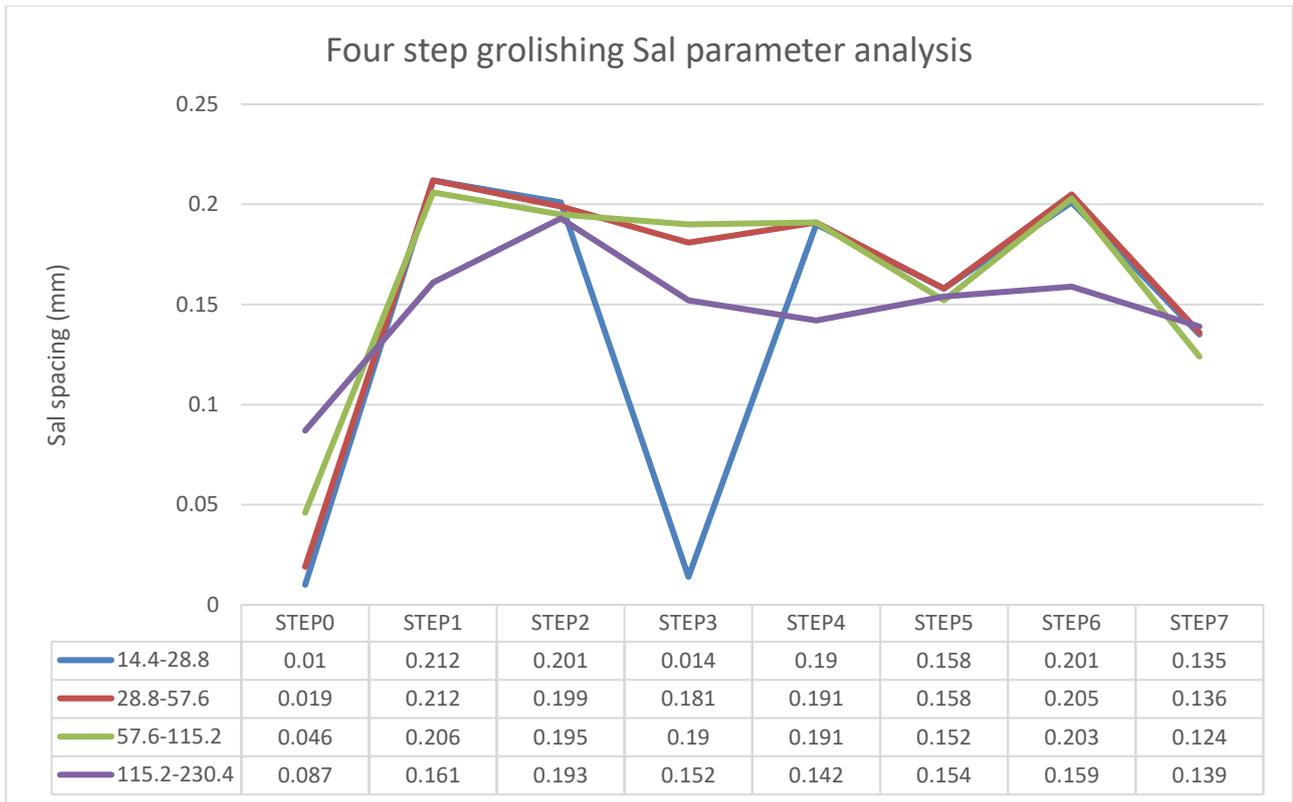
Figure 6-33:   Sal parameter analysis from seven step grolishing results showing the trend of tool path imprint on workpiece

6.4 Summary

This chapter investigated the grolishing ability of the designed machine. The grolishing process was developed by Walker et al [3] for smoothing surface roughness in a short period of time in order to be more attractive for industrial applications prior to a final finish polishing. Grolishing is also used for minor error form correction. Moreover, it has the capacity to attenuate machining marks without causing sub-surface damage. There are three main types of grolishing technique described in the literature: bonded abrasives on hard tool, bonded abrasives on soft tool, and loose abrasives with soft tool. This last form was used in the development of the present grolishing processes. Samples of P20 tool steel, a material widely used for mould tools, were ground flat. The surface roughness of the samples at this stage was around 0.55 µm Sa, which is equivalent to the finishing capability of CNC machining on P20 [223].

Grolishing is an aggressive process compared with polishing. The grolishing cloth wear from mechanical and chemical reaction can affect the performance of the process. The grolishing cloth therefore needs to be adapted to the material of the workpiece and its initial surface roughness condition. Ultrapad^{TM} cloth was chosen for coarse surfaces and Verdutex^{TM} cloth for intermediate surface conditions. Verdutex^{TM} was also used for the finishing process. 45 µm diamond abrasives were used to remove the grinding marks from the surface, followed by 9 µm diamond abrasives to smoothen the grolishing marks left from the previous grolishing process. Finally, 1 µm diamond paste was used for polishing to test whether surface roughness can be reduced to below 10 nm Sa using the grolishing method.

The theoretical spot sizes were calculated for different offsets and then evaluated experimentally. Offset spots measured from a Dino 2.0 microscope show two types of removal marks. The circular rings in the middle exhibit deep material removal and is caused by two body abrasion. The scratch marks on the periphery were caused by abrasives rolling freely between tool and workpiece, and is called three body abrasion. It was deduced that the two and three body abrasions resulted from the tool–workpiece contact. Indeed, the Hertz contact theory states that a rubber sphere pressed against a solid flat surface produces high pressure in the middle and lower pressure towards the edges, and this was reflected in the two and three body abrasions on the workpiece surface. Theoretical spot sizes are generally bigger than impact and contact spot sizes, except for the contact spot size of 0.1 mm offset. However, they all follow the same trend, with approximately 1 mm difference between theoretical and impact spot sizes. When line and areal grolishing was tested, it was found that 0.5 mm and 0.25 mm spacing on the tool path program produced 2.5 µm depth of material removal. However, 0.5 mm spacing is faster and produced a flatter surface than 0.25 mm spacing. Therefore, 0.5 mm spacing was chosen for development of the grolishing process.

A four step grolishing process was developed and performed. Results show the surface roughness was gradually improved from 461 nm Sa to 4 nm Sa on average. The waviness of the flat surface was improved from Wt = 1.33 µm to 0.61 µm. The spacing between peaks improved from WS = 828 µm to WS = 3048 µm. However, although the Four Step grolishing process improved surface topography in many ways, there was still some visible waviness on the surface, and for a surface supposed to be flat, some deep grinding marks were still visible. A Seven Step grolishing process was therefore designed in an attempt to remove the grinding marks and to improve the waviness error on the surface. The Seven Step grolishing process has gradually improved the surface roughness from 575 nm Sa to 7 nm Sa. The waviness of the flat surface was improved from Wt = 1.44 µm to 0.5 µm and the spacing between peaks improved from WS = 1138 µm to WS = 2084 µm. The grinding marks were totally removed from the surface. The PV of waviness was

smaller than that of the previous (four step) grolishing process; however, the spacing between peaks was shorter than produced by the previous grolishing process, which still affected the visual appearance. Where the Wt needs to be smaller than 0.5 µm and WS larger than 2 mm, form correction needs to be performed before final polishing. Nevertheless, the results obtained are better than those obtained by Walker et al. using IRP600 to grolish silicon carbide [190].

The improvement of surface roughness over each grolishing step was studied in frequency domain. It is interesting to note that high amplitude frequencies from the ground surface remain the dominant frequency on the surface until the surface roughness reach approximately 10 nm Sa. Only below 10 nm Sa, the high amplitude frequency is obtained at 1.087 Hz, which corresponds to the length of the data profile. Therefore, a 15 mm long roughness profile was measured on low force contacting stylus instrument (Dektak Bruker) for both the four and seven step grolished samples. A surface roughness Ra of 4.3 nm was obtained on the four step grolished sample and 5.74 nm Ra on the seven step grolished sample. These data were used to produce an amplitude spectrum in frequency domain. The results are presented in figure 6-34. The high amplitude frequency for the four step grolishing process is at 0.3334 Hz, which corresponds to peaks obtained every 2999 µm. This confirms the spacing between peaks WS = 3048 µm obtained on waviness error. The second highest amplitude frequency is at 0.4668 Hz, which corresponds to peaks obtained every 2142 µm. The third highest amplitude is at 2.134 Hz, which corresponds to one of the dominant frequencies identified on the ground surface. This indicates that, even at such smooth surface roughness, the effects of previous machining processes are still present.

By contrast, on seven step grolished sample, the highest amplitude frequency is at 0.4668 Hz. This confirms the spacing between peaks WS = 2084 µm obtained on waviness error. The second highest frequency is at 1.8 Hz, which corresponds to peaks every 555 µm, which might correspond to 0.5 mm tool path spacing distance printed on the surface topography. It was observed that the four Step grolishing process had high amplitude at both 0.3334 Hz and 0.4668 Hz, in contrast with the seven step grolishing process, which only had a high amplitude frequency of 0.4668 Hz.
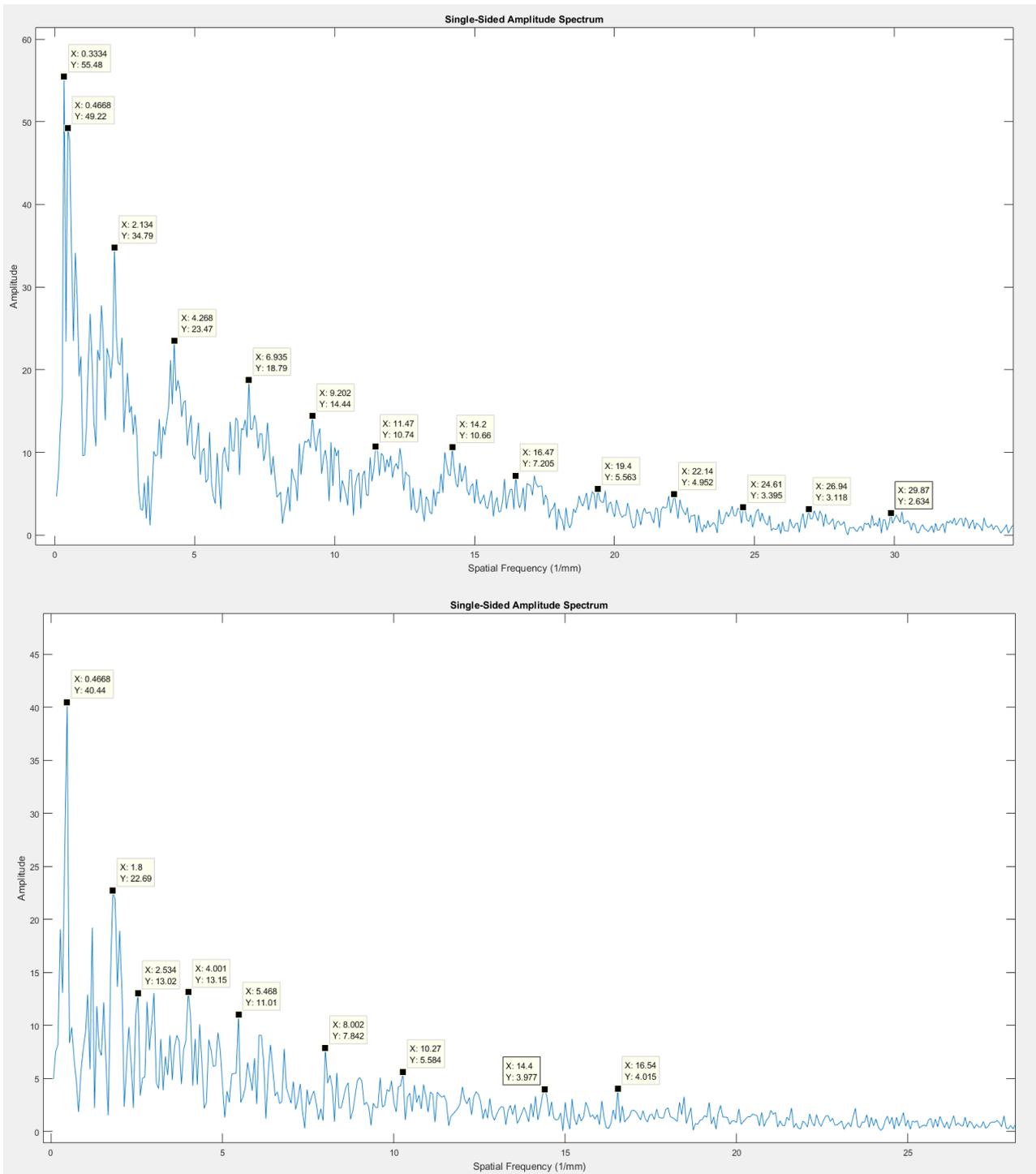
Figure 6-34:   Amplitude in frequency domain 15 mm profile: four step grolishing (top) & seven step grolishing (bottom)

Overall it is considered that grolishing is a process that can be implemented on the presently designed hexapod machine. The results above show that as using the present hexapod machine, grolishing can be implemented as an effective means for reducing surface roughness and effects of prior processes before final polishing is applied to workpieces.

7 OVERALL DISCUSSION

The need for a precision polishing machine is clearly expressed in Chapter 1. Based on the industrial pull for a low cost freeform polishing machine. A concept development process and prototype of the machine is conceived and constructed in chapter four of this thesis. The developed machine finishing capability is tested on Chapter five of the thesis. Further work is prepared for a grolishing process capable of improving surface roughness from ground finish (0.5 µm Ra) to mirror like finish with less than 10 nm Ra. The detail of the developed grolishing process is discussed on Chapter six of the thesis. This chapter will discuss and offer an overall summery of Chapters four, five and six of the thesis.

7.1 Machine design methodology

A new concept of an inexpensive polishing machine based on a parallel kinematic system is developed in chapter four of this thesis. Design methodology principles are followed to ensure the successful development of the machine. A BP machine with the ability to perform freeform movement within a workspace volume of 50 mm^3 is developed. The design machine has a footprint of less than 1 m^2, with low energy consumption (<1 kW). Further emphasis is put to keeping the cost of the developed machine as low as possible without compromising on the quality and reliability of the developed product. The use of parallel kinematic system as a precision multi-axis movement system enabled a workspace volume bigger than 50 mm^3. Using the design approach for an integrated system helps to obtain high precision movement at low cost. However, the slope inclination of the workpiece will limit the work volume range of the Hexapod. The tool path programme of the workpiece needs to be tested to check if the hexapod can reach the desired location of the workpiece and if it is within the range of the hexapod movements.

A number of machine design configurations are possible. Advantages and disadvantages of the design configuration are discussed. In precision machining horizontal spindle alignment is preferred over vertical spindle alignment. Indeed, during the machining process the chips are easily ejected from the cutting area which enable the achievement of a better surface finish than vertically aligned machine. However, this machine is developed on a vertical spindle alignment configuration for the following reasons. The designed machine is aimed to produce polishing and grolishing processes using paste based abrasives for economic process and quick change of paste material and size without any contamination. The efficiency of the polishing and grolishing process using paste abrasive is affected in horizontal positioning of the machine. The polishing paste will not adhere on the surface of the workpiece due to its consistency prone to flow downward following the gravitational field. Further, for a horizontal spindle alignment, the mass of the hexapod will dramatically affect the machine positioning due to deflection with the present machine structure assembled using aluminium extrusion frame for a cost effective prototype design.

The polishing tool is composed of a shank, rubber bonnet and polishing cloth. A standard Ø 6 mm rod is used as shank with a spherical rubber bonnet made of Ø 20 mm and polishing cloth glued on top. The shank diameter can be adapted to the polishing surface complexity from Ø 0.5 mm to Ø 6.35 mm. Rubber bonnets with different stiffness, size and shapes can be developed and tested. Indeed, rubber bonnets with flat end could benefit the polishing of flat surface. Cylindrical shape bonnet can be used for polishing side wall of a groove. Conical shapes could be developed for

polishing corners. Finally, aspherical shape bonnets could be developed to achieve evenly distributed force over the entire contact area.

The rubber bonnet is glued on a holder which is screwed to the shank. During the gluing process, the positioning could be off centred between bonnet and shanks which will dramatically increase the runout error of the spindle. Further the length of the shanks is longer than the spindle manufacturer instruction to achieve less than 1 µm runout error. This will also lead to an increased runout error of the tool. Although, the runout error of the tool will not affect the polishing process of a flat surface. It will definitely cause form errors on surfaces other than flat. Therefore, the holder of the rubber bonnet was redesigned to limit the runout error. Further, the assembly of the spindle holder was also redesigned to reduce tool shank length. The new design will be discussed in the future work section (Chapter 8).

All other components of the machine were carefully designed and manufactured or purchased to build a potentially freeform polishing machine. The workpiece is held on a tripod base used to align the workpiece with respect to hexapod X and Y axis. For flat surfaces the alignment in X and Y axis direction is performed manually. The distance in Z direction between tool end and workpiece is identified using shims of known thickness. The current machine design lacks in the ability to identify accurately the distance separating the tool and workpiece and also aligning the workpiece in X and Y axis with respect to hexapod axis. Preliminary work to solve this issue is developed and discussed on Future work section (Chapter 8).

Last but not least, a method is required to generate tool path program for components with curvature. The current hexapod controller reads GCS commands and executes movements accordingly. Manual writing is not a viable solution for industrial utilisation and certainly not a cost effective solution. A solution to generate program on GCS commands from a CAD model was developed and implemented on the machine. The detail is discussed in the future work section (Chapter 8). Although several elements of the design need further improvement, the initial aim of prototyping a low cost precision polishing machine capable of polishing freeform curvature is achieved.

7.2   Polishing process development on Hexapod polisher

The prototyped machine was evaluated for its ability as a precision polishing machine. Flat surfaces of P20 tool steel were used as test samples. The material P20 is widely used in injection mould industry for its purity and polishability. Very few research papers are available describing the finishing capability on this material. Unlike, the Zeeko-Classic process which uses an inclined tool during polishing, the designed machine aimed to perform polishing normal to the workpiece surface. The tool used is relatively small compared to the bonnet tool used on Zeeko polisher. Additionally, the workpiece material, and all other polishing parameters have an influence on the material removal rate and surface finish. Therefore, empirical experiments are performed to understand parameters which influences surface finish.

Empirical experiments helped to identify inconsistency in the obtained results. The causes of result inconsistency were identified and appropriate actions were taken to solve them. Further, it was noted that the consistency of the polishing paste has impact on the polishing performance. Indeed, it was found that a muddy consistency is ideal for polishing rough surface as it adheres better to the surface to remove large amounts of material and shorten the smoothing process time. Similarly, a liquid

consistency is found to be ideal in final finishing process for obtaining mirror like finish without visible scratch marks on the surface. The amount of paste applied needed to be consistent for process control as the material removal is related to the amount of paste applied. Indeed, for a same initial surface condition of a rough surface, higher paste concentration improved the surface roughness to a greater extent than a lower paste concentration. On the other hand, for a same initial surface condition of a relatively smooth surface, higher paste concentration resulted in increased scratch marks compared to lower paste concentration which improved further the surface roughness.

Empirical analysis showed that all parameters had an impact on the surface finish results. However, the variation of certain parameters such as polishing cloth, abrasive size, abrasive concentration, paste consistency (muddy or liquid) are related to the initial surface condition of the samples. Once these parameters are appropriately selected based on the initial surface condition, other parameters such as feed rate, spindle speed, tool offset and number of passes needed optimisation for surface finish improvement. Indeed, each combination of these parameters provided a different outcome. Therefore, Taguchi method were applied to identify the optimum polishing conditions for the smoothest finish. Optimum parameter conditions help to achieve 75% improvement with surface finish to below 10 nm Sa.

ANOVA statistical method was used to analyse the experimental results from Taguchi DOE. The purpose of the analysis was to identify the percentage of contribution of each parameter with respect to the overall outcome. Results showed that tool offset to be the largest contributor to surface finish improvement with 45.3% contribution. It is then followed by spindle speed with 39.14% contribution. The last remaining two factors had very little contribution; number of passes and feed rate having respectively 2.65% and 2.34% contributions. It is interesting to note that the two main contributors are important factor of material removal process dictated by Preston equation. The pressure applied by the tool onto the workpiece and the surface speed obtained from the interaction between spinning tool and workpiece improved the surface roughness by means of controlled removal of material.

Polishing with re-circulating slurry was lastly performed in chapter five of this thesis. In order to experiment this polishing process, a new workpiece holder which allowed smooth slurry flow for easy re-circulation around workpiece and slurry tank was developed. The other reason was to keep the slurry circulation area small, to reduce the possibility of external contamination and also reduce the amount of slurry required for the circulating process. A force sensor from Kistler was used to detect tool – workpiece contact and also used as an instrument for workpiece alignment in X and Y direction. Although, the sensor has performed the desired task, it remains an expensive solution (£3,000 - £4,500) for just identifying the contact and aligning manually using the same contact method. Further, the sensor could not position the workpiece on the tilt around Z axis. The re-circulating polishing was performed with the purpose to validate the slurry polishing process. After 25 passes the surface roughness was at 7.4 nm Sa with an initial surface condition of 6.4 nm Sa. A good slurry flow between workpiece holder and the tank was observed. Self-adhesive polishing cloth are prone to lose the glue effectiveness on a lengthy polishing process. Therefore, is it recommended to glue the pads or cloth manually for lengthy polishing process.

7.3   Development of grolishing process for P20 tool steel

The grolishing process is used as an intermediate process between grinding and polishing to smoothen the surface roughness quicker. It also has the ability to reduce mid-spacial frequency

errors and remove sub-surface damage left from previous machining process without affecting the form accuracy. Moreover, the grolishing process is used to correct minor form errors. There are three grolishing technics available in the literature; hard tool with bonded abrasives, soft bonnet with bonded abrasives, and soft bonnet with loose abrasives. The chapter six of this thesis presents the research work on implementing the grolishing process on the presently designed machine using soft bonnet with loose abrasive technics. It was noted in the literature that through CNC Milling process a surface finish of around 0.65 μm Ra can be achieved. In plastic injection moulding industry, the mould tools are often hand finished after CNC machining which requires high skilled technicians and are inclined to be affected by human errors. Therefore, the grolishing process was performed on ground P20 samples with similar surface finish achieved by CNC milling. The aim was to generate an automated, reliable process as an alternative to hand finishing.

The grolishing process requires surface finishing cloths and abrasives adapted to the rough condition of the sample surface. Indeed, the wear of the cloth or inefficiency of the abrasive particles can dramatically delay the process time. The Ultrapad™ cloth was chosen for coarse surfaces and Verdutex™ cloth for intermediate and fine surface conditions. Diamond abrasives with average particle size of 45 μm were used on coarse surface to remove the grinding marks from the surface. It was then followed by 9 μm to attenuate scratch marks produced by previous grolishing processes. Finally, 1 μm diamond paste was used for final finishing to verify if a surface roughness below 10 nm Sa could be attained using the grolishing method.

The experimental spot sizes are produced at three different offset values to compare with the theoretical spot. The experimental spots showed three distinct regions; (1) small circle in the middle with no material removal, (2) circular rings in the middle caused by micro cutting and ploughing, (3) scratch marks on the outer region caused by abrasives rolling freely between tool and workpiece. Theoretical and experimental spots followed the same trend with experimental results being slightly smaller than the theoretical spot size. This difference was considered to come from two sources; contact position error between tool and workpiece which modifies the contact area for a given offset and/or the grolishing process being inefficient towards the edge region of contact. The grolishing was then performed on a line cut and as a square patch to evaluate the material removal depth and material removal form achieved over an area. The results were used to prepare an efficient grolishing process which could remove all grinding marks from the surface. In standard bonnet grolishing processes an influence function is produced and used for the MRR calculation. MRR is then used for creating tool path with necessary dwell time to remove the desired layer of material. However, this is not an accurate process for the present machine and there is a need for measurement and additional grolishing steps as appropriate.

To improve the surface roughness of a ground sample to a mirror like finish, a four step grolishing process was designed and performed. The initial aim of reaching below 10 nm surface roughness was comfortably reached. However, visible waviness patches were noted on the surface and deep grinding marks which were not identified during the initial measurement stage became visible. It is assumed that the visible waviness patch may have come from the raster tool path performed in both X and Y axis of the machine. Therefore, a new Seven step grolishing process was designed to tackle both grinding marks and the waviness patch. In order to remove the grinding marks, the initial aggressive grolishing steps were extended. To reduce the visibility of the waviness patch, the tool paths were equally performed in every 45 degrees. This grolishing process achieved the desired surface roughness. The grinding marks were totally removed as expected. However, the waviness patch was much smaller but still visible.

Further, the measured results from each step were analysed in frequency domain. The aim was to identify high frequency spikes from the ground finish to verify their elimination process and identify any new spikes produced during grolishing process. It was noticed that all frequency spikes were attenuated in amplitude at each grolishing step. High amplitude frequencies noted after grinding remain the dominant frequency until the end. Four step grolishing improved W_t from 1.33 µm to 0.61 µm and WS from 828 µm to 3048 µm. The seven step grolishing improved the W_t from 1.44 µm to 0.5 µm and WS from 1133 µm to 2084 µm. Seven step grolishing was more effective than four step grolishing in reducing the gap between highest peak and lowest valley. However, the four step grolishing was more effective than seven step grolishing in increasing the spacing between two waviness peaks (i.e. increase the spacing between peaks would reduce waviness error). Further grolishing steps could be developed to reduce more these errors depending on the application requirement.

During the polishing/grolishing process, a soft rubber bonnet is pressed against the polishing workpiece vertically downwards creating a pressurised surface contact. The contact can be characterised as a Hertz contact with high pressure applied in the middle region and low pressure towards the circumferences. The rotating speed of the spindle produce surface speed on the contact region. It varies from zero in the centre to its maximum on the circumference of the contact region. The feed rate of the machine enables the contact region to be mobile. The continuous movement of the spindle during polishing process remove the effect of zero surface speed in the middle. The polishing abrasives penetrate between the polishing pad and the workpiece. The material removal is caused by two body abrasion in the impact region, where micro cutting and ploughing are obtained. On the other hand, the material removal is caused by three body abrasion on the region around the circumference of the contact spot, where micro cracks and micro fatigue are observed. The hardness of the polishing pad, the concentration of abrasives, the applied pressure, the rotating speed and feed rate have an impact on the material removal mechanism. Careful selection of these parameters allow these parameters have enabled to perform reliable polishing and grolishing on P20 tool steel samples.

Overall it is considered that the aims of developing a prototype inexpensive precision machine has been achieved. The machine was tested for its finishing ability and also for its ability to implement grolishing as an increased MRR process. The functionality of the machine is considered to be good for a prototype and the performance would be considerable optimised on future versions of the machine.

8 CONCLUSION AND FUTURE WORK

8.1 Conclusion

A need for a low cost freeform polishing machine is identified in earlier chapters. Industrial requirements were analysed in detail through a methodological design procedure which helped to produce a new concept design. Through careful market analysis relevant sub-systems were identified and purchased in order to facilitate an integrated design approach. The integrated design approach helped to reduce the time necessary for machine development, minimise risk associated with the developing system and reduced the cost associated with research and development. The developed polishing machine has the ability to move the tool end effector with microns precision in six degrees of freedom allowing precision freeform polishing.

A prototype of the bonnet polishing machine was assembled and tested as a precision polishing machine. Polishing and grolishing were performed on P20 tool steel used in the plastic injection industry for manufacturing mould tools. Empirical experiments gave a clear understanding of surface roughness improvement process and helped to eliminate result inconsistency for a robust polishing process. Taguchi method helped to optimise polishing parameters to successfully reach less than 6 nm surface roughness Ra with 75 % improvement ratio. Moreover, step grolishing process using soft bonnet loose abrasives method was developed. The developed process achieved a surface roughness of 4 nm Sa from a ground finish of 461 nm Sa.

The overall machine development cost was approximately £ 35,000 with it being possible for the machine to be built by two technicians in half day. The polishing process improved the surface roughness of a specimen of 30 mm^2 in 8 minutes going from 30 nm to 7 nm Ra. The grolishing process reached mirror like finish from a ground finish in around 75 minutes, though it is considered this could be improved considerably. The developed process for both polishing and grolishing are simple and inexpensive. Further, a re-circulating slurry system was designed to function with less than five litres of slurry which would reduce the cost associated with polishing consumables. The slurry circulating system was designed for easy maintenance. The parts used for slurry circulation can be easily removed from the machine and cleaned separately to avoid contamination. Finally, the integrated design approach provided a "near zero-breakdown" machine with the possibility to replace the faulty sub-system quickly.

The novel hexapod polisher has demonstrated its capability as a precision finishing process. It also has the ability to provide precision freeform movements. However, the machine does not yet have a easy access CAD/CAM system to generate polishing programs for surface other than flat. Moreover, there is not as yet a method to identify the distance separating hexapod and workpiece origins in machine X, Y and Z axis. These two features of the machine are crucial to qualify the machine to be fit for freeform polishing. Time did not permit the polishing of surfaces other than flat due to the size and complexity of this total project. Indeed, the use of hexapod for polishing purposes had several challenges which have been addressed with the manufacturer PI which has allowed for continuous improvement. The results inconsistency on empirical experiments has also taken considerable amount of time to identify the source of problems to solve them. However, preliminary works accomplished to implement freeform polishing to the machine will be presented in an extended future work section.

8.2 Future Work Programme

Future tool path programming and Tool – Workpiece relative distance sections are presented below in terms of illustrating the work that must be completed to implement geometrical shape polishing capabilities. Some completed preliminary work in the above areas in also presented in this future work section.

8.2.1 Tool path programming

The developed machine has a lack of method to quickly generate polishing programmes. The Hexapod reads GCS commands which is not a common programming command used in the machining industry. Further, the hexapod design concept with its machine kinematic makes it difficult to find a suitable CAM software for future development of the polishing machine. Fortunately, the software VisualCAM for SolidWorks 2017 developed by Mecsoft have been identified as a potential solution to solve this issue. Indeed, the vendors provide a more reasonable pricing for the CAM package than other competitors. Using the VisualCam software a request is made to generate programs for executing movements with program lines structured to fit the hexapod controller. The kinematics of the hexapod is setup in the CAM software with the correct assignments of the axes and taking into account their respective working range.

A part with random freeform curvature is designed on Solidworks (figure 8-1). The workpiece sample has cut grooves on four edges in line with X and Y axis of the sample. These grooves will be used to align the workpiece with respect to hexapod axis using the DRI. The intersection of the construction lines indicates the highest point of the freeform surface. The vertical distance (Z axes) separating hexapod origin and this point would be measured using DRI system. The origin of the program would be in the center of the workpiece in X and Y axis and at the highest point in Z axis. The virtual location of this origin can be located using the DRI.
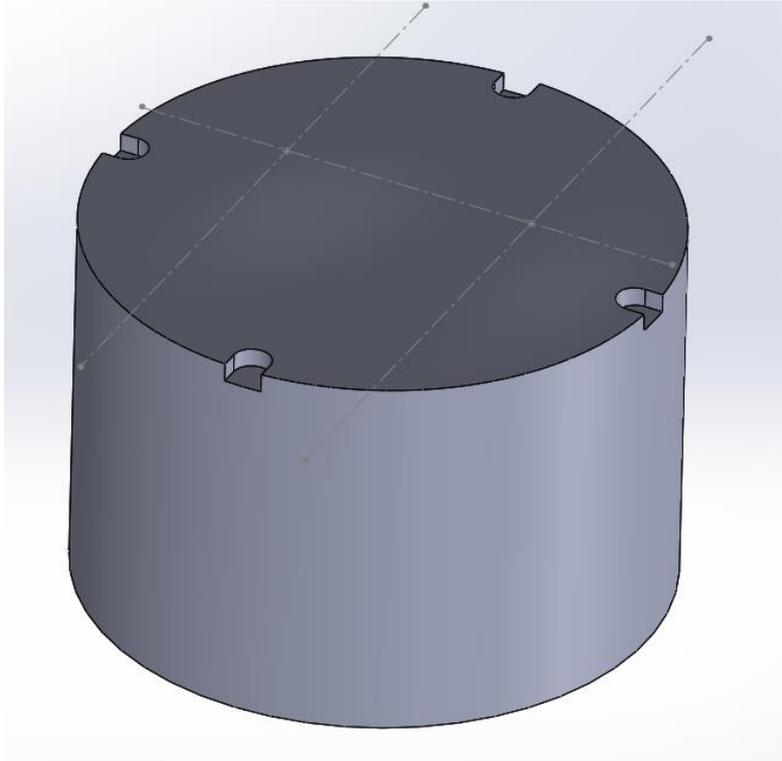
Figure 8-1:   Workpiece sample with freeform curvature

The designed part is used to program tool path using a raster scanning method. It is programmed to have the tool always perpendicular to the point of contact. figure 8-2 shows in yellow the tool entry, blue parallel lines represent the raster program and finally the red line shows the tool exit. The CAM software has the ability to generate programmes with microns incremental movements in X, Y and Z axis.
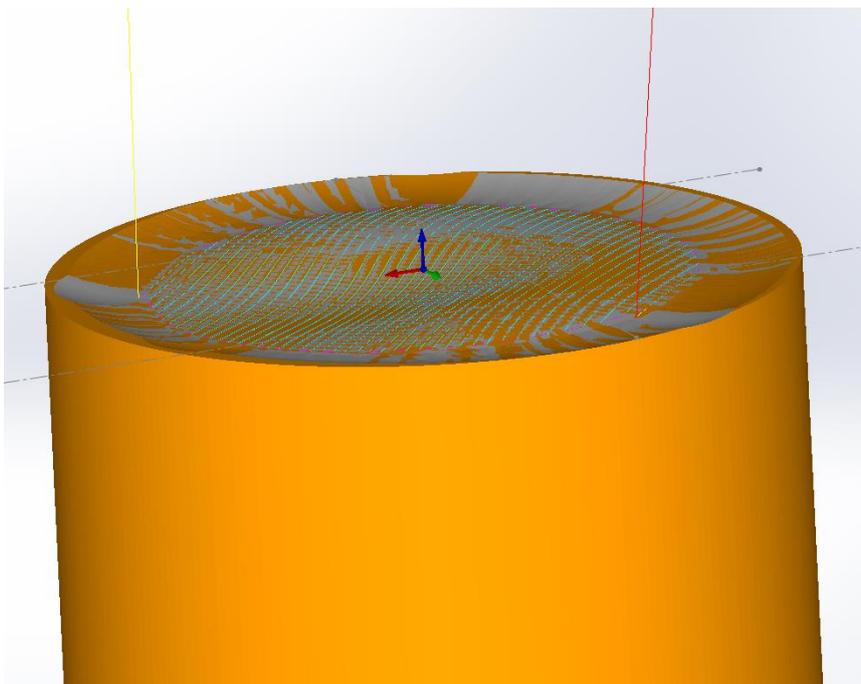
Figure 8-2:   Raster polishing tool path for potential freeform polish

The polishing program is generated using GCS commands. Figure 8-3 shows the first 30 lines of the program. Each line of movement is preceded by MOV and movement coordinates in three linear and two rotary axes. The program also automatically adds a verification line of command "WAC ONT? X = 1" to ensure that previous line is completed before executing the following line. The program is virtually executed on the hexapod to verify if it could be performed without reaching the limits of the hexapod arms movements. In this case, the program can be executed on the hexapod. As can be seen in figure 8-3, the program does not contain any information about machine feed, spindle speed, spindle start-stop or other relevant information about the polishing process. At least initially the polishing can be performed by manually activating these commands. However, there is the possibility of automatically activating this process by including these commands on the CAM program and executing the movements on the hexapod and spindle via a programmable logic controller (PLC) software.

```
MOV X -4.503 Y 12.713 Z -23.686 U -5.617 V 2.613
WAC ONT? X = 1
MOV X -4.503 Y 12.713 Z -19.454 U -5.617 V 2.613
WAC ONT? X = 1
MOV X -4.047 Y 11.735 Z -9.512 U -5.617 V 2.613
WAC ONT? X = 1
MOV X -3.591 Y 10.757 Z 0.429 U -5.617 V 2.613
WAC ONT? X = 1
MOV X -2.322 Y 10.749 Z 0.371 U -5.617 V 2.613
WAC ONT? X = 1
MOV X -2.066 Y 10.749 Z 0.360 U -5.875 V 2.535
WAC ONT? X = 1
MOV X -1.809 Y 10.749 Z 0.348 U -6.124 V 2.413
WAC ONT? X = 1
MOV X -1.553 Y 10.749 Z 0.338 U -6.357 V 2.248
WAC ONT? X = 1
MOV X -1.297 Y 10.749 Z 0.328 U -6.571 V 2.040
WAC ONT? X = 1
MOV X -1.124 Y 10.749 Z 0.322 U -6.702 V 1.893
WAC ONT? X = 1
MOV X -0.952 Y 10.749 Z 0.317 U -6.823 V 1.743
WAC ONT? X = 1
MOV X -0.779 Y 10.749 Z 0.312 U -6.934 V 1.593
WAC ONT? X = 1
MOV X -0.606 Y 10.749 Z 0.307 U -7.034 V 1.442
WAC ONT? X = 1
MOV X -0.434 Y 10.749 Z 0.303 U -7.124 V 1.289
WAC ONT? X = 1
MOV X -0.262 Y 10.749 Z 0.299 U -7.205 V 1.136
WAC ONT? X = 1
MOV X -0.089 Y 10.749 Z 0.296 U -7.275 V 0.981
WAC ONT? X = 1
```

Figure 8-3: GCS program generated by VisualCAM 2017

8.2.2 Tool – workpiece relative distance

The Hexapod was purchased with no persons in the group with experience on how to operate it effectively. The standard software available did not have collision checking before executing any movement. This situation was taken into consideration when the spindle holder was designed. The initially designed spindle holder held the spindle on the base level of the hexapod. Figure 8-4 shows the initial design of the spindle holder. It required a long tool shank to reach workpiece to avoid any chance of collision between hexapod base and workpiece.
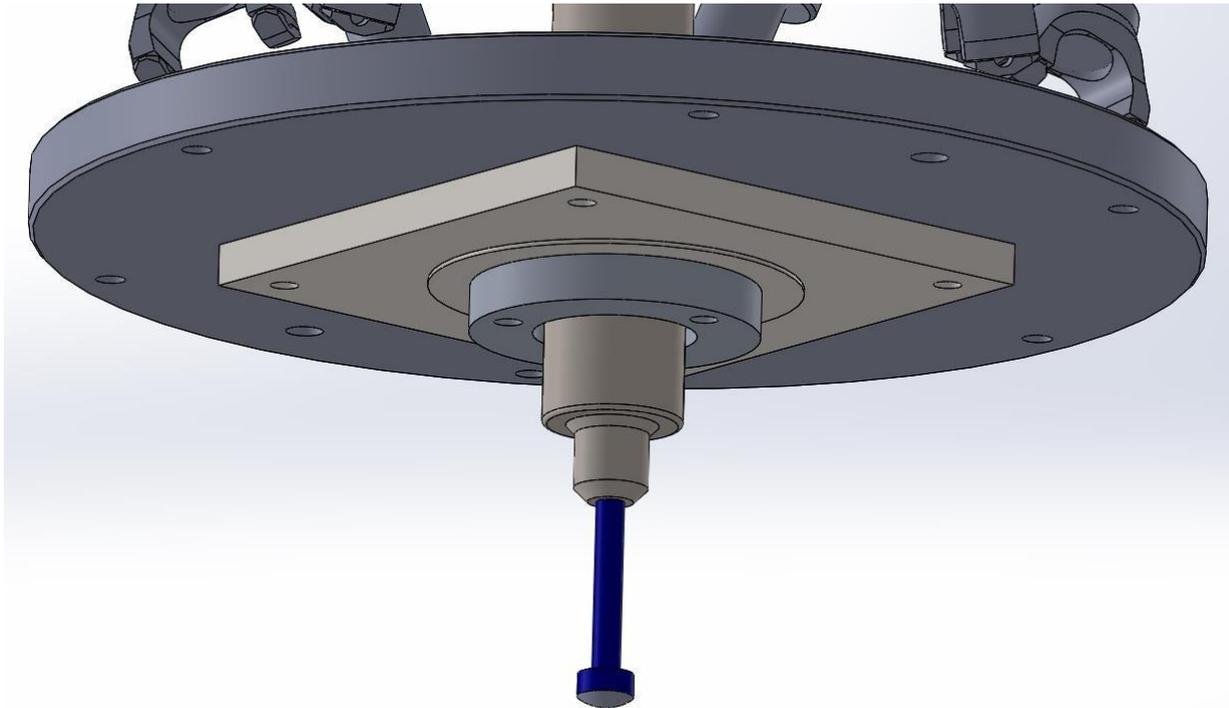
Figure 8-4:   Initial tool holder design

At the beginning of the project only flat surfaces were polished in order to understand parameters which influenced the polishing result. The use of long tool shank did not have issues when polishing flat surfaces. Once influential parameters were studied and understood, it was required to experiment these parameters on surfaces other than flat. At this stage the long shank was becoming an issue. In addition, the long shank had a bigger spindle runout which induced error on the polishing spot size, hence affecting the influence function of the polishing process and thus potentially causing error on the form accuracy. As far as form polishing is concerned, the spindle runout and the polishing spot size needed to be well controlled to replicate the form produced by the movement of the Hexapod.

Further, the contact between the tool and the workpiece is visually checked. This method does not provide a consistent tool position in Z direction. It affects the polishing process in many ways. The tool offset is not accurately know which induces error in the spot size and the pressure applied on the workpiece during polishing. Moreover, polishing programs are created from an imaginary origin on the workpiece. The tool end should reach this imaginary position in the X, Y and Z coordinates manually. As explained earlier for polishing flat only the positioning on Z axis is needed and this was achieved by visual checks and shims. In order to polish surfaces other that flat an instrument is required to locate the position of the tool with respect to the workpiece in X, Y and Z coordinates.

A Keyence LK-081 laser sensor was initially used as an instrument to locate the workpiece position. The laser point is crossed through the workpiece to identify the center position. Once the center of the workpiece is identified, then the hexapod is moved accordingly to reach the Workpiece origin location in X and Y direction. However, the laser could not identify the distance in Z direction between tool end and workpiece. figure 8-5 below shows the CAD design of the laser sensor fixed on a bracket which was mounted on the spindle mounting plate.

164
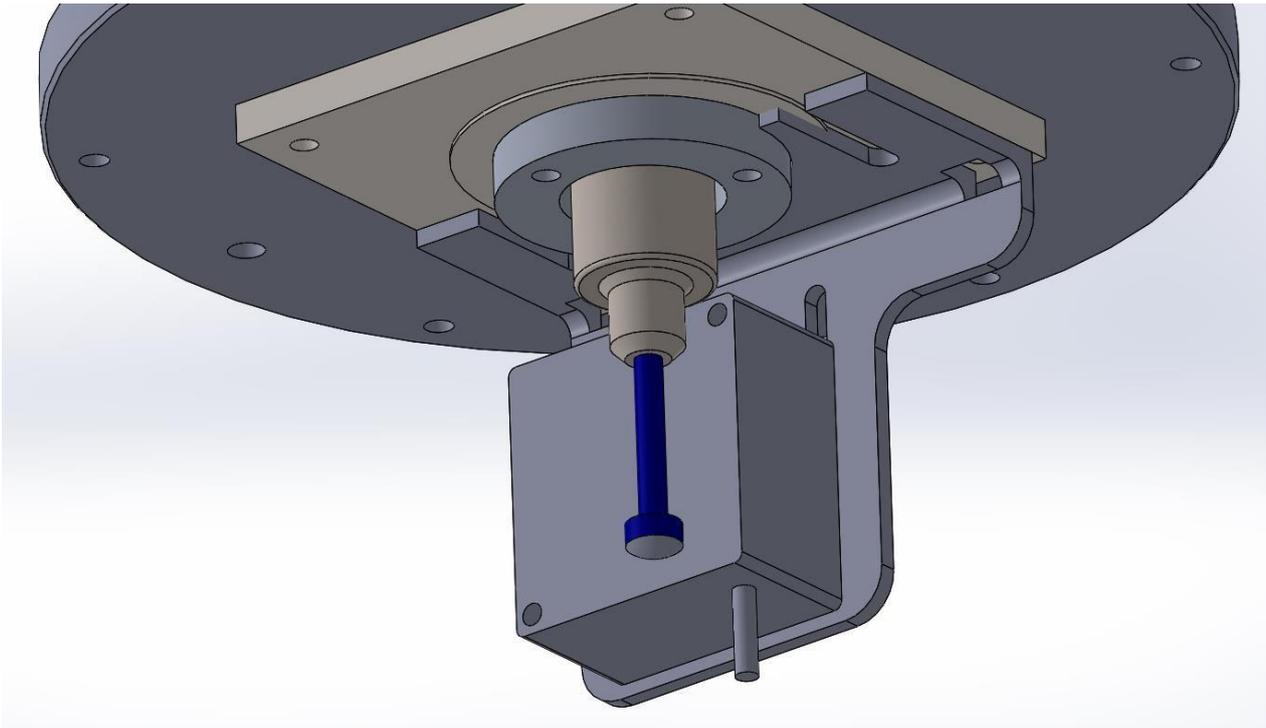
Figure 8-5:   Keyence laser sensor mounted on the hexapod

Although the sensor could accurately locate the workpiece in X and Y direction, this method was not retained for further development for the following reasons. As mentioned earlier, it could not identify the distance in the Z direction. If the size of the tool shank is reduced, then the sensor instrument is too big to be placed near the tool. Therefore, another instrument, small in size with the ability to identify the relative distances between tool-workpiece origins and a good standoff distance was required. Dispersed reference interferometry (DRI) using single point method seemed to be an ideal instrument to solve previously identified problem. DRI is designed to preform high precision linear measurements on a machining environment. The measurement probe is connected through an optical fibre to the DRI apparatus [226].

A new spindle holder system was designed to hold the spindle and the DRI on the Hexapod. This holder aimed to hold the spindle away from the Hexapod base to avoid chances of collision between hexapod base and workpiece holder during polishing process. The new spindle holder assembly is composed of a conical shape holder, a DRI fixture and L bracket. The detail of the concept design and their working process is explained in table 8-1.

Table 8-1:   New spindle holder design and working principles

	This is the overall assembly of the tool holder. Spindle holder DRI DRI fixture L bracket Polishing tool
	Section view shows the detail on fixings. The theoretical distance between the tool and the DRI is 10mm. The working distance of the DRI starts at 18mm. Therefore, there will be an 8mm distance clearance between tool and workpiece while the DRI is aligning the workpiece or measuring. This should avoid any chance of collision. 10mm
	There are four M6 threaded holes equally spaced on the hexapod base. The top of this part will be attached to the hexapod base using countersink screws for self-centring between hexapod and this part. The bottom face will be used as reference plane where the DRI holder will be mounted.
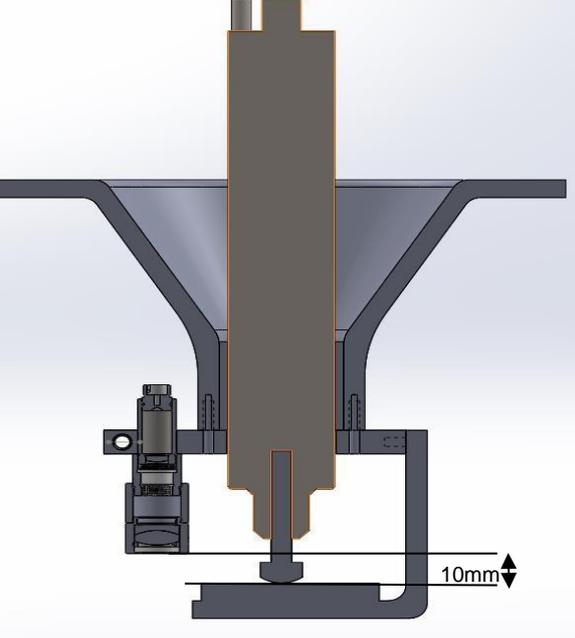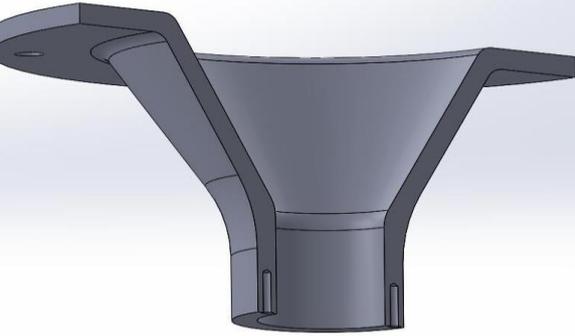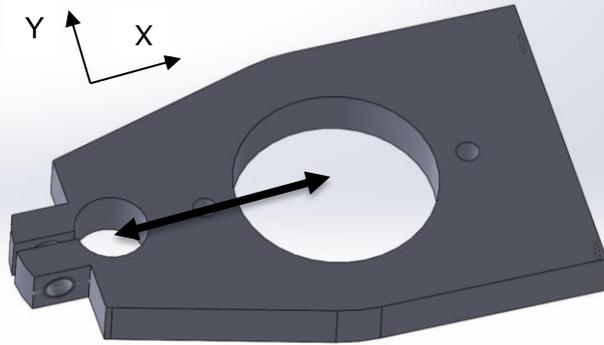
Table 8.1 continued	
Y, X	This is the DRI holder Through hole in the middle for spindle. The DRI will be assembled in the small hole. The distance separating the hexapod origin and DRI origin in X and Y axes will be measured on CMM once the system is assembled. The theoretical distance in X axis is 30 mm and Y axis 0 mm. The distance separating the DRI and Hexapod origins in Z axis is discussed on the next row.
	L bracket The L bracket is used for fixing the tool at the same position in Z direction all times. It has two dowel pin positioning holes for ensuring repeatable positioning and two threaded holes on DRI holder for fixturing. The tool shank will be placed inside the spindle chuck without tightening allowing the tool to move freely in the axial direction. The tool will touch the L bracket. At this position the chuck will be tightened using a digital torque spanner for a repeatable tightening process. During the tightening process the collet grips the shank and lifts the tool upwards. However, due to the repeatable tightening process the lifting distance remains the same each time. The process was tested and measured using a force sensor. The process is aimed to the obtain same distance between hexapod origin and tool end every time. The preliminary results showed the capability of this method to identify the distance separation hexapod origin and tool end in axial direction within 50 µm, however it needs further measurement for validation.
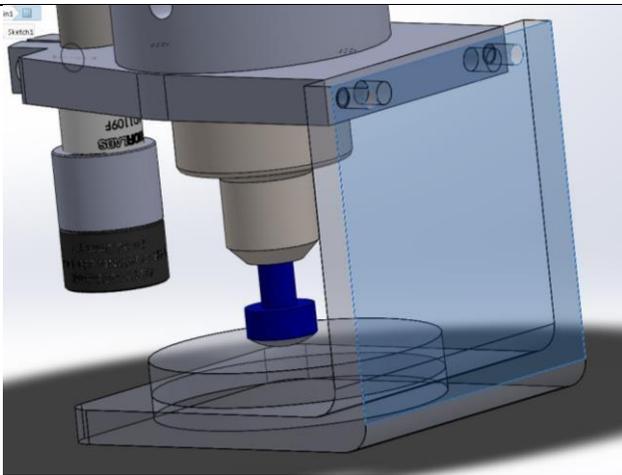
Table 8.1 continued	
	Hexapod and DRI origin distance in axial direction. To get the distance vertically between the both Hexapod and DRI origins; The distances A, B, C, and D need to be measured accurately on a CMM. They will be measured once all parts are assembled to account for error from the assembly process. The DRI will measure the workpiece position separating DRI origin and workpiece. This will be added to the permanent distance A-D to get the total distance from the hexapod origin to the workpiece. On the other hand, the distance separating hexapod origin to tool end is known from the previous method. Using these two pieces of information the distance separating the tool end to workpiece can be calculated.

Based on the design requirements, technical drawings were produced with necessary dimensions, tolerances and specifications for all these three components. Figure 8-6 shows the technical drawing of the spindle holder. The figure 8-7 shows the technical drawing of DRI holder. Figure 8-8 shows the technical drawing of L bracket. Further, the tool end part which holds the bonnet is redesigned to limit runout errors. Figure 8-9 shows the technical drawing of the tool end. All parts are made of aluminium alloy and anodised. Figure 8-10 shows the new spindle holder assembled on the hexapod unfortunately time constraints meant that the full capability of the new design was not able to be investigated.

Ø160

30

R5

R5

R10

R40

R40

85

5×[2]

Ø4 H7 (X2)

6

20.50

41 ±0.02

// 0.05 A

A

SECTION A-A

The parallelism is requested to ensure a precise base surface for fixing the DRI holder. Indeed, the DRI needs precision vertical alignment with the Hexapod for accurate measurements

M3 threaded hole for stopping the spindle movement in the holder

50 ±0.01

4 × 6.40 X 1 THRU
12.60 X 90°

Two dowel pin holes for aligning precisely the DRI center in the Y axis of the

A

50±0.01

41

Ø36

M 3 (X2) ▽8

Alu Alloy 1100

FW023

A 3

Figure 8-6: Spindle holder Technical drawing

169

84.98

4.25

A

5

M5

8.50

Ø 4.20 THRU
M5 - 6H THRU

41 ±0.02

// 0.01 A

Through hole for Spindle

DRI is clamped in this place

Ø4 H7

Ø11.05

35

44.75

35

Ø3.50

2 × Ø 2.50 ▽ 7.50
M3 - 6H ▽ 6

4

Ø5.50

1.50

40

Ø4 H7

30+0.02

Ø31

24.50

Ø4 H7

Ø49

Ø30

9.50

4.50

4.25

20.50

35

41

20.50

4

Ø3.50

5

5

49

Dowel pin holes for positioning DRI holder in the centre of Y axis of the

Dowel pins and threaded holes on the on the side for assembling the L bracket

Alu alloy 1100

FW024

A 3

Figure 8-7:   DRI holder technical drawing

170

Dowel pin and through holes for assembling the L bracket into DRI Holder

The length of the L bracket is chosen to ensure a 10 mm distance between tool and DRI position in axial direction

FW025
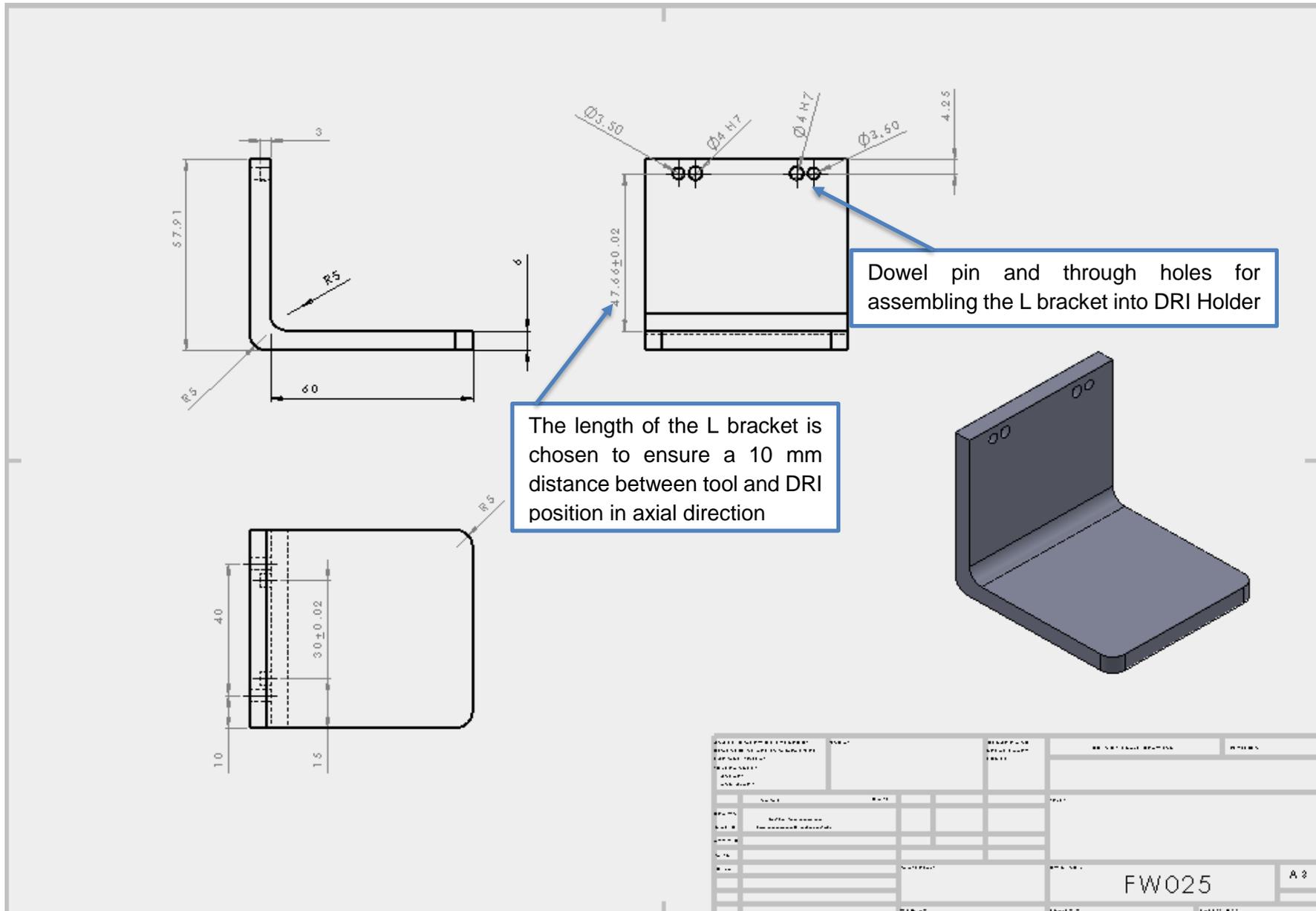
Figure 8-8:   L bracket technical drawing

171
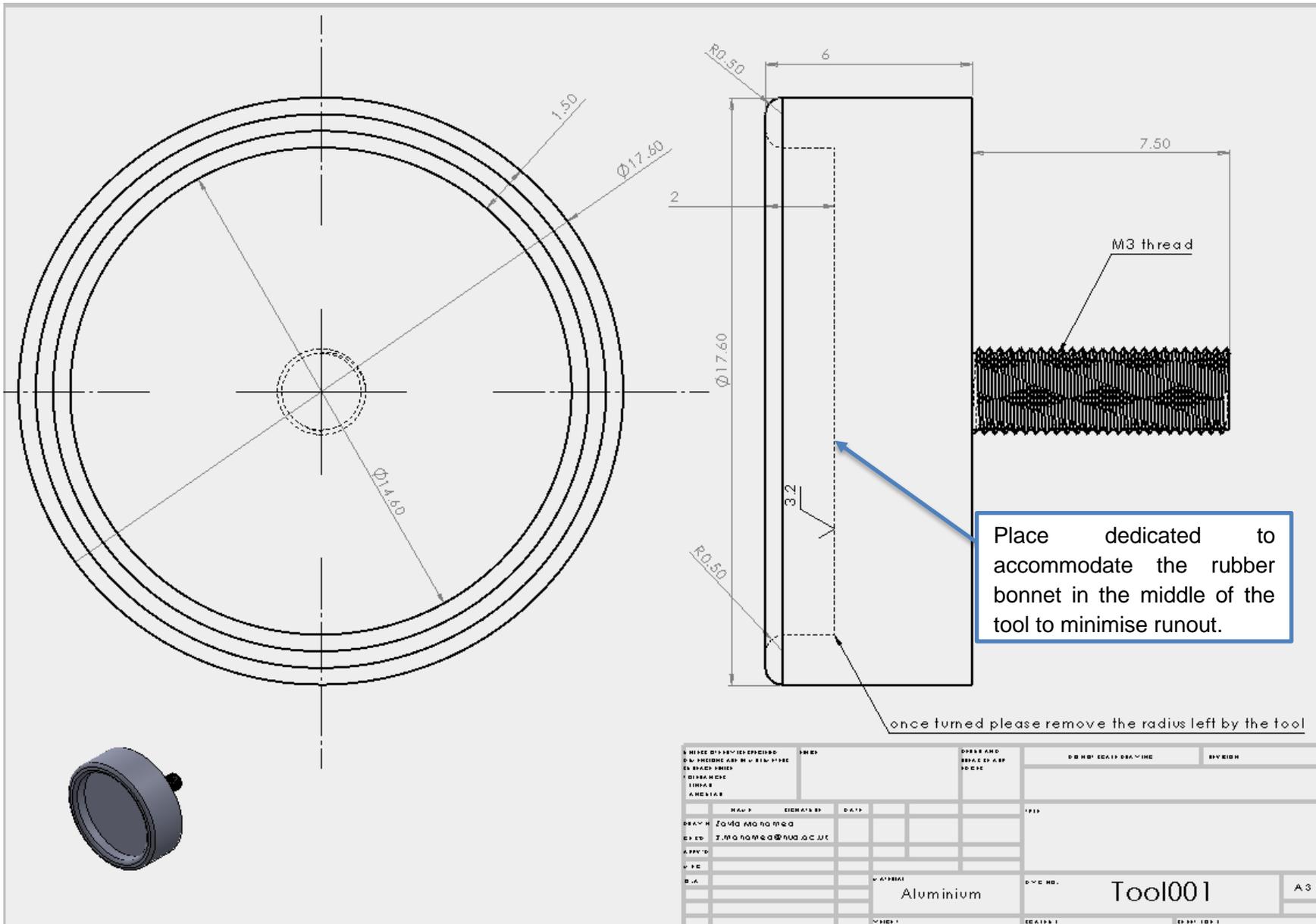
Figure 8-9: Rubber bonnet holder technical drawing
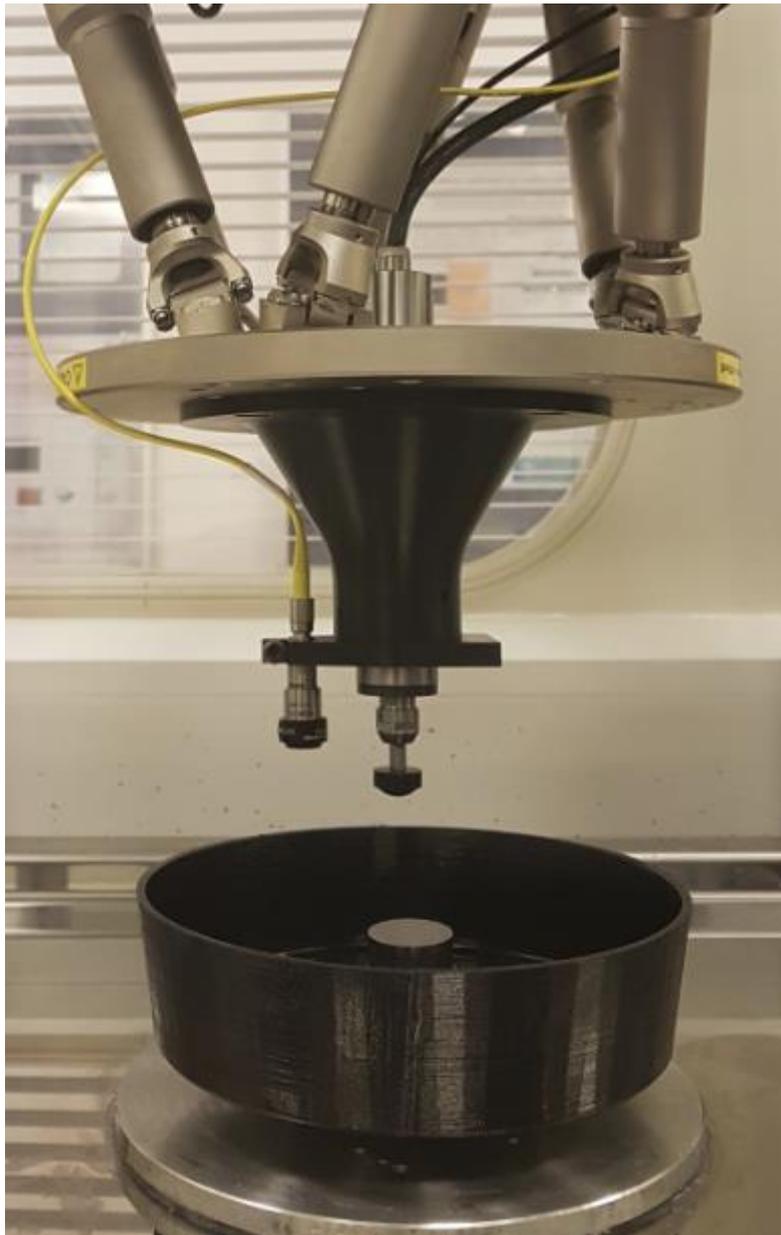
Figure 8-10:   Assembly of the spindle tool holder

In theory the distance separating Hexapod origin and tool end is 163.26 mm in the axial direction. In the X and Y axis the tool end should be combined on hexapod origin. Similarly, the theoretical distance separating the hexapod and DRI origins should be 153.26 mm in axial direction, 30 mm in the X axis and 0 mm in Y axis. These distances needs to be measured on a CMM for validation.

8.2.3   Future Work

Following the work completed towards the implementation of freeform polishing capabilities to the machine, there are still a number of tasks which need to be performed:

- The DRI is used to scan manually a flat mirror to evaluate the slope of the mirror with respect to hexapod axis. Figure 8-11 shows the obtained result. However, we are only in the developing stage which requires a series of work to obtain this result. The optimum working position in the Z axis needs to be identified by moving manually the hexapod Z axis. Then it needs to scan on X axis to collect data. And the collected data is processed using a separate MATLAB program. Fortunately, there are ways to automate this whole process to make the alignment quicker at accurate. It requires further work for optimisation.
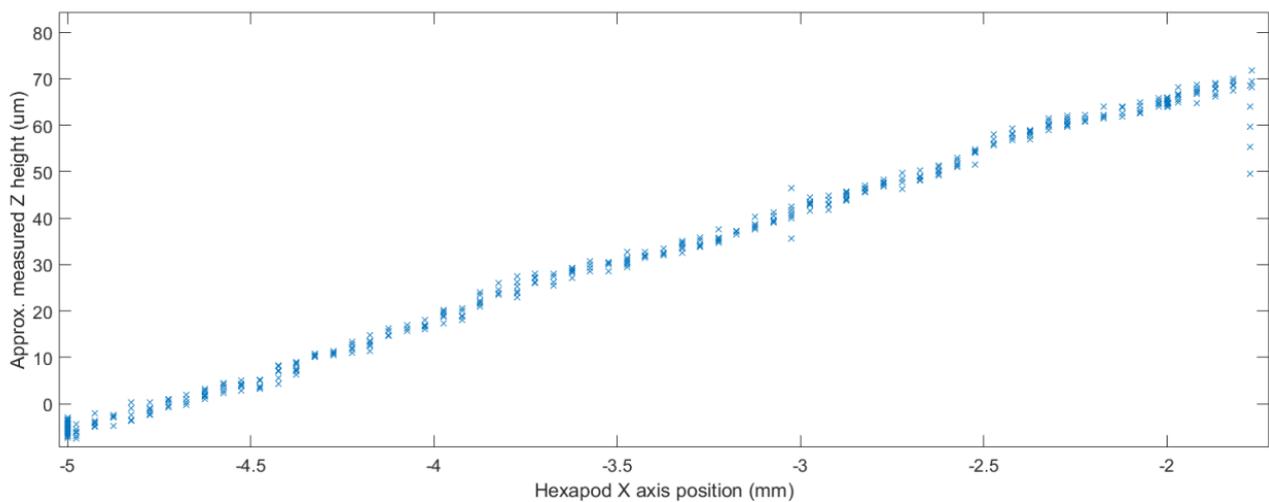
Figure 8-11:   DRI slope measurement data

- New spindle holder assembly needs to be measured accurately on a CMM to exactly know the distance separating the hexapod origin from tool end and DRI origin. Similarly, the distance separating the DRI and tool in X and Y axis with respect to hexapod origin.
- Demonstration of grolishing and polishing concave, convex and freeform shapes.
- Optimisation of parameters for re-circulating slurry polishing using Taguchi.
- A program of polish other materials such as glass, colbalt chrome or titanium.

REFERENCES

1. ISO7206-2, *Implants for surgery — Partial and total hip joint prostheses, in Part 2: Articulating surfaces made of metallic, ceramic and plastics materials*. 2011, British Standard: Switzerland.
2. Fang, F., et al., *Manufacturing and measurement of freeform optics.* CIRP Annals, 2013. **62**(2): p. 823-846.
3. Porter, M., et al., *National Joint Registry for England and Wales 9th Annual Report 2012.* Surgical data to December 2009, 2010. **7**.
4. McCann, L., et al., *An investigation of the effect of conformity of knee hemiarthroplasty designs on contact stress, friction and degeneration of articular cartilage: a tribological study.* Journal of biomechanics, 2009. **42**(9): p. 1326-1331.
5. Charlton, P., *The Application of Zeeko Polishing Technology to Freeform Femoral Knee Replacement Component Manufacture*. 2011, University of Huddersfield.
6. Zeng, S., *Bonnet Polishing of Cobalt Chrome Alloys for Artificial Implants*. 2014, University of Huddersfield.
7. Jiang, X., P. Scott, and D. Whitehouse, *Freeform Surface Characterisation - A Fresh Strategy.* CIRP Annals, 2007. **56**(1): p. 553-556.
8. Savio, E., L. De Chiffre, and R. Schmitt, *Metrology of freeform shaped parts.* CIRP Annals, 2007. **56**(2): p. 810-835.
9. Shorey, A., W. Kordonski, and M. Tricard. *Deterministic precision finishing of domes and conformal optics*. in *Window and Dome Technologies and Materials IX*. 2005. International Society for Optics and Photonics.
10. Brinksmeier, E., R. Gläbe, and C. Flucke, *Manufacturing of molds for replication of micro cube corner retroreflectors.* Production Engineering, 2008. **2**(1): p. 33-38.
11. Riemer, O., *Advances in ultra precision manufacturing.* Proc. Jpn. Soc. Precis. Eng, 2011.
12. Tamkin, J.M. and T.D. Milster, *Effects of structured mid-spatial frequency surface errors on image performance.* Applied optics, 2010. **49**(33): p. 6522-6536.
13. Beaucamp, A. and Y. Namba, *Super-smooth finishing of diamond turned hard X-ray molding dies by combined fluid jet and bonnet polishing.* CIRP Annals, 2013. **62**(1): p. 315-318.
14. Yu, G., H. Li, and D. Walker, *Removal of mid spatial-frequency features in mirror segments*. 2011. Vol. 6. 2011.
15. Cheung, C.F., L.T. Ho, and S. To, *An experimental investigation of surface generation using an integrated ultra-precision polishing process and different polishing trajectories.* Proceedings of the Institution of Mechanical Engineers, Part B: Journal of Engineering Manufacture, 2012. **226**(2): p. 203-220.
16. Walker, D.D., et al. *First aspheric form and texture results from a production machine embodying the precession process*. in *Optical manufacturing and Testing IV*. 2001. International Society for Optics and Photonics.
17. Organization, W.H., *World report on ageing and health*. 2015: World Health Organization.
18. Nations, U., *Population Division. World population prospects 2017*. 2017, United Nations New York.
19. Valdes, A.M. and J. Stocks, *Osteoarthritis and ageing.* European Medical Journal Rheumatology, 2018. **3**(1): p. 116-123.
20. Solutions, P. *Gel Injections for Osteoarthritis in the Knee.* 2016 29/04/2018]; Available from: http://physicalsolutionsli.com/gel-injections-osteoarthritis-knee/.
21. Raiss, P., et al., *Results of cemented total shoulder replacement with a minimum follow-up of ten years.* JBJS, 2012. **94**(23): p. e171.
22. Rush, S.M. and N. Todd, *Salto Talaris fixed-bearing total ankle replacement system.* Clinics in podiatric medicine and surgery, 2013. **30**(1): p. 69-80.
23. Gougoulias, N. and N. Maffulli, *History of total ankle replacement.* Clinics in podiatric medicine and surgery, 2013. **30**(1): p. 1-20.
24. Adams, B.D., *Wrist arthroplasty: partial and total.* Hand clinics, 2013. **29**(1): p. 79-89.

25. Tharin, S. and E.C. Benzel, *Cervical spine arthroplasty: fact or fiction: the absence of need for arthroplasty.* Neurosurgery, 2012. **59**(CN_Suppl_1): p. 82-90.

26. Wu, J.-C., T.-H. Tu, and P.V. Mummaneni, *Spinal arthroplasty: differences between the cervical and lumbar spine.* World neurosurgery, 2012. **78**(3-4): p. 245-246.

27. Joyce, T. and A. Unsworth, *A test procedure for artificial finger joints.* Proceedings of the Institution of Mechanical Engineers, Part H: Journal of Engineering in Medicine, 2002. **216**(2): p. 105-110.

28. Joyce, T. and A. Unsworth, *A literature review of" failures" of the Swanson finger prosthesis in the metacarpophalangeal joint.* Hand surgery, 2002. **7**(01): p. 139-146.

29. Quintana, J.M., et al., *Health-related quality of life and appropriateness of knee or hip joint replacement.* Archives of internal medicine, 2006. **166**(2): p. 220-226.

30. Long, M. and H. Rack, *Titanium alloys in total joint replacement—a materials science perspective.* Biomaterials, 1998. **19**(18): p. 1621-1639.

31. Research, A.M. *Orthopedic Implants Market Overview*. 2018 28/04/2018]; Available from: https://www.alliedmarketresearch.com/orthopedic-implants-market.

32. Board, N.E., *14th Annual Report 2017, National Joint Registry for England, Wales, Northern Ireland and the Isle of Man.* 2017.

33. Abu-Amer, Y., I. Darwech, and J.C. Clohisy, *Aseptic loosening of total joint replacements: mechanisms underlying osteolysis and potential therapies.* Arthritis research & therapy, 2007. **9**(1): p. S6.

34. Blumenfeld, T.J. and W.L. Bargar, *Early aseptic loosening of a modern acetabular component secondary to a change in manufacturing.* The Journal of arthroplasty, 2006. **21**(5): p. 689-695.

35. Miller, M.D., C.L. Peters, and B. Allen, *Early aseptic loosening of a total knee arthroplasty due to Gore-Tex particle–induced osteolysis.* The Journal of arthroplasty, 2006. **21**(5): p. 765-770.

36. Reina, R.J., et al., *Fixation and osteolysis in plasma-sprayed hemispherical cups with hybrid total hip arthroplasty.* The Journal of arthroplasty, 2007. **22**(4): p. 531-534.

37. Jiang, Y., et al., *Current research in the pathogenesis of aseptic implant loosening associated with particulate wear debris.* Acta Orthop Belg, 2013. **79**(1): p. 1-9.

38. DeFrate, L.E., et al., *The 6 degrees of freedom kinematics of the knee after anterior cruciate ligament deficiency: an in vivo imaging analysis.* The American journal of sports medicine, 2006. **34**(8): p. 1240-1246.

39. Hoshi, K., et al., *New Findings in Six-degrees-of-freedom Kinematics during Stationary Stepping in Patients with Knee Osteoarthritis.* Int J Phys Med Rehabil, 2016. **4**(381): p. 2.

40. Walldius, B., *Arthroplasty of the knee using an endoprosthesis.* Acta Orthopaedica Scandinavica, 1957. **28**(sup24): p. 1-112.

41. Sheehan, J.M., *Arthroplasty of the knee.* Bone & Joint Journal, 1978. **60**(3): p. 333-338.

42. Sheehan, J.M., *Arthroplasty of the Knee.* Clinical orthopaedics and related research, 1979(145): p. 101-109.

43. Goodfellow, J., et al., *Unicompartmental arthroplasty with the Oxford knee*. 2011: Goodfellow Publishers Limited.

44. Barnes, C.L., et al., *Kneeling Is Safe for Patients Implanted With Medial-Pivot Total Knee Arthroplasty Designs.* The Journal of Arthroplasty, 2011. **26**(4): p. 549-554.

45. Nishio, Y., et al., *Intraoperative medial pivot affects deep knee flexion angle and patient-reported outcomes after total knee arthroplasty.* The Journal of arthroplasty, 2014. **29**(4): p. 702-706.

46. Clinic, D.B.J., *Total Knee Replacement*. 2016.

47. Patel, N.R. and P.P. Gohil, *A review on biomaterials: scope, applications & human anatomy significance.* International Journal of Emerging Technology and Advanced Engineering, 2012. **2**(4): p. 91-101.

48. Matsumoto, T., et al., *Different pattern in gap balancing between the cruciate-retaining and posterior-stabilized total knee arthroplasty.* Knee Surgery, Sports Traumatology, Arthroscopy, 2013. **21**(10): p. 2338-2345.

49. Greengard, S. *Guide to Knee Replacement Implants and Their Manufacturers*. 2012 1/05/2018]; Available from: https://www.healthline.com/health/total-knee-replacement-surgery/implant-manufacturers#1.

50. Lizaur-Utrilla, A., J. Sanz-Reig, and M.A. Trigueros-Rentero, *Greater satisfaction in older patients with a mobile-bearing compared with fixed-bearing total knee arthroplasty.* The Journal of arthroplasty, 2012. **27**(2): p. 207-212.

51. Pitta, M., et al., *Failure after modern total knee arthroplasty: a prospective study of 18,065 knees.* The Journal of arthroplasty, 2018. **33**(2): p. 407-414.

52. Thiele, K., et al., *Current failure mechanisms after knee arthroplasty have changed: polyethylene wear is less common in revision surgery.* JBJS, 2015. **97**(9): p. 715-720.

53. Sharkey, P.F., et al., *Why are total knee arthroplasties failing today—has anything changed after 10 years?* The Journal of arthroplasty, 2014. **29**(9): p. 1774-1778.

54. Cheung, C.F., et al. *A study of wear characteristics of superpolished orthopaedic implant materials using ultra-precision polishing.* in *Key Engineering Materials.* 2010. Trans Tech Publ.

55. Sines, G. and Y.A. Sakellarakis, *Lenses in antiquity.* American Journal of Archaeology, 1987: p. 191-196.

56. O'Regan, D.E., *Rhetoric, Comedy, and the Violence of Language in Aristophanes' Clouds.* 1992: Oxford University Press on Demand.

57. Freestone, I.C., *Glass production in Late Antiquity and the Early Islamic period: a geochemical perspective.* Geological Society, London, Special Publications, 2006. **257**(1): p. 201-216.

58. White, L., *Eilmer of Malmesbury, an eleventh century aviator: A case study of technological innovation, its context and tradition.* Technology and Culture, 1961. **2**(2): p. 97-111.

59. al-Haitham, I., *The Optics of Ibn Al-Haytham: Books I-III: on Direct Vision.* 1989: Warburg Institute, University of London.

60. Cashell, G., *A short history of spectacles.* Proceedings of the Royal Society of Medicine, 1971. **64**(10): p. 1063.

61. Uluç, K., G.C. Kujoth, and M.K. Başkaya, *Operating microscopes: past, present, and future.* Neurosurgical focus, 2009. **27**(3): p. E4.

62. Gest, H., *The discovery of microorganisms by Robert Hooke and Antoni Van Leeuwenhoek, fellows of the Royal Society.* Notes and Records, 2004. **58**(2): p. 187-201.

63. Antiquespectacles. *Eyeglasses Through the Ages*. 2017 2/05/2018]; Available from: http://www.antiquespectacles.com/history/ages/through_the_ages.htm.

64. Discoveries, S.a. *Telescope*. 08/12/2018]; Available from: http://discoverysciencenews.blogspot.com/p/inventions-and-discovery-telescope.html#.

65. Galileo, M. *Galileo's microscope - The compound microscope*. 2007 08/12/2018]; Available from: https://brunelleschi.imss.fi.it/esplora/microscopio/dswmedia/storia/estoria1_st.html.

66. Leemik. *History and technical development of photographic camera lenses*. 2015 6/5/2018]; Available from: http://www.mike-lee.org/scripts/forum/discussforumgetmessages.htm?search=5461;post=18935.

67. P.Hess, J. *The Development of the Modern Lens*. 2017 6/5/2018]; Available from: https://filmmakeriq.com/lessons/the-modern-lens/.

68. Takahashi, S., *High relative aperture Gauss type lens.* 1988, Google Patents.

69. Britannica, T.E.o.E. *Lens*. 2018 2/5/2018]; Available from: https://www.britannica.com/technology/lens-optics.

70. Canon. *The history of Canon's L-series lenses*. 2018 5/5/2018]; Available from: https://www.canon.co.uk/pro/how-canon-lenses-are-made/history-of-canon-l-series-lenses/.

71. T. Plummer, W., *The origins of commercial free-form optics.* 2016.

72. Ye, J., et al., *Review of optical freeform surface representation technique and its application.* Optical Engineering, 2017. **56**(11): p. 110901.

73. Wu, R., et al., *Conceptual design of dedicated road lighting for city park and housing estate.* Applied optics, 2013. **52**(21): p. 5272-5278.

74. Feng, Z., et al., *Beam shaping system design using double freeform optical surfaces.* Optics express, 2013. **21**(12): p. 14728-14735.

75. Miñano, J.C., et al., *Free-form optics for Fresnel-lens-based photovoltaic concentrators.* Optics express, 2013. **21**(103): p. A494-A502.
76. Cheng, D., et al., *Design of an optical see-through head-mounted display with a low f-number and large field of view using a freeform prism.* Applied optics, 2009. **48**(14): p. 2655-2668.
77. Zhuang, Z., et al., *Field curvature correction method for ultrashort throw ratio projection optics design using an odd polynomial mirror surface.* Applied optics, 2014. **53**(22): p. E69-E76.
78. Fuerschbach, K., J.P. Rolland, and K.P. Thompson, *A new family of optical systems employing φ-polynomial surfaces.* Optics express, 2011. **19**(22): p. 21919-21928.
79. Liu, Y., Y. Li, and Z. Cao, *Design method of off-axis extreme ultraviolet lithographic objective system with a direct tilt process.* Optical Engineering, 2015. **54**(7): p. 075102.
80. Forkel, J., et al., *Personalized Progressive Addition Lenses: Correlation between Performance and Design.* Optometry and Vision Science, 2017. **94**(2): p. 208-218.
81. Tohme, Y. *Trends in ultra-precision machining of freeform optical surfaces.* in *Optical fabrication and testing.* 2008. Optical Society of America.
82. Pan, J.-W., et al., *High efficiency pocket-size projector with a compact projection lens and a light emitting diode-based light source system.* Applied optics, 2008. **47**(19): p. 3406-3414.
83. Pan, J.-W. and H.-H. Wang, *High contrast ratio prism design in a mini projector.* Applied optics, 2013. **52**(34): p. 8347-8354.
84. Hirata, K., et al., *Projection display system including lens group and reflecting mirror.* 2012, Google Patents.
85. Ogawa, J., *Reflection type image forming optical system and projector.* 2003, Google Patents.
86. RICOH. *Free-Form Mirror and Deflection Technology for Ultra-Close-Range Projection.* 2018 17/05/2018]; Available from: https://www.ricoh.com/technology/tech/040_projection.html.
87. Rodgers, J.M. *Unobscured mirror designs.* in *International Optical Design Conference 2002.* 2002. International Society for Optics and Photonics.
88. Rogers, J.R., *Aberrations of Unobscured Reflective Optical Systems.* 1983.
89. Wetherell, W.B. and D.A. Womble, *All-reflective three element objective.* 1980, Google Patents.
90. Wilson, R.N., *Reflecting telescope optics II: manufacture, testing, alignment, Modern Techniques.* 2013: Springer Science & Business Media.
91. Yang, T., et al., *Design method of freeform off-axis reflective imaging systems with a direct construction process.* Optics express, 2014. **22**(8): p. 9193-9205.
92. Thompson, K., *Description of the third-order optical aberrations of near-circular pupil optical systems without symmetry.* JOSA A, 2005. **22**(7): p. 1389-1401.
93. Liu, J.-f., F.-n. Long, and W. Zhang, *Study on computer-aided alignment method of off-axis three-mirror system.* Opt. Technol., 2004. **5**: p. 019.
94. Lee, D., et al. *Design of a compact wide field telescope for space situational awareness.* in *Ground-based and Airborne Telescopes IV.* 2012. International Society for Optics and Photonics.
95. Figoski, J.W. *Aberration characteristics of nonsymmetric systems.* in *1985 International Lens Design Conference.* 1986. International Society for Optics and Photonics.
96. Meng, Q., et al., *Easy-aligned off-axis three-mirror system with wide field of view using freeform surface based on integration of primary and tertiary mirror.* Applied optics, 2014. **53**(14): p. 3028-3034.
97. Hicks, R.A., *Controlling a ray bundle with a free-form reflector.* Optics letters, 2008. **33**(15): p. 1672-1674.
98. Cheng, D., Y. Wang, and H. Hua. *Free form optical system design with differential equations.* in *Optical Design and Testing IV.* 2010. International Society for Optics and Photonics.
99. Hou, J., et al., *Distortion correction for imaging on non-planar surface using freeform lens.* Optics Communications, 2012. **285**(6): p. 986-991.
100. Kaufmann, A., *The current role of high-resolution mass spectrometry in food analysis.* Analytical and bioanalytical chemistry, 2012. **403**(5): p. 1233-1249.
101. Peschel, T., et al. *Design of an imaging spectrometer for earth observation using freeform mirrors.* in *International Conference on Space Optics—ICSO 2016.* 2017. International Society for Optics and Photonics.

102. Reimers, J., et al., *Freeform spectrometer enabling increased compactness.* Light: Science & Applications, 2017. **6**(7): p. e17026.
103. Glasser, A. and M.C. Campbell, *Presbyopia and the optical changes in the human crystalline lens with age.* Vision research, 1998. **38**(2): p. 209-229.
104. Aves, O., *Improvements in and relating to multifocal lenses and the like, and the method of grinding same.* GB patent, 1908. **15735**.
105. Pope, D.R. *Progressive addition lenses: history, design, wearer satisfaction and trends.* in *Vision Science and Its Applications.* 2000. Optical Society of America.
106. Bernard, C.-M., *Machine for grinding an optical surface in a piece of refractive material.* 1959, Google Patents.
107. onlineopticianuk.com. *Varifocal & Progressive Lenses Explained.* 2018 28/05/2018]; Available from: http://www.onlineopticiansuk.com/varifocal-progressive-lenses-explained-i128.
108. Meister, D.J. and S.W. Fisher, *Progress in the spectacle correction of presbyopia. Part 1: Design and development of progressive lenses.* Clinical and experimental optometry, 2008. **91**(3): p. 240-250.
109. Meister, D. *Optics of progressive lenses.* 2018 30/05/2018]; Available from: http://64.50.176.246/cecourse.php?url=progressive_lenses/.
110. Zeiss. *Zeiss progressive lenses.* 2018 30/05/2018]; Available from: https://www.zeiss.com/vision-care/int/products/progressive-lenses.html.
111. Matthews. *Lens guide.* 2018 30/05/2018]; Available from: http://epsomeyecare.co.nz/lens-guide/.
112. Meister, D.J. and S.W. Fisher, *Progress in the spectacle correction of presbyopia. Part 2: Modern progressive lens technologies.* Clinical and experimental optometry, 2008. **91**(3): p. 251-264.
113. Hoya. *Choosing lenses.* 2018 30/05/2018]; Available from: https://www.hoyavision.com/what-i-need/for-spectacle-wearers/choosing-lenses/.
114. Crossbows-optical. *Freeform design features.* 2018 12/12/2018]; Available from: https://www.crossbowsoptical.com/freeform-designs/design-features/.
115. Guevara-Morales, A. and U. Figueroa-López, *Residual stresses in injection molded products.* Journal of materials science, 2014. **49**(13): p. 4399-4415.
116. Dick, L., S. Risse, and A. Tünnermann, *Injection molded high precision freeform optics for high volume applications*, in *Advanced Optical Technologies.* 2012. p. 39.
117. Bäumer, S., *Handbook of Plastic Optics.* 2011: Wiley.
118. Dick, L., S. Risse, and A. Tünnermann, *Injection molded high precision freeform optics for high volume applications.* Advanced Optical Technologies, 2012. **1**(1-2): p. 39-50.
119. Deng, P., et al., *Micro and macro injection molded parts of isotactic polypropylene/polyethylene blends: Shear-induced crystallization behaviors and morphological characteristics.* Journal of Macromolecular Science, Part B, 2014. **53**(1): p. 24-39.
120. Accumold. *What is Micro Injection Molding?* 2014 30/05/2014]; Available from: http://www.accu-mold.com/Accumold_What-is-Micro-Molding.html.
121. Theilade, U.A. and H.N. Hansen, *Surface microstructure replication in injection molding.* The International Journal of Advanced Manufacturing Technology, 2007. **33**(1-2): p. 157-166.
122. Shiou, F. and C. Cheng, *Ultra-precision surface finish of NAK80 mould tool steel using sequential ball burnishing and ball polishing processes.* Journal of materials processing technology, 2008. **201**(1-3): p. 554-559.
123. Goodfellow, J. and J. O'Connor, *The mechanics of the knee and prosthesis design.* Bone & Joint Journal, 1978. **60**(3): p. 358-369.
124. Cheung, C., et al., *Analysis of surface generation in the ultraprecision polishing of freeform surfaces.* Proceedings of the Institution of Mechanical Engineers, Part B: Journal of Engineering Manufacture, 2010. **224**(1): p. 59-73.
125. Bryce, D.M., *Plastic injection molding: Mold design and construction fundamentals.* Vol. 3. 1998: Society of Manufacturing Engineers.

126. DME. *Micro-Finish Mold & Tool Finish Guide.* 11/06/2018]; Available from: https://www.milacron.com/wp-content/uploads/2016/04/DME-Micro-Finish-Mold-Tool-Finish-Guide.pdf.
127. DME. *Micro-Finish Mold & Tool Finish Guide.* 2014 [cited 2014 30 JUIN]; Available from: http://www.dme.net/sites/default/files/technical-guides/DME%20Micro-Finish%20Mold%20%26%20Tool%20Finish%20Guide.pdf.
128. Thompson, S., *Handbook of mould, tool and die repair welding.* 1999: Elsevier.
129. Rosochowski, A. and A. Matuszak, *Rapid tooling: the state of the art.* Journal of materials processing technology, 2000. **106**(1-3): p. 191-198.
130. Ltd, M.P.S.u. *Silverline Wet And Dry Sandpaper 120 Grit 10Pk.* 11/06/2018]; Available from: https://www.metalpolishingsupplies.co.uk/wet-and-dry-sandpaper-120grit-10pk/.
131. Orvis, K.H. and H.D. Grissino-Mayer, *Standardizing the reporting of abrasive papers used to surface tree-ring samples.* Tree-Ring Research, 2002.
132. AWLGRIP. *Sanding and Sandpaper.* 2011 [cited 1/06/2018; Available from: http://www.awlgrip.com/support-and-advice/sanding-sandpaper.aspx.
133. Lee, H.S., et al., *Systematic finishing of dies and moulds.* International Journal of Machine Tools and Manufacture, 2006. **46**(9): p. 1027-1034.
134. doityourself. *A Complete Guide to Sandpaper Grit Classification.* 2018 1/06/2018]; Available from: https://www.doityourself.com/stry/a-complete-guide-to-sandpaper-grit-classification.
135. DiaMold, *Polishing Stone.* 2014, Engis Corporation.
136. Artco. *NSK Emax Evolution Motor.* 2018 02/06/2018]; Available from: http://www.artcotools.com/nsk-emax-evolution-motor/

137. Eternaltools. *Complete Guide to your Dremel Rotary Tool.* 2017 02/06/2018]; Available from: https://www.eternaltools.com/blog/complete-guide-to-your-dremel-rotary-tool.
138. Nakanishi. *Emax EVOlution.* 2018 02/06/2018]; Available from: http://www.nsk-nakanishi.co.jp/industrial-eng/mgt/emaxevolution/.
139. Cheung, C., et al., *Characterization of surface defects in fast tool servo machining of microlens array using a pattern recognition and analysis method.* Measurement, 2010. **43**(9): p. 1240-1249.
140. Mamedov, A. and I. Lazoglu, *An evaluation of micro milling chip thickness models for the process mechanics.* The International Journal of Advanced Manufacturing Technology, 2016. **87**(5-8): p. 1843-1849.
141. Liu, Q., et al., *Long-stroke fast tool servo and a tool setting method for freeform optics fabrication.* Optical Engineering, 2014. **53**(9): p. 092005.
142. Kong, L., C. Cheung, and W. Lee, *A theoretical and experimental investigation of orthogonal slow tool servo machining of wavy microstructured patterns on precision rollers.* Precision Engineering, 2016. **43**: p. 315-327.
143. Li, S., et al., *Improving the working surface condition of electroplated cubic boron nitride grinding Quill in surface grinding of Inconel 718 by the assistance of ultrasonic vibration.* Journal of Manufacturing Science and Engineering, 2016. **138**(7): p. 071008.
144. Zhang, S., et al., *A review of fly cutting applied to surface generation in ultra-precision machining.* International Journal of Machine Tools and Manufacture, 2016. **103**: p. 13-27.
145. Tian, F., Z. Yin, and S. Li, *A novel long range fast tool servo for diamond turning.* The International Journal of Advanced Manufacturing Technology, 2016. **86**(5-8): p. 1227-1234.
146. Feng, H., et al., *Fabrication of freeform progressive addition lenses using a self-developed long stroke fast tool servo.* The International Journal of Advanced Manufacturing Technology, 2017. **91**(9-12): p. 3799-3806.
147. Shi, X., L. Qiao, and P. Rao. *An Adaptive Constant Scallop-height Tool-Path Planning Method For Turn-Milling Machining of NURBS free-form surfaces.* in *Int. Conf. on Information Sciences, Machinery, Materials and Energy (ICISMME 2015).* 2015.
148. Corke, P., *Robotics, Vision and Control: Fundamental Algorithms In MATLAB® Second, Completely Revised.* Vol. 118. 2017: Springer.

149. Abdulshahed, A.M., A.P. Longstaff, and S. Fletcher, *The application of ANFIS prediction models for thermal error compensation on CNC machine tools.* Applied Soft Computing, 2015. **27**: p. 158-168.

150. Beyca, O.F., et al., *Heterogeneous sensor data fusion approach for real-time monitoring in ultraprecision machining (UPM) process using non-parametric bayesian clustering and evidence theory.* IEEE Transactions on Automation Science and Engineering, 2016. **13**(2): p. 1033-1044.

151. Li, Z., et al., *Machining approach of freeform optics on infrared materials via ultra-precision turning.* Optics Express, 2017. **25**(3): p. 2051-2062.

152. Lochegnies, D., et al., *3D modelling of thermal replication for designing progressive glass moulds.* New Journal of Glass and Ceramics, 2013. **3**(01): p. 34.

153. Hsu, W.-Y., et al. *Design and fabrication of the progressive addition lens.* in *Frontiers in Optics.* 2010. Optical Society of America.

154. Kong, L., et al., *A theoretical and experimental investigation of design and slow tool servo machining of freeform progressive addition lenses (PALs) for optometric applications.* The International Journal of Advanced Manufacturing Technology, 2014. **72**(1-4): p. 33-40.

155. Golini, D. *Precision optics manufacturing using magnetorheological finishing (MRF).* in *Optical fabrication and testing.* 1999. International Society for Optics and Photonics.

156. Shafrir, S.N., J.C. Lambropoulos, and S.D. Jacobs, *Toward magnetorheological finishing of magnetic materials.* Journal of Manufacturing Science and Engineering, 2007. **129**(5): p. 961-964.

157. Sankar, M.R., et al., *Nano-finishing techniques: a review.* Proceedings of the Institution of Mechanical Engineers, Part C: Journal of Mechanical Engineering Science, 2012. **226**(2): p. 327-346.

158. Shorey, A.B., et al., *Design and testing of a new magnetorheometer.* Review of scientific instruments, 1999. **70**(11): p. 4200-4206.

159. Sidpara, A., M. Das, and V.K. Jain, *Rheological characterization of magnetorheological finishing fluid.* Materials and Manufacturing Processes, 2009. **24**(12): p. 1467-1478.

160. Sidpara, A. and V. Jain, *Effect of fluid composition on nanofinishing of single-crystal silicon by magnetic field-assisted finishing process.* The International Journal of Advanced Manufacturing Technology, 2011. **55**(1-4): p. 243-252.

161. Sidpara, A.M. and V. Jain, *Nanofinishing of freeform surfaces of prosthetic knee joint implant.* Proceedings of the Institution of Mechanical Engineers, Part B: Journal of Engineering Manufacture, 2012. **226**(11): p. 1833-1846.

162. Jacobs, S.D., et al. *Magnetorheological finishing of IR materials.* in *Optical Manufacturing and Testing II.* 1997. International Society for Optics and Photonics.

163. Bingham, R.G., et al. *Novel automated process for aspheric surfaces.* in *Current developments in lens design and optical systems engineering.* 2000. International Society for Optics and Photonics.

164. Kim, S.-W., et al. *OGLP-400: an innovative computer-controlled polishing machine.* in *Specification, Production, and Testing of Optical Components and Systems.* 1996. International Society for Optics and Photonics.

165. Korhonen, T.K. and T. Lappalainen. *Computer-controlled figuring and testing.* in *Advanced Technology Optical Telescopes IV.* 1990. International Society for Optics and Photonics.

166. Zeeko. *Ultra-Precision Polishing.* 2018 [cited 02/06/2018; Available from: http://www.zeeko.co.uk/products.html.

167. Walker, D., et al. *Commissioning of the first Precessions 1.2 m CNC polishing machines for large optics.* in *Current Developments in Lens Design and Optical Engineering VII.* 2006. International Society for Optics and Photonics.

168. Walker, D.D., et al. *Zeeko/UCL process for polishing large lenses and prisms.* in *Large lenses and prisms.* 2002. International Society for Optics and Photonics.

169. Walker, D.D., et al., *The 'Precessions' tooling for polishing and figuring flat, spherical and aspheric surfaces.* Optics Express, 2003. **11**(8): p. 958-964.

170. Walker, D.D., et al. *Novel CNC polishing process for control of form and texture on aspheric surfaces.* in *Current Developments in Lens Design and Optical Engineering III.* 2002. International Society for Optics and Photonics.

171. Johnson, K.L. and K.L. Johnson, *Contact mechanics*. 1987: Cambridge university press.
172. Aikens, D., J.E. DeGroote, and R.N. Youngworth. *Specification and control of mid-spatial frequency wavefront errors in optical systems*. in *Optical Fabrication and Testing*. 2008. Optical Society of America.
173. Yu, G., H. Li, and D. Walker, *Removal of mid spatial-frequency features in mirror segments*. Journal of the European Optical Society-Rapid publications, 2011. **6**.
174. Dunn, C.R. and D.D. Walker, *Pseudo-random tool paths for CNC sub-aperture polishing and other applications*. Optics express, 2008. **16**(23): p. 18942-18949.
175. Walker, D.D., et al. *Precessions process for efficient production of aspheric optics for large telescopes and their instrumentation*. in *Specialized Optical Developments in Astronomy*. 2003. International Society for Optics and Photonics.
176. Li, H., et al., *Modelling and measurement of polishing tool influence functions for edge control*. Journal of the European Optical Society-Rapid publications, 2011. **6**.
177. Walker, D., et al., *Edges in CNC polishing: from mirror-segments towards semiconductors, paper 1: edges on processing the global surface*. Optics express, 2012. **20**(18): p. 19787-19798.
178. Li, H., *Research on manufacturing mirror segments for an extremely large telescope*. 2012, UCL (University College London).
179. Zeng, S. and L. Blunt, *Experimental investigation and analytical modelling of the effects of process parameters on material removal rate for bonnet polishing of cobalt chrome alloy*. 2014.
180. Cheung, C., et al., *Optical surface generation in ultra-precision polishing of freeform*. 红外与激光工程 (Infrared and laser engineering), 2010.
181. Walker, D., et al. *More steps towards process automation for optical fabrication*. in *Fourth European Seminar on Precision Optics Manufacturing*. 2017. International Society for Optics and Photonics.
182. Zeng, S., L. Blunt, and X. Jiang, *The application of Taguchi approach to optimise the processing conditions on bonnet polishing of CoCr*. 2011.
183. Zeng, S., L. Blunt, and X. Jiang, *The investigation of material removal in bonnet polishing of CoCr alloy artificial joints*. 2012, EUSPEN.
184. Beaucamp, A.T., et al. *Fluid jet and bonnet polishing of optical moulds for application from visible to x-ray*. in *Optical Manufacturing and Testing IX*. 2011. International Society for Optics and Photonics.
185. Marinescu, I.D., E. Uhlmann, and T. Doi, *Handbook of Lapping and Polishing*. 2006: Taylor & Francis.
186. Brinksmeier, E., O. Riemer, and A. Gessenharter, *Finishing of structured surfaces by abrasive polishing*. Precision Engineering, 2006. **30**(3): p. 325-336.
187. Preston, F.W., *The Theory and Design of Plate Glass Polishing Machines*. J. Soc. Glass Tech., 1927. **11**: p. 214.
188. Wang, C.-C., S.-C. Lin, and H. Hochen, *A material removal model for polishing glass–ceramic and aluminum magnesium storage disks*. International Journal of Machine Tools and Manufacture, 2002. **42**(8): p. 979-984.
189. Yu, G., D. Walker, and H. Li, *Implementing a grolishing process in Zeeko IRP machines*. Applied optics, 2012. **51**(27): p. 6637-6640.
190. Walker, D., et al. *A quantitative comparison of three grolishing techniques for the Precessions process*. in *Optical Manufacturing and Testing VII*. 2007. International Society for Optics and Photonics.
191. Booij, S.M., et al., *Nanometer deep shaping with fluid jet polishing*. Optical engineering, 2002. **41**(8): p. 1926-1932.
192. Guo, P., H. Fang, and J. Yu. *Computer-controlled fluid jet polishing*. in *3rd International Symposium on Advanced Optical Manufacturing and Testing Technologies: Advanced Optical Manufacturing Technologies*. 2007. International Society for Optics and Photonics.
193. Sampurno, Y., et al., *Feasibility of real-time detection of abnormality in inter layer dielectric slurry during chemical mechanical planarization using frictional analysis*. Thin Solid Films, 2008. **516**(21): p. 7667-7674.

194. Evans, C., et al., *Material removal mechanisms in lapping and polishing.* CIRP Annals-Manufacturing Technology, 2003. **52**(2): p. 611-633.
195. Belkhir, N., D. Bouzid, and V. Herold, *Morphological behavior and wear of polyurethane pads used in glass polishing process.* Precision Engineering, 2012. **36**(4): p. 641-649.
196. McGrath, J. and C. Davis, *Polishing pad surface characterisation in chemical mechanical planarisation.* Journal of Materials Processing Technology, 2004. **153**: p. 666-673.
197. McGrath, J. and C. Davis. *The effect of wafer and pad shape on removal uniformity a qualitative analysis using a mechanistic model.* in *CMP-MIC Conference.* 2003.
198. Liang, H., et al., *Wear phenomena in chemical mechanical polishing.* Wear, 1997. **211**(2): p. 271-279.
199. Todo, M., et al., *Strain-rate dependence of the tensile fracture behaviour of woven-cloth reinforced polyamide composites.* Composites Science and Technology, 2000. **60**(5): p. 763-771.
200. Kemet. *MATERIALOGRAPHIC EQUIPMENT & CONSUMABLES FOR SAMPLE PREPARATION.* 2018 5/6/2018]; Available from: https://www.kemet.co.uk/images/downloads/metallography-catalogue.pdf.
201. Buehler. *Polishing application guide.* 2012 10/06/2018]; Available from: https://www.buehler.com/Brochures/English/Grinding-Polishing/FN01465_0216_Polishing_Application_Guide_WEB.pdf.
202. Nguyen, N., Z. Zhong, and Y. Tian, *Analysis and improvement of the pad wear profile in fixed abrasive polishing.* The International Journal of Advanced Manufacturing Technology, 2016. **85**(5-8): p. 1159-1165.
203. Kemet. *Polishing Consumables.* 2018 05/06/2018]; Available from: https://www.kemet.co.uk/products/metallography/polishing-consumables.
204. Slocum, A.H., *Precision machine design.* 1992: Society of Manufacturing Engineers.
205. Liu, X.-W., *Five-axis NC cylindrical milling of sculptured surfaces.* Computer-Aided Design, 1995. **27**(12): p. 887-894.
206. Zeng, S., L. Blunt, and X. Jiang, *The application of Taguchi approach to optimise the processing conditions on bonnet polishing of CoCr.* 2011(Journal Article).
207. Gopalakrishnan, B., T. Yoshii, and S. Dappili, *Decision support system for machining center selection.* Journal of Manufacturing Technology Management, 2004. **15**(2): p. 144-154.
208. Rahman, M., J. Heikkala, and K. Lappalainen, *Modeling, measurement and error compensation of multi-axis machine tools. Part I: theory.* International Journal of Machine Tools and Manufacture, 2000. **40**(10): p. 1535-1546.
209. BLOG, P.T. *What is the Difference between Parallel Positioners and Stacked Serial Kinematics?* 2018 10/06/2018]; Available from: http://www.pi-usa.us/blog/what-is-the-difference-between-parallel-positioners-and-stacked-serial-kinematics/.
210. Instrumente, P. *Stacks of Single Axis Stages vs. Hexapods.* 2015 [cited 2018 18/03/2018]; Available from: http://www.pi-usa.us/blog/hexapods-vs-stacked-stages/.
211. Newport. *High Precision Hexapod, 200 mm Diameter Platform, 20 kg Load, M6.* 2018 [cited 2018 10/03/2018]; Available from: https://www.newport.com/p/HXP100-MECA.
212. Symetrie. *Breva.* 2018 [cited 2018 10/03/2018]; Available from: http://www.symetrie.fr/en/products/positioning-hexapods/breva/.
213. PhysikInstrumente. *H-840 6-Axis Hexapod.* 2018 [cited 2018 10/03/2018]; Available from: https://www.physikinstrumente.com/en/products/parallel-kinematic-hexapods/hexapods-with-motor-screw-drives/h-840-6-axis-hexapod-700810/.
214. Valuframe. *Valuframe - The Economy Aluminium Profile System.* 2018 08/12/2018]; Available from: http://www.valuframe.co.uk/Series-8-Aluminium-Profiles.html.
215. Wang, L., et al., *Ceria concentration effect on chemical mechanical polishing of optical glass.* Applied surface science, 2007. **253**(11): p. 4951-4954.
216. Zhang, L., et al., *An investigation of material removal in polishing with fixed abrasives.* Proceedings of the Institution of Mechanical Engineers, Part B: Journal of Engineering Manufacture, 2002. **216**(1): p. 103-112.
217. Zeng, S. and L. Blunt, *Experimental investigation and analytical modelling of the effects of process parameters on material removal rate for bonnet polishing of cobalt chrome alloy.* Precision Engineering, (0).

218. Anderson, E., et al., *Hexapods for precision motion and vibration control.* American Society for Precision Engineering, Control of Precision Systems, 2004: p. 1-5.
219. Zanatta, A.M., et al. *Surface Finish Assessment of Polishing Process of Tool Steels by Abrasion, Using Diamond and Alumina Particles.* in *Advanced Materials Research.* 2013. Trans Tech Publ.
220. Roy, R.K., *A primer on the Taguchi method.* 2010: Society of Manufacturing Engineers.
221. Kwak, J.-S., *Application of Taguchi and response surface methodologies for geometric error in surface grinding process.* International journal of machine tools and manufacture, 2005. **45**(3): p. 327-334.
222. Tsai, F., et al., *A Taguchi and experimental investigation into the optimal processing conditions for the abrasive jet polishing of SKD61 mold steel.* International Journal of Machine Tools and Manufacture, 2008. **48**(7): p. 932-945.
223. Vishnu Vardhan, M., et al., *Optimization of Parameters in CNC milling of P20 steel using Response Surface methodology and Taguchi Method.* Materials Today: Proceedings, 2017. **4**(8): p. 9163-9169.
224. Buehler. *Application guide Polishing.* 2015 20/03/2018]; Available from: https://www.buehler.com/Brochures/English/Grinding-Polishing/FN01465_0216_Polishing_Application_Guide_WEB.pdf.
225. Chang, Y., M. Hashimura, and D. Dornfeld, *An investigation of material removal mechanisms in lapping with grain size transition.* Journal of Manufacturing Science and Engineering, 2000. **122**(3): p. 413-419.
226. Williamson, J., H. Martin, and X. Jiang, *High resolution position measurement from dispersed reference interferometry using template matching.* Optics express, 2016. **24**(9): p. 10103-10114.

APPENDIX

Appendix 4-1

Hexapod specifications data showing four types of hexapod models with their own caracteristics. PI Hexapod H840-D2 is the model consider for the development of this polishing machine.

Specifications

	H-840.G2A	H-840.D2A	H-840.Gxx	H-840.Dxx	Unit	Tolerance
	BLDC gear motor with absolute encoder	BLDC motor with absolute encoder	DC gear motor	DC motor		
Active axes	X, Y, Z, θ_X, θ_Y, θ_Z	X, Y, Z, θ_X, θ_Y, θ_Z	X, Y, Z, θ_X, θ_Y, θ_Z	X, Y, Z, θ_X, θ_Y, θ_Z		
Motion and positioning						
Travel range* X, Y	±50	±50	±50	±50	mm	
Travel range* Z	±25	±25	±25	±25	mm	
Travel range* θ_X, θ_Y	±15	±15	±15	±15	°	
Travel range* θ_Z	±30	±30	±30	±30	°	
Actuator design resolution	0.0085	0.25	0.017	0.5	µm	
Min. incremental motion X, Y	1	3	1	3	µm	typ.
Min. incremental motion Z	0.5	1	0.5	1	µm	typ.
Minimum incremental motion θ_X, θ_Y, θ_Z	5	5	5	5	µrad	typ.
Backlash in X, Y	3	3	3	3	µm	typ.
Backlash in Z	0.2	0.2	0.2	0.2	µm	typ.
Backlash in θ_X, θ_Y	20	20	20	20	µrad	typ.
Backlash in θ_Z	30	30	30	30	µrad	typ.
Repeatability X, Y	±0.5	±0.5	±0.5	±0.5	µm	typ.
Repeatability in Z	±0.4	±0.4	±0.4	±0.4	µm	typ.
Repeatability in θ_X, θ_Y	±7	±7	±7	±7	µrad	typ.
Repeatability in θ_Z	±12	±12	±12	±12	µrad	typ.
Max. velocity in X, Y, Z	2.5	60	2.5	50	mm/s	
Max. velocity in θ_X, θ_Y, θ_Z	30	700	30	600	mrad/s	
Typ. Velocity in X, Y, Z	2	40	2	30	mm/s	
Typ. Velocity in θ_X, θ_Y, θ_Z	20	450	20	300	mrad/s	
Mechanical properties						
Load capacity (base plate horizontal / any orientation)	30 / 10	10 / 3	30 / 10	10 / 3	kg	max.
Holding force, power off (base plate horizontal / any orientation)	100 / 25	15 / 5	100 / 25	15 / 5	N	max.
Motor type	BLDC gear motor	BLDC motor	DC gear motor	DC motor		
Miscellaneous						
Operating temperature range	-10 to 50	-10 to 50	-10 to 50	-10 to 50	°C	
Material	Aluminum / steel	Aluminum / steel	Aluminum	Aluminum		
Mass	12	12	12	12	kg	±10 %
Cable length	3	3	3	3	m	±10 mm

Newport: HXP100-MECA technical specification sheet. The travel range limits of this model does not match developing machine requirements.

Technical Specs

Type	High Precision	**Pitch X, Y, Z - Guaranteed**	±75, ±75, ±75 µrad
Size	Ø300 x 209 mm	**Rigidity X, Y, Z**	5, 5, 40 N/µm
Platform Diameter	200 mm	**Bi-directional Repeatability with Compensation Typical (Guaranteed)**	X,Y,Z: ±2.0 (na), ±2.0 (na), ±1.0 (na) µm U,V,W: ±1.0 (na), ±1.0 (na), ±2.0 (na) mdeg
Centered Load Capacity	200 N		
Travel Range X, Y, Z	±27.5, ±25, ±14 mm		
Travel Range ΘX, ΘY, ΘZ	±11.5, ±10.5, ±19 °		
Minimum Incremental Motion X, Y, Z	0.5, 0.5, 0.25 µm	**Connectors**	DB25 M (6), non vacuum compatible
Minimum Incremental Motion ΘX, ΘY, ΘZ	0.25, 0.25, 0.5 mdeg	**Cable Length**	1.5 m
		Motor	DC Servo
Uni-directional Repeatability X, Y, Z - Typical	±0.25, ±0.25, ±0.125 µm	**Origin**	Optical, close to lower limit
Uni-directional Repeatability X, Y, Z - Guaranteed	±0.25, ±0.25, ±0.125 µm	**Origin Repeatability**	X,Y,Z: ±5.0, ±5.0, ±2.5 µm U,V,W: ±2.5, ±2.5, ±5.0 mdeg
Uni-directional Repeatability ΘX, ΘY, ΘZ - Typical	±0.125, ±0.125, ±0.25 mdeg	**Encoder Resolution**	0.005898864 µm
		Number of Axis	6
Maximum Speed X, Y, Z	2.5, 2, 1 mm/s	**Weight**	7.2 kg
Maximum Speed ΘX, ΘY, ΘZ	1.8, 1.7, 3 °/s	**MTBF**	5,000 h (25% load, 10% duty cycle)
Yaw X, Y, Z - Guaranteed	±75, ±75, ±75 µrad	**RoHS**	Compliant

Symetrie: BREVA technical specification sheet. Breva has precision and travel range matching our requirements. However, the cost of the hexapod is higher than our budget and speed capacity is slower than developing machine expectation.

	BREVA DC	BREVA ST	BREVA BL
	for lighter payload	for higher payload	for higher speed and payload
Motion and positioning			
Travel range Tx, Ty (mm)	± 75	± 75	± 75
Travel range Tz (mm)	± 50	± 50	± 50
Travel range Rx, Ry (deg)	± 20	± 20	± 20
Travel range Rz (deg)	± 22	± 22	± 22
Resolution Tx, Ty, Tz (µm)	0.5	0.5	0.5
Resolution Rx, Ry, Rz (µrad)	2.5	2.5	2.5
Repeatability Tx, Ty, Tz (µm)	± 1	± 1	± 1
Repeatability Rx, Ry, Rz (µrad)	± 5	± 5	± 5
Speed (mm/s; deg/s)	8; 2.5	0.8; 0.25	3; 1
Mechanical properties			
Stiffness X, Y (N/µm)	5	5	5
Stiffness Z (N/µm)	32	32	32
Payload capacity (kg) (vertical orientation / horizontal orientation)	25 / 10	200 / 80	200 / 80
Motor type	DC motor, gearhead	Stepper motor, gearhead	Brushless motor, gearhead
Miscellaneous			
Operating temperature range (°C)	0 to + 50	0 to + 50	0 to + 50
Material	Aluminum, steel, stainless steel, plastic	Aluminum, steel, stainless steel, plastic	Aluminum, steel, stainless steel, plastic
Size mobile platform (mm)	Ø 289	Ø 289	Ø 289
Central aperture (mm)	Ø120	Ø120	Ø120
Height in middle position (mm)	350	350	350
Mass (kg)	32	36	36
Cable length (m)	3	3	3
Options	Absolute encoders Clean room compatibility Vacuum compatibility Customized platform design		
Controller			
Controller type	ALPHA		
Interface	Ethernet, USB		
Power supply	110-240 VAC / 50-60 Hz		

The performances are specified for single axis motions, with all other axes at midrange and for a rotation center in the middle of the mobile platform.

Appendix 5-1

A program is manually produced to execute the following profile

Once this profile is expressed as a step movement, it is then converted into program using MOV function with X and Y values.

Between each line of command WAC ONT? X =1 is inserted to ensure that the previous line of command is executed.

These 4 lines command is repeated with a step change of 0.5 mm to cover the whole sample.

Yellow coloured lines create raster program parallel to X axe.

Bleu coloured lines create raster program parallel to Y axe.

| #	X	28	X	Y	-		X	28	X	Y	
1	X	28	X	Y	-		X	28	X	Y	
2	y	0.5	14	14		MOV X 14 Y 14	Y	0.5	14	14	MOV X 14 Y 14
3	-	-	-	-		WAC ONT? X =1	-	-	-	-	WAC ONT? X =1
4			-14	14		MOV X -14 Y 14			14	-14	MOV X 14 Y -14
5	-	-	-	-		WAC ONT? X =1	-	-	-	-	WAC ONT? X =1
6			-14	13.5		MOV X -14 Y 13.5			13.5	-14	MOV X 13.5 Y -14
7	-	-	-	-		WAC ONT? X =1	-	-	-	-	WAC ONT? X =1
8			14	13.5		MOV X 14 Y 13.5			13.5	14	MOV X 13.5 Y 14
9	-	-	-	-		WAC ONT? X =1	-	-	-	-	WAC ONT? X =1
10			14	13		MOV X 14 Y 13			13	14	MOV X 13 Y 14
11	-	-	-	-		WAC ONT? X =1	-	-	-	-	WAC ONT? X =1
12			-14	13		MOV X -14 Y 13			13	-14	MOV X 13 Y -14
13	-	-	-	-		WAC ONT? X =1	-	-	-	-	WAC ONT? X =1
14			-14	12.5		MOV X -14 Y 12.5			12.5	-14	MOV X 12.5 Y -14
15	-	-	-	-		WAC ONT? X =1	-	-	-	-	WAC ONT? X =1
16			14	12.5		MOV X 14 Y 12.5			12.5	14	MOV X 12.5 Y 14
17	-	-	-	-		WAC ONT? X =1	-	-	-	-	WAC ONT? X =1
18			14	12		MOV X 14 Y 12			12	14	MOV X 12 Y 14
19	-	-	-	-		WAC ONT? X =1	-	-	-	-	WAC ONT? X =1
20			-14	12		MOV X -14 Y 12			12	-14	MOV X 12 Y -14
21	-	-	-	-		WAC ONT? X =1	-	-	-	-	WAC ONT? X =1
22			-14	11.5		MOV X -14 Y 11.5			11.5	-14	MOV X 11.5 Y -14
23	-	-	-	-		WAC ONT? X =1	-	-	-	-	WAC ONT? X =1
24			14	11.5		MOV X 14 Y 11.5			11.5	14	MOV X 11.5 Y 14
25	-	-	-	-		WAC ONT? X =1	-	-	-	-	WAC ONT? X =1
26			14	11		MOV X 14 Y 11			11	14	MOV X 11 Y 14
27	-	-	-	-		WAC ONT? X =1	-	-	-	-	WAC ONT? X =1
28			-14	11		MOV X -14 Y 11			11	-14	MOV X 11 Y -14
29	-	-	-	-		WAC ONT? X =1	-	-	-	-	WAC ONT? X =1
30			-14	10.5		MOV X -14 Y 10.5			10.5	-14	MOV X 10.5 Y -14
31	-	-	-	-		WAC ONT? X =1	-	-	-	-	WAC ONT? X =1
32			14	10.5		MOV X 14 Y 10.5			10.5	14	MOV X 10.5 Y 14
33	-	-	-	-		WAC ONT? X =1	-	-	-	-	WAC ONT? X =1
34			14	10		MOV X 14 Y 10			10	14	MOV X 10 Y 14
35	-	-	-	-		WAC ONT? X =1	-	-	-	-	WAC ONT? X =1
36			-14	10		MOV X -14 Y 10			10	-14	MOV X 10 Y -14
37	-	-	-	-		WAC ONT? X =1	-	-	-	-	WAC ONT? X =1
38			-14	9.5		MOV X -14 Y 9.5			9.5	-14	MOV X 9.5 Y -14
39	-	-	-	-		WAC ONT? X =1	-	-	-	-	WAC ONT? X =1

Appendix 6-1

Seven step grolishing experimental condition and results

Appendix 6.1 Table 1:   Seven step grolishing parameters & results (step 0)

| Step 0	Surface condition from grinding process obtained from Semi- Automatic grinding machine	
Average Sa after grinding process	561 nm	
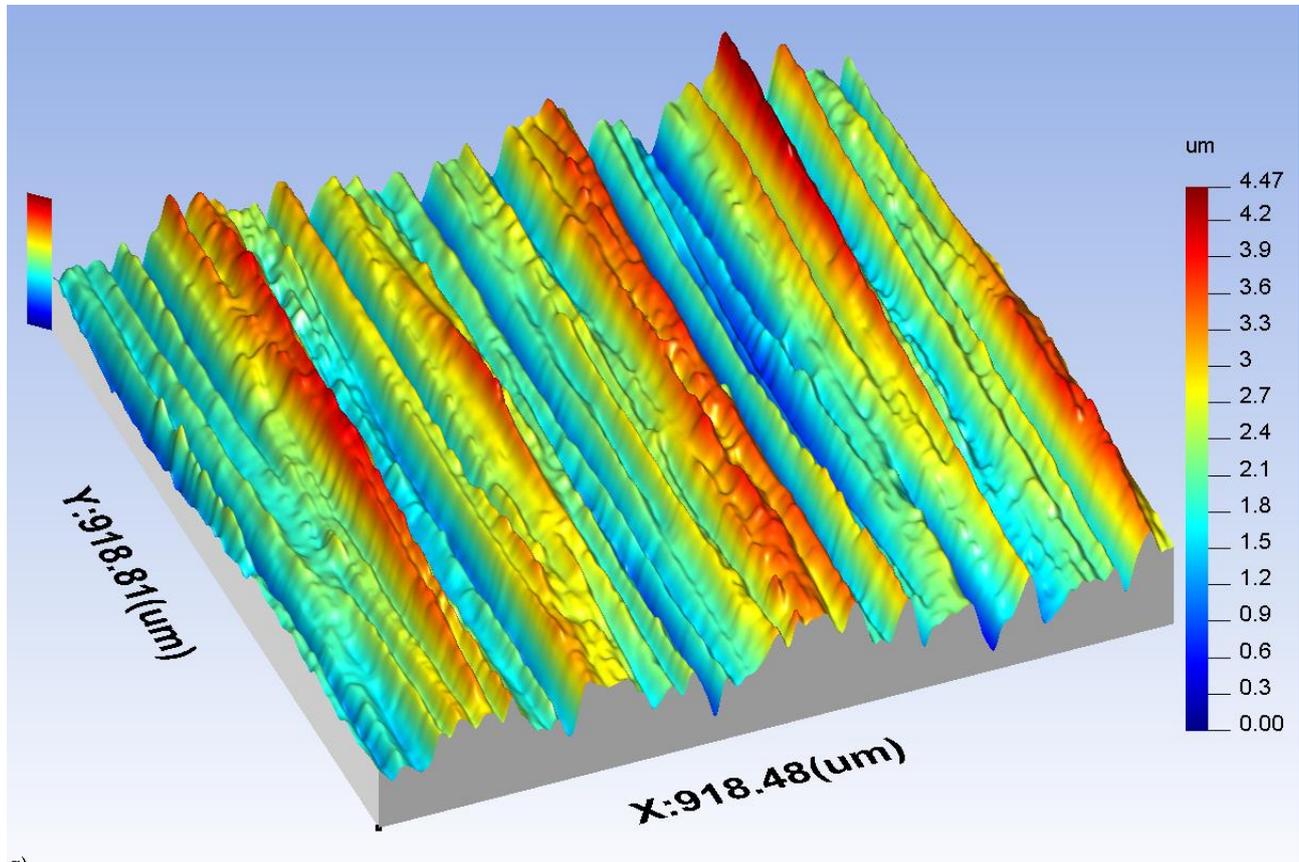
Appendix 6.1 Figure 1:   Seven step grolishing, step 0 surface topography
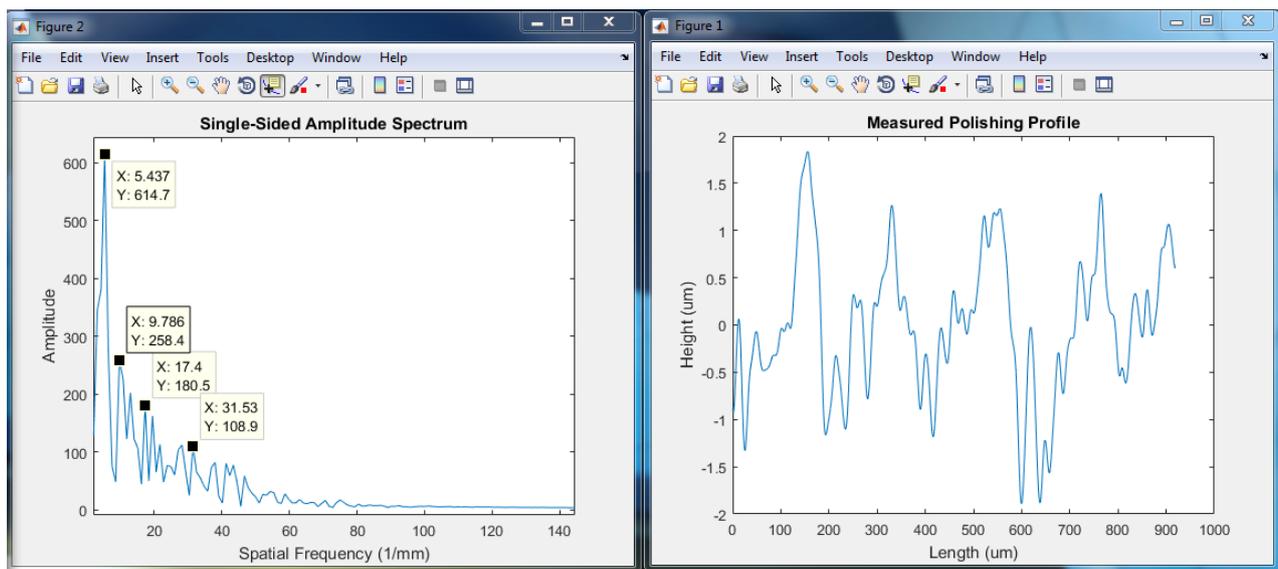

Appendix 6.1 Figure 2:   Seven step grolishing step 0, Amplitude in frequency domain (left) and surface profile (right)

Appendix 6.1 Table 2:   Seven step grolishing parameters & results (step 1)

Step 1	Speed (rpm)	Offset (mm)	Feed (mm/sec)	Number of Passes	Programme path direction	Abrasive size	Polishing Pad
	5000	0.3	0.75	1	Normal to X & Y Machine axis	45µm	Ultrapad
Average Sa before polishing process				561 nm			
Average Sa after polishing process				111 nm			
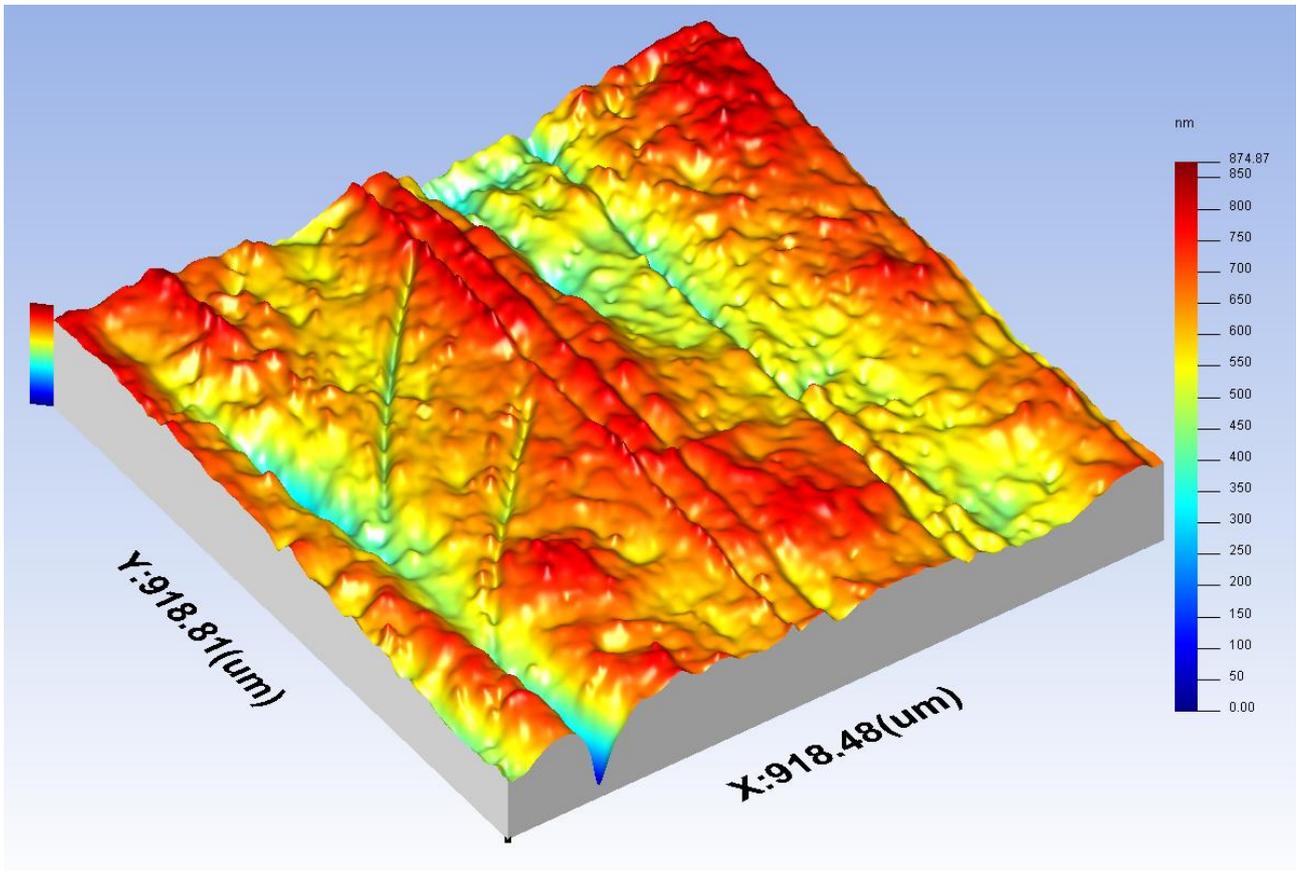
Appendix 6.1 Figure 3:   Seven step grolishing, step 1 surface topography
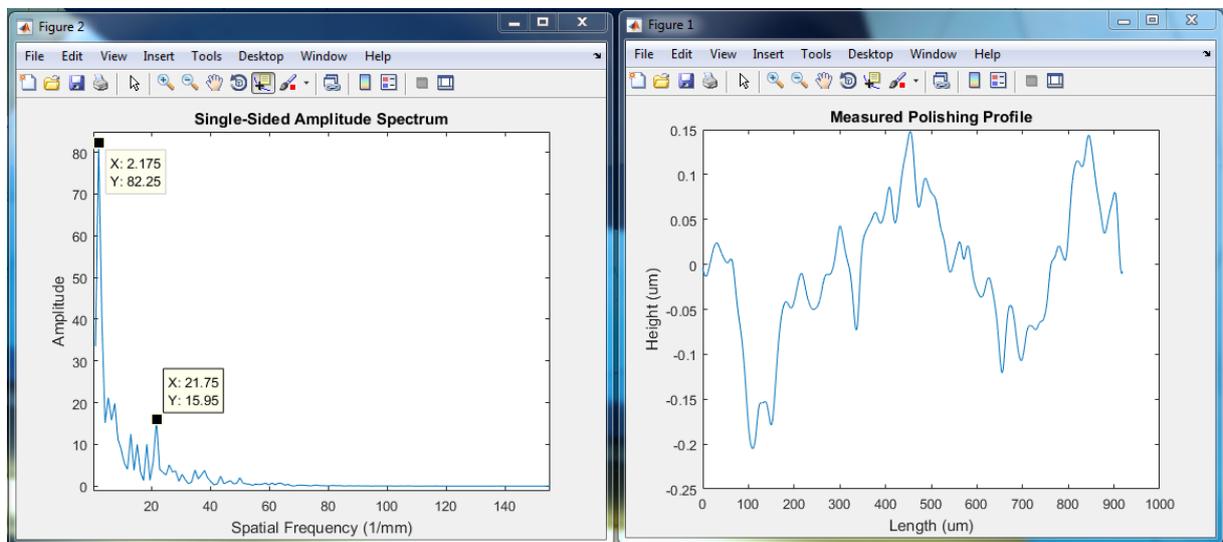

Appendix 6.1 Figure 4:   Seven step grolishing step 1, Amplitude in frequency domain (left) and surface profile (right)

Appendix 6.1 Table 3:   Seven step grolishing parameters & results (step 2)

Step 2	Speed (rpm)	Offset (mm)	Feed (mm/sec)	Number of Passes	Programme path direction	Abrasive size	Polishing Pad
	5000	0.3	0.75	1	45 Degree to X & Y Machine axis	45µm	Ultrapad
Average Sa before polishing process				111 nm			
Average Sa after polishing process				51 nm			
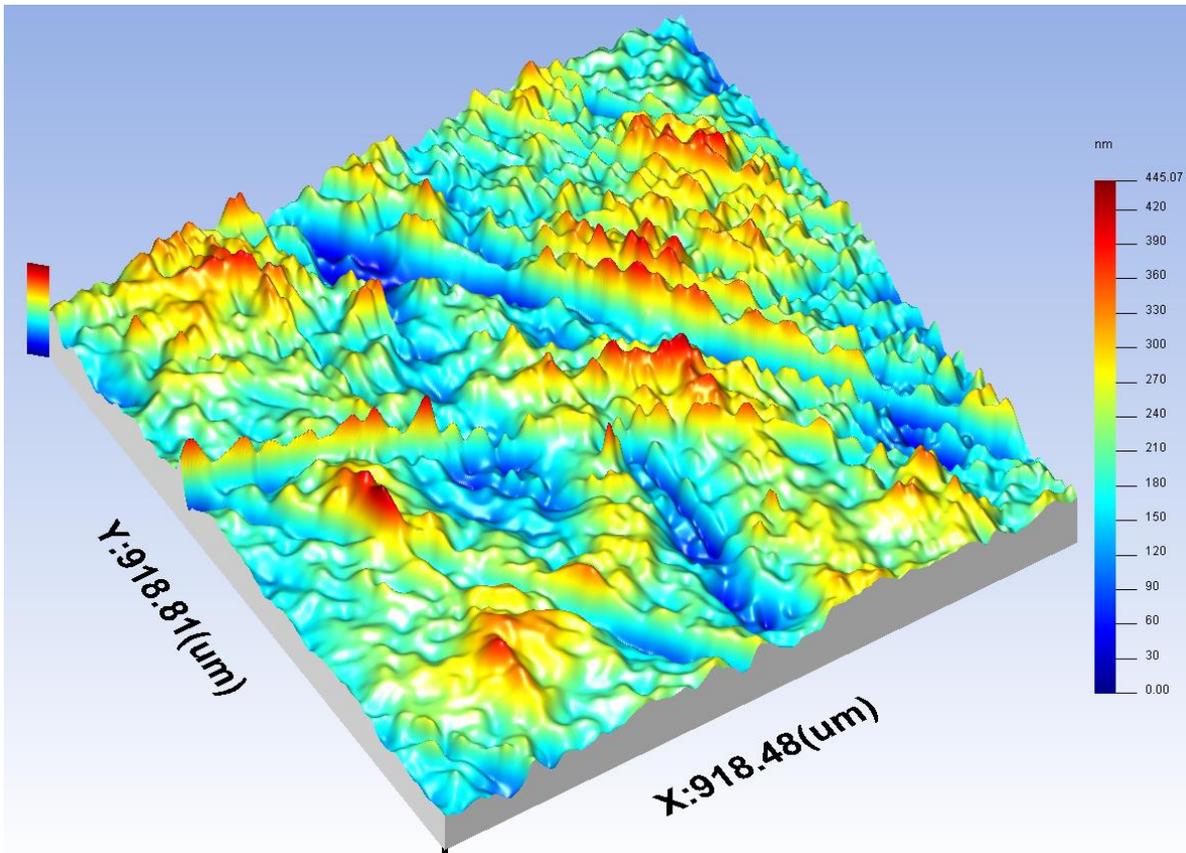
Appendix 6.1 Figure 5:   Seven step grolishing, step 2 surface topography
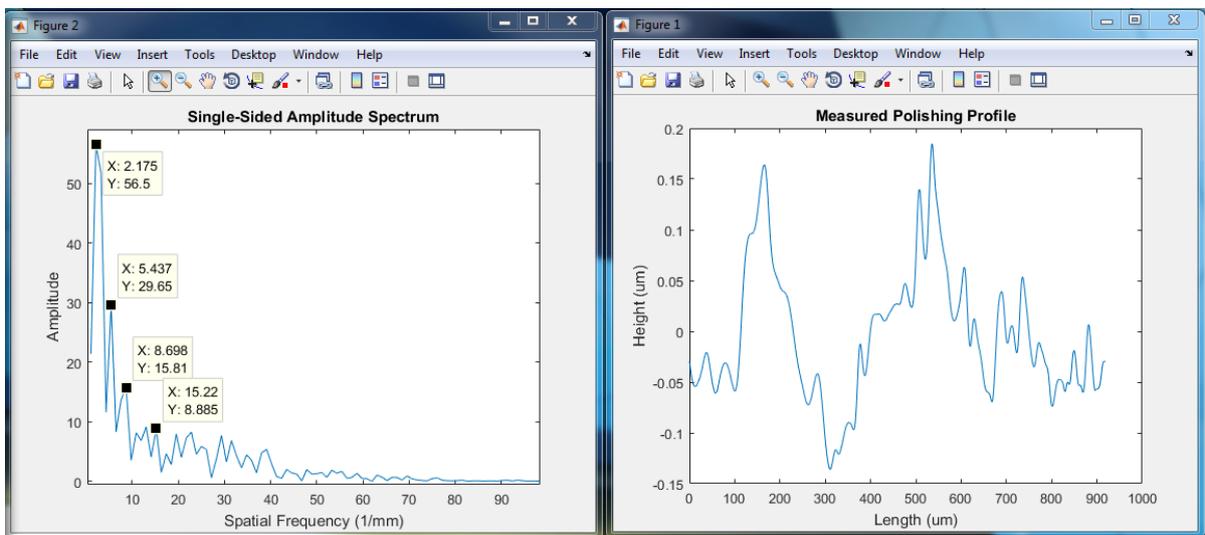
Appendix 6.1 Figure 6:   Seven step grolishing step 2, Amplitude in frequency domain (left) and surface profile (right)

Appendix 6.1 Table 4:   Seven step grolishing parameters & results (step 3)

Step 3	Speed (rpm)	Offset (mm)	Feed (mm/sec)	Number of Passes	Programme path direction	Abrasive size	Polishing Pad
	3000	0.3	3	1	Normal & 45 Degrees to X & Y axis	45µm	Ultrapad
Average Sa before polishing process				51 nm			
Average Sa after polishing process				39 nm			
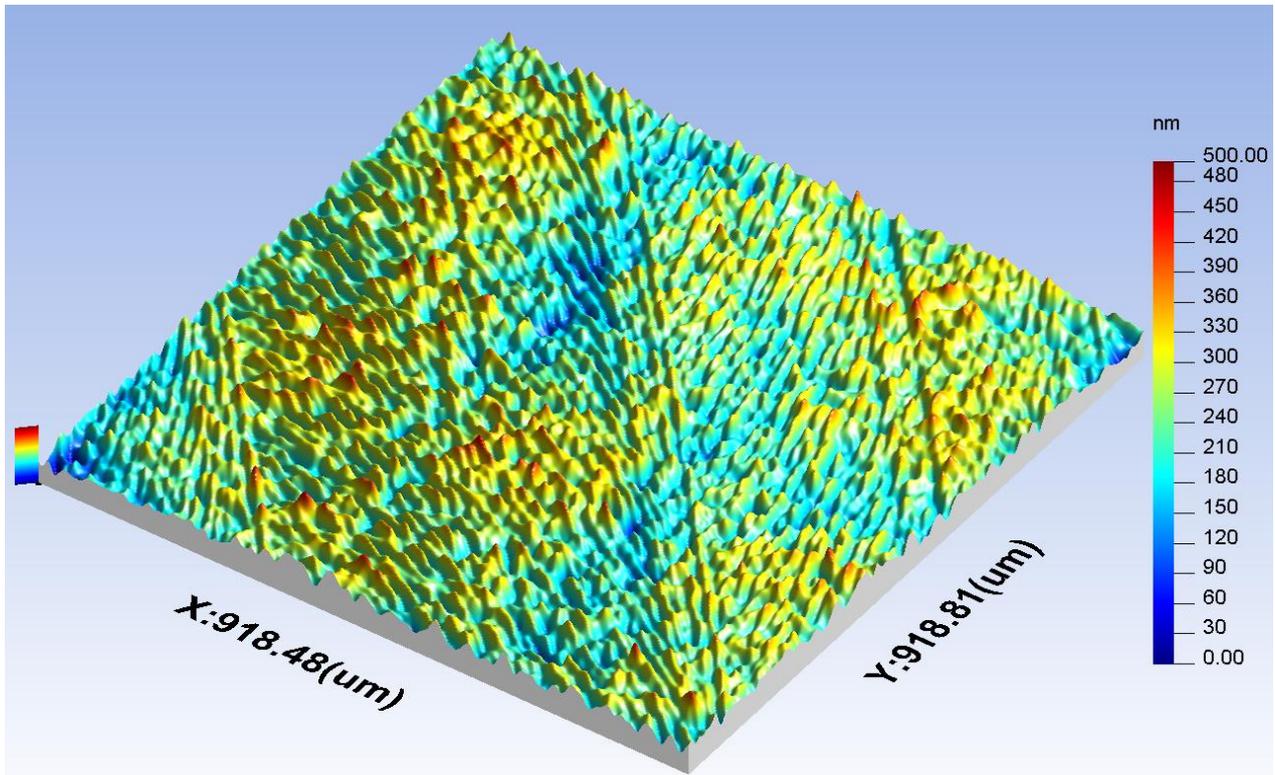
Appendix 6.1 Figure 7:   Seven step grolishing, step 3 surface topography
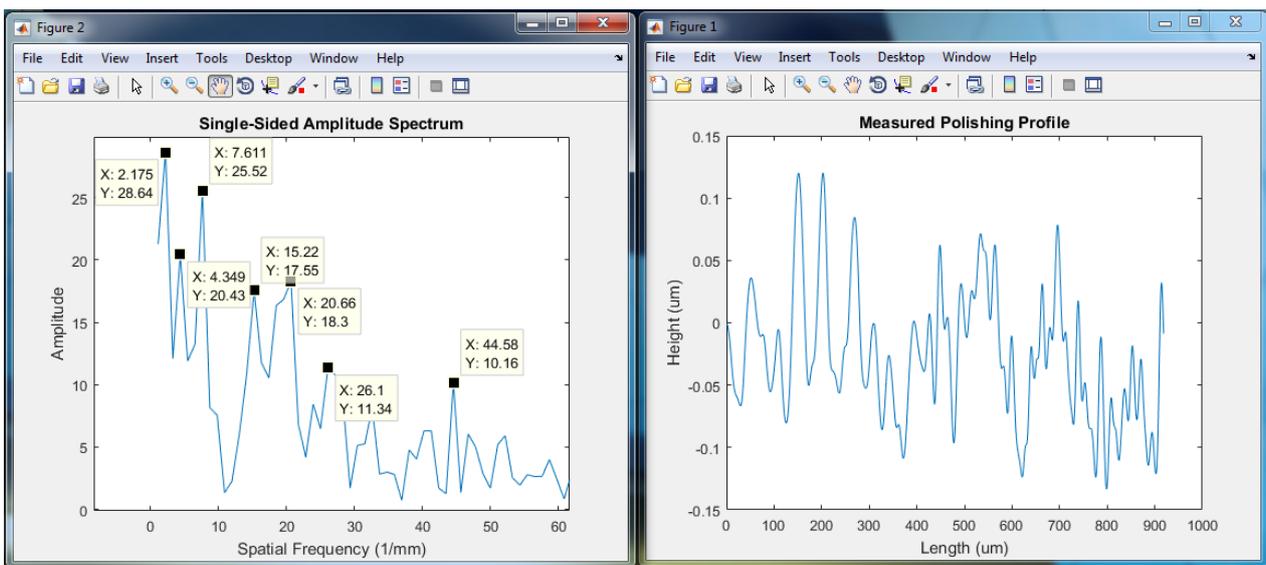
Appendix 6.1 Figure 8:   Seven step grolishing step 3, Amplitude in frequency domain (left) and surface profile (right)

Appendix 6.1 Table 5:   Seven step grolishing parameters & results (step 4)

| Step 4	Speed (rpm)	Offset (mm)	Feed (mm/sec)	Number of Passes	Programme path direction	Abrasive size	Polishing Pad
	2500	0.3	5	1	Normal to X & Y axis	9µm	Verdutex
Average Sa before polishing process			39 nm				
Average Sa after polishing process			16 nm				
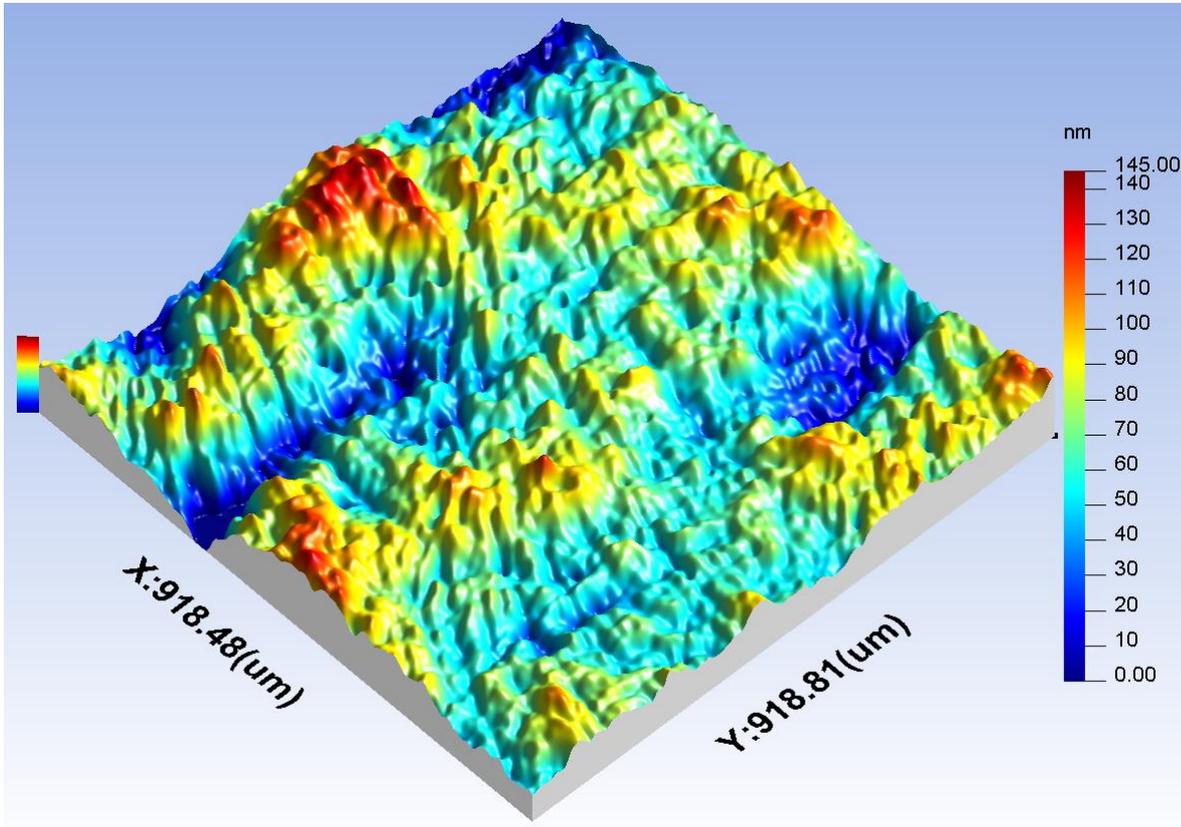
Appendix 6.1 Figure 9:   Seven step grolishing, step 4 surface topography
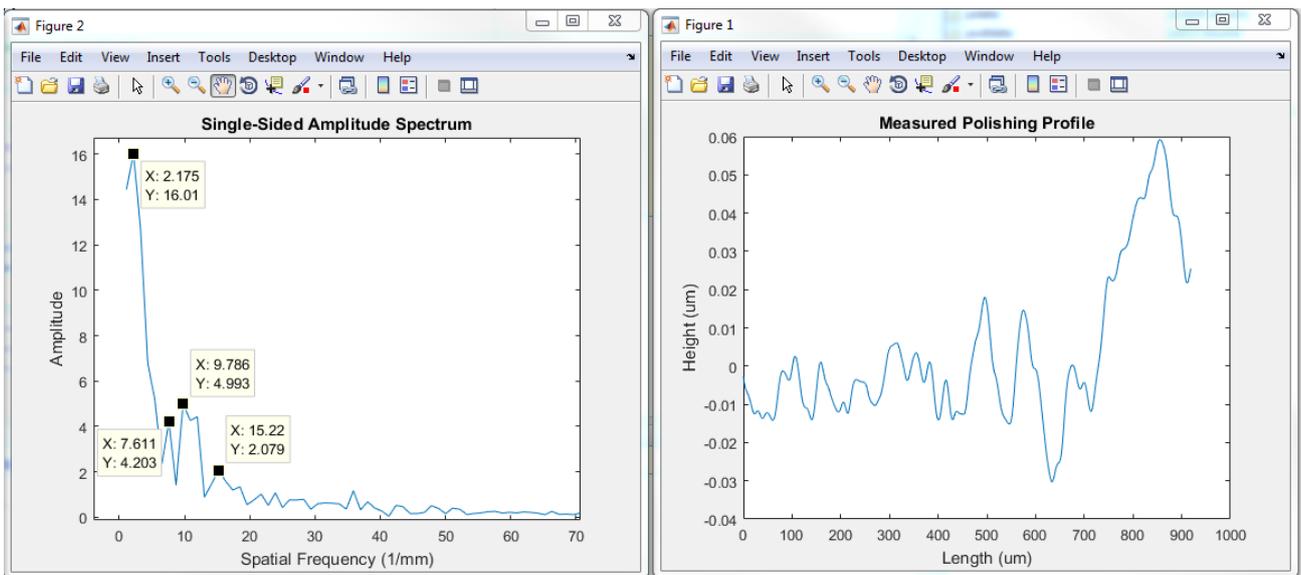

Appendix 6.1 Figure 10:   Seven step grolishing step 4, Amplitude in frequency domain (left) and surface profile (right)

Appendix 6.1 Table 6:   Seven step grolishing parameters & results (step 5)

| Step 5	Speed (rpm)	Offset (mm)	Feed (mm/sec)	Number of Passes	Programme path direction	Abrasive size	Polishing Pad
	2500	0.3	5	1	45 Degree to X & Y Machine axis	9μm	Verdutex
Average Sa before polishing process			16 nm				
Average Sa after polishing process			14 nm				
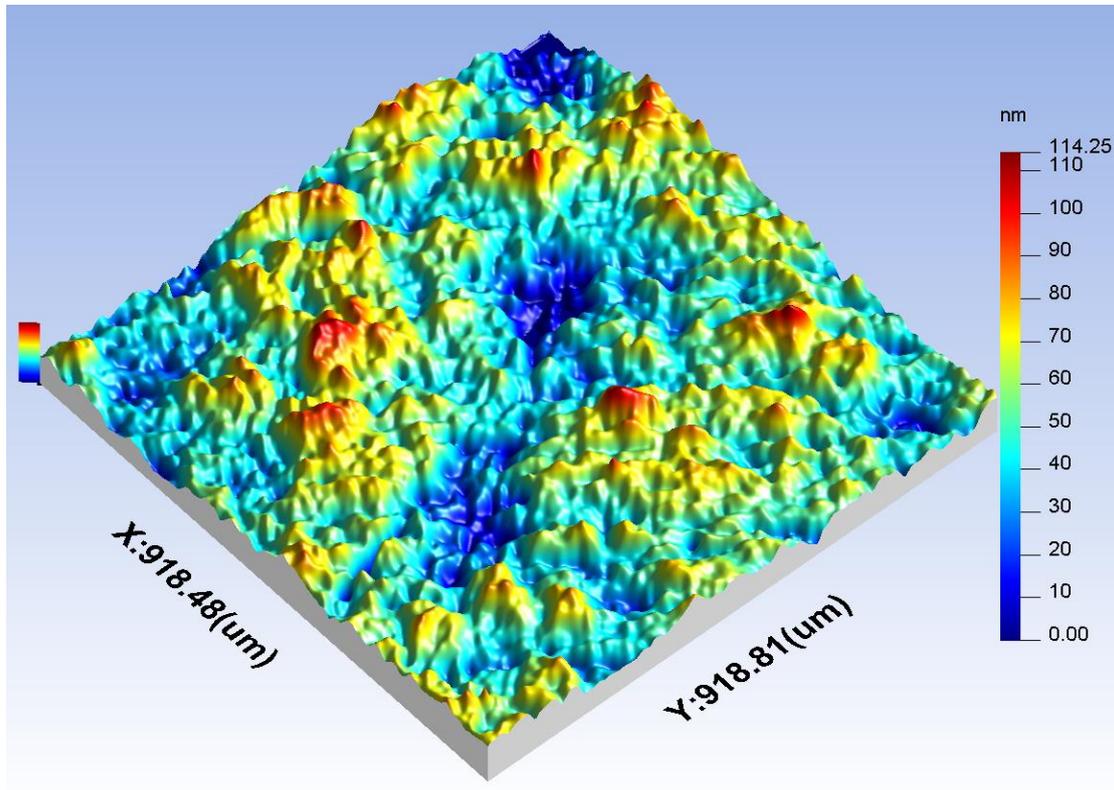
Appendix 6.1 Figure 11:   Seven step grolishing, step 5 surface topography
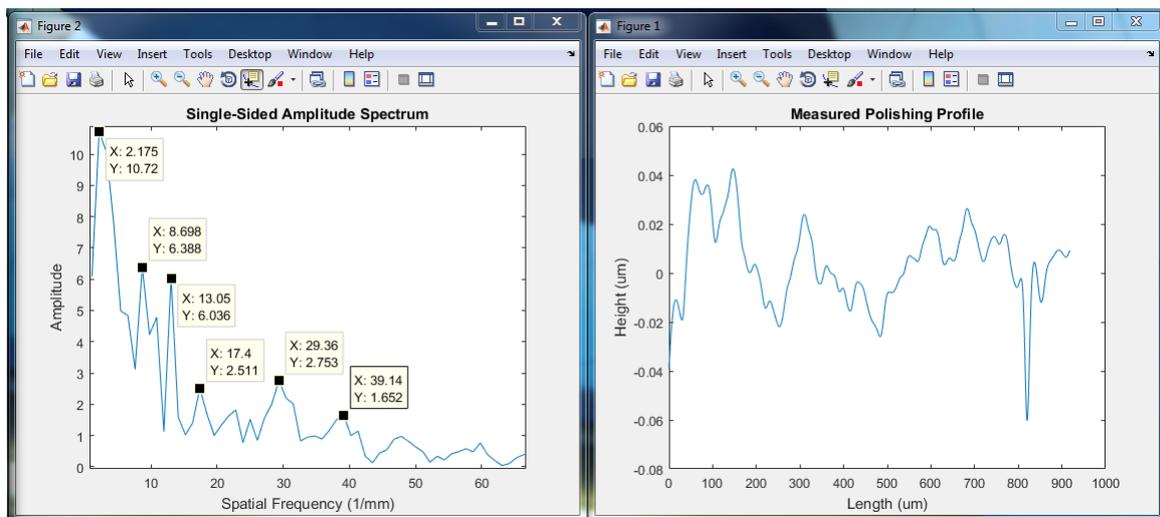
Appendix 6.1 Figure 12:   Seven step grolishing step 5, Amplitude in frequency domain (left) and surface profile (right)

| Step 6	Speed (rpm)	Offset (mm)	Feed (mm/sec)	Number of Passes	Programme path direction	Abrasive size	Polishing Pad
	1000	0.3	15	1	Normal to X & Y axis	1μm	Verdutex
Average Sa before polishing process			14 nm				
Average Sa after polishing process			13 nm				
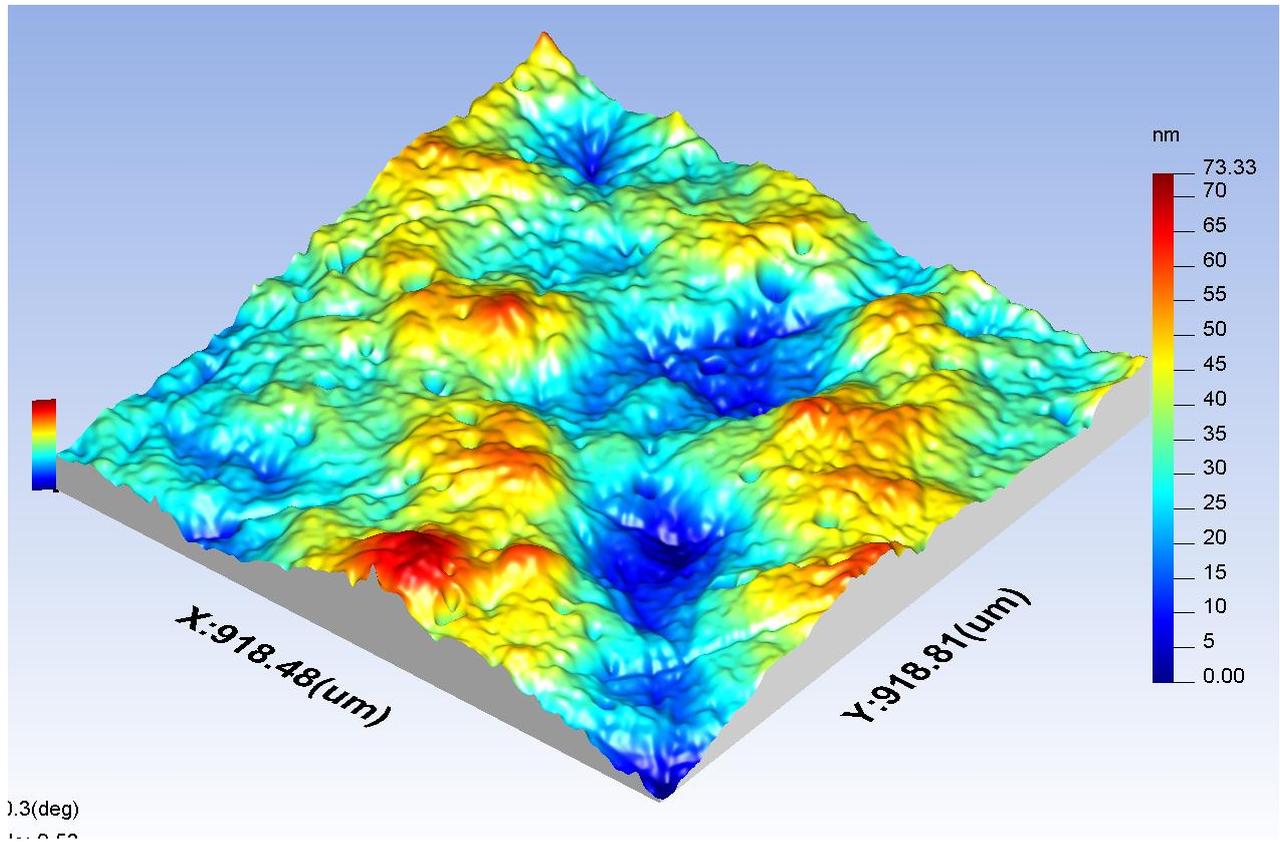
Appendix 6.1 Figure 13: Seven step grolishing, step 6 surface topography
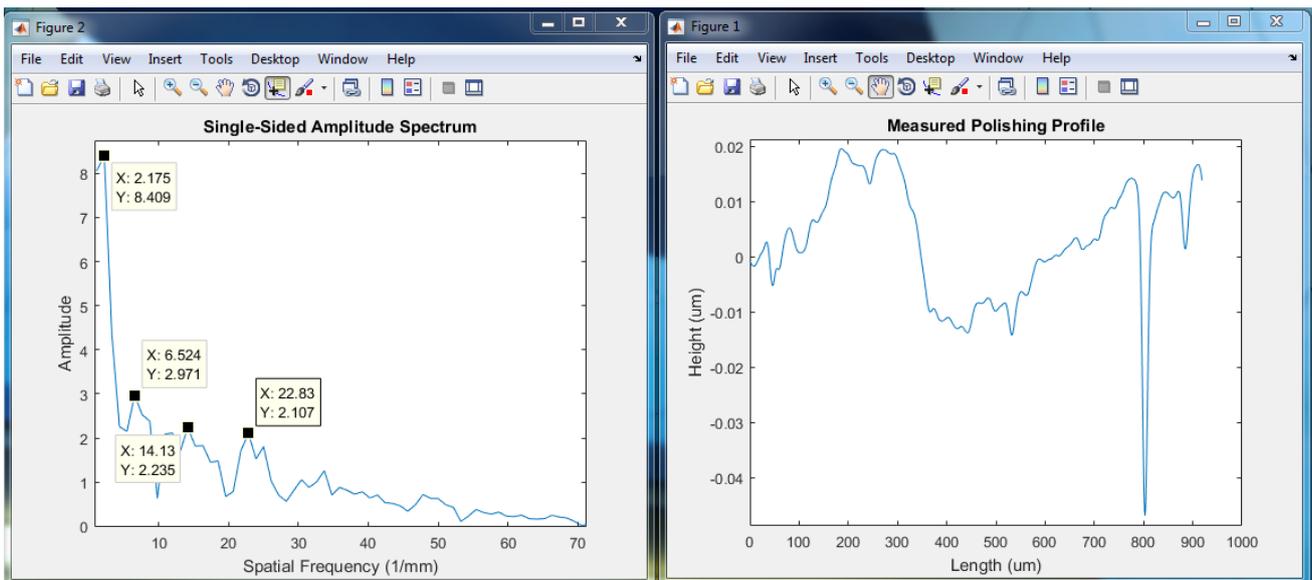

Appendix 6.1 Figure 14: Seven step grolishing step 6, Amplitude in frequency domain (left) and surface profile (right)

Appendix 6.1 Table 8:   Seven step grolishing parameters & results (step 7)

| Step 7	Speed (rpm)	Offset (mm)	Feed (mm/sec)	Number of Passes	Programme path direction	Abrasive size	Polishing Pad
	1000	0.3	15	1	45 Degree to X & Y Machine axis	1μm	Verdutex
Average Sa before polishing process			13 nm				
Average Sa after polishing process			7 nm				
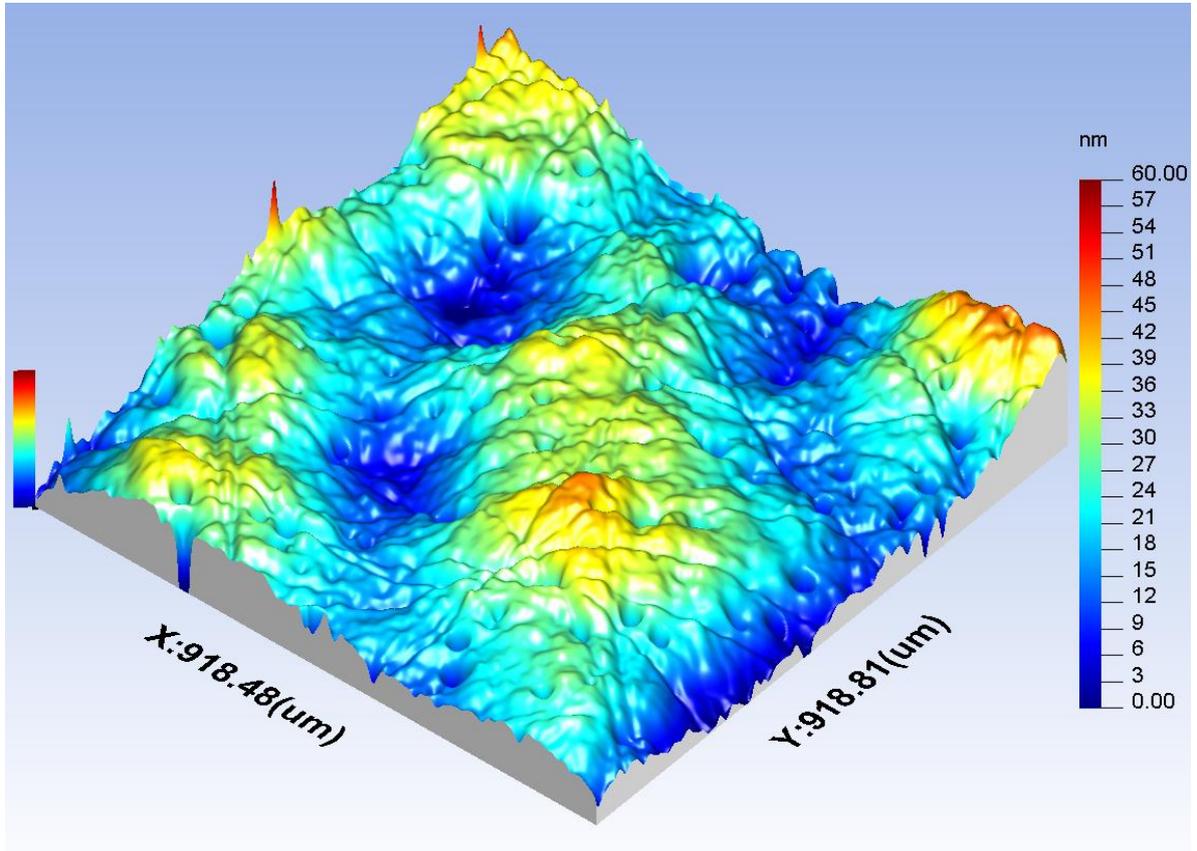
Appendix 6.1 Figure 15:   Seven step grolishing, step 7 surface topography
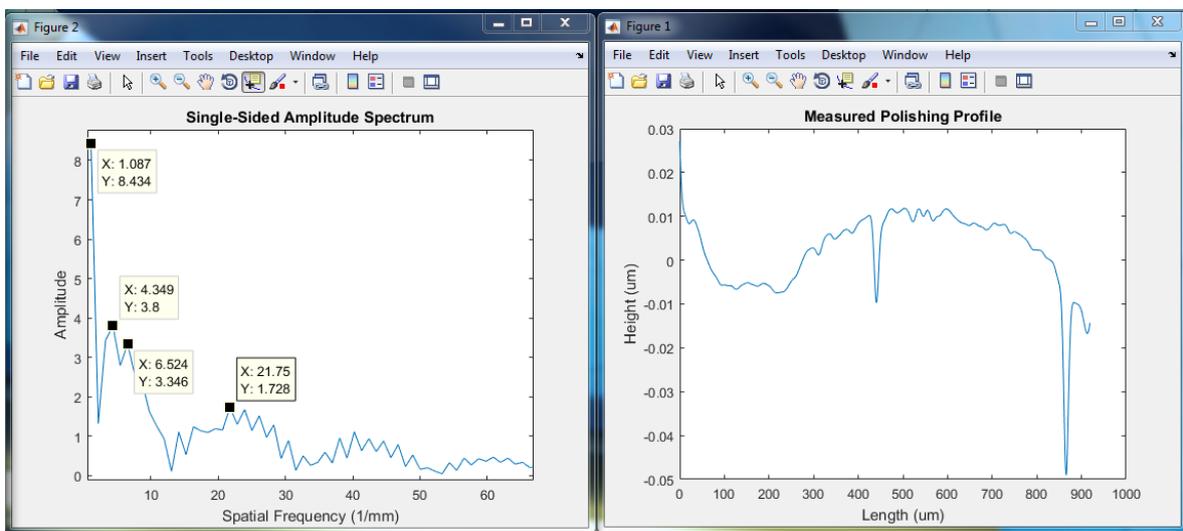
Appendix 6.1 Figure 16:   Seven step grolishing step 7, Amplitude in frequency domain (left) and surface profile (right)

Appendix 6-2.1

Multi-scale wavelet analysis of four step grolishing process showing the grinding marks removal process at four wavelet ranges. This also expose the tool path imprinted on the workpiece towards step 2 and the attenuation of those marks at step 4.

(μm)	STEP0	STEP1	STEP2	STEP3	STEP4
14.4-28.8					
28.8-57.6					
57.6-115.2					
115.2-230.4					
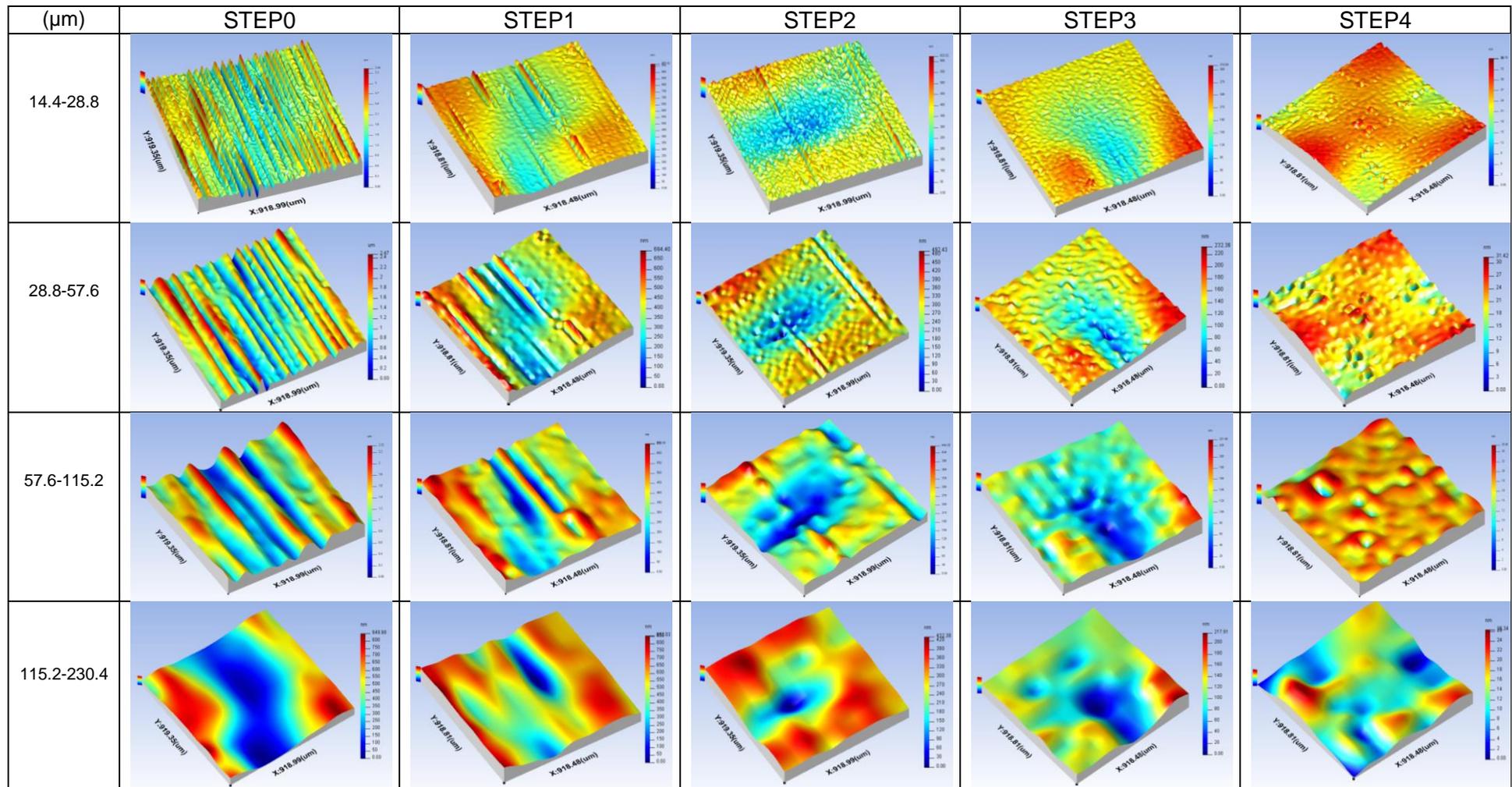
Appendix 6-2.2

Multi-scale wavelet analysis of seven step grolishing process showing the grinding marks removal process at four wavelet ranges. This also expose the tool path imprinted due to grolishing process and the change in direction of marks following the tool path. In all four wavelet range, the tool path marks are barely visible.

(µm)	STEP0	STEP1	STEP2	STEP3	STEP4	STEP5	STEP6	STEP7
14.4-28.8								
28.8-57.6								
57.6-115.2								
115.2-230.4								